HEINRICH HEINE
UNIVERSITÄT
DÜSSELDORF

Analysis of factors influencing enzyme activity and stability in the solid state

Inaugural-Dissertation

zur Erlangung des Doktorgrades
der Mathematisch-Naturwissenschaftlichen Fakultät
der Heinrich-Heine-Universität Düsseldorf

vorgelegt von

Liliya Kulishova
aus Pavlodar

Düsseldorf, April 2010

Aus dem Institut für Molekulare Enzymtechnologie (IMET)
der Heinrich-Heine Universität Düsseldorf
im Forschungszentrum Jülich

Gedruckt mit der Genehmigung der
Mathematisch-Naturwissenschaftlichen Fakultät der
Heinrich-Heine-Universität Düsseldorf

Referent: Frau Prof. Dr. Martina Pohl
Koreferent: Herr Prof. Dr. Karl-Erich Jäger

Tag der mündlichen Prüfung:

Die vorliegende Arbeit wurde in der Zeit von September 2006 bis September 2009 am Institut für Molekulare Enzymtechnologie der Heinrich-Heine-Universität Düsseldorf im Forschungszentrum Jülich unter der Anleitung von Frau Prof. Dr. Martina Pohl und Dr. Antje Spiess angefertigt.

Die Arbeit wurde von der Deutschen Forschungsgemeinschaft im Rahmen des Graduiertenkollegs 1166 "Biocatalysis in non-conventional media (BioNoCo)" gefördert.

Diese Dissertation wird u.a. in elektronischer Form auf dem WWW-Server der Universitätsund Landesbibliothek Düsseldorf veröffentlicht.

Table of Contents

Figures

Tables

Abbreviations

a_w	thermodynamic activity of water
a_{acphen}	thermodynamic activity of acetophenone
ADH	alcohol dehydrogenase
ADH T	alcohol dehydrogenase from *Thermo ¬anaerobacter species*
Amp	ampicillin
au	arbitrary units
bp	base pairs
BAL	benzaldehyde lyase from *Pseudomonas fluorescens*
BSA	bovine serum albumin
BFD	benzoylformate decarboxilase from *Pseudomonas putida*
CD	circular dichroism
ddH_2O	double distilled water
DRIVeR	diversity resulting from *in vitro* recombination
ee	enantiomeric excess
epPCR	error-prone polymerase chain reaction
FAD	flavin adenine dinucleotide
FIA	flow injection analysis
FIT	B-Factor Iterative Test
FMN	flavin mononucleotide
*Ff*ADH	alcohol dehydrogenase from *Flavobacterium frigidimaris*
GdnCl	guanidinium chloride
HLADH	horse liver alcohol dehydrogenase
HCD	high cell density
HPLC	high performance liquid chromatography
IPTG	isopropyl-β-D-thiogalactopyranosid
ISOR	incorporating synthetic oligonucleotides via gene reassembly
Km	Michaelis constant
LB	Luria-Bertani
*Lb*ADH	alcohol dehydrogenase from *Lactobacillus brevis*
MDR	medium-chain dehydrogenases
MS	mass spectroscopy
NADH	nicotinamide adenine dinucleotide
NADPH	nicotinamide adenine dinucleotide phosphate
OD	optical density
OSCARR	one-pot simple methodology for cassette randomization and recombination

PAGE	polyacrylamide gel electrophoresis
PDA	poly diode array
PCR	polymerase chain reaction
PEDEL-AA	programme for estimating amino acid diversity in error-prone PCR libraries
RAISE	random insertional-deletional strand exchange mutagenesis
RACHITT	random chimeragenesis of transient templates
RD-PCR	recombination-dependent polymerase chain reaction
RID	random insertion and deletion mutagenesis
RT	room temperature
rpm	rotations per minute
SDR	short-chain dehydrogenases
SDS	sodiumdodecylsulphate
SeSaM	sequence saturation mutagenesis
*Ss*ADH	alcohol dehydrogenase from *Sulfolobus sulfactarius*
StEP	staggered extention process
$\tau_{1/2}$	half-life time
TEA	triethanolamine
TEMED	tetramethylethylendiamine
ThDP	thiamine-diphosphate
TIM	transposon integration mediated mutagenesis
Tris	tris(hydroxymethyl)-aminomethan
*T*ADH	alcohol dehydrogenase from *Thermus sp.*
Tm	melting temperature
T_{md}	midpoint of thermal inactivation curve
v/v	volume pro volume
w/v	weight pro volume
*Y*ADH	baker's yeast alcohol dehydrogenase

Acknowledgment

I would like to give my grateful acknowledge to the *Forschungszentrum Jülich* and *Heinrich-Heine University of Düsseldorf* for the great chance to study in an international academic environment. I deeply appreciate an interesting, interactive and carefully designed graduate program "*Biocatalysis in Non-conventional Media*", which familiarized me with prominent research topics in biotechnology and biochemical engineering and trained critical scientific reasoning. I would like to thank all the people involved in its establishment. My gratitude goes to *Deutsche Forschungsgemeinschaft* for providing me a financial support during my Ph.D. studies and making this work possible.

I extend my sincere gratitude and appreciation to my supervisors *Apl. Prof. Dr. Martina Pohl and Dr. Antje Spiess* for an opportunity to conduct the research in their laboratories, their timely advices, guidance, consistent support and careful editing of the thesis. It was a great pleasure to work in their teams.

I owe my special gratitude to to *Dr. J. Fitter (Research Center Jülich)* for providing me a chance of performing the CD studies in his laboratory and for useful discussions concerning the spectra.

I would like to express my warm and sincere thanks *Ms. A. Wirtz* and *Dr. D. Hofmann (Research Center Jülich)* for performing the effort-consuming HPLC separation and MS analysis of cofactor degradation products. I am grateful *to Ms. C. Bösing* for her assistance in production and screening of the mutant library.

I am highly indebted to *K. Dimoula* and *M. Jordan (RWTH Aachen University)* for their collaboration and support in gas/solid reactor experiments.

I offer my deep appreciation to *Prof. Dr. A. Schmid (University of Dortmund)* and *Prof. Dr. T. Kazuoka (Kansai University, Japan)* for providing of highly thermostable alcohol dehydrogenases.

I would like to express my thanks to *Prof. Dr. J. Büchs, Dr. L. Greiner* and *Dr. M. Fioroni* (RWTH Aachen University) for right stimulating discussions and useful suggestions.

I am deeply indebted to my former and present lab mates *Dr. U. Krauss, Dr. D. Göcke, Dr. J. Guterl, Dr. B. Franken, Ms. M. Schwarz and Ms. G. Kolter* for their interest and enourmous contribution to the development of my scientific ideas and skills. I would like to thank Ms. I. Frindi-Wosch and Ms. K. Range to their help with experiment organisation.

Finally, my special gratitude goes to my husband *Dr. Alexander Kraynov* and my family for their cooperation, support and encouragement.

Publications

Kulishova, L., Dimoula, K., Jordan, M., Wirtz, A., Hofmann, D., Santiago-Schübel, B., Pohl, M., Spiess, A.C. (2010): Factors influencing the operational stability of NADPH-dependent alcohol dehydrogenase and an NADH-dependent variant thereof in gas/solid reactors. *Submitted.*

Conference contribution

Kulishova, L., Spiess, A.C., Pohl, M. (2007): Analysis of factors influencing enzyme activity and stability in the gas phase to allow high throughput screening for stabilized enzymes. Poster, BioTrans 2007 (Oviedo).

Kulishova, L., Spiess, A.C., Pohl, M. (2008): Factors influencing enzyme activity and stability in the solid state. Poster, BioCat 2008 (Hamburg).

Kulishova, L., Dimoula, K., Spiess, A.C., Pohl, M. (2009): NADPH- and NADH-dependent reduction of acetophenone in a solid-gas bioreactor. Poster, BioTrans 2009 (Bern).

Dimoula, K., Jordan, M., Kulishova, L., Büchs, J., Pohl, M., Spiess, A.C. (2009):
Enhanced operational stability of the *Lactobacillus brevis* alcohol dehydrogenase (*Lb*ADH) in a gas/solid reaction system. Presentation, ProStab 2009 (Graz).

Hofmann, D., Wirtz, A., Santiago-Schübel, B., Kulishova, L., Disco, U., Pohl, M. (2010): Strukturaufklärung der thermischen Abbauprodukte der enzymatischen Kofaktoren NADH und NADPH mittels ESI-FTICR-MS und HPLC-MS.

Abstract

The gas/solid biocatalysis represents a developing environmental-friendly technology for the production of volatile compounds like esters and alcohols, in which a dry enzyme catalyzes the reaction of the gaseous substrate to the gaseous product. This approach exhibits significant advantages, such as high conversion rates, higher stability of the immobilized biocatalyst and simplified product recovery. Furthermore, the gas/solid biocatalysis is efficient for investigation of the influence of thermodynamic parameters, such as water activity and substrate activity on activity and stability of a biocatalyst. However, progressive inactivation of the immobilized solid enzymes is usually observed under the operating conditions of a gas/solid reactor. Thus, studies of the temperature-dependent performance of the dry enzymes are important for both fundamental scientific understanding and engineering of novel thermostable biocatalysts.

The primary objectives of the current thesis were:

(i) Understanding of the key mechanisms responsible for the inactivation of solid enzymes in comparison to enzymes in aqueous solution.

(ii) Understanding of the processes leading to inactivation of the solid cofactors NADH and NADPH in comparison to cofactors in aqueous solution.

(iii) Generation of novel thermostable enzyme variants for the gas/solid biocatalysis and setup of an appropriate high-throughput screening procedure.

(iv) Investigation of the activity and stability of enzymes under operational conditions in the gas/solid reactor.

Studies were predominantly performed using the NADPH-dependent alcohol dehydrogenase from *Lactobacillus brevis* (*Lb*ADHwt) and a NADH-dependent variant thereof (*Lb*ADH G37D). A comparative study of the biocatalytic activity and protein structure through complementary techniques demonstrated that thermal inactivation of the dissolved and solid enzymes proceeds via different molecular mechanisms. Thermal degradation of NADH differed from NADPH. In the both cases, the main fragmentation routes included the cleavage of the nicotinamide ring as well as oxidative ring opening of the ribose ring. Construction and screening of a mutant library with 6000 enzyme variants resulted in identification of the variant *Lb*ADH G37D/V42F/E44C/K48Q with higher stability in the dry state. Comparative studies of *Lb*ADHwt and *Lb*ADH G37D in the gas/solid reactor demonstrated that thermodynamic activity of water and substrate was decisive for the operational activity and stability of enzymes. Furthermore, already a single amino acid exchange in the enzyme had significant impact on the kinetic characteristics and the stability of the biocatalyst.

Summary

Gas/solid biocatalysis represents an environmental-friendly reaction system, where a solid dry enzyme catalyzes conversion of gaseous substrates to gaseous products. The technology is used for the production of volatile fine chemicals, bioremediation of air pollution and elaboration of electrochemical biosensors. The possibility to control thermodynamic parameters in a gas/solid system allows precise adjusting the enzyme micro-environment, which is important for scientific purposes. However, the gas/solid reactor is operated at elevated temperature, and, in spite of increased resistance of the immobilized enzymes, their progressive inactivation is usually observed. Hitherto, the key mechanisms leading to inactivation of a biocatalyst in the gas/solid reactor have remained unclear. On the other hand, application of enzyme engineering techniques for the stabilization of enzymes in the gas/solid system requires detailed knowledge of the molecular effects relevant for inactivation of the solid biocatalyst. Thus, investigation of the factors that affect the stability of the solid enzymes is of great importance.

In this thesis, the stability of enzymes was characterized both in non-reactive and reactive systems. The aim was to elucidate factors that affect the operational stability in the gas/solid reactor and find parameters that may predict the biocatalyst performance in the gas/solid system. Two single-amino-acid exchange enzyme variants, the NADPH-dependent *Lb*ADHwt and the NADH-dependent *Lb*ADH G37D were used as model enzymes. Special emphasis was placed on the thermal stability of the solid cofactors, the thermal stability of the solid proteins, and application of the obtained knowledge for the design of a reliable high-throughput screening system and optimization of the target enzymes for gas/solid system.

(i) The first part of the present thesis is dedicated to the detailed studies of the thermal degradation of the dissolved and solid NAD(P)H, which were performed with the aim to elucidate the key processes responsible for the cofactor inactivation. It was found that the dissolved NADH was more thermostable by a factor of 3.5-5.5 than the phosphorylated cofactor, whereas both cofactors show significantly higher stability in the solid state. To gain deeper understanding of the cofactor degradation process, HPLC-MS analysis of the products of thermal degradation of the dissolved and solid NAD(P)H was carried out. It was discovered that thermal degradation of NADH and NADPH occured in different ways. More degradation products were detected after heat treatment of solid NADPH than of solid NADH. Main fragmentation routes included the cleavage of the nicotinamide ring as well as oxidative ring opening of the ribose ring. Additionally, the thermally degraded solid probe of NADPH

contained a product of cyclization. Both cofactors showed enzymatically inactive degradation products containing an intact reduced nicotinamide ring giving rise to absorbance at 340 nm.

(ii) The second part of the present work describes comparative studies of the thermal stability of *Lb*ADHwt and *Lb*ADH G37D performed in aqueous solution and in the solid state. In both cases heat-induced inactivation of the enzymes was irreversible. Drastic aggregation accompanied the heat-induced inactivation of the dissolved enzymes. Kinetic characterization of the thermal stability of the dissolved *Lb*ADHwt and *Lb*ADH G37D revealed 3-9 times higher thermostability of the variant. This effect was explained by location of the G37D exchange in the β-turn in close proximity to cofactor binding region, which is known to be a sensitive part. Manipulations in this region may significantly affect local and even global flexibility of the protein molecule, and, therefore, its thermal stability.

Both enzymes were approximately two orders of magnitude more stable in the solid state than in solution. Besides, no differences were observed between the stabilities of the solid *Lb*ADHwt and *Lb*ADH G37D. The key mechanisms responsible for the inactivation of the solid enzymes in comparison to enzymes in aqueous solution were inspected using fluorescence, CD and static light scattering spectroscopic techniques. Although certain structural changes were detected for both the dissolved and solid enzymes, the degree of structural unfolding was drastically lower in the absence of liquid water. So, in spite of the total inactivation, the fluorescence emission maxima of the solid samples showed only a minor red shift, the light scattering intensity stayed relatively constant and no remarkable differences were displayed by CD spectra of the solid protein samples.

(iii) The third part of this thesis focuses on generation of the novel thermostable enzyme variants advantageous for the gas/solid system. Because of the higher stability of NADH compared to NADPH also in the solid state, and its lower price, the variant *Lb*ADH G37D was chosen as a starting point for subsequent modifications. Focused mutagenesis strategy based on determination and randomization of most flexible enzyme regions was exploited. Based on the crystal structure of *Lb*ADH D37D, the amino acids V42, E44 and K48 were selected using the B-Fitter Iterativer Test (B-FIT) and subjected to saturation mutagenesis. All the three residues were randomized simultaneously in order to cover all possible cooperative effects. The focused mutant library of 6000 enzyme variants was created.

An effective and reliable high-throughput screening was developed for evaluation of variants with enhanced thermostability in the solid state.

Application of this system for the screening of the mutant library allowed identification of the variant *Lb*ADH G37D/V42F/E44C/K48Q as potentially suitable for the gas/solid biocatalysis. Additionally, the variants *Lb*ADH G37D/V42D, *Lb*ADH G37D/E44F/K48E, *Lb*ADH G37D/V42D/E44Y/K48E, *Lb*ADH G37D/V42L/E44Y/K48E and *Lb*ADH G37D/V42D/E44N/K48Q were found to possess increased thermostability in aqueous solution.

(iv) The last part of the thesis describes the behaviour of *Lb*ADHwt and *Lb*ADH G37D under operational conditions in the gas/solid reactor. In contrast to 15 times lower enzymatic activity of *Lb*ADH G37D in the aqueous solution at pH 7.0, the variant demonstrated unexpectedly high specific reaction rates in the gas/solid experiments. Thermostability of the dry enzymes without substrates has been proven to be predictive for the order of magnitude of the operational stability in the gas/solid reactor. Interestingly, the cofactor stability was not the decisive parameter for the operational stability in the gas/solid reactor system despite the low thermostability and increased number of degradation products of the cofactor NADPH in in the dissolved and solid state.

Increasing of thermodynamic activity of water and substrate in the gas/solid reactor caused differences in the operational stability of the two enzyme variants. The observed phenomenon was related to the probable impact of the single exchange G37D into the catalytic properties of the enzymes, such as substrate and co-substrate affinity or substrate inhibition. These effects could overlay with the high protein stability in the presence of the substrates. Importantly, some of these differences, *i.e.* the lower affinity of *Lb*ADH G37D to the substrate, were observed in the aqueous medium [8]. Thus, the appropriateness of an enzyme variant to the gas/solid biocatalysis can be fully predicted neither from its “offline” performance in aqueous solution nor in the solid dry state. The evaluation of suitable enzymes has to be performed through direct experimental test in the gas/solid reactor.

Zusammenfassung

Die Gas/Feststoff Biokatalyse ist ein umweltfreundliches Verfahren, bei dem ein festes trockenes Enzym die Umsetzung gasförmiger Substrate zu gasförmigen Produkten katalysiert. Diese Technologie findet Einsatz z.B. zur Herstellung flüchtiger Feinchemikalien, bei der Beseitigung der Luftverschmutzung und in elektrochemischen Biosensoren. Die Kontrolle thermodynamischer Parameter im Gas/Feststoff-Reaktor erlaubt die präzise Einstellung der Mikroumgebung des Enzyms. Allerdings werden Gas/Feststoff-Bioreaktoren bei erhöhter Temperatur betrieben, um eine hinreichende Flüchtigkeit der Substrate und Produkte zu bewirken, was trotz der Verwendung immobilisierter Enzyme zur progessiven Enzyminaktivierung führt. Bisher fehlten Untersuchungen zur Aufklärung der Schlüsselmechanismen der Enzyminaktivierung im Gas/Feststoff-Reaktor und geeignete Enzyme wurden durch Versuch und Irrtum ausgewählt. Um einen rationalen Zugang zu für die Gas/Feststoff-Biokatalyse geeigneten Enzyme zu ermöglichen, bedarf es detaillierter Kenntnisse der molekularen Effekte, die bei der Inaktivierung von festen Enzymen eine Rolle spielen. Deswegen ist die Untersuchung von Effekten, die die Stabilität trockener Enzyme beeinflüssen, besonders wichtig.

Im Rahmen der vorliegenden Arbeit wurde die Enzymstabilität sowohl in Abhängigkeit einzelner Parameter (z.B. pH, T) als auch im kompletten Reaktionssystem während der Gasphasenkatalyse mit Substrat-gekoppelter Kofaktorregenerierung charakterisiert. Das Ziel war, Faktoren, die die Betriebsstabilität im Gas/Feststoff Reaktor beeinflüssen, aufzuklären und, falls möglich, indikative Parameter zu identifizieren (z.B. Thermostabilität), mittels derer man die Betriebseigenschaften des Biokatalysators im Gas/Feststoff-Reaktor vorhersagen kann. Zwei Alkoholdehydrogenasen (ADH), die NADPH-abhängige ADH aus *Lactobacillus brevis* und ihre NADH-abhängige Variante *Lb*ADH G37D wurden als Modellenzyme benutzt. Beide unterscheiden sich lediglich in einem Aminosäureaustausch.

(i) Im ersten Teil dieser Arbeit wurde die Thermostabilität der Kofaktoren NAD(P)H untersucht, um deren Anteil am Inaktivierungsverhalten der festen ADHs im Gas/Feststoff-Reaktor zu bestimmen. Die Stabilitätsuntersuchungen zeigten, dass gelöstes NADH 3.5 - 5.5mal thermostabiler als der phosphorylierte Kofaktor NADPH ist. Im festen Zustand zeichnen sich hingegen beide Kofaktoren durch eine deutlich höhere Stabilität aus. Die thermische Degradation der Kofaktoren wurde unter anderem mittels HPLC-MS analysiert. Die Ergebnisse zeigen, dass beide Kofaktoren bei der thermischen Inaktivierung unterschiedliche Fragmentierungswege durchlaufen, die sich auch in Abhängigkeit von verfügbarem Wasser unterscheiden. In allen Fällen kommt es zur Fragmentierung des Nikotinamidrings und zur oxidativen Öffnung der Riboseringe.

(ii) Im zweiten Teil wird die vergleichende Untersuchung der Thermostabilität der beiden Enzyme *Lb*ADHwt und *Lb*ADH G37D in wässriger Lösung und im festen Zustand beschrieben. Bedingt durch die auftretende Aggregation der Enzyme verlief die thermische Inaktivierung bei beiden Enzymen im gelösten Zustand irreversibel. Dabei zeigte sich, dass die Variante *Lb*ADH G37D 3-9 mal thermostabiler als das Wildtyp-Enzym ist. Verantwortlich hierfür sind vermutlich strukturelle Effekte bedingt durch den Austausch G37D, der in einem *β-turn* in der Nähe der Kofaktor-bindenen Region liegt. Im festen Zustand zeigen beide Enzyme eine etwa um zwei Größenordnungen höhere Stabilität als in wässriger Lösung. Auch nivellieren sich die im gelösten Zustand beobachteten deutlichen Stabilitätsunterschiede zwischen beiden Enzymvarianten im festen Zustand; allerdings zeigte auch hier die Variante bei 40°C, der Betriebstemperatur des Gas/Feststoff-Reaktors, eine 10-20-fach höhere Thermostabilität. Strukturelle Änderungen wurden mittels verschiedener spektroskopischer Methoden, wie Tryptophanfluoreszenz, Circulardichoismus und statischer Lichtstreuung, verfolgt. Dabei waren die Strukturänderungen, die zur Enzyminaktivierung führen, in wässriger Lösung erwartungsgemäß deutlich ausgeprägter als im festen Zustand bei niedriger Wasseraktivität. Die Ergebnisse deuten auf unterschiedliche Enfaltungswege in der flüssigen und festen Phase hin.

(iii) Daher wurde im dritten Teil dieser Arbeit ein Hochdurchsatzscreening-Verfahren entwickelt, das die Durchmusterung von Enzymvarianten im festen und gelösten Zustand ermöglicht, um so neue optimierte Enzymvarianten für die Gas/Feststoff-Biokatalyse zu identifizieren. Aufgrund der höheren Stabilität und des niedrigeren Preises von NADH im Vergleich zu NADPH, wurde die NADH-abhängige Enzym-Variante *Lb*ADH G37D als Ausgangspunkt für eine Optimierung mittels Mutagenese gewählt. Dazu wurden thermolabile Bereiche in der Kristallstruktur der *Lb*ADH G37D mit dem „B-Fitter“ Verfahren identifiziert und der Sättigungs-mutagenese unterworfen. Die Aminosäure V42, E44 und K48 wurden gleichzeitig randomisiert, um alle möglichen kooperativen Effekte zu erfassen. So wurde eine fokussierte Mutanten-Bibliothek mit 6000 Varianten konstruiert.

Die Durchmusterung dieser Bibliothek führte zur Identifizierung einer Variante mit verbesserter Thermostabilität im festen Zustand, *Lb*ADH G37D/V42F/E44C/K48Q, die für die Gas/Feststoff-Biokatalyse potenziell vorteilhaft sein könnte. Zusätzlich zeigten vier weitere Varianten eine erhöhte Thermostabilität in wässriger Lösung.

(iv) Im letzten Teil der vorliegenden Arbeit wurde das Verhalten der *Lb*ADHwt und *Lb*ADH G37D im Gas/Feststoff-Reaktor untersucht. Als Testreaktion wurde die Reduktion von Acetophenon zu (*R*)-Phenylethanol gewählt, wobei der Redoxkofaktor durch die Zugabe von Isopropanol als zweitem Substrat regeneriert wurde. Im Gegensatz zu der 15-mal geringeren enzymatischen Aktivität der

*Lb*ADH G37D in wässriger Lösung bei pH 7.0, zeigte diese Variante eine unerwartet hohe spezifische Katalyseaktivität im Gasphasenreaktor auf. Die Thermostabilität im festen Zustand erwies sich als verlässliches Auswahlkriterium für die relative Stabilität im Gasphasenreaktor, wenn auch die weiteren Komponenten des Reaktionssystems, wie Substrataktivität und Wasseraktivität ebenfalls Einfluss auf die Betriebsstabilität haben. Für das untersuchte System kann die Stabilität der Kofaktoren vernachlässigt werden.

Als Fazit dieser Arbeit kann festgehalten werden, dass das Verhalten von Enzymen im Gas/Feststoff-Reaktor durch „offline“ Messungen in wässriger Lösung und auch in der festen Phase nur unzureichend vorhergesagt werden kann, da sich wesentliche kinetische- und Stabilitäts-Parameter drastisch ändern können und der Einfluss aller Komponenten im Reaktionssystem einkalkuliert werden muss. Jedoch kann die Thermostabilität der Enzyme im festen Zustand möglicherweise als indikativer Parameter für deren Eignung im Gas/Feststoff-Reaktor herangezogen werden. Dies erfordert noch weitere Untersuchungen.

Chapter 1
An introduction to enantioselective catalysis

1.1 Gas/solid biocatalysis

1.1.1 Industrial biocatalysis

Industrial biocatalysis represents a set of technologies utilizing biological systems for the synthesis of commodity and fine chemicals, pharmaceutical, agrochemicals and their building blocks [10]. Over the last 30 years, biocatalysis has become a fast developing field, and the number of its applications in organic synthesis has been significantly extended [11]. Both isolated enzymes and whole-cell microorganisms are widely exploited [10].

Historically, biocatalysis has been used in food processing for more than 8000 years. Based on empirical knowledge, entire microorganisms have been intensively implemented in fermentation of crops, fruits and milk to produce yogurt, cheese, bread, wine, beer and many more. The processes with cell-free enzymes were developed much later. Probably, the first example of the bioprocess with isolated enzyme was an application of the aspartic protease rennin, which was derived from a calf or a lamb stomach, to the cheese making. Rennin was the first commercially available biocatalyst (1914) [12]. An introduction of bacterial proteases into washing powders and the use of alpha-amylases and gluco-amylases for a strarch hydrolysis in 1960s fulfilled a breakthrough in a large-scale commercial application of enzymes [12]. The racemic resolution of amino acids using the acylase method started usage of biocatalysts in the industrial production of commodity and fine chemicals [13]. Since then, biocatalysis has developed into standard technology for the chemical synthesis [14]. More than 100 different biotransformations are already integrated into industrial processes [13, 14]. Examples include the preparation of semisynthetic penicillins using penicillin amidase [10, 15], hydration of acetonitrile into acrylamide by nitrile hydratase [10, 15], an efficient synthesis of the herbicide precursor *(S)*-methoxyisopropylamine with transaminase [10]. The predominantly used enzymes are hydrolases (44%) and oxidoreductases (30%) [14].

High □egion- and enantioselectivity of enzymes make them especially attractive for the bioorganic synthesis of chiral compounds [13]. Indeed, 89% of all the biocatalytically produced fine chemicals are chiral [14]. Both the kinetic resolution of racemic mixtures (mostly carried out by hydrolases) and the asymmetric synthesis (implemented by oxidoreductases and lyases) is broadly applied [14].

For a long time, application of biotransformation to the chemical synthesis had been limited by the general idea that biocatalysts (entire cells as well as cell-free enzymes) are exclusively active in aqueous environment under mild conditions [16]. Operation in aqueous solution, however, significantly lowers the range of applicable substrates and requires development of special methods for product recovery from the reaction medium [15]. Fortunately, many enzymes were found to function also in non-conventional media, such as water-free organic solvents, aqueous two-phase systems, ionic liquids, supercritical fluids, and gas/solid bioreactor [15, 16]. This finding had a huge impact on applicability of biocatalysis to the chemical manufacturing, providing access to bioconversions with poor water-soluble substrates and products, such as aliphatic, aromatic and heterocyclic compounds [15].

Nevertheless, the development of novel industrial applications is limited by enzyme instability under technical conditions [15]. Indeed, the presence of organic solvents, harsh operational conditions, such as extreme pH, high temperature and pressure, alter both activity and stability of biocatalysts [16]. As a result, biocatalytic processes often lack space-time yield, process mass intensity and catalytic efficiency [17], making the process feasibility questionable. To overcome these limitations, highly effective immobilization and stabilization methods based on physical, chemical and biological approaches have been developed [10]. Another alternative is the use of directed evolution and rational protein design for optimization of useful enzymes and creation of variants with improved properties [15, 17].

The recent advances in molecular biology, high-throughput screening methodology and instrumentation are widely used to fulfill this task [10, 15]. Moreover, ongoing research focuses on simultaneous evolving of multidimentional characteristics, such as activity, stability (pH, thermal, against organic components), and substrate scope. Therefore, the great potential of biocatalysis will be, probably, intensively exploited in industrial chemical synthesis [14, 15, 17].

1.1.2 Principles of gas/solid biocatalysis

Gas/solid biocatalysis is a novel perspective approach of non-conventional enzymology exploiting the ability of solid enzymes to catalyze reactions of gaseous substrates to gaseous products (Fig. 1-1). Technically, packed-bed type reactors filled with an immobilized, dehydrated biocatalyst are continuously percolated by a gas that delivers substrates and water (for defined water activity), and simultaneously allows the removal of the gaseous products from the reaction system [3, 18].

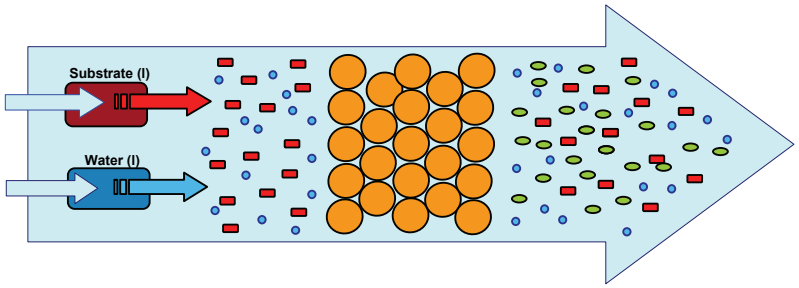

Figure 1-1. Schematic representation of the gas/solid biocatalysis. The carrier gas is represented by the light-blue arrow in the background, immobilized biocatalyst is shown as orange circles ●, substrate is depicted as a red rectangle ▬, product is symbolized by green ovals ●, and water vapour is represented by blue circles ◦.

In comparison to conventional biocatalysis, the gas/solid technology presents numerous advantages, such as:

(i) The immobilization of the enzyme and cofactor simplifies the technical process. Hereby, physical adsorption on a support material is sufficient. Alternatively, lyophilized enzyme powder can be used [19]. The use of lyophilized or immobilized biocatalyst allows the easy recycling of redox cofactors and the recovery of the biocatalyst after the conversion has been completed.

(ii) In many cases, the dehydrated enzyme is more stable than the dissolved aqueous preparations [6]. Therefore, the reactor can be operated at elevated temperatures and/or for longer times to improve product yields.

(iii) It is possible to modify the substrate specificity just by reducing water content in the system [20].

(iv) The constant removal of inhibitory products reduces the inactivation rate even more [3].

(v) Higher diffusion coefficients of substrates and products and effective mass transfer at the gas/solid interface ensure high conversion yields [3].

(vi) The low solubility of certain substrates and products in common aqueous systems can be easily overcome. Moreover, the addition of organic solvents can be avoided, thus, solvent toxicity effects are excluded and no undesired by-product formation can take place [3].

(vii) Low water availability and elevated operational temperatures ensure avoidance of microbial contamination [3, 21].

(viii) Downstream processing of products is simplified because no extraction and purification steps are necessary. The substrates and products can be separated by fractional condensation alone [4].

(ix) The circulation of gaseous phase makes the scale up process easier [1].

(x) A precise control of thermodynamic parameters (such as water activity, pressure, temperature etc.) allows the adjustment of enzyme micro-

environment, which in turn is important for studies of enzyme hydration or solvent influences [3, 22].

The main limitation of gas/solid biocatalysis is its restricted application to substrates and products with a relatively low boiling point. In spite of this limitation, many enzymes, such as alcohol oxidases [4, 5], cutinases [19, 23], lipases [19], esterases, alcohol dehydrogenases [7, 24-26], haloalkane dehalogenases [1, 27, 28], and carboligases have been used in gas/solid systems.

Moreover, from an academic perspective gas/solid biocatalysis opens new opportunities for fundamental research and allows the development of clean industrial technologies. It is already used in food industry for production of natural esters and aroma compounds [3, 9]. Additionally, the gas/solid systems are widely applied to the design of biosensors for bioanalytical determination of the ethanol, methanol or formaldehyde content in air [5, 21, 29]. Several other technologies are under development. For example, stereospecific alkylation, acylation or hydrolysis catalyzed by lipases can be utilized for resolution of racemic mixtures of acids, alcohols or esters [3]. Chiral reduction of ketones is interesting for the production of fine chemicals. Cost-beneficial and an environmental-friendly treatment of waste gases can be accomplished by haloalkane dehalogenases, alcohol oxidases and methane monooxygenases as well as by the use of dried cells of *Pseudomonas putida*, *Methylocistis trichsporium* and *Rhodococcus erythropolis* [3, 9, 30].

1.1.3 Activity and stability of enzymes in gas/solid reactors

1.1.3.1 Temperature

Enzymatic activity is highly dependent on the operational temperature employed in the gas/solid reactor. In gas/solid system with no mass transfer limitations the initial reaction rate exponentially increases with heating until thermal deactivation becomes significant [4, 25, 28]. This dependence is described by the Arrhenius law:

$$k = Ae^{-E_a / RT} \quad (1\text{-}1)$$

where

- k is the rate constant of a chemical reaction in s^{-1};
- A is the specific pre-exponential factor;
- R is the universal gas constant equal to 8.31 J K^{-1} mol^{-1} ;
- T is the absolute temperature in K.

Although dry enzymes are significantly more stable than dissolved ones, thermal inactivation under operational conditions takes place [25, 28]. For enzymes in aqueous solution several molecular mechanisms that influence thermostability

have been suggested (see section 1.4 for details). However, up to now, the mechanisms leading to enzyme inactivation in the solid state remain not fully investigated. Moreover, the flammable nature of some compounds (i.e. substrates or products) represents an additional challenge for the gas/solid system, and needs to be taken into account [27].

1.1.3.2 Influence of water

Water activity (a_w) is considered to be a key parameter in gas/solid catalysis [18]. It is defined as the ratio of the partial pressure of water in the system over the vapour pressure of pure water at the same temperature.

$$A_w = \frac{P}{Po} = \frac{RH}{100\%} \qquad (1\text{-}2)$$

where:

- P is the equilibrium partial pressure of water in the system in Pa,
- Po represents saturation vapour pressure of water in Pa,
- RH stays for relative humidity in %.

Early studies performed on enzyme-substrate powders, as well as later gas/solid reactor experiments performed with alcohol dehydrogenases [7, 31, 32], haloalkane dehaloganases [27] and carboligases [26] revealed the existence of a critical a_w level. Enzymatic activity could not be detected below the minimal required a_w, and the increase of a_w above this point drastically accelerated the reaction rates [7, 26, 31]. However, no critical a_w value was observed in transesterification reactions, i.e. the porcine pancreatic lipase exhibited enzymatic activity at a_w close to 0 (even after drying over P_2O_5) [19]. The cutinase from *Fusarium solani* also displayed enzyme activity at an a_w equal to zero [19, 23]. Lipase B from *Candida antarctica* (CalB) shows maximum activity at an a_w equal to 0, with decreasing reaction rates at higher a_w.

Studies performed using the gas/solid system demonstrated a great influence of a_w on both activity and thermostability of a biocatalyst. Usually, the increase of a_w leads to significant acceleration of gas/solid reactions accompanied by a decrease of the enzyme thermostability [4, 7, 18, 19, 23, 26, 27, 31]. Often, an optimal a_w is observed and the enzymatic activity continuously increases with increasing a_w until optimal a_w value is reached. Futher increase of a_w often leads to a rapid loss of activity due to fast thermal degradation processes [23, 26, 32] and/or mass transfer limitations caused by enzyme agglomeration [19].

Moreover, the variation of a_w in the gas/solid reactor influences the content of surface-bound water molecules. Solid protein placed in a gaseous environment containing water at a certain thermodynamic activity adsorbs water molecules until the system is equilibrated. Enzyme hydration plotted against the a_w of the system results in a characteristic curve (also known as water adsorption isotherm), that is common for many proteins (Fig. 1-2) [22].

A gas/solid reactor represents a multicomponent system, often containing in the gaseous phase several substrates, products, and sometimes additives. Each of these components can compete with water for adsorption at the protein surface. Therefore, the features of water adsorption isotherms may greatly vary depending on thermodynamic activities [3] and the surface area of the enzyme [22]. Usually, point B in Fig. 1-2 corresponds to optimal a_w value [23].

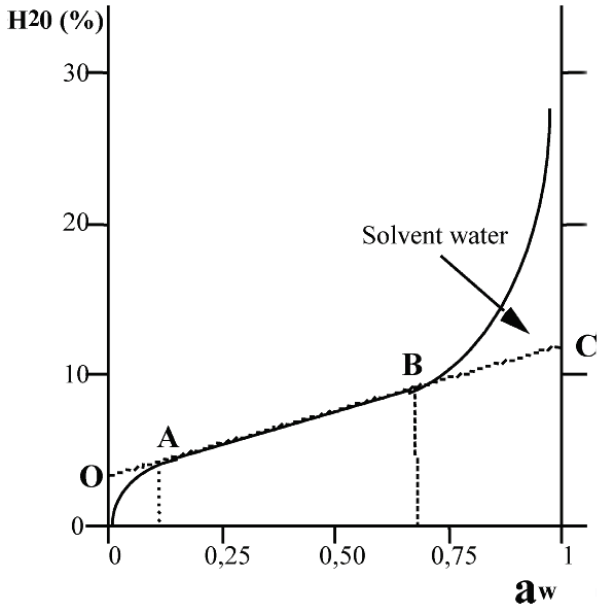

Figure 1-2. Isoterm adsorption curve (reprinted from Drapron 1985). (i) Point O represents tightly bound water molecules, buried in the structure. Segment O to A corresponds to highly structured water interacting with ionic and polar groups at the protein surface. (ii) Between point A and B the hydration layer is formed. In this region water content linearly increases with increasing a_w. (iii) At the point B free water appears at the protein surface. At a higher a_w water molecules not interacting with the protein surface condense on it and complete the hydration process. Point C gives the total quantity of non solvent water [3].

A_w apparently influences the substrate affinity in hydrolysis reactions. So, cutinase from *Fusarium solani* showed significant activity towards polar substrates at low a_w, whereas high values of a_w led to a preference of apolar compounds [30]. The effect was explained by the limited availability of water molecules bound to the polar residues in the active site at low a_w, which was partially overcome by interaction with polar substrates [30].

For CalB a drastic effect of a_w on the enantioselectivity towards enantiomers of secondary alcohols has been demonstrated [20, 33, 34]. A_w below 0.2 increased the enantioselectivity, of the reaction, whereas higher a_w values promoted its decrease. Molecular modeling studies suggested that at low a_w values water molecules can bind to polar residues in the substrate pocket of CalB. This results in a size reduction of the substrate pocket, thus acting as enantioselective inhibitors [33]. Above a_w 0.2, water mostly served as “solvent” with high inpact on

the intrinsic flexibility. Therefore, the a_w turning point 0.2 most probably corresponds to the full coverage of all polar groups by water in the substrate binding pocket [33].

1.1.3.3 Thermodynamic activity of substrates

The kinetics in gas/solid reactors often follows the Michaelis-Menten model [4]. The apparent Michaelis constant in the gas/solid system, however, is significantly lower than in aqueous solution [4, 35]. This effect relates to the differences in energy for substrate binding and product release in the liquid and solid state as well as to the influence of the solvent molecules [35].

Several cases of substrate inhibition have been demonstrated in experiments with increasing thermodynamic activities of substrates. In particular, acetic acid vapors irreversibly denatured porcine pancreatic lipase in transesterification reactions [2]. Inhibitory effect of gaseous propanol, 2-methyl-2-butanol, 2-methyl-2-pentanol and water on CalB was demonstrated by Letisse *et al*. [35, 36]. Remarkably, the inhibitory action of the alcohols became more pronounced after addition of non-reacting compounds to the gas phase, such as 2-hexane [35] or different ketones [36]. According to molecular simulation results, these chemicals might promote the dissociation of the alcohols from the active site, by competitive replacement and dead-end complex formation which in turn prevents the reaction to proceed [36]. Thiamine-diphosphate dependent enzymes like benzaldehyde lyase from *Pseudomonas fluorescens* (BAL) and benzoylformate decarboxilase from *Pseudomonas putida* (BFD), which were previously used for propioin synthesis in a gas/solid reactor system, were inhibited by high thermodynamic activities of propanal. Notably, BAL displayed a strong decrease of its half-life with increase of thermodynamic activity of propanal. In contrast, BFD showed a higher stability under the same conditions [26].

On the other hand, substrate activation effects could be observed as well. For example, various alcohols, which served as substrates in transesterification reactions, activated cutinase from *Fusarium solani* at low a_w values. After a_w was increased, the substrate activation effect was minimized. Therefore, the authors suggested that the alcohols might be able to take over the role of water and act as plasticizers, thus favoring flexibility of the enzyme [30, 37] which in turn results in the observed substrate activation.

1.1.3.4 Enzyme preparation

Principally, the use of simple lyophilized enzymes powders in the gas/solid system is possible [19, 27], but may cause mass transfer limitations. Additionally, free enzymes i.e. presented as lyophilized powder in the system, are noticeably less stable than the immobilized ones [18, 38]. Therefore, immobilization of enzyme on

a carrier support is commonly used. Usually, either physical absorption on a porous carrier or covalent linkage is employed. Significant differences in performance in gas/solid reactor systems were observed for crude extracts and the corresponding purified enzymes immobilized on a support [31, 39].
Because catalytic activity of an enzyme depends on its ionization state, which is stimulated by the last aqueous pH to which the enzyme was exposed prior to immobilization, a phenomenon know as “pH memory effect” is frequently observed in gas/solid systems [27, 28, 38, 40].
In principle, a biocatalyst deposited on a solid support behaves similar to a free enzyme. Its enzymatic activity is strongly dependent on the hydration level, with optimal a_w coinciding with point B on the water adsorption isotherm [23] (see Fig. 1-2). Immobilization, however, strongly affects the shape of water adsorption curve, which results in a different performance in the gas/solid reactor. Usually, point B, and, therefore, optimal a_w values, are between 0.4 and 0.5 for lyophilized enzyme powders and between 0.6 and 0.7 for the respective physically adsorbed enzymes [23]. On the contrary, covalently immobilized enzymes, never showed any optimum concerning water content [23]. Thus, point B of the water adsorption isotherm was not reached. Therefore, enzymatic activity increased linearly with increasing a_w, and thermal denaturation was either not observed [23] or is very slow [38]. In spite of significant improvement of enzyme stability, deposited biocatalysts can degrade under the gas/solid reactor conditions [7, 23, 31]. Nevertheless, deposition processes are widely used due to their simplicity. The techniques have been significantly optimized with respect to material choice, use of additives and the immobilization procedure itself [7, 31, 39, 41]. Considering the cost, the physical adsorption method is the method of choice in many cases.

1.1.4 State of the art of gas/solid biotransformations with isolated enzymes and whole cells

1.1.4.1 Hydrogenases

The first gas/solid biotransformation was demonstrated in 1969 by Yagi *et al*. [42]. The authors found, that purified hydrogenase from *Desulfovibrio desulfuricans* in its solid state bound hydrogen molecule and aligned the spins of the both in the same direction, which resulted into convertion of gaseous *para*-hydrogen to *ortho*-hydrogen. Additionally, exchanges between hydrogen isotopes were detected [42]. These observations were explained by the presence of protons in the dry hydrogenase molecule, which are directly exchangeable with H_2 during a catalytic process [42, 43]. In 1979 Kimura *et al.* found out, that the dry enzyme catalyzed reversible oxidoreduction of the electron carrier cytochrome C3 with molecular hydrogen [43].

1.1.4.2 Alcohol oxidases

A purified alcohol oxidase from *Pichia pastoris* was intensively studied in batch gas/solid reactor. Dehydrated enzyme adsorbed on DEAE-cellulose or glass beads was shown to effectively oxidize methanol and ethanol vapors at 5-70°C [4, 5]. Since oxygen-mediated oxidation was found to be the main reason for the inactivation of the enzyme, co-immobilization with enzymes decomposing H_2O_2 (catalase or peroxidase) significantly prolonged its half-life [5]. Water activity greatly affected thermostability of the alcohol oxidase and as well as the rate of conversion [4].

1.1.4.3 Lipolytic enzymes

Lipases and cutinases are enzymes catalyzing the hydrolysis of esters and the reverse reaction in so-called transesterifications. These enzymes are intensively used in biotechnology because of their high regio-, chemo- and enantioselectivity, broad substrate spectrum, and significant activity and stability in non-conventional media.

Cutinase from *Fusarium solani* was successfully employed in gas/solid reaction systems for both transesterification [19, 23, 30, 37] and hydrolysis reactions [30, 37] of volatile components. Free lyophilized, deposited as well as covalently immobilized enzyme preparations were used to catalyze several transesterification reactions, whereas the lyophilized enzyme was found to form large clumps or agglomerates [30]. For those systems a strong dependence of the reaction rate and substrate affinity on a_w and temperature was demonstrated [30, 37]. Local hydration of the substrate pocket and cooperative binding of water and substrate molecules were suggested to be essential for the affinity towards polar or apolar substrates [30, 37] CalB was used for enantioselective acylation of *(R)*-2-pentanol in a gas/solid reactor at 45°C [34]. Although CalB showed some activity even at a_w 0.02, a pronounced effect of the water content on the enzyme activity and enantioselectivity was observed. The reaction rate drastically increased with increase of a_w from 0.02 to 0.1. At higher a_w values, however, water acted as competitive inhibitor and promoted hydrolysis, which resulted in a decrease of the transesterification rate [20, 33]. Interestingly, tightly bound water molecules in the stereospecific substrate pocket of CalB significantly affected its enantioselectivity towards enantiomers of secondary alcohols, which varied with variation of a_w [20, 33] (*vide supra*).

1.1.4.4 Thiamine-diphosphate dependent lyases

Thiamine-diphosphate (ThDP) dependent enzymes are able to catalyze the ligation of aldehydes and ketones to chiral 2-hydroxy ketones in a carboligation reaction and, *vice versa,* catalyze the cleavage of carbon-carbon bonds, e.g. in

decarboxylation reactions. The feasibility of gas/solid biocatalysis empoying benzaldehyde lyase from *Pseudomonas fluorescens* (BAL) and benzoylformate decarboxylase from *Pseudomonas putida* (BFD) was demonstrated in studies of Mikolajek *et al*. [26]. Ligation of two propanal molecules to propioin at 40°C was used as a model reaction. In spite of similar tertiary structure and common catalytic mechanisms, both enzymes behaved differently in the gas/solid reactor system. BAL did not show any detectable activity below a critical a_w of 0.4 [26]. Above this point, the reaction rate increased exponentially until a_w reached 1.0 [26]. BFD, in contrast, displayed catalytic activity already at a_w 0.1 (at 40°C). The initial reaction rate grew with variation of a_w from 0.1 to 0.5, and distinctly decreased at higher a_w values [26]. Both enzymes were prone to substrate inhibition. However, the effect on BAL was more pronounced [26]. Unexpected results were obtained by comparatively investigating the thermostability of BAL and BFD in the gas/solid reactor system. In contrast to all previous studies performed with other enzymes, the half-life of both enzymes at 40°C increased with increasing a_w values and reached a maximum at a_w of about 0.8 and 0.9 for BFD and BAL, respectively [26].
The ability of BAL and BFD to catalyze a stereospecific ligation of two benzaldehyde molecules into (*R*)-benzoin was investigated using a similar setup. Indeed, using BAL benzoin was produced in the gas/solid reactor [44]. However, online detection of benzoin was impaired due to its poor volatility [44].

1.1.4.5 Haloalkane dehalogenases

Haloalkane dehalogenases catalyze the hydrolytic cleavage between a primary carbon atom and the halogen atom in aliphatic haloalkanes to the corresponding alcohol and halide ion. No cofactors or oxygen are needed for this reaction.
Because of the widespread contamination of the environment with haloalkanes i.e. from pesticides and herbicides, the application of these enzymes in bioremediation of industrial pollution is under intensive investigation [27, 38, 40, 45].
The haloalkane dehalogenase from *Rhodococcus rhodochlorus* is active towards aliphatic halogenated hydrocarbons. The enzyme prefers smaller substrates (C_2-C_4) over larger ones (C_4-C_8) [27]. Studies performed on lyophilized enzyme powders revealed a significant pH memory effect and a strong dependence on the water content. The critical a_w of approximately 0.1 (at 30°C) was demonstrated, with the enzymatic activity linearly increased with futher increase of a_w [27]. Covalent immobilization on alumina impregnated with polyethyleneimine enhanced both the chemical and thermal stability of the haloalkane dehalogenase [38]. Interestingly, addition of volatile triethylamine to the system increased the reaction rate by an order of magnitude [27]. Most probably, triethylamine scavenged the chloride ions produced during the reaction [40], and therefore prevented enzyme inhibition.

Haloalkane dehalogenase from *Rhodococcus erythropolis* is known to show a broad substrate range [28]. Its ability to convert halogenated compounds in gas/solid system was proven by using lyophilized lysed cells of *R. erythropolis* as a solid phase [28, 40]. In contrast to conventional catalysis, where preference of short chain substrates was demonstrated, the conversion rates in the gas/solid reactor increased with increasing chain-length of the halogenated substrate [28]. A critical a_w value of 0.4 (at 40°C) was necessary for the enzyme to become active, whereas the optimal a_w in this system was found to be at around 0.9. Increase of operational temperature caused increase of enzymatic activity but lowered the half-life time of the biocatalyst; thus 40°C was chosen as a compromise [28, 40]. Loss of stability, however, was apparently not due to thermal degradation of the enzyme, but rather related to an accumulation of chloride ions produced during the reaction [28]. Similar to the haloalkane dehalogenase from *Rhodococcus rhodochlorus*, addition of volatile triethylamine to the gas phase was found to be beneficial [28, 40].

1.1.4.6 Alcohol dehydrogenases

Alcohol dehydrogenases (ADHs) catalyze the oxidation of alcohols to the corresponding aldehydes and ketones using (phosphorylated) nicotinamide dinucleotide ($NAD(P)^+$) as a cofactor. Depending on the reaction conditions, these enzymes usually also catalyze the reduction of carbonyl compounds to chiral alcohols [46], which makes this enzyme class especially attractive for the biotechological production of flavor aldehydes and chiral secondary alcohols [47].

The gas/solid reactor setup used to test the performance of ADHs is more complicated than with other enzymes. This relates to the fact that all ADHs require stoichiometric amounts of cofactors to perform the desired reaction. Thus, the cofactor has to be co-immobilized with the enzyme and needs to be constantly regenerated during the reaction. Usually, this is achieved by the same ADH by comcomitant oxidation or reduction of a second substrate (see section 1.3 for more details). Nevertheless, also for ADHs, the gas/solid reaction system overcomes many limitations which are present for ADH-dependent processes carried out in conventional reaction media, such as low solubility of substrates, instability of the enzyme, product inhibition etc. [24].

Therefore, the experiments in the gas/solid reactor were performed with many ADHs, such as horse liver ADH (*HL*ADH), baker's yeast ADH (*Y*ADH), ADHs from the thermophilic organisms *Sulfolobus solfactaricus* (*Ss*ADH) and *Thermo-anaerobacter* sp. (ADH *T*), psychophilic ADH from *Flavobacterium frigidimaris* (*Ff*ADH) and mesophilic ADH from *Lactobacillus brevis* (*Lb*ADH). Unfortunately, all these studies were performed under widely different conditions. In particular, substrates, temperatures, purity of enzymes, flow rates as well as the employed enzyme immobilization methods varied, thus making a direct comparison of the

data difficult. Table 1-1 provides an overview over the studies performed on ADHs in gas/solid reactions.

Yang and Russel studied the activity of lyophilized *Y*ADH in a continous gas/solid reactor using the oxidation of 3-methyl-2-butel-1-ol as a model reaction. The enzyme behaved “classically”: the relationship between initial reaction rates and substrate concentrations followed the Michaelis-Menten equation; the effect of temperature on the enzyme activity could be described by the Arrhenius equation [6]. Conversion curves, detected at 22-50°C and a_w of 1.0, displayed a steady-state period of 4-16 days followed by an activity decay period [6]. The critical hydration level of 0.16 g_{water} g_{enzyme}^{-1}, which corresponded to a critical a_w 0.11 at 40°C, was required to activate *Y*ADH [6]. Investigation of *Y*ADH thermostability revealed that a temperature-independent critical hydration level of 0.16 g_{water} g_{enzyme}^{-1}, the same as for enzyme activation, was necessary to stabilize dry *Y*ADH in the gas/solid reactor. This level corresponded to 46% surface coverage of the protein [6]. Beyond the critical water content, stability of *Y*ADH gradually decreased with increase of temperature or/and hydration [6].

Covalently immobilized dry *HL*ADH and *Ss*ADH were comparatively investigated by Pulvin *et al*. [48]. Both enzymes were able to catalyze the oxidation of butanol, pentanol and hexanol in a gas/solid reactor at 60°C. The simultaneous reduction of acetaldehyde served for regeneration of the co-immobilized cofactor NAD^+. Similar to *Y*ADH, steady-state and decay periods were observed. The steady-state period of *HL*ADH activity lasted for approximately 24 h, whereas *Ss*ADH was stable for 48 h [48].

Comparative studies of the $NADP^+$-dependent *Lb*ADH and ADH *T* were conducted by Trivedi et al. [25, 31]. Crude extracts of *E. coli* cells with recombinantly expressed *Lb*ADH or ADH *T* were deposited on porous glass beads and used in the gas/solid reactor. Acetophenone conversion, performed at 60°C, was used as a model reaction. A critical a_w 0.3 had to be maintained to activate both *Lb*ADH and ADH *T*. At higher a_w values initial reaction rates rapidly increased, accompanied by simultaneous decrease of the half-life of the immobilized ADHs [25]. The influence of temperature both on immobilized *Lb*ADH and immobilized ADH *T* followed a similar trend: the initial reaction rate exponentially grew with increasing temperatures, while the half-life followed an exponential decay. A Arrhenius-like temperature dependence of the reaction rate constants and the deactivation rate constants was observed [25]. Surprisingly, the thermostability of the mesophilic *Lb*ADH was higher than that of the thermophilic ADH *T* under the gas/solid reactor conditions [25].

The performance of NAD^+-dependent *Ff*ADH in the gas/solid system was investigated by Ullish [49]. Crude extracts of recombinant *E. coli* cells were deposited on porous glass beads and used for the experiments. Oxidation of 2-butanol as well as reduction of 2-butanone were examined at 40°C. A_w had a strong influence on reaction rate and on the half-life of immobilized *Ff*ADH.

Enzymatic activity linearly grew with increase of a_w from 0.4 to 0.9. Half-life linearly rose till an optimal a_w of 0.7 was reached, and rapidly decayed at higher a_w [49]. In this respect, *Ff*ADH behaved similar to the BFD, as reported by Mikolajek *et al*. [26]. Investigations of enantioselectivity elucidated that a_w had no significant influence on the achieved enantiomeric excess. However, increasing thermodynamic activity of 2-butanone decreased the *ee* values by about 20 % [26].

Table 1-1. ADHs in gas/solid biocatalysis.

Protein	Substrate	Cosubstrate	Reference
*Y*ADH	3-Methyl-2-buten-1-ol	Acetone	[6]
*Ss*ADH	1-Butanol	Acetaldehyde	[48]
	1-Pentanol		
	1-Hexanol		
*HL*ADH	1-Butanol	Acetaldehyde	[48]
	1-Pentanol		
	1-Hexanol		
*Ff*ADH	2-Butanone	Isopropanol	[49]
	2-Butanol	Acetone	
ADH *T*	Acetophenone	Isopropanol	[25]
*Lb*ADH	Acetophenone	Isopropanol	[25]

1.1.4.7 Whole cells

Commonly, a whole cell approach is intensively used in gas/solid biocatalysis. Dried cells of many different microorganisms were successfully applied for the treatment of contaminated air effluents. For example, immobilized dried *Methylocistis trichsporium* cells were able to decompose trichloroethylene in a gas/solid bioreactor with 80-90% efficiency [50]. Biofilters packed with dry *Pseudomonas putida* cells continuously removed phenol from waste gases [51, 52]. Lyophilized cells of *Rhodococcus erythropolis* and *Xanthobacter autotrophicus*, and later recombinant *E. coli* BL21 (DE3) cells expressing haloalkane dehalogenase from *Rhodococcus erythropolis* directly converted 1-chlorobutane to 1-butanol and HCl in a gas/solid reactor [1, 28, 40]. Continuous reduction of aldehydes and ketones with simultaneous regeneration of NADH was enabled by dried cells of *S. cerevisiae* [32].

All the whole cell systems that were studied so far, showed several characteristic features. Firstly, the dependence of conversion on the total flow rate. Erable *et al*. reported that the initial rate of 1-butanol formation by lyophilized cells of *R. erythropolis* increased with decreasing of the total flow. Probably, longer residence time of the substrate in the bioreactor made the difference [28]. Secondly, the cellular matrix apparently caused a different partitioning of water in the system. Therefore, a higher critical a_w was required to promote catalytic activity of

immobilized cells in comparison to the corresponding pure enzyme preparations. So, whole baker's yeast cells, investigated in a gas/solid reactor at 65°C using a hexanal reduction model, became active at an a_w of 0.4 [53]. Under the same conditions, pure *Y*ADH needed an a_w of 0.1 to display catalytic properties [6, 53]. Another example was reported by Dravis *et al*. Here, a critical a_w value of 0.4 was necessary for the *R. erythropolis* cells to show catalytic properties, whereas the pure dehalogenase remained active even at a_w as low as 0.1 [27].
Whole cells appear to be attractive candidates for gas/solid biocatalysis. A tempting option for the future would be to realize multistep reaction cascades within the cells. It is known, that degradation of trichloroethylene by lyophilized cells of *Methylosinus trichosporium* in a gas/solid biofilter proceeds through sequential action of methane monooxygenase and other dehydrogenases, thus several enzymatic systems might be involved in the decontamination process [3]. However, fundamental studies and a separate characterization of each component are still missing. Therefore, more fundamental research is necessary for futher development in this direction [3].

1.2 Alcohol dehydrogenases

1.2.1 Classification

Alcohol dehydrogenases (EC 1.1.1.1) are enzymes, which catalyze the inter-conversion between alcohols and the corresponding aldehydes and ketones. These enzymes require $NAD(P)^+$ as cofactor for their activity. The general reaction mechanism is depicted in Fig. 1-3. ADHs are widely distributed in all three kingdoms of life [54].

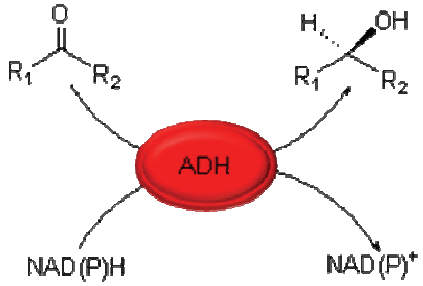

Figure 1-3. ADH catalyzed reaction. ADHs catalyze the interconversion between alcohols and the corresponding aldehydes and ketones with a simultaneous utilization of the cofactor $NAD(P)^+$ or NAD(P)H.

ADHs can generally be subdivided into three distinct classes: (i) short chain dehydrogenases/reductases (SDR), (ii) medium chain dehydrogenases/reductases (MDR) and (iii) iron-activated long chain dehydrogenases/reductases. MDRs

consist of about ~350 residues per subunit and are Zn^{2+}-dependent. They form dimers (in higher eukaryotes) or tetramers (in bacteria) [55]. SDRs have approximately 250 residues per chain, and rarely contain metals. Usually they possess a tetrameric quarternary structure [55]. LDRs consist of over 385 amino acids per subunit, sometimes as many as 900. Enzymes of this class can be activated not only by Fe^{2+}, but by a range of divalent cations. They display little sequence homology to SDRs and MDRs. Table 1-2 summarizes the main characteristics of these three groups [56, 57].

Table 1-2. Basic characteristics of ADH classes [54-56].

Feature	SDR	MDR	LDR
Amino acids pro unit	~250	~350	~385
Quarternary structure	dimer or tetramer	tetramer	dimer
Metal requirement	seldom, Mg^{2+}	often, Zn^{2+}	always Fe^{2+}
Cofactor	NAD^+ or $NADP^+$	NAD^+ or $NADP^+$	NAD^+
Cofactor binding motive	GxxxGxG	GxGxxG	GxGxxG

1.2.2 Short-chain ADHs

SDRs form a large and diverse protein family, which contains more than 2000 members. Despite their low sequence homology (15-30%), the members share s high degree of structural similarity [58]. The most SDRs possess a one-domain architecture with the highly variable C-terminal region containing a substrate binding site, and the N-terminal region binding the nucleotide cofactor, and the second one containing the substrate binding site. The latter domain determines the substrate specificity and contains amino acids involved in catalysis. The cofactor binding domain is located at the amino terminus of the protein. It contains a structural motif called Rossmann fold [59]. This motif consists of three or more parallel β-strands linked by two α-helices in the order –βαβα- and contains a highly conserved GxxxGxG sequence motif [60]. In this fold parallel β–sheets are sandwiched between two arrays of parallel α-helices (Fig.1-6A) [60]. Generally, SDRs contain a conserved charged residue (aspartic acid or arginine) located in a loop between the βB-sheet and αC-helix approximately 20 residues downstream of the Gly-rich motif of the Rossmann fold (Fig.1-4). This residue is found to be involved in stabilization of adenine moiety of the cofactor [61].

SDRs can use either NAD^+ or $NADP^+$. Since the intracellular ratio of NADPH to $NADP^+$ is generally high, and the ratio of NADH to NAD^+ is low, it is assumed, that NADP-dependent SDRs have evolved as reductases, whereas NAD-dependent SDRs are preferably oxidases. The cofactor preference of a SDR is assumed to be specified by amino acid residues in the cofactor binding region. The basic residue

in the loop between βB and αC (Arg38 of *Lb*ADH) is responsible for NADP preference, whereas presence of Asp in this loop leads to preference of NAD [8]. The role of these residues was confirmed by site-directed mutagenesis studies [8, 62].

A catalytic triad, which consists of a serine, a tyrosine and a lysine, is often located in the loop between βE and αF (Fig. 1-4) [61]. Additionally, a highly conserved asparagine located in the helix αE is involved in catalysis [58, 63]. This residue promotes the formation of the proton relay necessary for the catalysis [58].

Most SDRs are homodimers or homotetramers. Coupling between two monomers is accomplished through a four-helix bundle, which is composed of two parallel α-helices from each subunit. Dimers can interact with each other via the C-terminal parts [59].

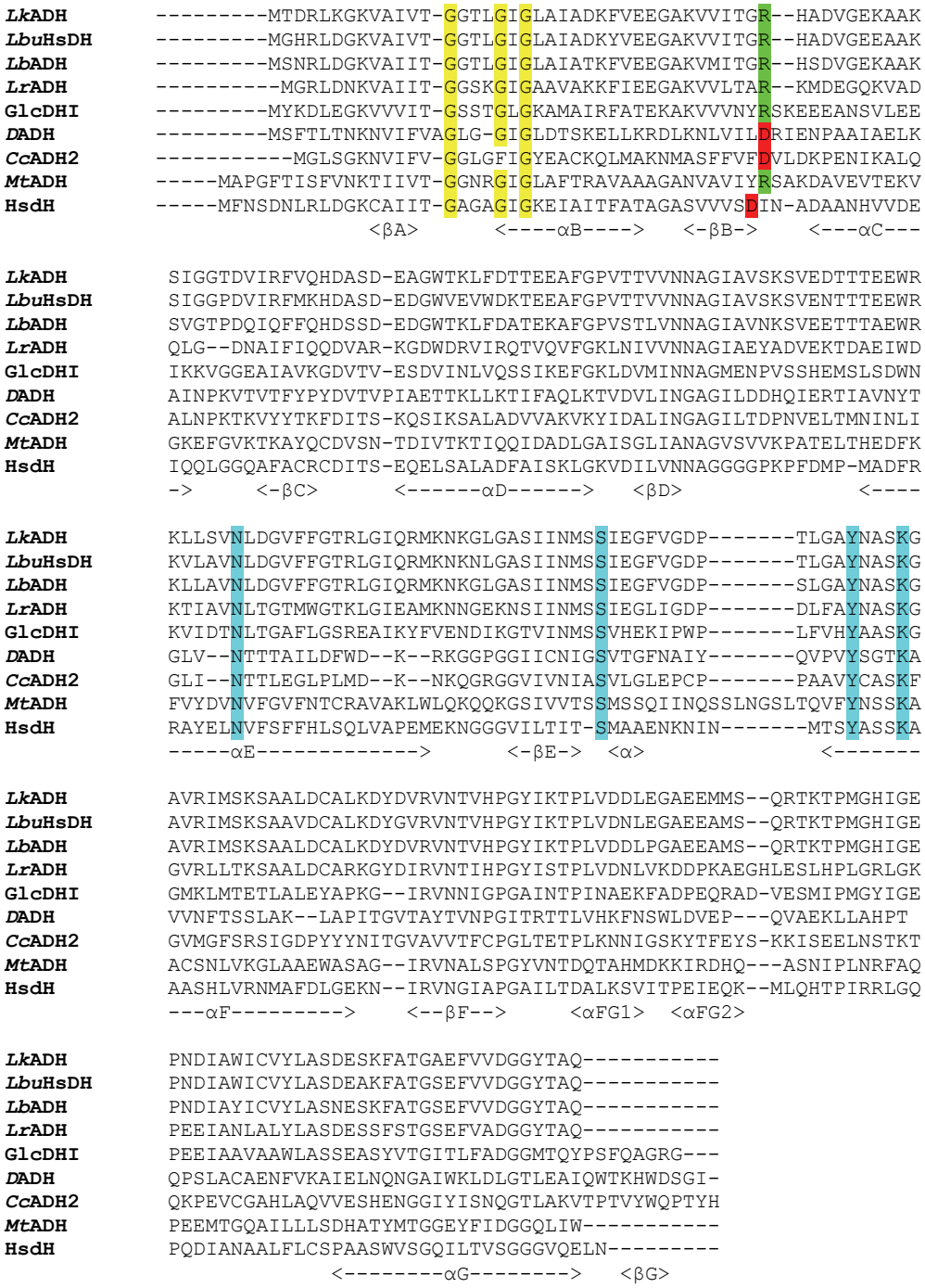

Figure 1-4. Multiple sequence aligment of several SDR enzymes. Nicotinamide nucleotide recognition pattern is marked with yellow, NADP-specifying N residue with green, NAD-specifying D with red, and catalytic triad with cyan. Structure-based sequence alignment was prepared with T-coffee [64]. The following proteins were aligned: *Lk*ADH, ADH from *Lactobacillus kefir*; *Lbu*HsDH, 3α-hydroxysteroid DH from *Lactobacillus buchneri*; *Lb*ADH from *Lactobacillus brevis*; *Lr*ADH, ADH from *Lactobacillus reuteri*; GlcDHI, glucose DH 1 from *Bacillus megaterium*; *D*ADH, ADH from *Drosophila melanogaster*; *Cc*ADH$_2$, ADH2 from *Ceratitis capatita; MtDH*, mannitol DH from *Agaricus bisporus*; HsdH, 7α-hydroxysteroid DH from *Escherichia coli*.

According to the literature, all SDRs share a common catalytic mechanism, which is of sequential nature [65, 66] (Fig. 1-5):

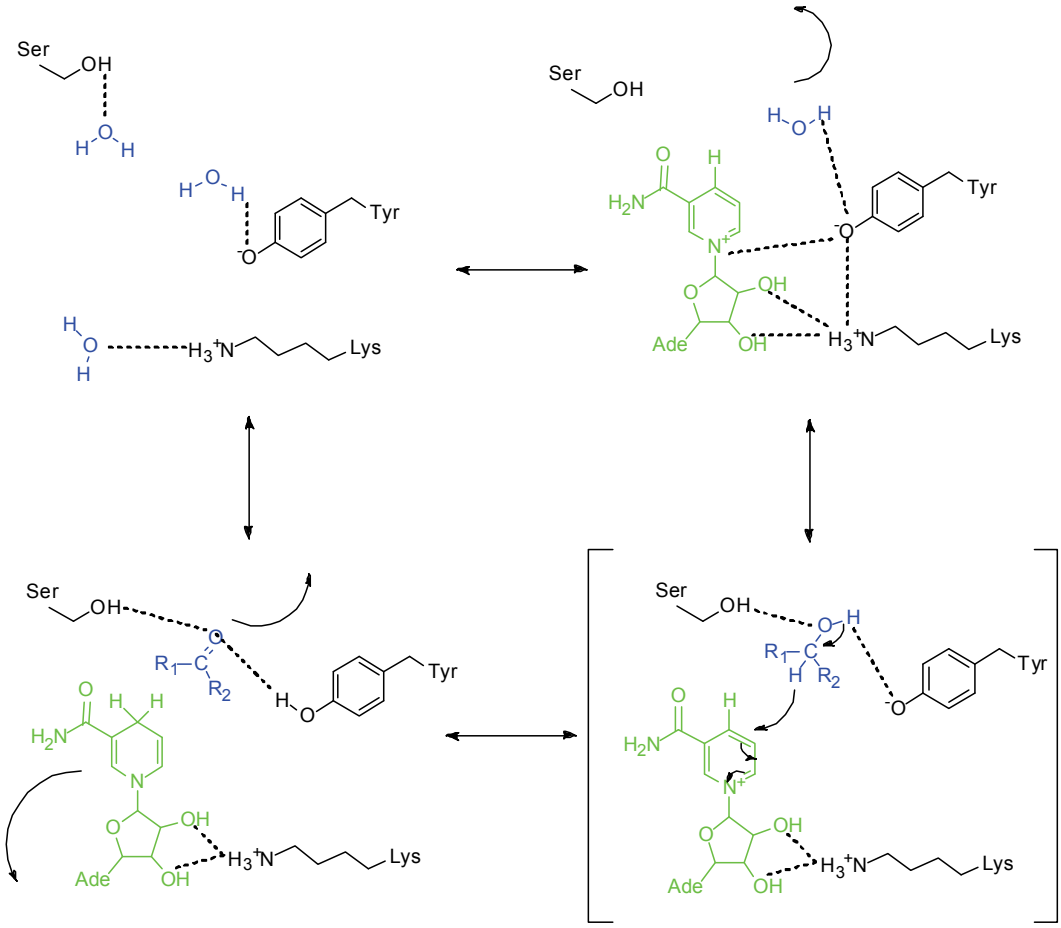

Figure 1-5. Proposed catalytic reaction mechanism of SDRs. (A) Apo state: three water molecules hydrogen-bonded to the catalytic triad. (B) Binary state: NAD^+ at the active site and one water molecule hydrogen-bonded to the catalytic triad. (C) Ternary state: binding of alcohol, proton transfer and hydride transfer. (D) Ternary state: ketone and NADH at the active site. (According to Benach *et al*. [66]).

(i) **Apo state** of the SDRs represents the "free state", where neither the cofactor nor the substrate molecules are bound to the enzyme. The loop regions are relaxed. The catalytic triad residues form hydrogen bonds to three water molecules.

(ii) **Binary state** formation starts with the binding of the cofactor $NAD(P)^+$ to the enzyme, which induces a large conformational change in the protein [65, 66]. The substrate-binding loop and the C-terminus drastically change their conformation bringing the catalytic triad residues into close proximity resulting in an optimization of the active site geometry [65]. One water molecule stays bound to the catalytic triad [66].

(iii) Transition from the binary to the **ternary state** occurs after binding of the substrate. The substrate-binding loop becomes less flexible and shields the

active center from the solvent [65, 66]. The last water molecule leaves the catalytic center.

(iv) The deprotonated phenolic group of the tyrosine residue and the hydroxyl group of the substrate form a hydrogen bond. The hydroxyl group of the catalytic serine also contributes to the stabilization of the substrate in the active site by hydrogen bonding. The lysine lowers the pKa value of the tyrosine through strong electrostatic interaction and orients the nicotinamide nucleotide moiety of the cofactor by forming a bifurcated hydrogen bond to the 2' and 3'-hydroxyl groups of the ribose moiety. An asparagin residue, located close to the active site, plays an important role in stabilizing the position of the catalytic lysine via a conserved water molecule, extending the previously recognised catalytic triad to form a tetrad of Asn-Ser-Tyr-Lys [65] (Filling et al. 2002).

(v) The tyrosine extracts a hydride ion from the substrate and transfers it to $NAD(P)^+$, thus the substrate is oxidized, and in turn the cofactor reduced.

(vi) Finally, the ketone and NADH leave the active site.

1.2.3 ADH from *Lactobacillus brevis*

The alcohol dehydrogenase from *Lactobacillus brevis* (*Lb*ADH) catalyzes the reversible reduction of the ketones to the corresponding alcohols with high *R*-selectivity using the cofactor NADPH as a reducing agent and the reverse reaction of oxidation with the cofactor $NADP^+$. The enzyme is a homotetramer with a molecular weight of 107 kDa (26.6 kDa pro subunit), with each of the monomers containing a single Rossmann-fold cofactor-binding domain with a central β-scaffold composed of 8 parallel β-strands linked by α-helices (Fig. 1-6). The tetramer contains two Mg^{2+} binding sites and four active centers (one per subunit) [67]. Each Mg^{2+} ion is coordinated by the carboxylic groups of two C-terminal glutamine residues (Q251), which stabilizes the quaternary structure. Their removal, however, does not disrupt the homotetrameric assembly, but fully inactivates the enzyme [67].

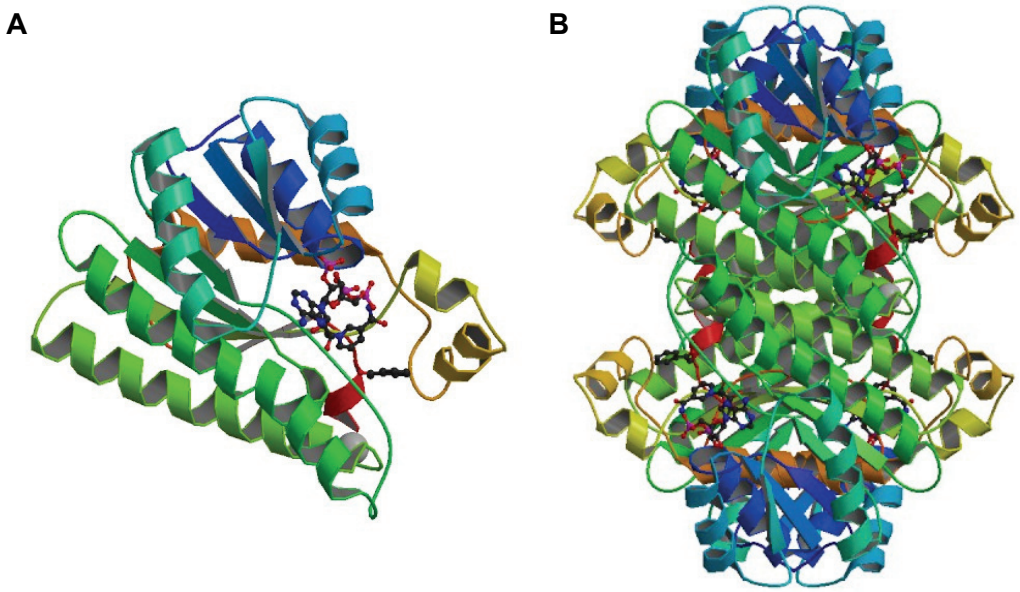

Figure 1-6. Tertiary and quaternary structure of the wild type *Lb*ADH. The structures were derived from the database UniProt, PDB entry 1zk4.

*Lb*ADH belongs to the SDR superfamily of dehydrogenases and displays the common group reaction mechanism (Fig. 1-5). Its active site is located at the C-terminal part, in a cleft, which can be covered from the solvent by moving the substrate-binding loop (positions 185-210) [67]. Residues of the catalytic triad are Ser142, Tyr155, Lys159, the conserved Asn corresponds to Asn113 in *Lb*ADH [8, 67]. Additionally, active site residues together with several other highly conserved residues and a cluster of internal water molecules form an “extended proton relay system”, which ensures rapid transfer of a proton from the bulk solvent to the active site, where it is consumed in the reductive reaction direction (Fig. 1-7) [8].
Due to the broad substrate range and high regio- and enantioselectivity, *Lb*ADH is suitable for numerous industrial applications. It was successfully used for the production of chiral secondary alcohols [7, 25, 68], δ-hydroxy-β-keto esters [69], for the dynamic kinetic resolution of α- and γ-alkyl substituted β,δ-diketoesters [70], the reduction of aryl alkynones [71], *n*-alkyl ethynyl ketones [71, 72], and of α-halogenated propargylic ketones [69, 71]. In all these reactions NADPH was applied as cofactor in catalytic amounts and regenerated using isopropanol as a second substrate [71].

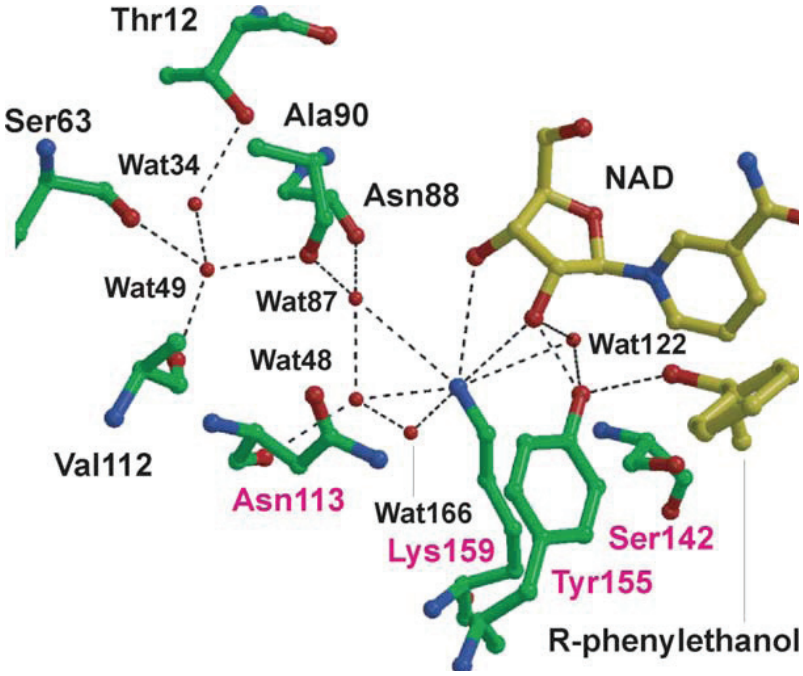

Figure 1-7. Close-up view of the most important residues of the extended proton relay system (reprinted from Schlieben *et al*., [8]). The catalytic tetrad is labeled in magenta. Hydrogen bonds are indicated by broken black lines.

Although cofactor regeneration methods are well established for NADPH, NADH is preferred over NADPH in technical processes due to its lower cost [73] and higher stability [74]. Therefore, several attempts to create an NADH-dependent variant of *Lb*ADH have been performed. Based on the current knowledge of cofactor specificity determination in SDRs and multiple sequence alignments, Schieben *et al*. identified residue G37 as a target and introduced a single amino acid exchange G37D [8] into *Lb*ADH. Indeed, the variant *Lb*ADH G37D was able to utilize both NAD(H) and NADP(H) with a distinctly higher affinity towards NAD(H) [8]. The D37 is located in the cofactor-binding domain, and stabilizes NADH through interaction with the 2',3'-hydroxyl groups of the ribose moiety (Fig. 1-8). It is negatively charged and imposes electrostatic repulsion to the phosphate group of NADPH, so, the varaint has significantly lower affinity towards NADPH [8]. However, *Lb*ADH G37D exhibited significantly lower enzymatic activity compared to the wild-type (wt) enzyme [8], which might represent an obstacle for industrial applications. No data about thermostability of this variant were presented.

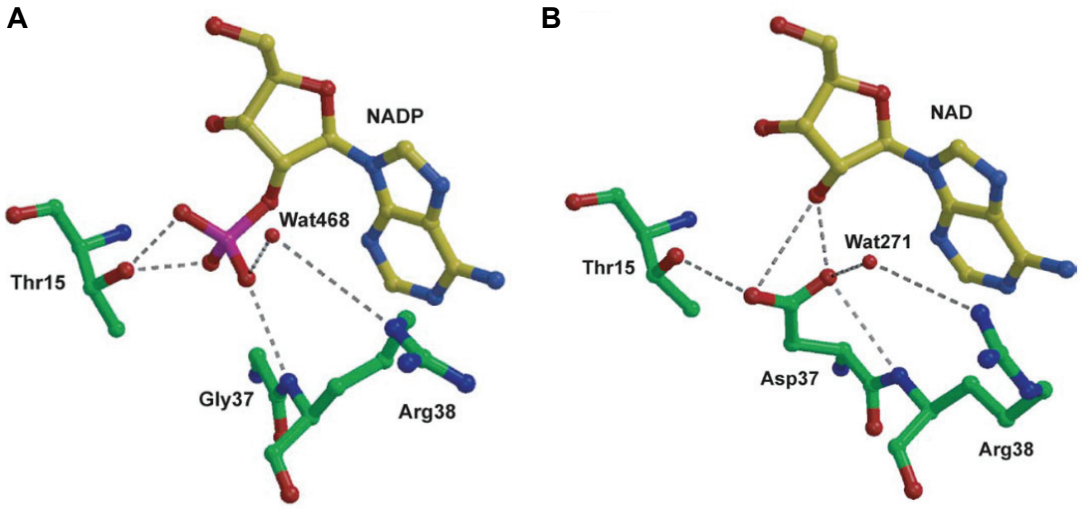

Figure 1-8. Comparison of the (A) NADP-dependent *Lb*ADHwt with the (B) NAD-dependent *Lb*ADH G37D (after Shieben *et al.*) [8]. Oxygen, nitrogen and phosphorus atoms are colored red, blue and magenta, respectively. Carbon atoms of an enzyme are drawn in green, whereas whose of the cofactor are in yellow.

Machielsen *et al*. exploited computational methods and structure-guided protein design for the same purpose [62] and four mutations R38P, A90S, V112D, and M140I were predicted by molecular modeling. However, the *Lb*ADH single variants A90S, V112D, and M140I showed no activity in an acetophenone conversion assay neither with NADPH nor with NADH as a cofactor. The *Lb*ADH R38P, however, displayed enzymatic activity with both NADPH (323 U/mg) and NADH (80.3 U/mg) at an optimal pH of 5.5 [62]. Molecular modeling studies suggested that the removal of the NADPH phosphate might liberate two unsaturated hydrogen bonds towards R38 (Fig. 1-8). Mutation to P compensates this effect and, additionally, partially occupies the phosphate cavity [62]. Biochemical characterization of *Lb*ADH R38P revealed a shift of the pH optimum for the reduction reaction from 6.5 for the wild-type to 5.5 for the variant [62]. The variant showed higher thermostability than the wild-type enzyme at 30°C and 42°C, [62]. The double variant *Lb*ADH G37D/R38P displayed significantly lower activity than the *Lb*ADH R38P, and was not futher investigated.

It is important to mention that biochemical data obtained by Machielsen *et al*. disagree with those published earlier. So, Machielsen *et al*. reported an enzymatic activity of 22 U/mg for the purified *Lb*ADHwt with NADH as a cofactor [62], whereas Shieben *et al*. had not observed any activity at all [8]. As the purity of the enzymatic preparations obtained by Machielsen *et al*. and Shieben *et al*. was proved by SDS-PAGE electrophoresis, the observed differences should be explained by great variations in the composition of the enzymatic assay mixture. Such parameters, as buffering component, ionic strength, pH of the assay mixture, as well as concentrations of the substrate and the cofactor considerably varied [8, 62].

In the present work, *Lb*ADHwt and the variant *Lb*ADH G37D were studied with respect to their properties in aqueous solution and in the gas/solid system. The variant was taken as a starting point for subsequent directed evolution experiments.

1.2.4 ADH from *Thermus sp.*

The ADH from *Thermus sp.* ATNI (*T*ADH) represents a new thermophilic NADH-dependent enzyme, which belongs to the MDR family of oxidoreductases [75]. Its natural host grows at an optimal temperature of 70°C and utilizes alkanes in its metabolism. Hereby, *T*ADH is assumed to be involved in the alkane degradation pathway. The enzyme is a homotetramer with a molecular weight of 38 kDa pro subunit, with each subunit containing one Zn^{2+} ion [75].

*T*ADH effectively converts a variety of compounds, including primary, secondary, cyclic and aromatic alcohols as well as the corresponding aldehydes and ketones. Cyclohexanol, cyclohexanone and their derivatives were shown to be excellent substrates for *T*ADH; even compounds with large substituents at the ring were accepted [75]. The double-ring compound 2-decalone was reduced with relatively high catalytic activity (28% relative to cyclohexanone) [75]. The enzyme is *(S)*-selective and produces *(S)*-alcohols with more than 99% enantiomeric excess [75].

*T*ADH is stable in various organic solvents over a broad range of $logP_{o/w}$. Water immiscible solvents, such as hexane and octane, are especially suited and can be used as a second phase in bioconversions providing a high solubility for a wide range of substrates and products [76]. The water-miscible solvents isopropanol and acetone induce inactivation of the enzyme, but can be applied in concentrations up to 10% (v/v) (without complete loss of enzymatic activity) [75].

*T*ADH has already been successfully employed for the enzymatic production of chiral alcohols in systems with a chemoenzymatic [77] or electroenzymatic [76] regeneration of NADH at 60°C. Therefore, this thermophilic ADH might represent a potent target enzyme for application in the gas/solid reaction system, too.

1.2.5 ADH from *Flavobacterium frigidimaris*

The ADH from the psychotolerant organism *Flavobacterium frigidimaris (Ff*ADH) is a NAD-dependent cold-active thermostable oxidoreductase [78]. It belongs to the MDR family of enzymes, has a homotetrameric structure and contains two Zn^{2+} ions per 40 kDa subunit [79]. One of these Zn^{2+} ions is located in the center of a subunit and is essential for biocatalysis, whereas the second one is located at the interface between the subunits and is considered to be structurally important [79]. A multiple sequence alignment with the other members of the MDR family revealed a highly conserved catalytic triad with the Ser (of other ADHs) being presumable replaced by a Thr [79].

*Ff*ADH effectively oxidizes primary and secondary aliphatic and aromatic alcohols and reduces the corresponding aldehydes and ketones, with high *(R)*-selectivity [79]. Unique characteristics of this enzymes are the significant activity at low temperatures and the high stability at elevated temperatures [79]. The enzyme displays its maximal activity at 70°C with half-life of 6 min (0.3 min for *Lb*ADH at the same temperature) [79]. Incubation of the enzyme at 40°C for 210 min did not affect its catalytic activity [79]. The half-lifes at 50°C and 60°C were found to be 304 min and 50 min, respectively [79].
The high enantioselectivity and significant thermostability renders *Ff*ADH attractive for industrial applications. Its performance in the gas/solid reaction system has already been investigated by Ullish et al. (see section 1.1.2.6 for details) [49].

1.3 Nicotinamide cofactors

The nicotinamide cofactors NAD(H) and NADP(H) are important electron carriers in all living cells. These molecules possess a closely related structure and consist of two nucleotides connected two phosphate groups, with one nucleotide containing an adenine base, and the second containing nicotinamide (Fig. 1-8). NAD^+ and $NADP^+$ each can accept two electrons and a proton (= hydride ion), being reduced to NADH and NADPH, respectively (Fig.1-9) [80]. The hydride ion, can be donated in subsequent reactions, in which the substrate becomes reduced and NAD(P)H oxidized. Transfer of the hydride ion occurs with a large negative change of free energy, which makes it energetically favourable [80].

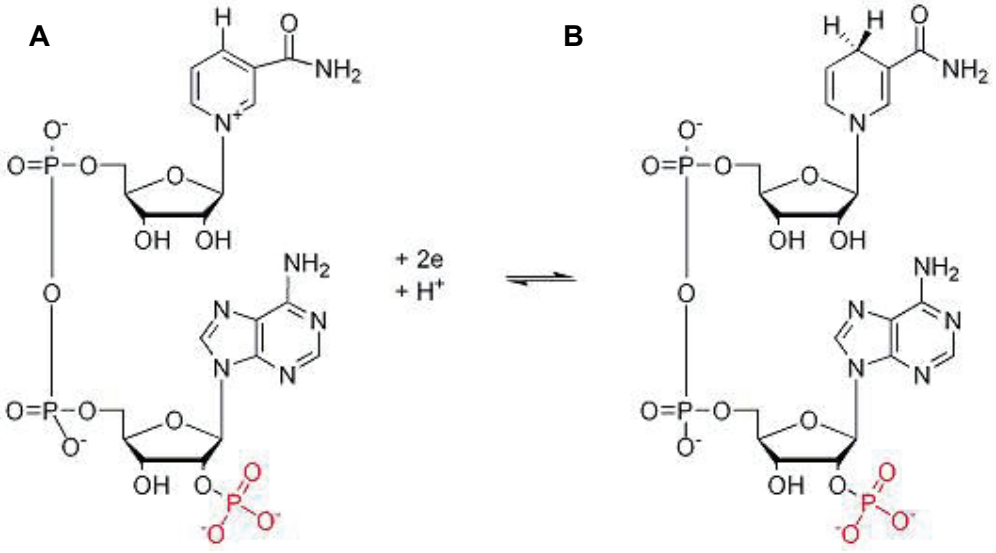

Figure 1-9. $NAD(P)^+$ (A) and NAD(P)H (B). The phosphate group, which distinguishes NADPH from NADH, is highlighted by red.

The phosphate group of NADP(H) does not affect the redox properties of the cofactor, but gives it a different “shape” and polarity. Therefore, NAD(H) and

NADP(H) are bound by different enzymes and are used for different sets of reactions. NADPH is mostly involved in anabolic pathways, whereas NADH transfers a hydride ion in many catabolic reactions [80]. The intracellular ratio of NADPH to $NADP^+$ is kept high, and the ratio of NADH to NAD^+ is kept low, so that, at all times plenty of NAD^+ as oxidizing agent and NADPH as reducing agent are available within the cell [80].

Due to the adenine base, the oxidized cofactor $NAD(P)^+$ absorbs light in the UV region of the spectrum with the maximal absorbance at 259 nm (ε = 16.9 $M^{-1}cm^{-1}$). Because of the presence of a conjugated π-system in the fully reduced nicotinamide ring of NAD(P)H, an additional absorption peak with maximum at 340 nm (ε = 6.22 $M^{-1}cm^{-1}$) is found [81]. The reduced and oxidized cofactor species differ also in their fluorescence properties. Being excited at 330-370 nm, the reduced cofactor NAD(P)H exhibits a broad emission peak with a maximum at 460 nm, while oxidized $NAD(P)^+$ does not [82]. As for the absorption properties, the observed emission peak at 460 nm is also due to the electronic nature of the reduced nicotinamide ring in NAD(P)H. The differences in the spectral characteristics of the oxidized and reduced cofactor species are widely used in bioanalytics, for example in spectrophotometric enzyme assays and fluorescence microscpy. [84, 86, 87]. The rate of decomposition strongly depends on the actual pH and buffering components. There is a correlation between the half-life of $NAD(P)^+$ and the pKa value of the buffering component at a fixed pH. In particular, the most pronounced degradation of the reduced cofactor will be caused by components with a pKa almost equal to the pH of the solution (since only undissociated acid can catalyze cofactor decomposition). Phosphate and citrate, however, represent exceptions from this rule as they induce NAD(P)H degradation more effectively than expected [84].

1.3.1 Stability of nicotinamide cofactors

Nicotinamide cofactors show only limited stability in aqueous solution, either in the oxidized or in the reduced form. NAD(P)H decomposes under acidic conditions, but is relatively stable in an basic environment [83-85]. NAD(P)+, in contrast, is less stable under basic compared to acidic conditions [83, 84] [85] (Fig.1-10).

Decomposition of the reduced cofactor into enzymatically inactive substances proceeds through acid-catalyzed hydration [86], epimerisation [87] and cyclization.

In general, NADPH follows the same degradation pathways as NADH. In addition, there is evidence for intramolecular acid-catalyzed interaction of the ionized 2'-phosphate group with the nicotimamide ring [83, 84, 86]. Therefore, at low pH values, NADPH is decomposed 3 times faster than NADH [83].

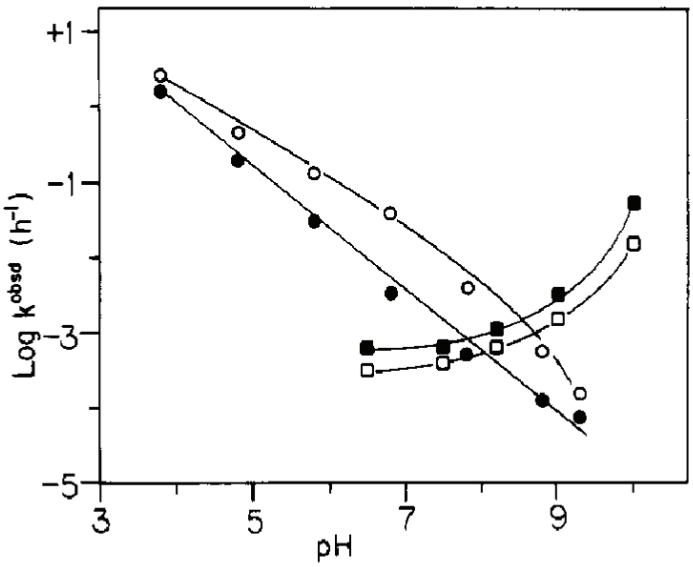

Figure 1-10. Rate constants for the decomposition of the cofactors. NAD^+ is depicted in black squares, $NADP^+$ in white squares, NADH in black circles and NADPH in white circles. Reprinted from Wong and Whitesides [83].

At a pH below 8.0 oxidized cofactor species ($NAD(P)^+$) are more stable than the reduced ones (in the absence of strong nucleophiles). At higher pH values their structure is mainly broken via base-catalyzed hydrolytic cleavage of the nicotinamide-ribose bond or nucleophilic addition to the nicotinamide ring [84]. Presence of phosphate, citrate, maleate, sulphate, oxalate, carbonate or chloride anions have been shown to accelerate the rate of hydrolysis [84, 85]. Moreover, it has been shown that prolonged incubation under highly alkaline conditions can induce the cleavage of the pyrophosphate bond of $NAD(P)^+$.

Degradation of NAD(P)H is temperature-dependent, with both cofactors being significantly less stable at elevated temperatures. The temperature coefficient of destruction equals to 9% per °C for NADH and 11% per °C for NAD^+ [85]. Phosphorylated cofactors degrade faster, but temperature and pH act cooperatively in a strong non-linear way. For example, at pH 6.0 at the same temperature the rates of decomposition of the NADPH and NADH differ by a factor of 5, whereas, at pH 3.7, the rates are almost identical [88]. Additional factors, such as buffering component type and the ionic strength can influence the speed of cofactor degradation [74, 84, 85, 88]. Therefore, thermal stability of $NAD(P)^+$ and NAD(P)H has to be separately elucidated for each system, under the buffer, ionic strength and pH conditions as being used later for bioconversion.

The stability of nicotinamide cofactors in the solid state was studied in relation to their storage conditions. It was shown, that lyophilized NADPH was stable for at least two years at -80°C, thereas 20% of it was decompoused in one week during the storage at -20°C [89]. The presence of a liquid phase in a equilibrium with a solid phase was suggested as an explanation for this phenomenon [89]. Lyophilized NADH, as expected, demonstrated higher storage stability. It could

retain 98% of its activity after 5 weeks of storage at 33°C [90]. In spite of these findings, no studies concerning thermal stability of cofactors in the solid state have been published.

1.3.2 Regeneration of NAD(P)H

The industrial application of oxidoreductase-catalyzed processes requires continuous recycling of the nicotineamide cofactor. Common strategies for recovery of NAD(P)H in cell-free biocatalytic systems can be classified into four categories: enzymatic, chemical, electrochemical and photochemical [84].

Enzymatic strategies for the recovery of reduced cofactor are preferred in industrial processes because of their high efficiency and selectivity [91, 92]. They include substrate-coupled and enzyme-coupled approaches [84]. The substrate-coupled approach is commonly used with ADHs. Reduction of $NAD(P)^+$ is achieved through oxidation of a second “cheaper” substrate (usually isopropanol or ethanol) and is generally achieved by the same enzyme, which carries out the target conversion to the more valuable product (Fig. 1-11 A) [84, 91-93]. This approach is widely employed in bioreactor design. However, presence of two substrates and two products induces thermodynamic limitations into the reaction system. Moreover, the second substrate has to be supplied in a large excess, which might induce inactivation of an enzyme [84, 91-93].

In the enzyme-coupled regeneration method a second enzyme, which is highly selective towards a sacrificial substrate, is involved in the process (Fig. 1-11 B) [84, 92, 93]. It helps to avoid thermodynamic restrictions and at the same time provides high reaction rates. NADH is generally regenerated by a formate dehydrogenase from *Candida boidinii Cb*FDH), which oxidizes formate to CO_2 and H_2O [84, 94, 95]. The process is advantageous, since the generation of CO_2 provides a strong driving force for NADH regeneration by rendering the reaction irreversible. However, FDH possesses only a low activity (6 U mg^{-1}) [91]. The phosphite dehydrogenase from *Pseudomonas stutzeri* (*Ps*PtDH) catalyzing NAD-dependent oxidation of the phosphite to phosphate represents an alternative for the regeneration of NADH [91].

NADPH is recycled either by a glucose dehydrogenase from *Bacillus megaterium* (*Bm*GDH), glucose-6-phosphate dehydrogenase from *Saccharomyces cerevisiae* (*Cc*G6PDH) or an engineered FDH and PTDH with altered cofactor specificity [91, 96]. *Bm*GDH renders reduction of $NADP^+$ to NADPH via simultaneous oxidation of glucose to gluconolactone. Spontaneous hydrolysis of gluconolactone to gluconate shifts the equilibrium of the whole system towards the production of the desired compound. *Cc*G6DH oxidizing glucose-6-phosphate has been widely used for NADPH regeneration in the past [84]. Protein engineered variants of *Cb*FDH D195Q/Z196H [97] and *Ps*PtDH E175A/A176R [98] possess altered cofactor specificity and are more specific for NADP(H) than NAD(H).

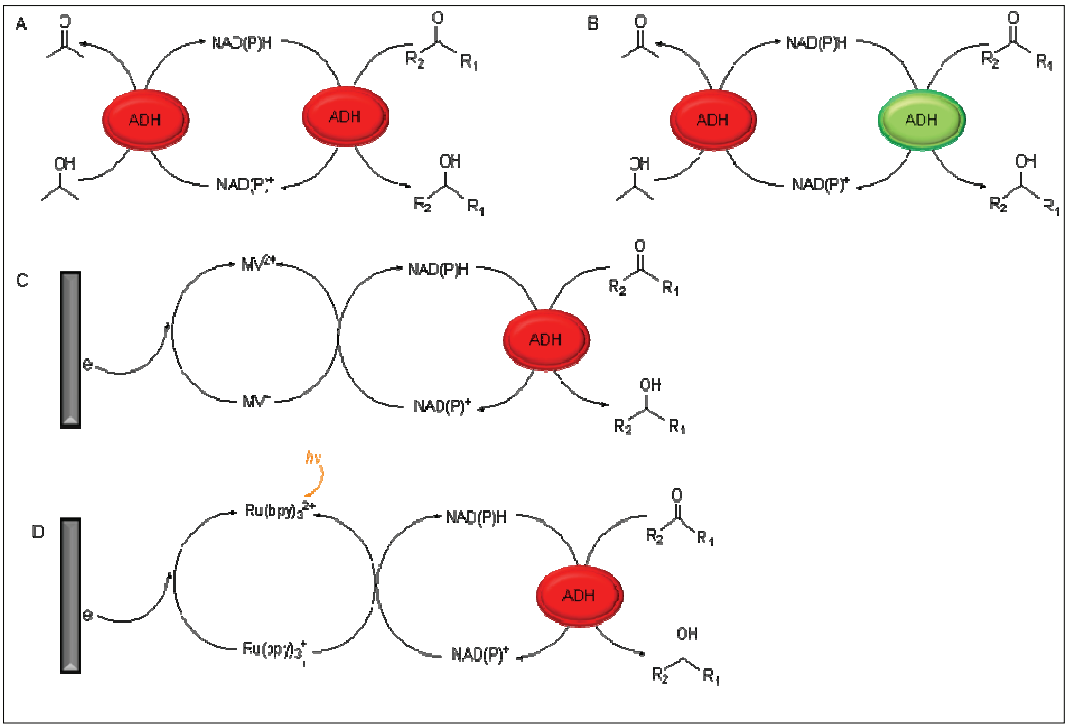

Figure 1-11. Schematic representation of cofactor regeneration strategies. A: substrate-coupled regeneration; B: enzyme-coupled regeneration; C: electroregeneration; D: photoregeneration.

Chemical regeneration of NADH was performed by addition of dithionite [84]. Although dithionite is relatively inexpensive, the method is disadvantageous due to direct reduction of both the biocatalyst and a product [84].

The electrochemical approach uses electrons supplied by an electric current for the recovery of NAD(P)H (Fig. 1-11 C) [93, 99]. Potentially, the process is more simple and economical than the others. Direct reduction of $NAD(P)^+$ on the electrode surface is possible [100]. However, this method is currently applicable for very low amounts of cofactor only, because of an non-selective dimerization process, which takes place if higher amounts of $NAD(P)^+$ undergo electro-reduction [99]. Therefore, chemical mediators have to be added to transfer two electrons from the cathode to the cofactor molecule, producing enzymatically active 1,4-NAD(P)H [99]. Compounds such as rhodium complexes with substituted 2,2′-bipyridine or pentamethylcyclopentadienyl ligands ensure high reduction potentials and fast reaction rates, and prevent overpotentials [99, 101]. Therefore, such mediators were widely applied in lab scale to promote ADH-catalyzed enantiospecific reduction reactions and oxidative kinetic resolutions [76, 101-105]. The main disadvantage of mediator usage is the potential toxicity of the employed enzyme to the mediator [106]. Cystein, histidine and tryptophan as well as the proteins containing these amino acids at the surface drastically reduce activity of the rhodium 2,2'-bipiridine [106]. Nevertheless, reactor engineering provides

several possibilities to overcome this obstacle be spatial separation of the processes [99, 105, 106].

Since NADPH plays an important role as an electron carrier in photosynthesis, photochemical systems for NAD(P)H regeneration are of special interest. *In situ*, a photochemical method utilizes special mediators called photosensitizers, such as tris(bypyridine)ruthenium II, *meso*-tetramethylpyridinium-porphyrin-zinc II or TiO_2 [84, 107]. First, the photosensitizers have to be reduced by an electron donor (electric current). Than the resulting photoproduct can reduce $NAD(P)^+$ in a reaction induced by light (Fig. 1-11 D). This system can be coupled to enzyme-catalyzed conversions to ensure constant cofactor recycling [107]. However, turnover numbers and conversion rates in such systems are quite low [84]. Therefore, an additional artificial electron mediator as well as a corresponding enzyme might be needed.

Alternatively, targeted asymmetric reductions can be performed in living recombinant cyanobacteria or algae [108]. Whole cell biotransformations do, probably, provide the easiest possibility to regenerate the consumed cofactor [92]. The recovery is achieved by shifting the cellular metabolism with special feeding strategies. Additionally, enzyme-coupled and substrate-coupled strategies are often be applied to whole cell systems by percolation of cell cultures with isopropanol or recombinant coexpression of enzymes involved in cofactor regeneration [91, 92, 109].

1.4 Thermostability

1.4.1 Factors contributing to enzyme thermostability

Protein thermostability is a complex and complicated phenomenon, which is rather influenced through a combination of several small effects, than the results of major changes in structure [110-112]. Comparative studies between enzymes from thermophilic sources and their mesophilic counterparts revealed that their amino acid sequences are often homologous [113], the 3D structures are superimposable and catalytic mechanisms are maintained [110]. Some important differences were, nevertheless, observed:

(i) Different amino acids are preferrentially present in thermophilic and mesophilic enzymes.
(ii) Additional intramolecular interactions (hydrogen bonds, salt bridges, hydrophobic interactions, metal binding etc.) exist in thermophilic enzymes.
(iii) Conformational stabilization (rigidity of protein structure, compact packing, α-helix stabilization, loop shortening etc.) occurs in thermophilic enzymes.

Hereby, a structure-based comparison of the **amino acids distribution** among thermophilic and mesophilic enzymes revealed several key points:

(i) Alanine appears with higher frequency in the core of thermophilic proteins, but with lower frequency being exposed to the solvent [114-116]. The content of Ile is also higher [117].

(i) (ii)There are less β-branched residues (valine, isoleucine and threonine) in α-helices of thermophilic proteins [118, 119].

(ii) Thermophilic enzymes contain proline more frequenty than mesophilic ones, especially in loops and β-turns [116].

(iii) A higher percentage of charged and polar amino acids, especially arginine, glutamic acid and tyrosine, on the protein surface is characteristic for thermophilic proteins [114, 116]. Interestingly, arginine is preferred over lysine, since it has more potential to form electrostatic interactions [116, 119].

(iv) Hyperthermophilic proteins apparently possess less thermolabile residues, such as glutamine, asparagine, cysteine and methionine [114, 115].

Hydrophobic interactions, leading to burial of non-polar side chains in the protein core, are the main energetic factor for protein folding and stability [120, 121]. The contribution of a single buried methyl group to conformational stability of an enzyme equals about 1.3 kcal mol^{-1} [122]. Indeed, introduction of point mutations V74Land V74I increased the melting temperature (Tm) of ribonuclease HI from *E. coli* by 2.1 - 3.7°C [123]. Enzymes, such as DNA polymerase from *Thermus aquaticus*, 3-Isopropylmalate dehydrogenase and seryl-tRNA synthase from *Thermus thermophilus* and 3-phosphoglycerate kinase from *Bacillus stearothermophilus* display a significantly expanded hydrophobic core compared to their mesophilic counterparts [110]. Perpendicular ring-ring interaction of aromatic amino acid side chains provides about 1 kcal mol^{-1}. A large number of aromatic interactions is observed in thermitase from *Thermoacetomyces vulgaris* and citrate synthase from *Thermoplasma acidophilum* [110].

Hydrogen bonds play a significant role in maintenance of protein structure and function at elevated temperatures. Vogt *et al*. showed that the overall number and density of hydrogen bonds directly correlates with the protein thermostability [119]. Introduction of additional hydrogen bonds in numerious mutagenesis studies improved the enzyme thermostability by stabilizing local interactions or by participating in hydrogen-bonding network [124-128].

As indicated by the higher content of arginine, tyrosine and glutamic acid, **electrostatic interactions** between oppositely charged residues represent a great stabilizing force in thermophilic proteins [114, 115, 117, 119]. Each salt-bridge has a stabilizing effect of 3-5 kcal mol^{-1} [129]. Buried salt bridges are quite rare. In contrast, electrostatic networks are often formed on the protein surface and at the interfaces between subunits [129]. Moreover, the stabilizing role of ion pairing was confirmed by many site-directed mutagenesis experiments [130-133].

The presence of intramolecular **disulfide bonds** introduces additional conformational stability into proteins. Disulfide bridges can enhance the melting

temperature (Tm) of enzymes and improve their long-term thermostability [134-137].

Comparative studies of thermophilic and mesophilic enzymes revealed a stabilizing role of incorporated **metal ions** [119, 138]. The presence of incorporated Ca^{2+} was shown to be a single factor, which differed between ferredoxins and proteases from *Sulfolobus sp. Bacillus AK1, Thermoactinomyces vulgaris* [129] and *Thermus aquaticus* [139] and their mesophilic homologs. Zn^{2+}-dependent L-amino acylases from *Pyrococcus furiosus* and *Pyrococcus horikoshii* were significantly stabilized by the presence of extra Zn^{2+}, Mn^{2+} or Ni^{2+} ions [140, 141]. Indirect evidence for the stabilizing effect of metals could be provided by the fact that most of thermophilic ADHs belong to the Fe^{2+}-dependent LDR or the Zn^{2+}-dependent MDR families [113].

1.4.2 Structural features of thermostable proteins

The increased rigidity of thermophilic proteins protects them against unfolding at high temperatures [111, 129, 142]. As extra benefits, thermophilic proteins are often more resistant to chemical denaturation (urea, GdnCl organic solvents) [142] and are able to accumulate a higher number of mutations without significant destabilizing effects [143]. Enhanced rigidity is achieved by optimized packing of protein structural elements, e.g. by an expanded hydrophobic core, fewer internal cavities, stabilization of secondary structure elements, stabilization of N'- and C'-termini, and tighter binding of subunits [110-112, 129]. The role of molecular rigidity was clearly demonstrated by Russel *et al.*, who compared three homologous citrate synthases from *Pyrococcus furiosus*, *Thermoplasma acidophilum* and pig (*Sus domestica)*. The enzymes shared a similar 3D structure and differed mainly in the strength of subunit association in the oligomer, the number of inter-subunit ion pairs and their overall compactness [144].

The **reduction of the solvent-accessible hydrophobic surface area** (ASA) is another important stabilization mechanism. In thermophilic proteins the number of solvent-accessible cavities and voids is reduced in comparison to their mesophilic counterparts. The number of buried non-polar amino acids is increased, whereas non-polar residues at the surface are often exchanged by polar ones [129, 142].

The **reduction of conformational constraints** plays a significant role in **stabilization of secondary structure elements**. For example, non-glycine residues with a left-handed conformation, if they do not participate in compensating non-covalent interactions, can create steric hindrance and destabilize turn regions [110, 111, 129, 145, 146]. Thus, elimination of conformational constraints by exchange to Gly at certain positions of β-turns or in C-caps of α-helices can increase protein stability up to 70% [111, 145-149]. Introduction of proline into the second position of β-turns or into the N-cap end of α-helices can strengthen the interaction between secondary structure elements and might increase overall

compactness of the protein [110, 150, 151]. Stabilization of α-helices in thermophilic enzymes is achieved through removal of β-branched amino acids (isoleucine, valine, threonine), which display low helical propensity, and introduction of alanine [118, 129, 152]. Another option lies in compensation of the α-helix dipole moment by placing negatively charged residues (e.g. glutamic acid) near its N-cap, as well as by introducing positively charged residues (e.g. arginine) near the C-cap of the helix [110, 111, 129, 152].

1.4.3 Engineering of protein thermostability

1.4.3.1 Rational design

Rational design is a powerful tool to enhance thermostability of an enzyme, when based on a detailed understanding of structure-function relationships. Site-directed mutagenesis based on comparison of 3D structures of the target protein and its thermophilic homolog would be the best option [153]. However, such cases are relatively rare. Alternative routes to obtain high thermostability are: introduction of additional hydrogen bonds, salt-bridges and disulfide bonds [119, 126, 127, 130, 132, 134, 136, 137, 154]; stabilization of α-helices [118, 147, 152] and β-turns [146, 151, 155]; improvement of molecular packing by filling of internal cavities [123] and shortening of loops, strengthening of interactions between oligomer subunits and thus stabilization of the oligomeric state [156].

1.4.3.2 Directed evolution

Directed evolution is a commonly used and effective method for the improvement of enzymatic thermostability by repeated rounds of creating diversity, screening and selection of the best variants (Fig. 1-12). Experimental techniques used for each of these steps can significantly vary. The routine methods to create genetic diversity are error-prone PCR (epPCR) and DNA shuffling [124, 125, 157]. The first method, however, faces limitations such as mutational bias of the employed polymerases and low mutational frequency, partially due to organization of genetic code itself [158]. Enhancement of protein thermostability, in contrast, requires generation of new intramolecular interactions, e.g. by exchanges in distant regions of sequence space. EpPCR with a high mutation rate (22.5 nucleotide exchanges per gene) is beneficial for this purpose, since it enables to generate and screen more diverse protein sequences, and, therefore, increases probability to find a positive hint [159]. However, such high mutational load significantly increases screening efforts, as many inactive enzyme variants are generated. Thus, fast and efficient screening systems need to be employed.

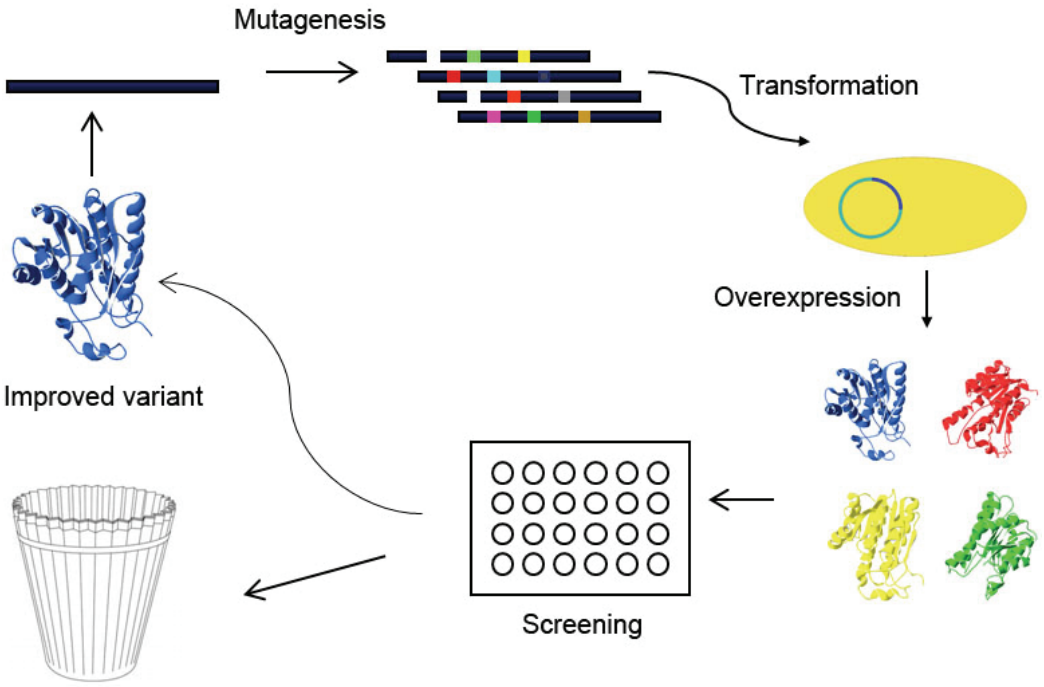

Figure 1-12. Schematic outline of a typical directed evolution experiment. First, the gene encoding the enzyme of interest is randomly modified by mutation or/ and recombination technique. Then, the modified genes are overexpressed in a host organism. Next, the mutant library is screened for the presence of protein variants with desired property. The improved variants are isolated, amplified, and used for the further experiments, whereas the non-functional ones are eliminated.

To overcome the main challenges of epPCR, many mutagenesis methods have been developed. They include commercially available Sequence Saturation Mutagenesis (SeSaM), Random Insertion and Deletion (RID) mutagenesis, Random Insertional-deletional Strand Exchange (RAISE) mutagenesis as well as utilization of base analogue 8-hydroxy-dGTP, mRNA mutagenesis by Q_β replicase and use of human family X and Y DNA polymerases for epPCR [158]. Another possibility lies in random integration of degenerate codon(s) into the gene of interest. Transposon Integration mediated Mutagenesis (TIM) [160] and Trinucleotide Exchange (TriNEx) [161] methods exploit this strategy [158].
DNA shuffling is a procedure for *in vitro* recombination of homologous genes [162]. The genes to be recombined have to be randomly digested by DNase I and then reassembled by PCR, such that DNA fragments from different parents can recombine in cross-over regions with high sequence identity [157, 162, 163]. After screening, the chimeric proteins with improved thermostability can be isolated from the pool [157, 164, 165]. DNA shuffling techniques can be combined with epPCR [125, 128, 166, 167] or performed with highly homologous genes (70% homology is needed) from meso- and thermophilic sources [168-170]. Despite of the wide use in protein engineering, gene shuffling is a skill-demanding, time- and effort-

consuming method. The reported drawbacks are recombination bias, low yield of chimeras and a parental background of about 20% [171]. Several modifications of the DNA shuffling method, such as Random Chimeragenesis of Transient Templates (RACHITT), Staggered Extention Process (StEP), recombination-dependent PCR (RD-PCR), have been developed to address these problems.

1.4.3.3 Semi-rational design

Semi-rational approaches represent another strategy to enhance thermostability of enzymes. They randomize amino acids at one or more rationally chosen positions. Generated focused libraries are significantly smaller, than random libraries, and are faster to screen. Additionally, these libraries are based on certain theoretical concepts, which help to develop a better understanding of structure-function relationship and ensure an increased chance for success [172].

The **consensus method** relies on the hypothesis that amino acids highly conserved within an enzyme family are crucial for the stability. Therefore, substitution of non-conserved residues by conserved ones should be beneficial for overall thermostability [173, 174]. So, Lehmann *et al.* calculated a consensus sequence from an alignment of 13 phytases, synthesized the gene artificially and obtained a more thermostable phytase with showed an increase in T_m by 15 - 26°C [173].

Iterative saturation mutagenesis is based on available X-ray data. The atomic displacement factor (B-factor), which reflects smearing of atomic electron densities as a consequence of thermal motion of amino acids, serves as a criterion for the choice of randomization sites [172]. The most flexible amino acids in a protein (those with the highest B-factor) are subjected to saturation mutagenesis and the resulting variants screened for increased thermostability. The cycle can be repeated using the “best hint” as a template [172]. Alternatively, several residues can be randomized and screen simultaneously [158, 172].

Cassette mutagenesis is helpful for dealing with flexible protein regions, identified by a structure-guided alignment of protein sequences. One or several regions in any given position of a gene can be randomized in a focused way by a One-pot Simple methodology for Cassette Randomization and Recombination (OSCARR) [175] or by Incorporating Synthetic Oligonucleotides via Gene Reassembly (ISOR) [176] approaches.

1.4.3.4 Computational methods

Computational methods for rational protein design are increasingly employed. Homologous modelling and molecular dynamic simulation are powerful tools for identification of flexible protein regions and *in silico* introduction of stabilizing interactions. Generation and screening of combinatorial libraries is possible *in*

silico, on the primary sequence level, which is very helpful for reducting the experimental work load. Special tools such as the Programme for Estimating Amino Acid Diversity in Error-prone PCR Libraries (PEDEL-AA) and Diversity Resulting from *In Vitro* Recombination (DRIVeR) allow the estimation of the number of distinct protein variants encoded by epPCR or DNA shuffled libraries, respectively [158]. The structure-guided approach SCHEMA was designed for choosing the least disruptive crossover locations and was shown to be an effective instrument for generation of diverse shuffled libraries [177, 178]. Evaluation of variants is based on calculation of sequence fitness [179]. Several approaches, such as Monte-Carlo simulations, genetic algorithms, and side-chain topology and energy refinement (FASTER) are routinely used to examine large combinatorial libraries and evaluate promising candidates [180, 181]. Often, the target is compared with statistical information for known thermophilic proteins, e.g. amino acids and dipeptide distribution, patterns of residues with minimized energy and/or preferred structural elements. In that way, computational methods allow *in silico* screening of large combinatorial library [177, 178, 182, 183].

Significant progress has been achieved in design of focused libraries. Structure-based multiple sequence alignment algoritms, such as STAMP, MATLIGN [184], and many others are helpful for calculation of consensus sequences. B-Fitter is used for visualization of B-factors and planning of mutagenesis sites [172]. There are methods, which permit to apply and evaluate *in silico* rational stabilization strategies, for example, amino acid replacements, mutations in α-helices and β-sheets, introduction of hydrogen bonds and ionic interaction at the protein surface [185-187]. CodonCalculator and AA-Calculator tools can assist in the appropriate design of degenerate primers for saturation mutagenesis [158].

1.4.3.5 B-FIT approach to enhance thermostability

According to Reetz and Carballeira, “the B-FIT approach constitutes a symbiosis of rational design and combinatorial randomization” [172]. The method aims to enhance enzymatic thermostability by increasing the rigidity of the enzyme, which is achieved by randomization of the most flexible site(s) in the protein structure and subsequent screening of the variants. Identification of the flexible sites is accomplished through analysis of the known crystallographic structure of the target enzyme. The B-factor value, which reflects the degree of atomic displacement with respect to the equilibrium position, is used as a criterion for the choice of amino acids to be randomized. This information can be extracted from X-ray data using the B-Fitter tool.

The chosen amino acids have to be randomized by saturation mutagenesis in hierarchical order. The focused library, derived from randomization of the first site, should be screened, and the best hint can serve as a template for randomization of

the next positions. Alternatively, several sites can be randomized simultaneously with the larger mutant library to be screened.

The right choice of degenerate codons and the size of the mutant library are equally important for a successful experiment. So, comparison of in three codon positions randomized libraries of the epoxide hydrolase gene from *Aspergillus niger,* created with the routinely used degenerate codon NNK (32 codons/ 20 amino acids) and the codon NDT (12 codons/ 12 amino acids) revealed a significantly higher quality of the second (smaller) library. 511 positive hints were found in the NDT-library of 5000 mutants, whereas the NNK-library of the same size contained only 38 positive hints [188]. This phenomenon is in fact statistically well-founded. Indeed, one needs to screen 98163 variants to cover 95% of the sequence space created by NNK, compared with 5175 clones for the NDT-codon library (table 3) [188]. Thus, the 5000 mutants screened in the approach, cover nearly the complete possible sequence space for the NDT-codon library, but barely cover 5% of the available genetic diversity created by using the NNK degenerate codon. The worksheet CASTER, supplied together with B-Fitter, is helpful in selection of the appropriate codon and in further planning of the experimental work [172].

Chapter 2
Objectives of the present project

Gas/solid biocatalysis represents a perspective biotechnological approach in which the solid dry enzyme catalyzes the reaction of the gaseous substrate to the gaseous product. This technique exhibits significant advantages, such as increased resistance of the immobilized enzymes, simplified recovery of the product, possibility for the continuous removal of the toxic or inhibitory substances [3]. However, despite of increasing attention, there have been quite a few studies answering fundamental questions about protein structure performance in the low-hydrated, solid state. Further, no investigations were performed on the stability of the solid cofactors.

Additionally, only volatile substrates are suitable for the gas/solid catalytic systems. To use certain substrates in the gas phase system, the reactor is usually operated at elevated temperature; therefore, highly thermostable enzymes are needed. Application of directed evolution techniques for the improvement of enzyme thermostability in the solid state requires a reliable screening system. Thus knowing the molecular factors relevant for inactivation of the enzyme in solid state is a first step to develop such a system.

Considering the facts mentioned above, this work had the following aims:

(i) **Elucidation of the key mechanisms responsible for the inactivation of the solid enzymes in comparison to enzymes in aqueous solvents.** To fulfill this aim, a comparative study of the biocatalytic activity and the protein structure through complementary techniques was carried out. The NADPH-dependent *Lb*ADHwt and its variant *Lb*ADH G37D, which has higher affinity towards NADH, were used as model enzymes.

(ii) **Elucidation of the key mechanisms responsible for the inactivation of the solid cofactors NAD(P)H.** Up to now, the stability of the redox cofactors has exclusively been studied in solution, demonstrating that NADH is significantly more stable than NADPH under various conditions, such as alkaline or acidic pH or increased temperature [74, 84, 85, 88]. To obtain reliable data for the gas/solid system, comparative studies of the dissolved and solid NAD(P)H should be performed.

(iii) **Design of the high-throughput screening system, which would be reliable for production of the thermostable enzyme variants suitable for the gas/solid system.**

(iv) **Generation of thermostable enzyme variants suitable for the gas/solid system using protein engineering.**

(v) **Testing of the resulting enzyme variants in the gas/solid bioreactor.**

Chapter 3
Materials and Methods

3.1 Materials

3.1.1 Chemicals

All chemicals used in this work were of highest purity grade.
The chemicals were supplied by Sigma-Aldrich GmbH (Taufkirchen), Fluka Biochemika GmbH (Steinheim), Merck KGaA (Darmstadt) or Carl Roth GmbH (Karlsruhe).
Media components were purchased from Carl Roth GmbH (Karlsruhe).
The cofactors β-NADPH, β-NADH, β-$NADP^+$ and β-NAD^+ used for thermal degradation studies were ordered from Biomol GmbH (Hamburg) with 99% purity. The cofactors β-NADPH and β-NADH with 98% purity used for enzymatic assays were obtained from Carl Roth GmbH (Karlsruhe).

Restriction enzymes with corresponding buffers were supplied by Fermentas (St. Leon-Roth) or Roche Diagnostics (Mannheim), *pfu* polymerase was ordered from Roche Diagnostics (Mannheim) and the KOD polymerase was from Novagen (Madison, USA).

DNA purification kits were supplied by QiaGen (Hilden), BioanalytikJena (Jena), and Macherey-Nagel.
The cell lysis master Bugbuster was purchased by Novagen (Madison, USA).
PAGE and Coomassie dye components were produced by BioRad.

3.1.2 Equipment and software

Table 3-1. Equipment and software.

Equipment	Supplier
Cells cultivation	
Electroporator	BioRad
Reaction tube rotator	Stuart
Thermostated incubator	Infors AG
Microtiter plates shaker	Edmund Bühler GmbH

Table 3-1. Equipment and software, continued.

Equipment	Supplier
Centrifugation	
Sorvall	DuPont
Rotina 35R	Hettich Zentrifugen
Rotanta 460R	Hettich Zentrifugen
Cells disintegration	
Sonopuls HD 2070	Bandelin
Chromatography	
Äkta explorer protein purification system	GE Healthcare
Q-Sepharose matrix	Pharmacia
Sephadex G-25 matrix	Pharmacia
Sephadex G-25 minicolumns	GE Healthcare
Lyophilization	
Lyovac GT2	GEA Process Engineering
PCR	
Thermocycler	Eppendorf
Electrophoresis	
DNA electrophoresis chamber GT system	Bio-Rad
EagleEye II videodocumentation system	Stratagene
MiniProtean II	BioRad
Spectroscopy	
UV-Vis spectrophotometer	Beckman
Microtiter plates reader SpectraMax	Molecular Devises
Fluorescence spectrophotometer	Perkin Elmer
CD polarimeter	Jasco GmbH
BioPhotometer	Eppendorf
NanoDrop ND 3300	NanoDrop Technologies
Automated systems	
Colony picking robot QPix2	Genetix
Pipetting robot	Bio-Tek
Software	
Clone Manager	Sci-Ed Software
BioEdit	Ibis Biosciences
Spdb Viewer	Swiss Institute of Bioinformatics
Unicorn Manager	GE
SoftMaxPro 3.1.2	Molecular Devises
FL WinLab	Perkin Elmer
Spectra Manager	JascoGmbH
OriginPro 7.0	OriginLab Corporation
MS Office	Microsoft

3.1.3 Bacterial strains and plasmids

The *E. coli* strain DH5α was used for production of genetic material. The BL21(DE3) strain was used for the overexpression of desired enzymes.

Table 3-2. Bacterial Strains.

Bacterial Strain	Genotype	Source
E. coli DH5α	*F*-φ80*lac*ZΔM15Δ(*lac*ZYA-*arg*F) U169 *rec*A1 *end*A1 *hsd*R17 (r_k-m_k+) *pho*A *sup*E44 λ-*thi*-1 *gyr*A96 *rel*A1	Invitrogen (Karlsruhe)
E. coli BL21(DE3)	*F-omp*T *hsd*S_b(rB^-mB^-) *gal dcm (λclts857 ind1Sam7 nin5 lacUV5-T7gene1)*	Novagen (Madison, USA)

Table 3-3. Vectors.

Plasmid	Description	Source
pET21a+	Ap^R, ori_{pBR322}, P_{T7lac},	Novagen (Madison, USA)
pET21a-*Lb*ADH	Recombinant pET21a with 751 bp gene for *Lb*ADH	Prof. Dr. W. Hummel (Research Center Jülich, Germany)
pET3a -*Ff*ADH	Recombinant	Prof. Dr. T. Kazuoka (Osaka University, Japan)
pET11b-*T*ADH	Recombinant	A. Schmid (University of Dortmund, Germany)
pET21a-*Lb*ADH G37D	Recombinant pET21a with 751 bp gene for *Lb*ADH G37D	Present work
pLK17 B5	Recombinant pET21a with 751 bp gene for *Lb*ADH G37D/V42F/E44N/ K48R	Present work
pLK18 G4	Recombinant pET21a with 751 bp gene for *Lb*ADH G37D/V42D/E44N/ K48Q	Present work
pLK19 A11	Recombinant pET21a with 751 bp gene for *Lb*ADH G37D/V42D	Present work
pLK19 F11	Recombinant pET21a with 751 bp gene for *Lb*ADH G37D/V42L/E44Y/ K48E	Present work
pLK26 A9	Recombinant pET21a with 751 bp gene for *Lb*ADH G37D/V42I/E44Y/ K48R	Present work

Table 3-3. Vectors, continued.

Plasmid	Description	Source
pLK27 F1	Recombinant pET21a with 751 bp gene for *Lb*ADH G37D/V42I/E44F/ K48L	Present work
pLK34 G3	Recombinant pET21a with 751 bp gene for *Lb*ADH G37D/V42D/E44Y/ K48E	Present work
pLK38 G3	Recombinant pET21a with 751 bp gene for *Lb*ADH G37D/V42I/E44S	Present work
pLK41 C12	Recombinant pET21a with 751 bp gene for *Lb*ADH G37D/V42D/E44Y/ K48E	Present work
pLK41 H7	Recombinant pET21a with 751 bp gene for *Lb*ADH G37D/V42F/E44C/ K48Q	Present work
pLK42 C3	Recombinant pET21a with 751 bp gene for *Lb*ADH G37D/E44F/K48E	Present work
pCB13 C4	Recombinant pET21a with 751 bp gene for *Lb*ADH G37D/V42D/E44N/ K48S	Christina Bösing [189]
pCB11 E6	Recombinant pET21a with 751 bp gene for *Lb*ADH G37D/V42I/E44F K48A	Christina Bösing [189]

3.1.4 Oligonucleotides

Table 3-4. Oligonucleotides.

Oligonucleotide	Sequence 5'→3'	Remark
G37D for	GGTCATGATTACCGACCGGCACAGCGA TGTTG	Point mutation G37D
G37D rev	CAACATCGCTGTGCCGGTCGGTAATCA TGACC	Point mutation G37D
42/44/48 for	CGGCACAGCGATNDTGGTWDTAAAGCA GCTNNKAGTGTCGGC	Randomization of positions 42, 44 and 48
42/44/48 rev	GCCGACACTMNNAGCTGCTTTAHWACC AHNATCGCTGTGGTGCCG	Randomization of positions 42, 44 and 48

All the oligonucleotides used in this work were purchased in Thermo Hybaid (Ulm).

Concentrations of the oligonucleotides were calculated from absorbance at 260 nm using extinction coefficients provided by company.

3.2 Molecular Biological Methods

3.2.1 Electro-competent *E. coli* cells

Production of electrocompetent *E. coli* cells was performed according to Dower *et al.* [190]. BL21(DE3) or DH5α cells were transferred on LB agar plate and incubated at 37°C over night. The next day a single bacterial colony was isolated from the plate with a sterile toothpick and resuspended in 10 ml of LB media. This preculture was grown overnight at 37°C with constant shaking (115 rpm). 0.5 ml of the preculture was used to inoculate 1 L of LB media. The main culture was grown at 37°C with shaking at 120 rpm until it reached an optical density OD_{600} of 0.7. At this point, the cells were cooled on ice for 5 min and harvested by centrifugation for 15 min at 4000 rpm at 4°C. After removal of the supernatant, the pellet was resuspended twice in 1 l of ice-cold 10% (v/v) glycerol in ddH_2O and centrifuged for 10 min at 4000 rpm, 4°C. The collected cells were resuspended in 40 ml of ice-cold 10% glycerol and centrifuged for 10 min at 7000 rpm. Finally, the pellet was then resuspended in 2 ml of ice-cold 10% glycerol and devided into 40 µl aliquots under sterile conditions. Afterwards, the electrocompetent cells were frozen at –80 °C and stored until further use.

Transformation of electrocompetent *E. coli* cells was performed by electroporation. For this purpose, 40 µl aliquots of electrocompetent cells were thawed on ice. 10-100 ng of vector DNA was added by gentle pipetting, and the cells were transferred to a precooled sterile electroporation cuvette. After one pulse (EcnII) the cells were resuspended in 900 ml of LB medium, incubated with shaking for 1 hour at 37 °C and plated on LB-agar plates, containing ampicillin (100 µg ml^{-1}).

3.2.2 Chemically competent *E. coli* cells

Chemically competent *E. coli* cells were prepared as described by Hanahan [191]. The following buffers were used:

The BL21(DE3) or DH5α cells were plated on LB agar plate from a frozen stock and incubated at 37°C over night. The next day a single bacterial colony was picked up with sterile toothpick and resuspended in 5 ml of YETM media. This preculture was grown overnight at 37°C constantly rotating, and 0.5 ml of the preculture was used to inoculate 1 L of YETM media. The main culture was grown at 37°C with 120 rpm shaking until it reached the OD_{600} of 0.7. After cooling on ice for 5 min and centrifugation for 15 min at 2000 rpm and 4°C, the supernatant was carefully removed, and the pellet was resuspended in 200 ml of ice-cold TFB1 by

gentle re-pipetting and centrifugedagain for 10 min at 2000 rpm, 4°C. The supernatant was immediately removed by aspiration, and the cells were gently resuspended in 40 ml of ice-cold TFB2. The suspension was incubated on ice for 15 min and finally divided into 80 µl aliquots under sterile conditions. The cells were frozen at –80 ^{o}C and kept frozen until further use.

The heat-shock method was used for transformation of the chemically competent cells. For this purpose, 80 µl aliquots were thawed on ice for 30 min, mixed with 30-300 ng of plasmid DNA and left on ice for additional 20 min. After incubation, the cells were heat-shocked at 42°C for 90 sec and then returned on ice for 2 min. 900 ml of LB medium was added and the sample was incubated with shaking for 1 hour at 37°C. The transformed cells were plated on LB-agar selection plates, containing ampicillin (100 µg ml^{-1}).

Table 3-5. Chemically competent cells.

Solution	Component	
YETM medium	10 g l^{-1}	Tryptone
	2.5 g l^{-1}	Yeast extract
	5 g l^{-1}	$MgSO_4$*$7H_20$
		in ddH_2O, pH 7.5
TFB1	30 mM	KOAc
	100 mM	RbCl
	10 mM	$CaCl_2$
	50 mM	$MnCl_2$
	15% (v/v)	Glycerol
		in ddH_2O, pH 5.8
TFB2	10 mM	MOPS
	10 mM	RbCl
	75 mM	$CaCl_2$
	15% (v/v)	Glycerol
		in ddH_2O, pH 6.5

3.2.3 Cultivation of *E. coli* cells

Unless otherwise stated, growth of *E. coli* cells and expression of desired proteins with the T7*lac* expression system took place on LB agar or in sterile LB medium at 37°C:

After preparation, growth media were sterilized for 20 min at 121°C. Thermally unstable components were filtered sterile.

5 ml mini-cultures were grown in 10 ml reaction tubes in reaction tube rotator (NeoLab, Heidelberg). Cell cultures of higher volume were placed in Erlenmeyer flasks of at least 5 x bigger volume than the culture and grown in a thermostated shaker (Unitron, Bottmingen) at 115 rpm. Recombinant bacteria containing

plasmids, which encode resistance markers, were selectively cultivated after addition of corresponding antibiotics.

Table 3-6. Media and solutions.

Medium	Component	
LB medium	10 g l^{-1}	Tryptone
	5 g l^{-1}	Yeast extract
	10 g l^{-1}	NaCl
		in ddH_2O, pH 7.0
LB Agar	10 g l^{-1}	Tryptone
	5 g l^{-1}	Yeast extract
	10 g l^{-1}	NaCl
	15 g l^{-1}	Agar
		in ddH_2O, pH 7.0

3.2.4 Heterologous expression of proteins in *E. coli*

3.2.4.1 Protein production in shaking flasks

E. coli BL21(DE3) electro- or chemically competent cells were transformed with the pET21a plasmid encoding the *Lb*ADH variant, the pET11b-*T*ADH or the pET3a-*Ff*ADH. The next day single bacterial colonies were isolated from the plates with sterile toothpicks and transferred into 100 ml of LB media containing 100 µg ml^{-1} ampicillin. The preculture was grown overnight at 37°C with constant shaking (115 rpm). 1 ml of the preculture was used for inoculation of 1 L of LB media containing 100 µg ml^{-1} ampicillin. Further incubation took place at 37°C with vigorous shaking until they reached the OD_{600} of 0.7. After induction of the protein expression with 1 mM IPTG, the overexpression of *Lb*ADH and *T*ADH continued for 4-6 h at 37°C (115 rpm); for the overexpression of *Ff*ADH the cells were incubated for 16 h at 30°C (115 rpm). After this period, cells were harvested by centrifugation (40 min, 4000 rpm, 4°C). The supernatant was discarded and the cell pellets were collected in plastic bags and kept at –80 °C for further use.

3.2.4.2 Cultivation of *Lb*ADH variants in 96-well plates

Cultivation of cells in 96-well plates was performed at 37°C in a thermostated room on a microtiter plate shaker at 700 rpm. Precultures were grown in sterile 96-well microtiter plates, with a volume of 200 µl per well (Greiner Bio One), in non-inducing ZYP-505 medium with 100 µg ml^{-1} ampicillin at 37°C for 6-8 h. Main cultures were produced by transferring of 50 µl of the preculture to 950 µl of the autoinducing medium ZYP-5052 with 100 µg ml^{-1} ampicillin. The main cultures were

grown in 96-well deep-well plates in a total volume of 1 ml per well at 37°C for 16 h [172, 193]. The cells were harvested by centrifugation (20 min, 3500 rpm, 4°C, Rotanta 460 R) and kept at -80°C. To simplify the further use, all the mutants were numbered according to their position in the microtiter plate.

Table 3-7. Autoinduction media and stock solutions.

Media				**Stock Solutions**		
ZYP-505 medium	20 ml l^{-1} 50 ml l^{-1} 2 ml l^{-1}	Solution 505 Solution NPS 1M $MgSO_4$ in ZYP medium, pH 7.0		505 Solution	250 g l^{-1} 25 g l^{-1}	Glycerol Glucose in ddH_2O
ZYP-5052 medium	20 ml l^{-1} 50 ml l^{-1} 2 ml l^{-1}	Solution 5052 Solution NPS 1 M $MgSO_4$ in ZYP medium, pH 7.0		5052 Solution	250 g l^{-1} 25 g l^{-1} 100 g l^{-1}	Glycerol Glucose α-Lactose in ddH_2O
ZYP Medium	10 g l^{-1} 5 g l^{-1}	Tryptone Yeast extract in ddH_2O, pH 7.0		NPS solution	66 g l^{-1} 136 g l^{-1} 142 g l^{-1}	$(NH_4)_2SO_4$ KH_2PO_4 Na_2HPO_4 in ddH_2O

3.2.4.3 Protein production by high cell density cultivation

To obtain high cell densities, heterologous expression of wt *Lb*ADH and *Lb*ADH G37D in BL21(DE3) *E. coli* strain was performed in a fed batch fermenter under substrate-limiting conditions [192]. Glucose served as a carbon source.

Cultivation was carried out in 15 L Techfors (Infors AG, Switzeland) fermenter at 30°C and pH 7.0. Dissolved oxygen concentration, pressure and agitation rate were kept constant. First, the bioreactor was filled with HCD batch solution, ddH_2O and Anti-foam 289 (Table 3-8.1) and autoclaved. Then the thermo sensitive components of the HCD batch medium (Table 3-8.2) were added by sterile filtration.

After temperature equilibration at 30°C, fermentation was started by inoculation of the batch medium with 100 ml of a freshly prepared *E. coli* preculture. Cell growth was stabilized for 3 h, and then exponential addition of feed medium (Table 3-8.2) was started. The speed of nutrient components addition was regulated automatically in order to keep specific growth rate of the cells under critical value of 0.14 h^{-1}. The protein expression was started after 27 h by addition of IPTG to a

final concentration of 1 mM. The cultivation process was continued for additional 14 h. Finally, the cells were harvested by centrifugation (45 min, 6000 rpm, 4°C, Sorvall RC-5B) and frozen at -80°C until futher use.

Table 3-8.1. Stock solutions for Fermentation.

HDC-Batch	2	g l^{-1}	NH_4Cl
	20	g l^{-1}	$(NH_4)_2SO_4$
	130	g l^{-1}	KH_2PO_4
	100	g l^{-1}	K_2HPO_4
	60	g l^{-1}	NaH_2PO_4 x H_2O
	30 to 1.5	g l^{-1} l	Yeast extract in ddH_2O
HDC-Feed	180	g l^{-1}	Yeast extract in HDC-Batch
Vitamin Solution	0,1	g l^{-1}	Riboflavin /(Vit B2)
	10	g l^{-1}	Thiamin-HCl (B1)
	0,5	g l^{-1}	Nicotin acid
	0,5	g l^{-1}	Pyridoxin-HCl
	0,5	g l^{-1}	Ca-Phanthotenat
	0,001	g l^{-1}	Biotin
	0,002	g l^{-1}	Foleic acid
	0,01	g l^{-1}	Cyanocobalamin (B12)
	to 1.0	l	in ddH_2O
Thiamin Solution	200	g l^{-1}	Thiamin HCl in ddH_2O
Trace elements	10	g l^{-1}	$CaCl_2$ x $2H_2O$
	0,5	g l^{-1}	$ZnSO_4$ x $7H_2O$
	0,25	g l^{-1}	$CuCl_2$ x $2H_2O$
	2,5	g l^{-1}	$MnSO_4$ x H_2O
	1,75	g l^{-1}	$CoCl_2$ x $6H_2O$
	0,125	g l^{-1}	H_3BO_3
	2,5	g l^{-1}	$AlCl_3$ x $6H_2O$
	0,5	g l^{-1}	Na_2MoO_4 x $2H_2O$
	10	g l^{-1}	$FeSO_4$ x $7H_2O$ in ddH_2O
Glucose Batch	400	g l^{-1}	Glucose in ddH_2O
Glucose Feed	717.7	g l^{-1}	Glucose in ddH_2O
$MgSO_4$ Solution	200	g l^{-1}	$MgSO_4$ x$7H_2O$ in ddH_2O
IPTG	300	g l^{-1}	IPTG in ddH_2O
Ampicil-lin	200	g l^{-1}	Ampicillin in 70% ethanol
Other compo-nents	5	ml	Antifoam 289
	100	ml	Preculture ddH_2O

Table 3-8.2. Media for fermentation.

Component	Batch Medium		Feed Medium	
HDC batch	1000	ml		
HDC feed			500	ml
Glucose batch	50	ml		
Glucose feed			4180	ml
$MgSO_4$ Solution	50	ml	250	ml
Vitamin Solution	50	ml	25	ml
Trace elements	40	ml	20	ml
Thiamin Solution	5	ml	25	ml
Antifoam 289	3	ml	2	ml
Preculture	100	ml		
ddH_2O	8702	ml		
Total Volume	10000	ml	5002	ml

3.2.5 Extraction of plasmid DNA from *E. coli*

3.2.5.1 Miniprep DNA isolation

Selected colonies were isolated from plates using sterile toothpicks and suspended in 5 ml of LB with ampicillin (100 µg ml^{-1}). The colonies were allowed to grow overnight at 37°C constantly rotating. The plasmid DNA was isolated from the cells using an alkaline plasmid purification kit either the NucleoSpin Plasmid Quick Pure (Macherey-Nagel), QIAprep Spin Miniprep (QIAGEN) or InnuPREP Plasmid Mini (AnalytikJena) according to the manufacturer protocol.

3.2.5.2 Midiprep DNA isolation

Selected colonies were picked from the plates with sterile toothpicks, transferred to 300 ml of LB with ampicillin (100 µg ml^{-1}) and subsequently incubated overnight at 37°C and 115 rpm. The plasmid DNA was isolated from the cells using an alkaline plasmid purification kit NucleoBond AX Midi (Macherey-Nagel) as suggested by producer.

3.2.6 Quick-change PCR

The Quick-change PCR method was used to generate the protein variant *Lb*ADH G37D (by introduction of the point mutation G114A in the corresponding gene *lbadh*) and to generate mutant library randomized at positions 42, 44 and 48. To obtain the desired mutations, a methylated dsDNA vector containing the insert of

interest and two mutagenic oligonucleotide primers are needed. During temperature cycling, the primers hybridize to opposite strands of the vector and the DNA polymerase extends them creating a novel mutated plasmid with stagged nicks. High fidelity DNA polymerases (*Pfu* or KOD) were used to avoid generation of additional mutations. The template vector was then digested by the endonuclease *Dpn*I, which is specific for methylated and hemimethylated DNA. The nicked plasmids are repaired after transformation of *E. coli* cells via cellular ligases.

3.2.6.1 Site-directed mutagenesis

The mutagenic primers contained G114A substitution which could subsequently remove the *Nae* I restriction site. The PCR was performed with *Pfu* proof reading DNA polymerase (NEB), pET21a-*Lb*ADH vector as a template and combination of mutagenic oligonucleotides, which contains the G114A substitution. Reaction took place in 50 µl volume using the Biometra^{T1} Thermocycler.

Table 3-2. Site-directed mutagenesis.

Reaction mixture:		**PCR Program:**		
40 ng	Template DNA	1 min	98°C	
10% (v/v)	Pfu Buffer (NEB)	30 sec	98°C	
0.2 µM	dNTPs	30 sec	60°C	x 25
0.2 µM	Each primer	7 min	68°C	
1U	*Pfu* pol	10 min	68°C	
	In dd H_2O	∞	4°C	

The PCR products were treated with *Dpn*I. 2 µL of *Dpn*I were added to 20 µL of non-purified PCR mixture and incubated at 37^{o}C for 2 hour. 5 µL of the treated plasmid was used for electroporation.
Plasmid DNA of obtained clones was analysed by a) restriction digest; b) sequencing.

3.2.6.2 Randomization of positions 42, 44 and 48

Randomization of the three codons was performed simultaneously by creating a set of PCR primers containing degenerate codons:
5'- CGGCACAGCGAT**NDT**GGT**WDT**AAAGCAGCT**NNK**AGTGTCGGC-3' and
5'- GCCGACACT**MNN**AGCTGCTTT**AHW**ACC**AHN**ATCGCTGTGGTGCCG-3'.
The PCR was performed with the proof reading KOD polymerase under following conditions shown in Tab. 3-10.
The PCR template was digested with *DpnI*. 2 µL of DpnI were added to 20 µL of non-purified PCR mixture and incubated at 37 ^{o}C for 3 hour. 20 µL of the treated

plasmid was used for electroporation.

Table 3-3. Codon randomization PCR.

Reaction mixture:		**PCR Program:**		
20-40 ng	Template DNA	3 min	94°C	
10% (v/v)	KOD Buffer	1 min	98°C	x 25
0.2 µM	dNTPs	1 min	57°C	
0.25 µM	Each primer	1 min	72°C	
1 mM	$MgSO_4$	8 min	72°C	
0.4 U	KOD pol	∞	4°C	
	In dd H_2O			

3.2.7 Restriction digest

Restriction of DNA fragments was performed according to recommendations of enzymes manufacturer. Corresponding buffers were supplied by manufacturer as well.

3.2.8 Sequencing

Sequencing reactions were carried out by Sequiserve. Each sequence was proofread in forward and reverse directions; T7 and T7rev were used for the sequencing of pET vectors. The ClustalX program was used to interpret sequencing results.

3.2.9 Agarose gel electrophoresis

Table 3-4. Agarose gel electrophoresis.

Buffer	**Component**	**Concentration**
0.5 TAE:	Tris	20 mM
	EDTA	0.5 mM
	Acetic acid	10 mM
DNA loading dye:	Bromphenol blue	0.05 % (w/v)
	EDTA	100 mM
	Glycerol	43 % (v/v)

1%-agarose gels were prepared in 0.5 × TAE buffer. For each gel 50 ml of molten agarose was used resulting in a gel thickness of approximately 5-7 mm. Ethidium bromide was added to the final concentration of 0.01% (v/v). The DNA/loading dye mixture (6-10µl) was loaded into each well. 5 µl of a DNA ladder mix (Fermentas) was pipetted into the first lane. Samples were electrophoresed at 135 V for 25 min.

After electrophoresis, DNA was visualized under UV light and documented using EagleEyeII videosystem.

3.2.10 SDS-PAGE

Proteins were visualized on the SDS-polyacrylamide gels as described by Laemmli [194]. Protein SDS-PAGE gel was typically composed of two layers. The top layer served as the stacking gel, and it comprised about 10-20% of the gel height. The lower layer, which comprised the remaining portion of the gel, was the separating one. The difference in pH and acrylamide concentration at the stacking and separating gel functions to compress the sample at the interface and provides better resolution and sharper bands in the separating gel.

Table 3-5. SDS PAGE stock solutions

Stacking gel	5% (v/v)	Polyacrylamide	**5xProtein loading buffer:**	0.15 % (w/v)	Bromphenol blue
	0.125% (w/v)	SDS		25 mM	Tris-HCl
	0.125% (w/v)	APS		50 % (v/v)	Glycerol
	0.25% (v/v)	TEMED			In ddH_20, pH 6.8
	125 mM	Tris-HCl	**1xRunning buffer**	25 mM	Tris-HCl
		In ddH_2O, pH 6.8		129 mM	Glycine
				0.1% (w/v)	SDS
Separating gel	12% (v/v)	Polyacrylamide			In ddH_20, pH 8.3
	0.1% (w/v)	SDS	**Coomassie solution**	0.1%	Coomassie Brillant Blue R-350
	0.1% (w/v)	APS		50%	Ethanol
	0.1% (v/v)	TEMED		10%	Acetic acid
	375 mM	Tris-HCl			In ddH_20
		In ddH_2O, pH 8.8			

Before the electrophoresis protein samples were mixed with a 5x loading buffer and heated up at 95 ^oC for 5 min. Whole cell samples were mixed with 45 µl of 1x-loading buffer and incubated at 95 ^oC for 15 min. PAGE Ruler Prestained Protein Ladder (Fermentas) served as a molecular weight marker. Gels were always prepared freshly and run in vertical electrophoresis apparatus (BioRad) at 150 V

for 1 hour in 1x running buffer. The gels were rinsed with water and stained for 1 h in Coomassie solution with subsequent destaining for 12 h in distilled water.

3.3 Chromatographic purification of proteins

3.3.1 Ion-exchange purification of *Lb*ADH and its variants

Purification of the wild type *Lb*ADH and *Lb*ADH G37D was performed at room temperature by ion exchange chromatography [195]. An automated pump system Äkta was used; it allowed to collect sample fractions and to monitor constantly the volume of liquid, UV_{280} signal, conductivity and pressure.

The frozen cell pellets, containing the protein of interest, were thawed on ice for 30 min in 40 ml of lysis buffer and disrupted by sonication (4 cycles x 3 min with 3 min gaps, 70 mV, 4°C). After sonication, cell debris was removed by centrifugation (40 min, 18000 rpm, 4°C).

Table 3-6. Buffers for ion exchange chromatography of *Lb*ADH.

Buffer	Component	Concentration
Lysis buffer	Tris	100 mM
	$MgSO_4$	1 mM
	Lysozime	1 mg ml^{-1}
	in ddH_2O, pH 7.5	
Equilibration buffer	TEA	50 mM
	$MgCl_2$	1 mM
	in ddH_2O, pH 7.2	
Elution buffer	TEA	50 mM
	$MgCl_2$	1 mM
	NaCl	1 M
	in ddH_2O, pH 7.2	

The 25 ml column filled with Q-Sepharose beads was assembled into the Äkta purifier (Amersham Biosciences) and washed with 125-150 ml of the equilibration buffer until the UV_{280} signal was stable. The supernatant was filtered (4.5 µm pore size) and applied to the column under the constant flow rate of 1 ml min^{-1}. Subsequently, the column was treated again with the equilibration buffer until the non bounded protein was washed out and the UV_{280} signal was stable. The desired protein was eluted from the column in 10 ml fractions by application of an isocratic NaCl-gradient from 0 to 100% of the 1 L of elution buffer over a fixed period of 150 min. The fractions were subjected to the *Lb*ADH activity assay and the Bradford

test (described below). The fractions with the highest values of specific activity and protein concentration were combined for the desalting step (see section 3.3.3).

3.3.2 Ion-exchange purification of *T*ADH

Purification of *T*ADH took place at room temperature by ion exchange chromatography using automated pump system Äkta. The volume, UV_{280} signal, conductivity and pressure were constantly monitored. The cell pellets were thawed for 30 minutes in 30 ml of lysis buffer and disrupted by ultrasonication (4 cycles x 3 min with 3 min gaps, 70 mV, 4°C). The cells fragments were sedimented by centrifugation (40 min, 18000 rpm, 4°C).

The supernatant was filtered (4.5 µm pore size) and applied to a 25 ml Q-Sepharose column, which was preliminary equilibrated with at least five volumes of the equilibration buffer. The unbound molecules were removed by sequential column washing with the equilibration buffer. Afterwards the target protein was eluted by slow pumping of the elution buffer (without gradient). Elution fractions were collected and analyzed for enzymatic activity and protein concentration. The fractions with the highest values of specific activity and protein concentration were desalted and lyophilized.

Table 3-7. Buffers for ion exchange purification of *T*ADH.

Buffer	Component	Concentration
Lysis buffer	Kpi Lysozyme in ddH_2O, pH 7.5	50 mM 1 mg ml^{-1}
Equilibration buffer	Kpi in ddH_2O, pH 7.5	50 mM
Elution buffer	Kpi NaCl in ddH_2O, pH 7.5	50 mM 1 M

3.3.3 Desalting of proteins

Gel filtration was exploited to desalt the proteins. The 1 L column filled with Sephadex G25 material (Pharmacia) was connected to the automated pump system Äkta and equilibrated with at least 1 L of desalting buffer with a pumping rate of 10 ml min^{-1}. The collected elution fractions of enzyme, which had been obtained after ion-exchange purification step, were applied to the column and eluted in desalting buffer. To remove the remaining salt, the Sephadex G25 column was washed with 1 L of ddH_2O and 1 L of 20% Ethanol after use.

To desalt smaller protein amounts 5 ml Sephadex G25 columns (GE Healthcare) were used. Therefore, the columns were equilibrated with 25 ml of desalting buffer

under gravitation flow. Then 2.5 ml of the protein solution obtained from the ion-exchange purification step was applied onto each column. Finally, the protein was eluted by addition of 4.5 ml of desalting buffer.

Table 3-8. Desalting buffers.

Protein	Component	Concentration
*Lb*ADH	TEA	10 mM
	$MgCl_2$	1 mM
	in ddH_2O, pH 7.5	
*T*ADH	Kpi	10 mM
	in ddH_2O, pH 7.5	

3.3.4 Lyophilisation

Enzymes were diluted in corresponding desalting buffer to a final concentration of 1 mg ml^{-1}. The obtained protein solution was divided into aliquots of approximately 150 ml, frozen at -20°C and freeze-dried under vacuum in the LyoLac lyophilizator.

3.4 Analytical methods

3.4.1 Determination of the protein concentration

Table 3-9. Bradford reagent composition.

Bradford solution	Coomassie Brilliant Blue G-250	100 mg l^{-1}
	Ethanol	5% (v/v)
	Phosphoric acid in ddH_2O	8.5% (v/v)

The amount of protein was determined by the Bradford method [196], which is grounded on the ability of the dye Coomassie Blue G25 to interact with the protein, this results in a shift of the absorption maximum to a wavelength of 595 nm. 100 µl of a sample solution was added to 900 µl of Bradford solution and incubated at room temperature for 15 min to allow the protein binding to proceed. Afterwards, the OD_{595} was measured against a buffer control. The protein concentrations were determined by using a standard curve, created in advance with a BSA reference sample and its dilutions.

3.4.2 *Lb*ADH activity assay

3.4.2.1 Photometric assay

*Lb*ADH activity was determined spectrophotometrically by monitoring the changes of NAD(P)H absorbance at 340 nm. Acetophenone reduction and isopropanol oxidation served as model reactions.

Substrate and cofactor solutions were prepared separately; the cofactor solution was kept on ice. The standard reaction mixture consisted of following components:

- 970 µl substrate solution,
- 20 µl cofactor solution, and
- 10 µl enzyme.

Just before the kinetic measurement the cofactor solution was mixed with the substrate solution in a plastic cuvette and pre-incubated at 30°C for 5 min inside the photometer. The enzymatic reaction was started by addition of appropriately diluted *Lb*ADH; kinetic detection was started immediately after short mixing by measuring absorbance$_{340}$ against air as a reference. The reactions were followed for 1 min at 30°C. Initial reaction rates were calculated according to equation 3-1.

Table 3-10. *Lb*ADH activity assay.

Buffer	Substrate reduction		Substrate oxidation	
Substrate solution	50 mM 1 mM 11 mM	TEA $MgCl_2$ Acetophenone in ddH_2O, pH 7.0	50 mM 1 mM 200 mM	TEA $MgCl_2$ Isopropanol in ddH_2O, pH 7.0
Cofactor solution	9.5 mM	NAD(P)H in 50 mM TEA, 1 mM $MgCl_2$, pH 7.0	9.5 mM	$NAD(P)^+$ in 50 mM TEA, 1 mM $MgCl_2$, pH 7.0

The result of enzyme activity in a cuvette accounts for:

$$Activity(U/ml) = \frac{\Delta A/\min}{\varepsilon \bullet d} \qquad (3\text{-}1),$$

where:

- ΔA/min is a change of absorbance at 340 nm per minute,
- $\varepsilon_{NAD(P)H}$ = 6.22 ml µmol^{-1} cm^{-1},
- d stays for the optical pathway in cm.
- Taking into consideration dilution of the enzyme stock solution:

$$Activity(U/ml) = \frac{\Delta A/\min \bullet V_{total} \bullet f_{dilution}}{\varepsilon \bullet d \bullet V_{enzyme}} \qquad (3\text{-}2),$$

where:

- ΔA/min is a change of absorbance at 340 nm per minute,
- V_{total} represents the volume of an assay solution in µl,
- $f_{dilution}$ stays for the dilution factor of an enzyme stock solution,
- V_{enzyme} is the volume of an added enzyme in µl.

Duplicate or triplicate measurement was performed for every tested enzyme probe. Average enzymatic activity was accounted as a result.

3.4.2.2 Microtiter plate based assay

To screen *Lb*ADH G37D variants cultivated in 96-well plates for enzymatic activity, the acetophenone activity assay was used as well. First, the cell pellets obtained as described in section 3.2.4.3 were thawn down at room temperature and lysed by addition of 100 µl of Bugbuster Master Mix (Novagen, USA) and incubated for an additional 1 h at room temperature. Then, the crude extracts were diluted 1:400 in buffer (Tab. 3-18), and 20 µl aliquots of the diluted crude extracts were transferred to an optically transparent 96-well microtiter plate (Greiner Bio-One). The reaction was started by addition of 180 µl of assay solution (Tab. 3-18) to each well and took place for 10 min at 30°C. The enzymatic activity was measured by following the NADH decay at 340 nm in a 96-well format (SpectraMax).

Table 3-11. Microtiter plate based assay for *Lb*ADH enzymatic activity.

Buffer	Component	Concentration
Dilution buffer	TEA	10 mM
	$MgCl_2$	1 mM
	in ddH_2O, pH 7.0	
Assay solution	TEA	50 mM
	$MgCl_2$	1 mM
	Acetophenone	11 µM
	NADH	0.19 mM
	in ddH_2O, pH 7.0	

3.4.3 *T*ADH activity assay

Activity of *T*ADH was detected spectrophotometrically as well. The oxidation of 1-propanol was chosen as a model reaction. The reaction progress was monitored by following the increase of the absorbance at 340 nm, caused by reduction of the cofactor NAD^+.

The standard reaction mixture contained in a total volume of 1 ml:

- 970 µl substrate solution,

- 20 µl cofactor solution, and
- 10 µl enzyme.

Table 3-12. *T*ADH activity assay.

Buffer	Component	Concentration
Substrate solution	Glycine 1-Propanol in ddH_2O, pH 10.0	50 mM 25 mM
Cofactor solution	NAD^+ in ddH_2O	10 mM

Substrate and cofactor solutions were prepared separately. The first one was preheated at 65°C in a thermocase, the second one was kept on ice. Just before the kinetic measurement 20 µl of the cofactor solution was added to 970 µl of the substrate solution in a plastic cuvette and thermostated inside the photometer at 65°C for 5 min. Reaction was started by addition of 10 µL of appropriately diluted *T*ADH. The increase of $absorbance_{340}$ was monitored against air as a reference at 65°C for 1 min. *T*ADH activity was calculated as described above.

3.4.4 *Ff*ADH activity assay

Table 3-20. *Ff*ADH activity assay.

Buffer	Component	Concentration
Substrate solution	Tris Isopropanol in ddH_2O, pH 7.5	50 mM 25 mM
Cofactor solution	NAD^+ in 50 mM Tris, pH 7.5	10 mM

*Ff*ADH activity was determined spectrophotometrically by monitoring the increase of NADH absorbance at 340 nm. Oxidation of isopropanol was chosen as model reactions.

As described above, the substrate and the cofactor solutions were prepared separately according to the table 3-20; the cofactor solution was kept on ice. The standard reaction mixture consisted of following components:

- 970 µl substrate solution,
- 20 µl cofactor solution, and

- 10 µl enzyme.

The enzymatic reaction was started by addition of appropriately diluted *Lb*ADH; kinetic detection was started immediately after short mixing by measuring absorbance$_{340}$ against air as a reference. The reactions were followed for 1 min at 30°C; three replicate measurements were performed. Initial reaction rates were calculated according to equation 3-1.

3.4.5 Water activity adjustment

The water activity (a_w) values were set up in desiccators using the "saturated salt solutions" method. The LiCl, $Mg(NO_3)_2$, NaCl and K_2SO_4 were implemented to create a_w of 0.1, 0.3, 0.5 and 0.9, respectively. Lyophilized aliquots of both enzymes were opened and equilibrated in dissicator at mentioned a_w for 24 h and then subjected to analysis.

3.5 Enzyme characterization

3.5.1 *Lb*ADH thermostability studies

3.5.1.1 Thermostability in the dissolved state

*Lb*ADHwt and *Lb*ADH G37D were dissolved in dilution buffer (Table 17) to the final concentration of 0.1 mg ml^{-1} and divided into 100 µl aliquots. The samples were placed in a thermocase and heated at 30-70°C for different time intervals, taken off, and assayed for residual enzymatic activity and protein concentration as described above. The inactivation curves were described by second-order exponential decay model; half-life of enzymatic activity was manually extracted from the plot. Three independent inactivation curves were obtained for every temperature, the average half life was accounted as a result.

3.5.1.2 Thermostability in the solid state

*Lb*ADHwt and *Lb*ADH G37D were dissolved in dilution buffer (Table 17) to the final concentration of 0.1 mg ml^{-1}, divided into 100 µl aliquots, frozen at -20°C and lyophilized. The solid samples were incubated in a thermocase at 30-80°C for different time intervals, taken off, cooled down on ice and redissolved in 100 µl ddH_2O. The residual enzymatic activity and protein concentration of the

redissolved samples were measured. The data were plotted and half-life of enzymatic activity was manually extracted from the plot. Three independent inactivation curves were obtained for every of the investigated temperatures, yielding the average half-life.

3.5.2 High-throughput screening of *Lb*ADH G37D variants for enhanced thermostability

3.5.2.1 Screening in the dissolved state

Crude extracts of *Lb*ADH G37D variants were prepared as described above. Then, the crude extracts were diluted 1:400 in dilution buffer (Table 17), and 80 µl aliquots of the diluted crude extracts were transferred to two 96-well PCR plates. The first plate was immediately subjected to the enzymatic activity assay, as described in the section 3.3.2.2. The second plate was incubated at 50°C for 10 min in a PCR cycler, cooled down, and screened for the residual enzymatic activity (section 3.3.2.2). To obtain reliable results, the residual activity values determined after screening on the heated variants (the 2nd plate) were normalized to the activity values of the intact samples (the 1st plate). The ration calculated in this manner for the *Lb*ADH G37D equaled to 0.5. Variants, which displayed a ratio >0.75 were considered as thermostabilized.

3.5.2.2 Screening in the solid state

ADH variants were screened for improved thermostability in the solid state as well. For that purpose the crude extracts were diluted in ddH_2O 1:200. The diluted samples were transfered to a PCR plate (100 µl pro well), then frozen at -20°C and lyophilized. After lyophilization of the samples the PCR plates were heated in a PCR cycler to 80°C for 10 min. After cooling, the samples on ice for 1-2 min they were redissolved in 100 µl ddH_2O and screened for their residual enzymatic activity as described above.

Enzymatic activity was determined spectrophotometrically by monitoring the NADH decay at 340 nm in a 96-well format. The assay mixture was composed of 22 mM acetophenone, 380 µM NADH and 2 mM $MgCl_2$ in 100 mM TEA buffer, pH 7.0. Just before the kinetic measurement 100 µl of the redissolved enzymatic samples were added to the assay solution. Kinetic measurement was started immediately and took place for 10 min at 30°C.

3.5.2.3 Validation of the screening system

Protein variants were screened for improved thermostability in a solid state as well. For that purpose 20 µl aliquots of the crude extracts were transferred to 96-well PCR plates. Afterwards 380 µl of ddH_2O was added in each well, creating dilution of the crude extract 1:20. The diluted samples were transferred to a PCR plate (100 µl pro well), then frozen at -20°C and lyophilized. After lyophilization of the samples the PCR plates were heated in a PCR cycler at 80°C for 10 min. After cooling, the samples were redissolved in 100 µl ddH_2O and screened for their residual enzymatic activity as described above.

Enzymatic activity was determined spectrophotometrically by monitoring the NADH decay at 340 nm in a 96-well format. The assay mixture was composed of 22 mM acetophenone, 380 µM NADH and 2 mM $MgCl_2$ in 100 mM TEA buffer, pH 7.0. Just before the kinetic measurement 100 µl of the redissolved enzymatic samples were added to the assay solution. Kinetic measurement was started immediately and took place for 10 min at 30°C.

The reliability of the quantitative results obtained by this HTS assay was evaluated by analyzing a control plate containing *E. coli* BL21(DE3) clones overexpressing the *Lb*ADH G37D variant. The following statistical parameters were applied [197]:

$$S/B = \mu_s/\mu_b \quad (3\text{-}3),$$

The signal to background ratio, which indicates separation of positive and negative controls. The value S/B is assay-dependent; usually the S/B above 3 is considered to be sufficient.

$$S/N = \frac{\mu_s \quad \mu_b}{\sqrt{\sigma_s{}^2 + \sigma_b{}^2}} \quad (3\text{-}4),$$

The signal-to-noise ratio, which evaluates separation between a signal and the background. S/N should be higher than 10.

$$CV = \frac{100 \times \sigma_s}{\mu_s} \quad (3\text{-}5),$$

The coefficient of variation, estimating signal variation; less than 10% is acceptable.

$$Z = 1 - \frac{3\sigma_s + 3\sigma_b}{\mu_s - \mu_b} \quad (3\text{-}6).$$

The Z factor, a specific statistical parameter for HTS assays characterization. It relatively indicates separation of the signal from the background. Z factor should be lower than 0.4.

In the formulas S stays for the signal, B for the background, N for the noise, µ for the mean value and σ for the standard deviation.

3.5.3 Cofactor thermostability studies

3.5.3.1 Thermostability in the dissolved state

NADPH and NADH were diluted in 50 mM TEA buffer, pH 7.2, to the final concentration of 9.5 mM. The solutions were divided into 100 µl aliquots and heated in a thermocase at 30-70°C for 0-8 h. The half-life was determined by measuring the residual reducing activity in the standard activity assay by following the decay of absorbance at 340 nm. *Lb*ADHwt enzymatic assay was used to measure the residual reducing activity of the heat-treated NADPH samples, *Lb*ADH G37D was taken for the NADH probes. The enzymatic assay was performed as described in the section 3.4.2.1. The highest activity value was taken as 100% and used to normalize the rest of the data. The cofactor concentration in the heat-treated probe was 9.5 mM. The absorption and the enzymatic activity tests were performed with 0.19 mM of cofactor, which resulted from dilution of the previously mentioned 9.5 mM probe.

The cofactor degradation curves were fitted with a single order exponential decay model given by Eq. 3-7 and 3-8 and the deactivation constant k_d were determined.

$$A = Ao \cdot \exp^{-k_d \cdot t} \quad (3\text{-}7)$$

$$v = v_0 \cdot \exp^{-k_d \cdot t} \quad (3\text{-}8)$$

where:

- A stays for absorbance at 340 nm
- u represents reaction rate in U ml^{-1}
- *t* is time, min.

The half life time $t_{1/2}$ of the enzyme in the gas/solid reactor was calculated through:

$$t_{1/2} = \frac{\ln 2}{k_d} \quad (3\text{-}9).$$

Three independent curves were obtained for every investigated temperature, the average half-life was taken as a result.

3.5.3.2 Thermostability in the solid state

Solid samples of NADPH and NADH were exposed to 50°C for a time period of 0-24 days, then redissolved in 50 mM TEA buffer (pH 7.2) and tested for absorption at 340 nm and reducing activity (*Lb*ADHwt enzymatic assay was performed with NADPH samples, *Lb*ADH G37D with NADH probes). The highest activity value was taken as 100% and used to normalize the rest of the data. This experiment was performed only.

3.5.4 Determination of substrate spectrum

Enzymatic activity was investigated for a broad range of substrates. Both the oxidation and the reduction propertied were tested. The substrate concentration was always 10 mM. The measurement was performed at the respective optimal pH-values using standard parameters of the photometric assay, in triplicates.

3.5.5 Determination of temperature optimum

Dependence of the reaction rate on the temperature was examined in a range from 25°C to 75°C under otherwise standard assay conditions. Before the reaction was started 20 µl of the cofactor solution was added to 970 µl of the substrate solution in a plastic cuvette and thermostated inside the photometer until it reached the desired temperature (checked with external thermometer). The effect of temperature on the cofactor absorbance was measured at 340 nm for 1 min against and frozen at -80°C until futher use air as a reference. After this, the reaction was started by addition of 10 µL of the appropriately diluted enzyme. The change of absorbance$_{340}$ was followed for 1 min. Enzymatic activity was calculated according to the formula:

$$Activity(U/ml) = \frac{(\Delta A_{enz} - \Delta A_{cof}) \bullet V_{total} \bullet f_{dilution}}{\varepsilon \bullet d \bullet V_{enzyme}} \qquad (3\text{-}10),$$

where:

- ΔA_{enz} is a change of absorbance at 340 nm per minute after the reaction was started,
- ΔA_{cof} is a change of absorbance at 340 nm per minute caused by temperature-induced degradation of cofactor,
- V_{total} represents the volume of an assay solution in µl,
- $f_{dilution}$ stays for dilution factor of an enzyme stock solution,
- V_{enzyme} is a volume of an added enzyme in µl
- $\varepsilon_{NAD(P)H} = 6.22$ ml / µmol / cm.

Every activity value was measured in triplicates.

3.5.6 Determination of pH optimum

The influence of pH on enzymatic activity was determined in the pH range of 4-12 and otherwise under standard assay conditions. Concentration of buffering component was always 50 mM.

Table 3-21. Buffers for pH optimum determination.

pH range	Buffering component
4.0-5.5	Sodium acetate
6.0-7.0	Kalium hydrogen phosphate
7.5-8.5	Tris-HCl
9.0-11.5	Glycine

3.5.7 Determination of kinetic parameters

Kinetic parameters were determined based on initial rate measurements depending on the substrate concentration. The cofactor concentration was always kept 9.5 mM to fulfil the requirements of spectophotometric assay. All measurement was performed at least in duplicates.

Equation 3-11 was used as a fitting model:

$$\upsilon o = \frac{\upsilon_{\max} \cdot S}{K_m + S} \quad (3\text{-}11),$$

where:

- v represents the reaction rate [U/mg],
- S is substrate concentration [mM],
- K_m stays for Michaelis-Menten constant [mM].

3.6 Spectroscopic studies of enzyme thermostability

3.6.1 Tryptophan fluorescence spectroscopy

3.6.1.1 Theoretical principles of the tryptophan fluorescence spectroscopy

Fluorescence spectroscopy is a sensitive analytical method, which can be used to obtain qualitative and quantitative information about protein structure, tracking of solvation dynamics and to follow the progress of biochemical reactions. The molecular principles of fluorescence are usually illustrated by the Jablonski diagram (Fig.1-13).

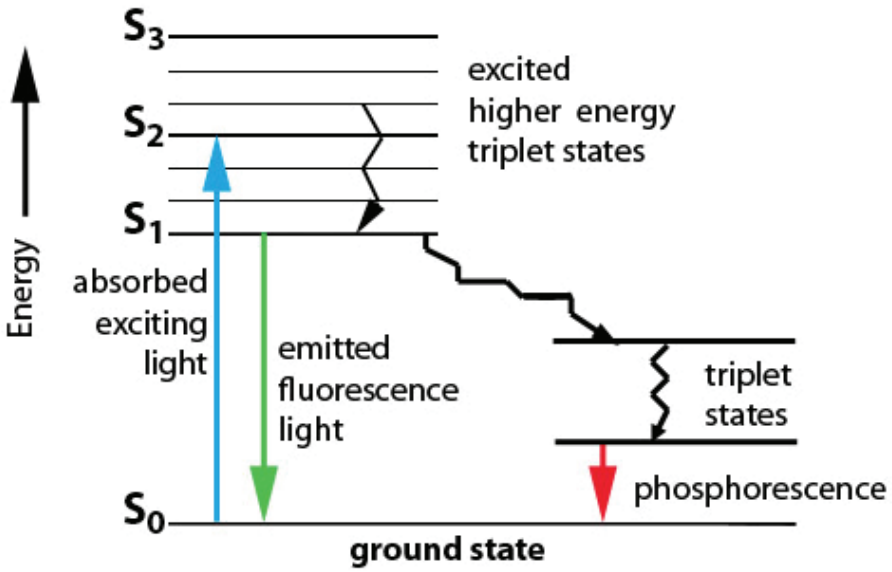

Figure 3-1. Jablonski diagram. Singlet electrons in the ground, 1st, 2nd and 3rd states are depicted as S_0, S_1, S_2 and S_3 [199].

Absorption of UV/Vis light energy by a certain molecule called fluorophore causes excitation of its electrons to higher energetic states called singlet states (S_1, S_2 … S_n) illustrated by bold solid lines in the Jablonski diagram. Each of these electronic states, in its order, contains a number of vibrational states (thin lines in the Jablonski diagram). After excitation, an electron rapidly looses its energy by a variety of processes. It may relax to the lowest vibrational level of the S_1 (interconversion), may be "quenched" by solvent relaxation (external conversion) or might enter the triplet state by intersystem crossing (due to spin-orbit coupling between singlet and triplet states). Return from the excited electronic state S_1 to the ground state S_0 by emission of a photon causes fluorescence, whereas transition $T_1 \rightarrow S_0$ results in phosphorescence [198]. Due to the excitation to higher electronic/or vibrational singlet states and the rapid loss of energy by interconversion to the S_1 state from that fluorescence emission occurs, the as fluorescence emitted photons are always of lower energy then the photon absorbed by the fluorophore. Therefore, the emission spectrum is shifted to the red relative to the absorption spectrum (Stokes shift) [198].

An important characteristic of a given fluorophore is the quantum yield, which is defined as the ratio of the number of emitted photons to the number of absorbed photons. It is given by:

$$Q = \frac{\Gamma}{\Gamma + k_{nr}} \qquad (3\text{-}12),$$

where:

- Q stays for the quantum yield,
- Γ represents the fluorophore emission rate in relative units, and

- k_{nr} is the rate of non-radiative loss of energy in relative units.

With respect to the protein, all fluorophores can be classified into intrinsic and extrinsic. Intrinsic protein fluorescence is normally caused by aromatic amino acids such as tryptophan, tyrosine and phenylalanine and/or bound molecules, like cofactors (NAD(P)H, FAD or FMN [200]), chromophores, pigments. Due to their relatively high quantum yield and extinction coefficient tryptophan residues dominate the intrinsic protein absorption and fluorescence [198, 201]. Tyrosine has a quantum yield similar to tryptophan, but displays emission of narrower distribution on the wavelength scale (Fig. 1-14 B). In native proteins tyrosine emission is barely seen, because it can be absorbed by tryptophan residues [198, 201]. Since excited electrons of phenylalanine possess very low quantum yield, its fluorescence properties can be neglected [198]. Since both tryptophan and tyrosine strongly absorb at around 280 nm (Fig. 1-14 A), exclusive investigation of the tryptophan contribution has to be performed by excitation at 295 nm [201], a wavelength where the excitation of tyrosine is neglectable.

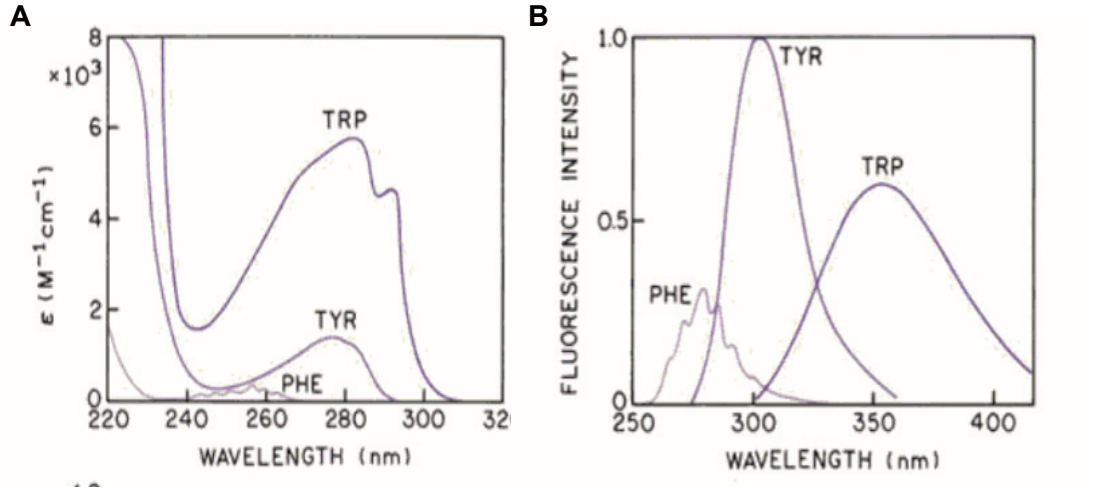

Figure 3-2. Absorption (A) and emission (B) spectra of aromatic amino acids in water, pH 7.0 (reprinted from Lakowicz, 2006 [198]).

Like for all fluorophores, the fluorescence emission of tryptophan is sensitive to the micro-environment of the fluorophor [201], and can be exploited to monitor conformational changes in the 3D protein structure. In a hydrophobic surrounding of the protein core Trp has a high quantum yield and, consequently, high emission intensity. Enzyme unfolding leads to exposure of tryptophan residues to the solvent, which causes the red shift of emission maxima and the loss of signal intensity [198, 200, 201]. Thus, protein intrinsic fluorescence spectroscopy can be used for accurate monitoring of protein unfolding kinetics and detection of stable folding intermediates [200]. The reduced nicotinamide ring of NAD(P)H is fluorescent, with absorption and emission maxima at 340 nm and 460 nm, respectively [198]. FMN and FAD, in contrast, are strongly fluorescent only in their

oxidized form. They absorb approximately at 450 nm and emit at 495 nm and 525 nm [198]. Fluorescence intensity changes upon protein binding to the cofactor, can also be used for certain structural studies [198]. For some tasks, such as investigation of non-fluorescent enzymes or protein surface studies, the labeling with extrinsic fluorophores might be required. Usually, extrinsic fluorophores,such as fluorescein and rhodamides, can be attached to the protein in a site-specific or random manner. They have longer excitation and emission wavelengths (usually in the visible region of the spectrum), than the intrinsic ones [198]. The majority of these compounds are commercially available.

3.6.1.2 Experimental setup

The fluorescence protein spectra were recorded in Perkin Elmer LS 50B fluorescence photometer at 25°C. Excitation was performed at 295 nm to minimize interference from tyrosine fluorescence. The tryptophan emission spectra were measured in the range from 300 to 450 nm with a speed of 120 nm min^{-1}, excitation and emission slits were adjust to 7.5 nm; a quartz cuvette with 1 cm optical pathway was used. Each spectrum was an average of three scans, which were corrected by base-line spectra recorded in buffer.

Effect of denaturants was studied first. The aliquots with 0.1 mg ml^{-1} of wt *Lb*ADH and *Lb*ADH G37D in 0-8 M urea or 0-6 M GdnCl were incubated at room temperature for 24 h, placed into the quartz cuvette and investigated for their spectral characteristics. Subsequently, the residual enzymatic activity of the enzyme samples was checked.

Thermal denaturation of the dissolved proteins was investigated in the following manner: 0.1 mg ml^{-1} solution of wt *Lb*ADH or *Lb*ADH G37D in 10 mM TEA, 1 mM $MgCl_2$ buffer at pH 7.2 was divided into aliquots of 800 µl each, then directly heated at 50°C for different time intervals and subjected to analysis by fluorescence spectroscopy in correlation with the residual enzymatic activity.

Investigation of thermal denaturation of the solid enzyme samples was more complicated. 1 mg ml^{-1} solution of wt *Lb*ADH or *Lb*ADH G37D in 10 mM TEA, 1 mM $MgCl_2$ buffer at pH 7.0 was divided into aliquots of 100 µl each as before, then frozen at -20°C and lyophilized. After lyophilization the solid enzyme samples were equilibrated with saturated salt solutions for 24 h to reach defined values of water activity, then heated at 80°C, cooled down to room temperature, re-dissolved in 800 µl of distilled water and immediately tested for fluorescence properties in correlation with the residual enzymatic activity.

3.6.2 CD spectroscopy

3.6.2.1 Theoretical principles of the CD spectroscopy

Circular dichroism (CD) spectroscopy is a variation of UV/Vis absorption spectroscopy, and is based on interaction of circular polarized light with optically active molecules. Linearly polarized light can be described as a superposition of two circularly polarized light components. If the linearly polarized light passes through an optically active substance, its plane of vibration is rotated by an angle α. This phenomenon is called optical rotatory dispersion and is caused by the different speed of left- and right circulary polarized light waves in a chiral medium. Additionally, one of the circulary polarized components can be absorbed to a larger extent than another due to different absorption coefficient. This phenomemom is called circular dichroism [202].

Differential absorbtion of left- and right circulary polarized light components results in elliptically polarized light. Therefore, CD is historically reported as a quantity called ellipticity (θ). By definition,

$$\tan(\theta) = \frac{E_R - E_L}{E_R + E_L} \qquad (3\text{-}13),$$

where:

- E_R and E_L stay for the amplitudes of the electric field vectors of the right-circularly and left-circularly polarized light in N C^{-1}.

Practically, elipticity is determined automatically as

$$\theta = \frac{180}{4\pi} \ln(10) * (\varepsilon_L - \varepsilon_R) * c * d \qquad (3\text{-}14),$$

where:

- ε_L and ε_R are absorption coefficients of the right-circularly and left-circularly polarized waves in mol^{-1} cm^{-1},
- c represents concentration of a chiral substance in mol, and
- d stays for the optical pathway in cm [202].

Measuring the ellipticity as a function of wavelength gives a CD spectrum. Depending on the wavelength, both the positive and the negative circular dichroism can be observed [202].

Usually, CD signals of proteins are observed in two wavelength regions. The far-UV CD spectrum (170-250 nm) originates from the amide bonds and amino acid side chains [201]. It is particularly useful for analyzing the secondary structure of a protein: α-helix, β-sheet, and random coil elements contribute to the characteristic shape and magnitude of the CD band (Fig. 1-15) [203]. So, proteins rich in α-helices display two negative peaks at 222 nm and at 208 nm, and one positive peak near 192 nm [204, 205]. Interestingly, the amplitude of the peak at 222 nm is independent on the length of the α-helix, whereas the intensity of the two further

peaks is reduced in short helices [204]. β-sheets give rise to a negative peak at about 216 nm, a positive peak between 195 and 200 nm, and another negative band near 175 nm [204, 205]. Random coils give a strong negative CD signal below 200 nm, and a positive one up to 218 nm [205]. The relative content of each type of secondary structure in a protein can be calculated by deconvolution of the far-UV CD spectrum using component curves for assignment.
Aromatic amino acids give rise to a further CD signal in the near-UV region (250-300 nm). Disulfide bonds bring in minor CD bands at about 250 nm. However, often these contributions are small [201].

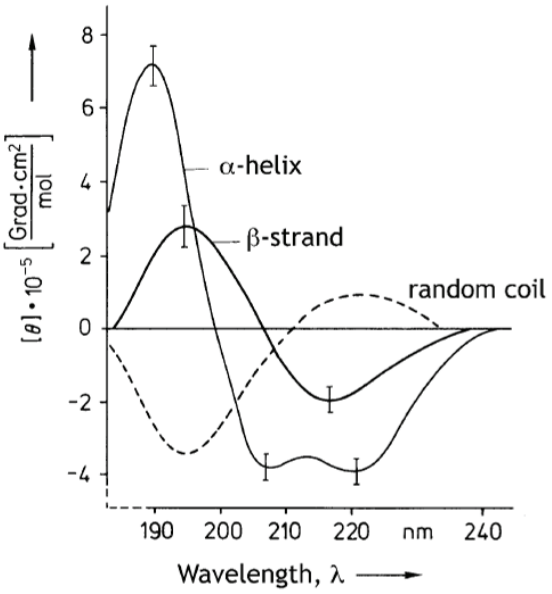

Figure 3-3. Conformational changes and CD spectra of poly-L-Lys in aqueous solution (according to Greenfield and Fasman, 1969) [203].

Due to drastic differences of CD spectra of folded and unfolded proteins, this technique is particularly sensitive for monitoring structural perturbations over a wide range of denaturing conditions, including high temperature [204]. Since the contribution of α-helices to the CD signal intensity predominates even in mixed α/β-proteins, the degree of helix→coil transition was chosen as a characteristic for the unfolding process [206]. Ellipticity at 222 nm serves for comparison of different spectra [205, 206].

3.6.2.2 Experimental setup

CD spectra of *Lb*ADHwt and *Lb*ADH G37D were recorded using a Jasco J-810 spectropolarimeter. The measurements were carried out in the range of 190 to 310 nm, with a scan rate of 50 nm min^{-1}. Dissolved proteins were investigated in a

quartz cuvette with 1 mm optical pathway, while the solid ones were immobilized by lyophilization on a quartz glass and covered with a second glass. Base line spectra, which were obtained either with buffer or with quartz glasses, were used to correct the data.

To study chemically induced unfolding, 0.1 mg ml^{-1} samples of *Lb*ADHwt and *Lb*ADH G37D in 0-8 M urea or 0-6 M GdnCl were prepared. After incubation at room temperature for 24 h, the CD spectra of the samples were recorded. The test of residual enzymatic activity followed the CD spectra measurement.

Two different experimental setups were exploited for investigation of the thermal degradation of *Lb*ADHwt and *Lb*ADH G37D in the dissolved and the solid state. First, protein solution was placed in a quartz cuvette and heated inside the CD-photometer cell with a speed of 1°C min^{-1}. Alternatively, enzymes were lyophilized on a quartz glass, covered with another one, placed in the CD polarimeter cell and heated up there. Temperature was varied over the range of 20-80°C with 5°C intervals. The CD spectra were recorded at the sample temperature, which excludes the possibility of protein renaturation. This method allowed usage of a single protein sample to monitor the conformational changes in a broad temperature range and to determine the midpoint of thermal inactivation curve (Tmd). However, it was impossible to test the residual enzymatic activity and to check the exact temperature values inside the photometer cell.

Second, 0.1 mg ml^{-1} solution of *Lb*ADHwt or *Lb*ADH G37D was divided into aliquots and incubated at certain temperatures (60°C for dissolved variants and 80°C for solid) in an external heating block. After redissolving in ddH_2O and investigation of the CD properties, the residual enzymatic activity and protein concentration were determined. In this case CD spectra were obtained at room temperature. The possibility of protein renaturation in solution could be excluded indirectly, through the activity values. Intact samples of *Lb*ADHwt or *Lb*ADH G37D were used as a reference in the both setups.

3.6.3 Static light scattering spectroscopy

3.6.3.1 Theoretical principles of the static light scattering spectroscopy

Static light scattering (Rayleigh scattering) spectroscopy is an important tool to characterize macromolecules. Physically, it is based on elastic scattering of electromagnetic waves by particles with a size smaller than the wavelength of the incident light beam [207]. The basic equation used in static light scattering spectroscopy is the Debye-Zimm relation:

$$Kc/\Delta R_\theta \cong \left\{1+\left(16\pi^2 R_G{}^2/3\lambda^2\right)\sin^2\left[(\theta/2)\right]\right\}\left[(1/M_w)+2Bc\right] \quad \text{(3-15)},$$

where:

$$K = 4\pi^2 n_0^2 (dn/dc)^2 / N_A \lambda^4 \quad (3\text{-}16)$$

and

$$R_\theta \approx I_\theta / I_0 \quad (3\text{-}18).$$

- θ is a scattering angle in rad;
- K represents an experimental constant dependent on solution properties;
- n_0 stands for refractive index of the solvent;
- λ is the wavelength of the light source in nm;
- dn/dc denotes an increment of the refractive index in mol^{-1};
- N_A is Avogadro number;
- I_0 and I_θ are intensities of the incident and scattered light at the angle θ in W m^{-2}, respectively;
- R_θ denotes the Rayleigh excess ratio;
- c symbolizes the solute concentration in mol;
- B stands for non-linearity;
- R_G represents the hydrodynamic radius of the investigated particle in m;
- M_w stands for the molecular weight in g mol^{-1}[207].

For particles of a size ≤ λ/20 (*e.g.* macromolecules), the angular dependence can be neglected, and M_w and R_G can be easierly obtained [207, 208]. Therefore, by measuring the intensity of light scattered from the sample one can deduce the molecular weight and the conformation of the target molecule. This can be used to determine the oligomeric state of the native protein or to elucidate the masses and the sizes of aggregated species [208, 209]. Macromolecular interaction challenges, such as self-association and aggregation [208, 210-213], reversibility of these processes [208, 214] and prediction of crystallization properties of an enzyme [215] are of increasing interest. Additionally, modern instrumentation and computational modeling allow the estimation of the stoichiometry of multicomponent protein complexes, *e.g.* receptor-ligand complexes, antibody-antigen complexes or protein-polymer complexes [215-217], and enable the elucidation of driving forces for intermolecular associations [212, 218].

3.6.3.2 Experimental setup

Static light scattering measurements were performed using a Perkin Elmer LS 50B fluorescence photometer at 450 nm (±15 nm slit). The scattering curve was obtained at a fixed angle of 90°, in a 400-500 nm range with a 5 nm slit and a scanning rate of 120 nm min^{-1}. For a single spectrum, 3 scans were accumulated. The spectra were corrected for the buffer base line. The scattering light intensity was determined at 450 nm. For the easier interpretation of results, the scattering light intensity was normalized to that one of the respective intact enzyme. Experiments with the previously heat incubated *Lb*ADHwt and *Lb*ADH G37D were

carried out at room temperature with. The samples were prepared as described in section 3.5.1.

3.7 Analytical procedures for separation and analysis of cofactor degradation products

3.7.1 HPLC setup

Hydrophilic interaction chromatography (HILIC) was used to separate cofactor degradation products. This method is a variant of normal phase chromatography and offers a sensitive alternative [219].

This technique consists of a hydrophilic stationary phase, which is modified with e.g. the following groups (diols, SiOH, NH_2 or zwitterionic methacrylate). The mobile phase is composed of an aqueous/organic solvent system, basically acetonitrile, in water respectively buffer (5-40%). This is a normal phase chromatography, but with reverse phase eluents. The order of elution in HILIC appears as an opposite elution to that seen in reversed phase separations. The polar analytes will be retained by partitioning between the water layer on the surface of the polar stationary phase [219]. The range of applications includes polar, mid polar and ionic compounds.

HPLC analyses were performed on an LC-10Ai series (Shimadzu, Kyoto, Japan) liquid chromatography system equipped with a SPD-M10Avp photodiode array detector, a RF-10AXL fluorescence detector, and a FRC-10A fraction collector. Data processing was carried out with LabSolution / LCSolution program.

For the separation, a ZIC-pHILIC-column PEEK (150°×°4.6°mm, I.D., 5°µm particle diameter, 200°Å pore size) (SeQuant, Marl, Deutschland) and a precolumn (20°×°2.1 mm, I.D.) filled with the same material were used. The PDA-detection wavelengths were set at 260°nm and 340°nm. The reduced cofactors NADH and NADPH were parallel monitored fluorometrically by activation at 340°nm and emission at 457°nm. The column oven temperature was maintained at 30°C.

The mobile phase was a mixture of 50 mM ammonium carbonate (pH 8.0) and acetonitrile (30:70). The mobile phases were filtered through a 0.2 µm Sartorius filter. The separation was performed by isocratic elution at a flow rate of 0.5 ml min^{-1}. The injection volume was 5 µL. The mobile phase was freshly prepared daily.

3.7.2 MS setup

The MS was operated in the positive and negative Enhanced MS (EMS) mode scanning from 100 – 900 Da with a LIT fill time of 2 msec and a scan rate of 4000 Da s^{-1}. The parameters used for all methods were optimized first performing a Flow

Injection Analysis (FIA) with NADH as a standard and led to the following parameter settings: IS -4500 V, Declustering Potential (DP) -145 V, Curtain Gas (N_2) 10 arbitrary units (au), Source Temperature 650°C, Nebulizer Gas (N_2) 50 au and Heater Gas (N_2) 20 au. CE and Q3-Entry barrier were set to -5 V and 8 V, respectively, to minimize fragmentation entering the LIT (line ion trap).
For structure elucidation/ confirmation of selected ions highly resolved mass spectra were recorded using a ESI-LTQ-FT Ultra (ThermoFisher Scientific, San Jose, CA, USA), equipped with a 7 T supra-conducting magnet and coupled with the chip-based micro-ESI system NanoMate (Advion BioServices, Ithaca, NY, USA).
The mass spectrometer, used in positive and negative mode, is tuned and external mass calibrated following a standard procedure for all voltages and settings with a calibration solution composed of caffeine, the peptide MRFA and ultramark. Therefore, the settings of the ion optics vary slightly from day to day. The transfer capillary temperature was set to 175°C. Hand cut fractions from the analytical HPLC were put in a 96-well plate (zero-carryover) and sprayed continuously by the NanoMate source. The automatic gain control (AGC) was set at 1E4 for ion trap MS scan and 5E5 for FTMS full scan, respectively. Fourier-transform mass spectra were recorded from 100 – 1000 Da at a resolution of 100.000 (at m/z 400), each scan consists from 30 transients.

3.8 Gas/solid reactor experiments

A continuous gas/solid enzymatic reactor was constructed by Kerasina Dimoula (RWTH Aachen) according to [18]. The reactor consisted of two units: saturation unit and operational unit. The saturation unit of the reactor was used to mix the gases under saturation conditions. It was operated at 45°C; N_2 was used as a carrier gas. Partial pressure of the mixture components (substrates and water) was adjusted by variation of the flow rate of the carrier gas through each flask containing reaction mixture components. The calculation was performed as described by Lamare et al. [3]. Total volumetric flow rate always equaled to 20 ml min^{-1}. The enzymatically catalyzed conversion took place in the reaction unit, which was operated at 40°C. The progress of the reaction was followed by means of an online gas chromatograph (GC) connected to the outlet of the reactor. The partial pressure of the reactants and products of the reaction mixture were measured by means of the online GC at 15 min intervals, during the reaction progress.

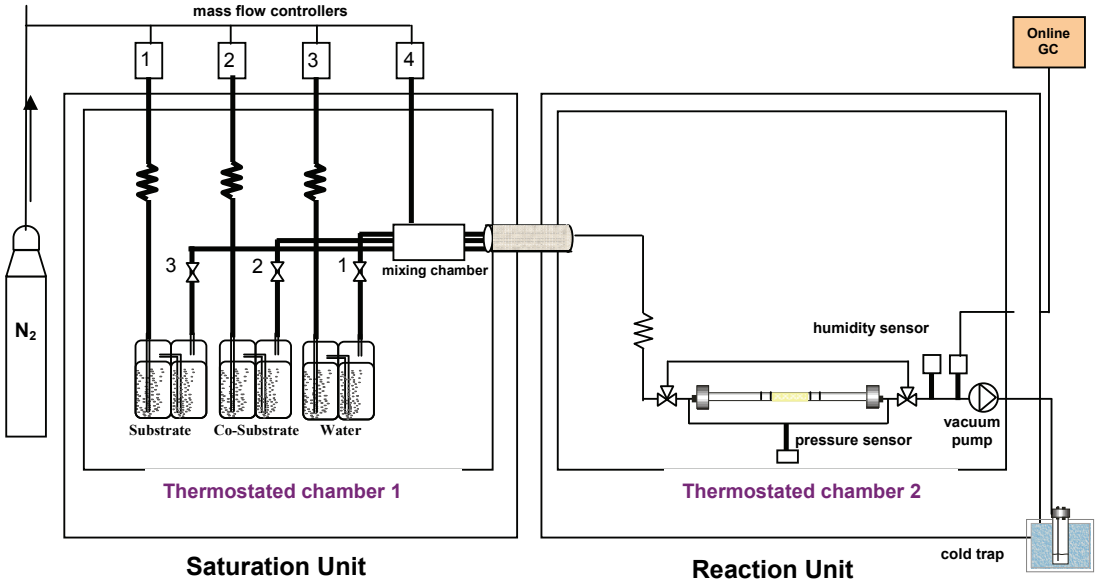

Figure 3-4. Schematic representation of a continuous gas/solid reactor. Adopted from Lamare et al. [3].

3.8.1 Enzyme immobilization on glass beads

The enzyme immobilization on the glass beads is based on a simple physical adsorption. The non-porous glass beads (0.450 – 0.600 mm in diameter, Sigma Aldrich) were first rinsed with distilled water 10-20 times and than dried at 100°C; 1 g of the clean beads was used for each immobilization.

The amount of wild type *Lb*ADH being immobilized was calculated based on its activity in solution. According to the experimental setup (planned by K. Dimoula), the reactor has to be operated under the substrate mass flow limit, which corresponds to the starting enzymatic activity equal or lower than 100 U per 1 g of beads. That "activity amount" is contained in 0.9 g of the wild type *Lb*ADH (2.8 mg of the lyophilizate from 21.12.07).

To produce comparable results with the wild type *Lb*ADH and the *Lb*ADH G37D, the same amount (e.g. 0.9 mg of protein per 1 g of beads) of both proteins was immobilized. It contained approximately 5 U of catalytic activity in the case of *Lb*ADH G37D. The amount of co-immobilized cofactor was calculated to give a 3:1 molar ratio to the protein subunits amount; the oxidized cofactor form was always used.

The protein and the cofactor were dissolved in 2 ml of 100 mM phosphate buffer (pH 7.5) and added to a falcon tube with 1 g of the glass beads (no additives, such as sucrose, were used). The components were mixed for 30 min at 4°C, and then the falcon was opened and placed into the vacuum desiccator, filled with silica particles. The pressure of 300 mbar was applied, and pre-immobilization continued for 3 h at 4°C. After that the pressure was lowered to 40 mbar, and immobilization

took place till the end.

3.8.2 Solid-gas reactor operation

To obtain necessary thermodynamic activity of each component of the reaction mixture, flow rate calculation was performed. After adjustment of the desired flow rates the solid-gas reactor was equilibrated with the resulting gas mixture for 6-7 h in disconnected mode. The acetophenone and isopropanol peaks on incorporated GC analytics had to stay constant, whereas the *(R)*-phenylethanol peak had to disappear. After that, 50 mg of glass beads with immobilized *Lb*ADHwt or 100 mg of glass beads with immobilized *Lb*ADH G37D were packed into the glass bed, the bed was placed inside the reactor in the disconnected mode and left there for 30 min to equilibrate temperature. The bed was then connected to the system, and the gas mixture was allowed to pass through reactor. Enzymatic conversion took place for 16-30 h, the reaction rates were monitored using incorporated automated GC.

Chapter 4 Results and Discussion

4.1 Comparative investigation of the thermal stability of NADH and NADPH

The cofactors NADPH and/or NADH, co-immobilized with the corresponding enzyme, are used in equimolar amounts for the reduction of ketones in a gas/solid reactor. Therefore, the stability of the solid cofactors is important for the stability of the overall biocatalytic system. In the liquid systems the oxidized and reduced cofactor molecules are able to diffuse from bulk solution to the binding site of the enzyme and reverse, making substrate coupled and enzyme coupled cofactor regeneration possible [93]. The situation is different in gas/solid biocatalysis, when the cofactor remains bound to the active site of the enzyme and must be regenerated by a substrate coupled approach. As a consequence, inactivated cofactor molecules remain in the active sites and render the respective site inactive. There are currently no data available concerning the stability of the NAD(P)H in the dry solid state. Thus, we started our studies from a detailed investigation of the stability of the reduced cofactors in the liquid and solid state.

4.1.1 Thermostability of cofactors in aqueous solution

Up to now, the stability of the redox cofactors has exclusively been studied in solution, demonstrating that NADH is significantly more stable than NADPH under various conditions, such as alkaline or acidic pH or increased temperature [74, 84, 85, 88]. Additionally, these studies showed, that such factors as buffer salt, ionic strength, and pH increase the rate of NAD(P)H degradation even at moderate temperatures [74, 84, 85, 88, 220]. To obtain reliable data for the gas/solid system, comparative studies of the dissolved and solid NAD(P)H were performed under the same conditions (buffer, ionic strength and pH) as used for the immobilization of the enzyme.

The stability of the dissolved cofactor was analyzed in a temperature range of 30-70°C by two independent methods. First, the decay of absorbance at 340 nm was measured, which is proportional to the concentration of reduced nicotinamide moieties. Second, residual reducing activity of the heat-treated cofactor samples was determined in the standard activity assay using the *Lb*ADHwt for NADPH and the *Lb*ADH G37D for NADH. The absorption at 340 nm and the residual activity were found to decrease over time both following a linear decay model at lower temperatures and a single-order exponential decay at higher temperatures. As indicated, the absorption at 340 nm predominantly arose from the intact cofactor (Fig. 4-1).

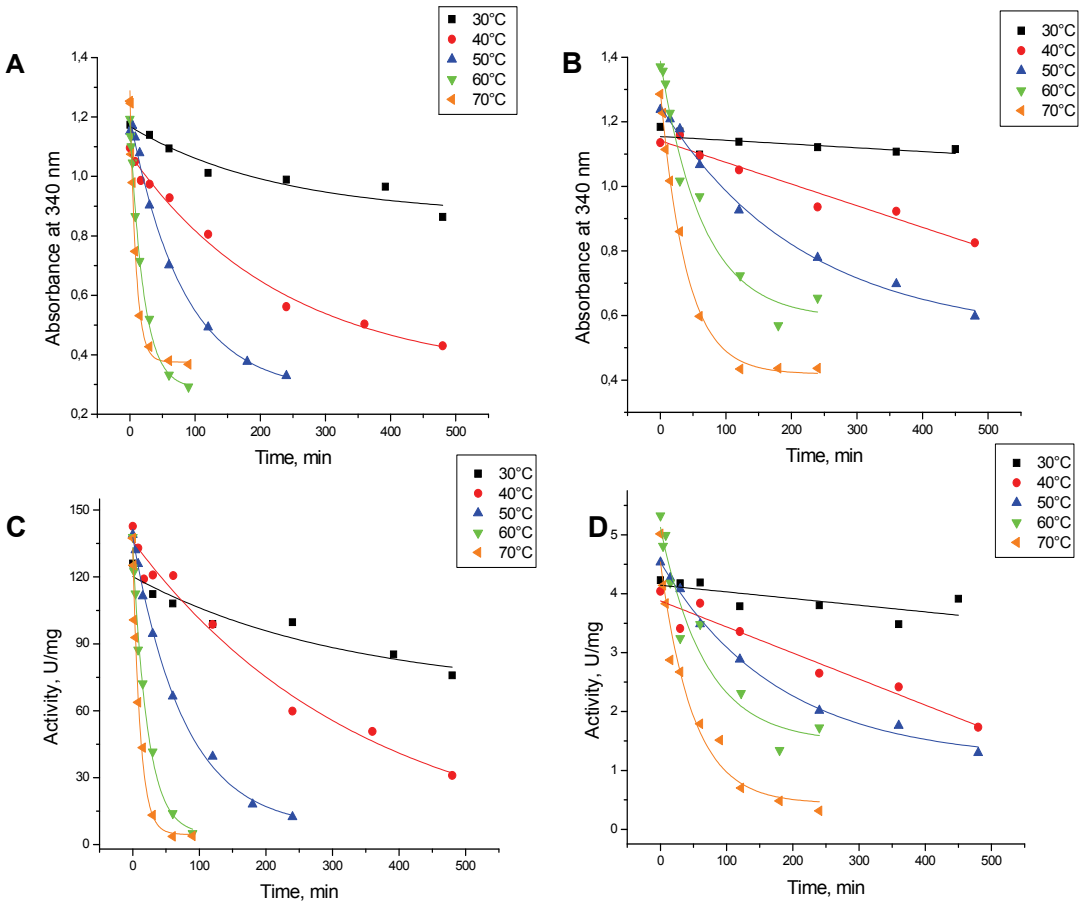

Figure 4-1. Thermal stability of the dissolved NADH and NADPH. A: NADPH after thermal treatment, absorbance at 340 nm; B: NADH after thermal treatment, absorbance at 340 nm; C: NADPH after thermal treatment, residual activity was measured with *Lb*ADHwt; D: NADH after thermal treatment, residual activity was measured with *Lb*ADH G37D. Initial cofactor concentration was 9.5 mM in 50 mM TEA, pH 7.2, for the activity tests it was diluted to 0.19 mM.

It was found that the dissolved NADH was more thermostable by a factor of 3.5-5.5 than the phosphorylated cofactor. The values of the half-life time derived using residual activity measurement were 20-50% lower than the ones determined from the absorbance$_{340}$ decay curves in a range of 30-60°C (Fig. 4-2). The tendency was even more pronounced for NADPH. The half-life time values measured by the both methods at 70°C were statistically indistinguishable. This fact indirectly suggests the presence of degradation products containing a reduced nicotinamide ring, but which are catalytically inactive. The relative content of these species in the thermally degraded cofactor samples is difficult to estimate using enzymatic tests only. The enzymatic activity assay mixture contains a large excess of cofactor molecules over protein molecules (10^6 for NADH test by *Lb*ADH G37D and 10^7 for NADPH test by *Lb*ADHwt). Therefore, a significant decrease of intact reduced cofactor molecules might not be visible. Further, the observed decay in enzymatic

activity might be related to potential competitive inhibition effects of the cofactor degradation products, which could diffuse to the active center of the enzyme and reversibly bind.

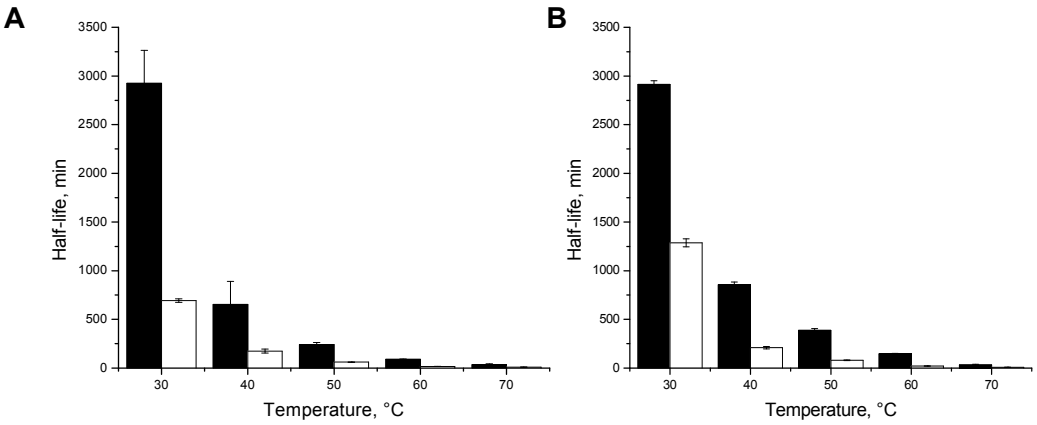

Figure 4-2. Half-lifes of the dissolved NADH (black) and NADPH (white). Half-life was determined by measuring the residual reducing activity in the standard activity assay (A) and by following the decay of absorbance at 340 nm (B). Initial cofactor concentration was 9.5 mM in 50 mM TEA, pH 7.2, for the tests it was diluted to 0.19 mM.

4.1.2 Thermostability of cofactors in the dry solid state

Thermal stability of the solid cofactor samples was examined by the same methods, which were used for the dissolved ones. The studies were performed at 50^{o}C which is in the range of the typical temperature at which gas/solid reactor is operated.

Surprisingly, both cofactors were found to be stable for several weeks in the solid state, which was evidenced by a constant absorbance at 340 nm while exposing samples to 50°C for 24 days (Fig. 4-3). For comparison, half-life times of the dissolved NADPH and NADH at 50°C equaled to 60±1 min and 240±20 min, respectively. However, the corresponding reducing activity of NADPH gradually decreased to approximately 60% of its initial activity. For the solid NADH both the absorbance at 340 nm and the reducing activity remained almost unchanged (Fig. 4-3).

As already mentioned for the dissolved cofactors, these result might suggest the presence of the catalytically inactive degradation products containing a reduced nicotinamide ring. To check this hypothesis, the thermal degradation products derived after thermal treatment of the dissolved and solid cofactor probes were analysed by HPLC/MS analysis in separate experiments (section 4.1.3).

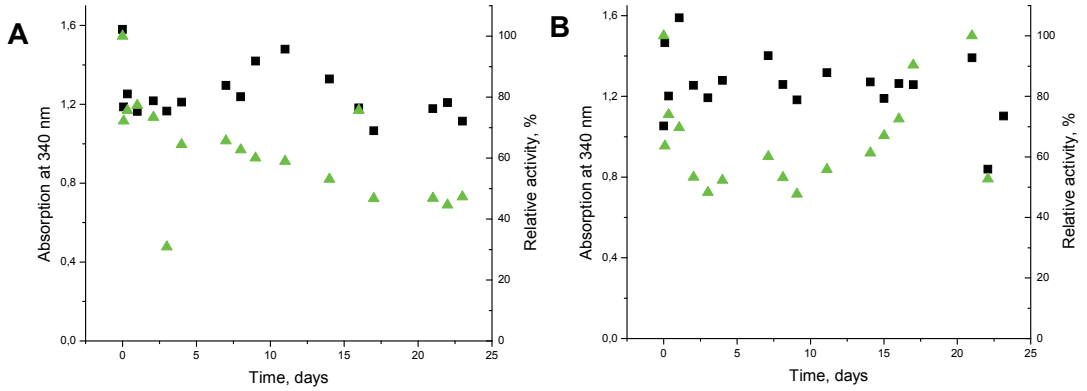

Figure 4-3. Thermal stability of solid NADPH (A) and NADH (B) at 50°C by analysis of absorption$_{340}$ ■ and relative activity ▲. Solid cofactor samples were incubated at 50°C for a time intervals of 0-23 days, dissolved in 50 mM TEA buffer, pH 7.2 and analysed for the absorbance at 340 nm and the residual reducing activity in the standard activity assay. Initial cofactor concentration was 9.5 mM in 50 mM TEA, pH 7.2, for the tests it was diluted to 0.19 mM.

4.1.3 Spectroscopic analysis and separation of the cofactor degradation products

To further analyze the cofactor degradation products, the heat-treated cofactors were subjected to UV-absorbance and fluorescence spectroscopy. The cofactor species used in this study were the following: intact NADPH and NADH, intact $NADP^+$ and NAD^+, dissolved in water and heated at 60°C for 12 h. NADPH and NADH heated to 95°C for 12 h in solid state. All the heat-treated cofactor samples completely lost their reducing activity, which was confirmed by the enzymatic activity assay (*Lb*ADHwt for NADPH and the *Lb*ADH G37D for NADH). Due to the slow degradation process, thermal treatment of the dry cofactor samples was performed under harsh conditions.

The absorption spectra of cofactors were screened in the range of 200-700 nm in 50 mM TEA buffer (pH 7.0), with a final cofactor concentration of 0.19 µM in each case. As expected, the oxidized cofactors were not able to absorb light at 340 nm. The reduced NADH and NADPH displayed almost identical absorption spectra. The spectra had three absorption peaks with maxima at 225, 280 and 340 nm (Fig. 4). Absolute values of A_{225} and A_{280} were, however, much above the detection limit at reliable cofactor concentrations, so A_{340} was usually used for comparison. The most pronounced absorption decay was displayed by the product of heat degradation of the NADPH in aqueous solution. The products of thermal degradation of the solid NADPH and the dissolved and solid NADH showed a decrease of the absorbtion intensity at 340 nm by approximately 25%, in comparison to the A_{340} values of the intact samples. (Fig. 4-4).

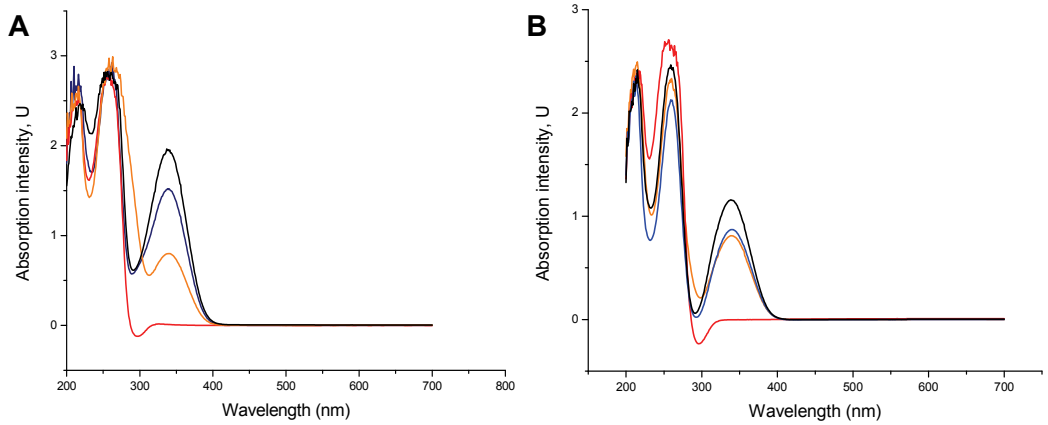

Figure 4-4. Absorption spectra of the nicotinamide cofactors and products of their thermal degradation. A: $NADP^+$ (red), NADPH (black), the dissolved NADPH incubated at 60°C for 12 h (orange), the solid NADPH incubated at 95°C for 12 h (blue); B: NAD^+ (red), NADH (black), the dissolved NADH incubated at 60°C for 12 h (orange), the solid NADH incubated at 95°C for 12 h (blue). The absorption spectra were determined at RT.

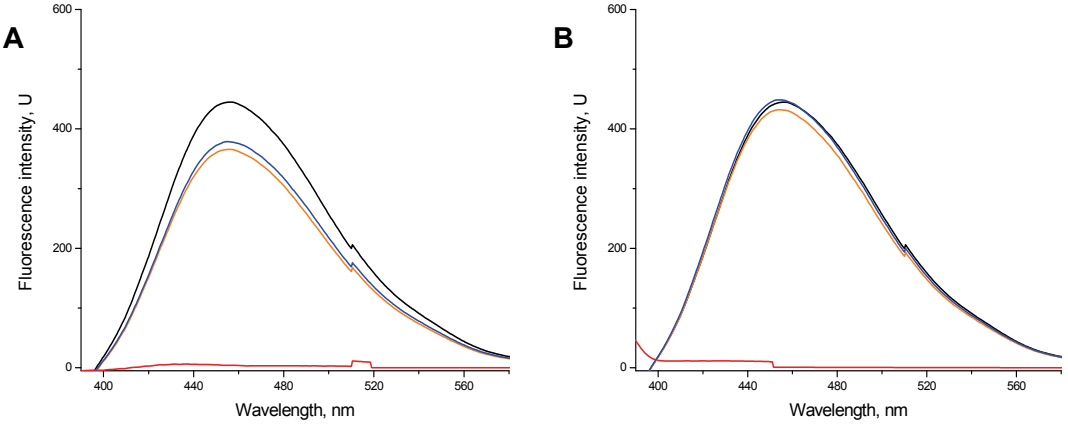

Figure 4-5. Fluorescence emission spectra of the nicotinamide cofactors and products of their thermal degradation. A: $NADP^+$ (red), NADPH (black), the dissolved NADPH incubated at 60°C for 12 h (orange), the solid NADPH incubated at 95°C for 12 h (blue); B: NAD^+ (red), NADH (black), the dissolved NADH incubated at 60°C for 12 h (orange), the solid NADH incubated at 95°C for 12 h (blue). Fluorescence emission spectra were measured at RT after an excitation performed at 340 nm. The excitation and emission slits were adjusted to ±7.5.

The fluorescence emission spectra of these cofactor samples obtained after excitation at 340 nm are represented in Fig. 4-5. Similar to the absorption profiles, the fluorescence properties of the intact NADH and NADPH were almost identical. Thermal treatment of the dissolved and solid cofactors neither led to considerable decay of fluorescence intensity, nor induced a shift of the spectral maximum (Fig. 4-5). So, most likely the catalytically inactive products of thermal degradation of NADH and NADPH contained a reduced nicotinamide ring.

The results of the HPLC separation, which was kindly performed by A. Wirtz, FZ-Jülich, are represented in Fig. 4-6. Indeed, the samples of the thermally treated cofactors contained a mixture of degradation species. Although the degradation species demonstrated dramatic changes of HPLC retention time, some of them kept the ability to absorb at 340 nm. Thermal treatment of the dissolved and solid probes of the cofactor NADH resulted in at least four different degradation products. Five degradation products were visible in the chromatogram of the heat-treated dissolved NADPH. The solid NADPH broke into at least eight different fragments (Fig. 4-6 C). However, the separation of many different degradation product was not really sharp. Thus a LC-MS analysis was performed to identify the degradation products.

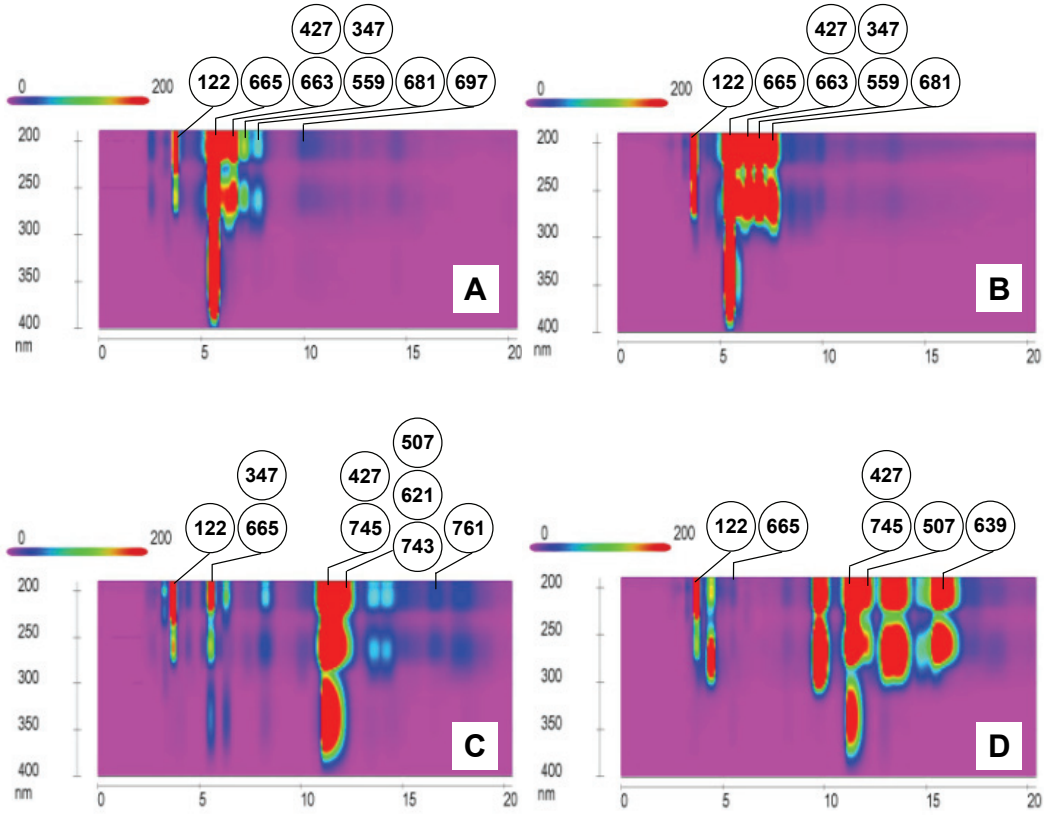

Figure 4-6. 2D-HPLC-chromatograms of NADH and NADPH. A: Freshly solved samples without thermal treatment; B: Dissolved samples incubated at 50°C for 16h and C: solid samples incubated at 95°C for 16h. Corresponding masses of the degradation products were obtained by nano-ESI-FTICR-MS- and LC-MS measurements (section 3.7.2). The picture was obtained by A. Wirtz and D. Hofmann.

LC-MS measurements were carried out by Dr. D. Hofmann, FZ-Jülich. From the data in Tab. 4-1 it is clearly visible that the thermal degradation of NADH and NADPH occurs in different ways. More degradation products were detected after heat treatment of solid NADPH than of solid NADH. Whereas in case of NADH

almost all observed fragments occur in both the liquid and the solid sample, differences concerning the fragmentation pattern were observed with NADPH, where fragments 2a, 3a, 6a, 9a and 10a were only observed in the solid state. Main fragmentation routes include the cleavage of the nicotin amide ring as well as oxidative ring opening of the ribose rings. Further, cleavage of the phosphoester bonds is observed yielding adenosine mono-, di- and tri-phosphate.

According to the different retention times observed in HPLC the AMP (9a and 8b) and ADP fragments (8a and 7b) can be regarded as different concerning the position of the phosphate groups (Tab. 4-1). Both cofactors show enzymatically inactive degradation products containing an intact reduced nicotinamide ring (3a, 4a, 3b, 5b) (Tab. 4-1 and 4-2) giving rise to absorbance at 340 nm, which explains the differences observed in half-life determination based on residual activity determinations and absorbance measurements at 340 nm (described above).

To conclude, although the stability of redox cofactors in the solid state is significantly higher than in solution, the higher stability of NADH compared to NADPH has been proven also in the solid state. Therefore, the use of NADH-dependent oxidoreductases in solid/gas systems might be one possibility to increase the stability of such systems.

Table 4-1. Comparison of thermal degradation of NADPH in the solid state and in water solution obtained by HPLC/MS. Neutral masses are given in Dalton. X: Fragment observed; -: fagment not found.

Degradation products of NADPH					
peak number	**mass** (Da)	**Structure**	**NADPH** solid	**NADPH** dissolved	**retention time** (min)
1a	745	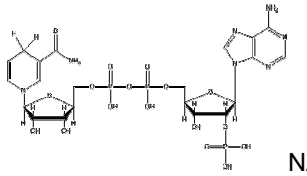 NADPH	x	x	14.5
2a	743	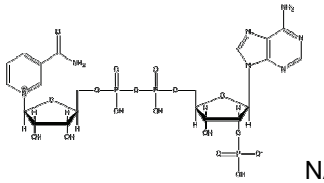 $NADP^+$	x	-	16.0
3a	761	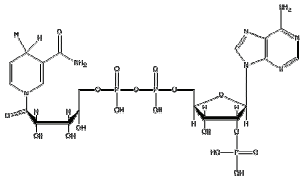	x	-	24.3
4a	665	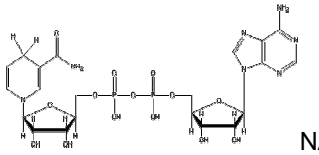 NADH	x	x	6.5

Table 4-1, continued. Comparison of thermal degradation of NADPH in the solid state and in water solution obtained by HPLC/MS. Neutral masses are given in Dalton. X: Fragment observed; -: fagment not found.

Degradation products of NADPH					
peak number	**mass** (Da)	**Structure**	**NADPH** solid	**NADPH** dissolved	**retention time** (min)
5a	639	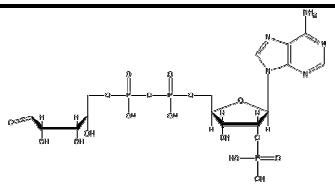	x	x	22.3
6a	621	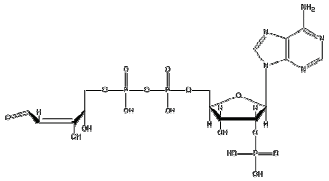	x	-	15.7
7a	507	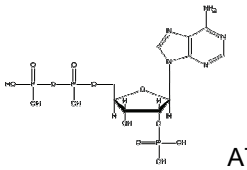 ATP	x	x	15.8
8a	427	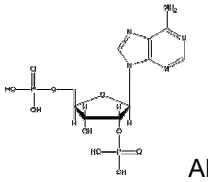 ADP	x	x	14.0
9a	347	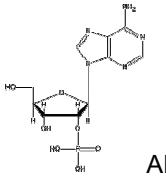 AMP	x	-	6.0
10a	329	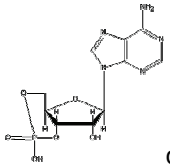 cAMP	x	-	10.0
11a	122	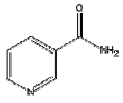	x	x	3.9

Table 4-2. Comparison of thermal degradation of NADH in the solid state and in water solution obtained by HPLC/MS. Neutral masses are given in Dalton. x: fragment observed; -: fagment not found.

Degradation products of NADH					
peak number	**mass** (Da)	**Structure**	**NADH** solid	**NADH** dissolved	**retention time** (min)
1b	665	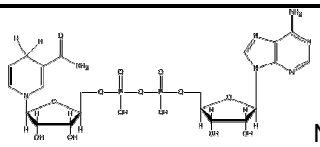 NADH	x	x	6.5
2b	663	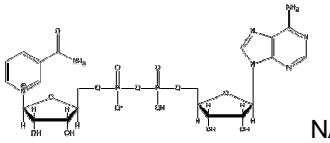 NAD^+	x	x	7.8
3b	697	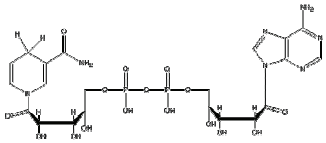	x	-	12.3
4b	679	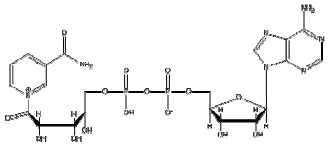	x	-	8.0
5b	681	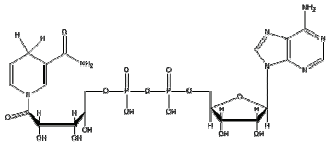	x	x	9.3
6b	559	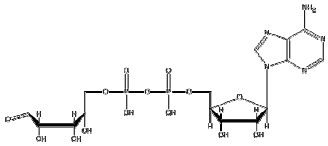	x	x	8.5
7b	427	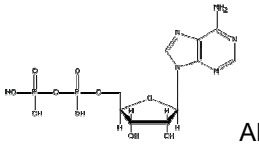 ADP	x	x	7.9
8b	347	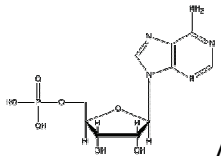 AMP	x	x	8.5
9b	122	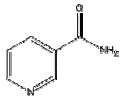	x	x	3.9

4.2 Characterization of *Lb*ADHwt and *Lb*ADH G37D

To elucidate the temperature-induced inactivation mechanisms and to elaborate methods for the enhancement of the operational stability of the enzymes in a gas/solid reactor, we focused our studies on the alcohol dehydrogenase from *Lactobacillus brevis* (*Lb*ADHwt) and its variant *Lb*ADH G37D. These model enzymes were chosen for the investigation because of their known potential in the gas/solid catalysis [7, 25, 31]. The available crystal structures of *Lb*ADHwt and *Lb*ADH G37D [8, 67] represented an additional advantage.

Prior to direct comparison of the performance of *Lb*ADHwt and *Lb*ADH G37D in the solid/gas reactor, both enzyme variants were characterized concerning their substrate range, pH optima and thermostability in both the dissolved and the solid state.

4.2.1 Thermostability in aqueous solution

The thermal stability of *Lb*ADHwt and *Lb*ADH G37D were characterized kinetically by measuring the residual catalytic activity after exposure to elevated temperature for the certain period of time. The corresponding half-life values were determined from the plots. The standard acetophenone conversion assay was used to measure the residual catalytic activity of the both enzyme variants. The assay allowed to compare the results with previously published data (Schieben et al. [8]), as well as to neglect the effect of cofactor instability.

It should be emphasized here that a pH of 7.0 was not optimal for *Lb*ADH G37D (see section 4.2.3 for details). The variant showed a specific activity of 7.0-9.3 U/mg, which was significantly lower compared to 75-115 U/mg for the wild type enzyme. In other words, *Lb*ADH G37D was found to be approximately 12-15 times less active than *Lb*ADHwt in solution.

The dissolved enzymes were investigated in the temperature range of 30-70°C. The role of thermal inactivation of the cofactors in the overall enzyme inactivation could not be evaluated from the obtained experimental results, because 0.19 mM of fresh cofactor were added in the activity assay.

The heat-induced decrease of the catalytic activity of *Lb*ADHwt and *Lb*ADH G37D could be described by linear, one- and two-order exponential decay models, depending on the respective temperature (Fig. 4-7). Therefore, a combination of several consecutive mechanisms, each of which individually could be described by the Arrhenius low (equation 1-1 in section 1.1.2.1), is highly probable [221, 222].

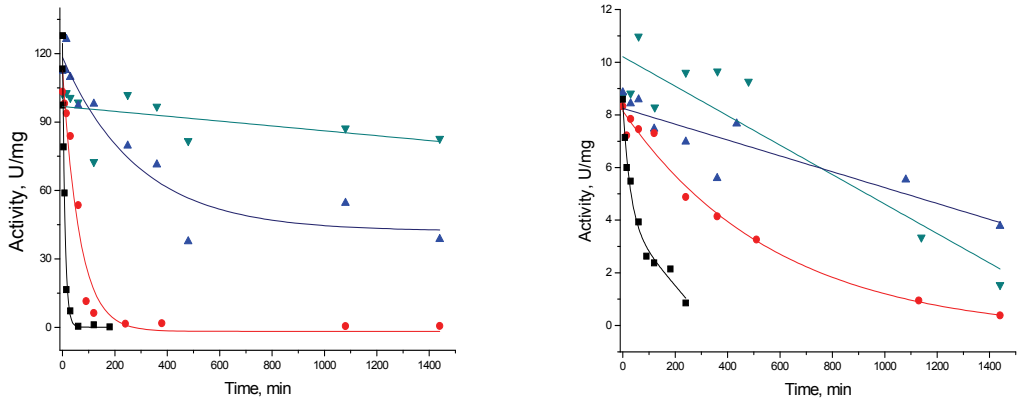

Figure 4-7. Thermal inactivation of the dissolved *Lb*ADHwt (A) and *Lb*ADH G37D (B). The heat inactivation profiles obtained at 30°C ▼, 35°C ▲, 40°C ● and 45°C ■ are represented. Experimental parameters: 100 µL of the enzyme variant (0.1 mg/ml) were incubated in 10 mM TEA buffer, with 1 mM $MgCl_2$, pH 7.5. Samles were withdrawn at the given time points and residual activity was assayed in duplicates using the standard assay (section 3.4.2.1). The enzyme inactivation curves were fitted by a linear, one- and two-order exponential decay.

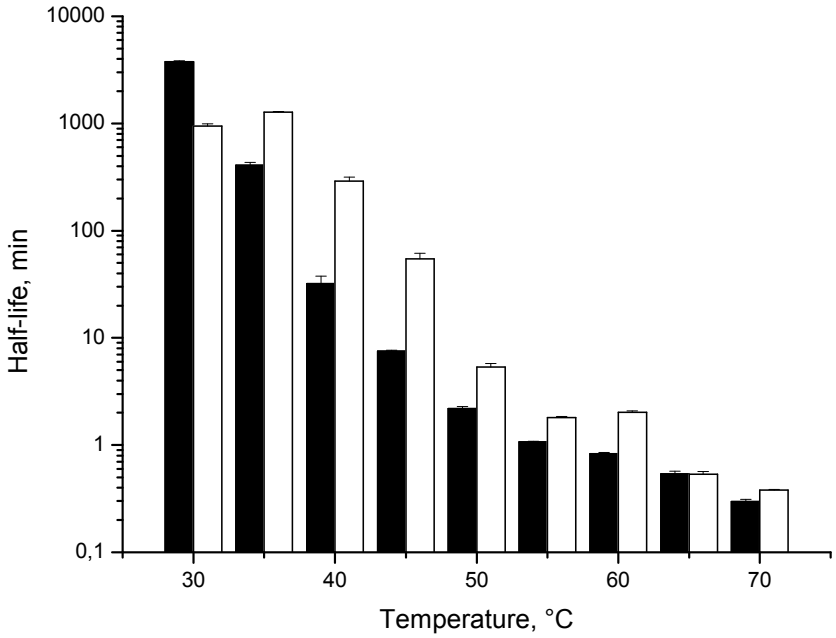

Figure 4-8. Thermal stability of the dissolved *Lb*ADHwt (black) and *Lb*ADH G37D (white). Heat inactivation experiments were performed with 100 µl of the 0.1 mg/ml enzyme solution in 10 mM TEA, 1 mM $MgCl_2$, pH 7.5. Residual activity was measured in duplicates using the standard assay (section 3.4.2.1).

Fig. 4-8 and Table 4-3 display half-lifes of dissolved *Lb*ADHwt and *Lb*ADH G37D at elevated temperatures. For both enzymes the half-life values decrease exponentially with increasing temperature. In the temperature range of of 35-60°C

the variant showes considerably higher thermostability than the wild type enzyme (Fig. 4-8 and Table 4-3). For example, the half-life values of *Lb*ADHwt and *Lb*ADH G37D at 40°C (a typical operational temperature in the gas/solid reactor) were 32±6 min and 289±26 min, respectively.

The higher thermostability of the variant *Lb*ADH G37D can be explained due to structural reasons. The G37D exchange is located in a β-turn in close proximity to the cofactor binding region. This β-turn, which connects two α-helices, is known to be a sensitive part [146, 150, 151]. Manipulations in this region, such as partial deletions or point mutations, may significantly affect the local and even global flexibility of protein molecule, and, therefore, its thermal stability.

Thermal inactivation of the enzymes was irreversible. According to Lumry and Eyling, the simplest model of irreversible protein denaturation involves at least two steps [223]. The first step is a reversible unfolding of the native, catalytically active enzyme (N). This is followed by an irreversible change of the denatured protein (D) into an irreversible inactivated state (I) that cannot fold back into the native state.

$$N \underset{k_{-1}}{\overset{k_1}{\rightleftharpoons}} D \xrightarrow{k_2} I$$

The transition from N to D is considered to be the rate-limiting step, whereas the irreversible inactivation step is fast [224]. In solution the last one is often caused by aggregation of partially unfolded enzyme molecules [225]. Indeed, drastic aggregation accompanied this process of thermal inactivation of the dissolved *Lb*ADHwt and *Lb*ADH G37D. The following observations support this conclusion:

(i) Visible precipitates were formed during heating of the dissolved *Lb*ADHwt and *Lb*ADH G37D (concentration range 0.1-3.6 mg. Subsequent centrifugation (5 min at 13000 rpm) of the heat-treated enzyme solutions resulted in significant reduction in the concentration of the dissolved protein measured by Bradford's method.

(ii) The inactivation kinetics of the thermal inactivation of *Lb*ADH depended on the initial concentration of the dissolved enzyme (Fig. 4-9).

(iii) The Arrhenius plots of the dissolved enzymes consists of two linear segments crossing at the so called transition temperature of 50°C, which indicates a change in the rate-limiting mechanism (Fig. 4-10).

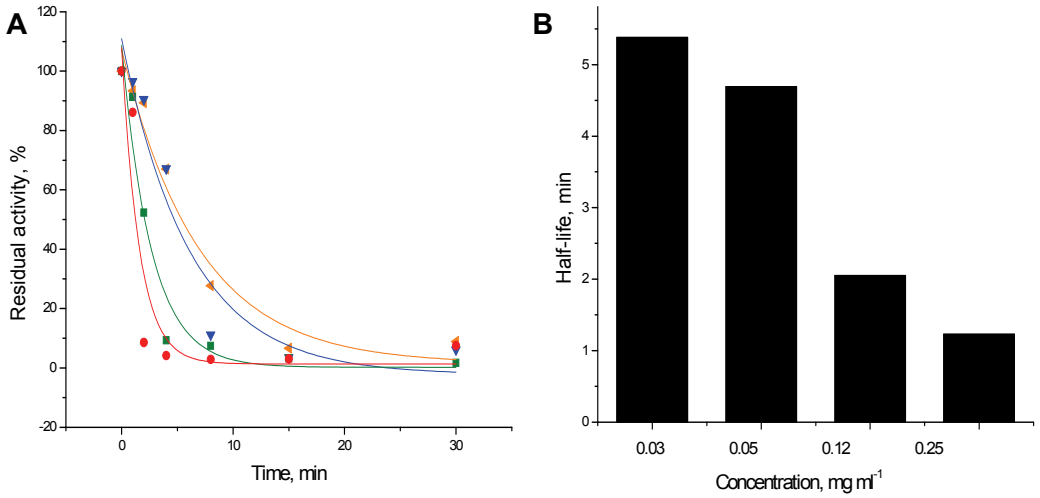

Figure 4-9. Concentration-dependent inactivation of *Lb*ADHwt at 55°C. A: Temperature-dependent inactivation of 0.03 ◀, 0.05 ▼, 0.12 ■ and 0.25 ● mg ml^{-1} *Lb*ADHwt; B: Half-lifes of 0.03, 0.05, 0.12 and 0.25 mg/ml *Lb*ADHwt. Heat inactivation experiments were performed with 100 µl of the enzyme solution in 10 mM TEA, 1 mM $MgCl_2$, pH 7.5. Residual activity was measured in duplicates using the standard assay (section 3.4.2.1). Data were fitted by one- and two-order exponential decay models.

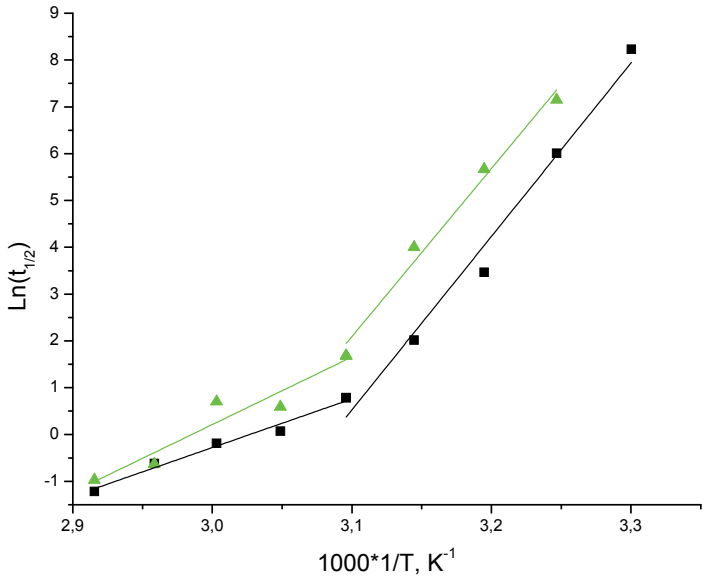

Figure 4-10. Arrhenius plot of inactivation constants of the dissolved *Lb*ADHwt ■ and *Lb*ADH G37D ▲. Heat inactivation experiments were performed with 100 µl of the enzyme solution in 10 mM TEA, 1 mM $MgCl_2$, pH 7.5. Residual activity was measured in duplicates using the standard assay (section 3.4.2.1).

Although the complex nature of the heat inactivation process does not allow calculation of the actual activation energy (E_A), the strickt linear behaviour of both enzyme variants in the temperature ranges of 30-50°C and 50-70°C made the

determination of the apparent E_A possible. At temperatures below 50°C, apparent E_A-values of 308±3 kJ mol^{-1} and 299±7 kJ mol^{-1} were calculated for the *Lb*ADHwt and *Lb*ADH G37D, respectively. At higher temperatures, the apparent E_A-values of the *Lb*ADHwt and *Lb*ADH G37D were calculated to 86±8 kJ mol^{-1} and 120±7 kJ mol^{-1}, respectively. The published values of the activation energy of protein denaturation caused by unfolding of the tertiary and/or quaternary structure vary between 200–502 kJ mol^{-1}, dependent of the nature of proteins [226, 227]. Thus, structural decomposition is a probable mechanism leading to the loss of catalytic activity of both variants at temperatures below 50°C. Undoubtly, protein structure denatures at higher temperatures as well. However, above 50°C another reaction limits the rate of observable inactivation. Most probably, it is a reaction of intermolecular association, leading to aggregation, with reported values for E_A between 100 and 120 kJ mol^{-1} [228]. A similar model of thermal denaturation was described for ß-lactoglobulins A and B and for α-lactoalbumin in whey or milk. The denaturation proceeds through two consecutive steps with the rate-limiting step of unfolding at the temperature range of 70-90°C for ß-lactoglobulins or 70-85°C for α-lactoalbumin (E_A 250-390 kJ mol^{-1}) and aggregation at the higher temperatures (54-120 kJ mol^{-1}) [228, 229].

Table 4-3. Thermal stability of the dissolved and solid *Lb*ADHwt and *Lb*ADH G37D. Heat inactivation experiments were performed with either 100 µl of the 0.1 mg/ml enzyme solution in 10 mM TEA, 1 mM $MgCl_2$, pH 7.5 or solid samples obtained after freeze-drying of 100 µl of the 0.1 mg/ml enzyme solution in 10 mM TEA, 1 mM $MgCl_2$, pH 7.5. Residual activity was measured after redisolving the thermally incubated samples by the standard activity assay (section 3.4.2.1).

Temperature, °C	**Half-life, min**			
	Dissolved		**Solid**	
	***Lb*ADHwt**	***Lb*ADH G37D**	***Lb*ADHwt**	***Lb*ADH G37D**
30	3770±72	946±47	6809±0	6650±629
35	407±27	1276±22	5873±2002	3279±563
40	32±6	289±26	1967±289	3661±401
45	7.5±0.2	54±7	2902±487	2160±205
50	2.2±0.1	5.4±0.4	763±268	620±112
55	1.07±0.02	1.8±0.05	1229±144	568±94
60	0.83±0.02	2.02±0.03	117±32	45±9
65	0.54±0.03	0.53±0.03	79±22	190±26
70	0.3±0.01	0.38±0.005	1.9±0.3	286±31
75	ND	ND	2.1±0.8	30±4
80	ND	ND	18±2	19±3

4.2.2 Thermostability in the solid state

Both enzymes are approximately two orders of magnitude more stable in the solid state than in solution (Fig. 4-11 and Table 4-3). For example, the half-life values at 50°C of wild type *Lb*ADH in the dissolved and in the solid state are 2.2±0.1 min and 763±268 min, respectively; corresponding values for the variant are 5.4±0.4 min and 620±112 min. The apparent differences between the half-life of *Lb*ADHwt and *Lb*ADH G37D are not significant, but are within the range of errors of the used methods.

The dependence of the half-life values of the solid *Lb*ADHwt and *Lb*ADH G37D on the temperature showed a first-order (or a pseudo-first-order) kinetics, which could be demonstrated by linear Arrhenius plot (Fig. 4-12). The E_A of heat inactivation (30-80°C) of the solid enzymes were calculated to be 110±9 and 100±6 kJ mol^{-1} for *Lb*ADHwt and *Lb*ADH G37D, respectively. The lower values of E_A of the solid enzymes can be attributed to the mass transfer limitation in the system.

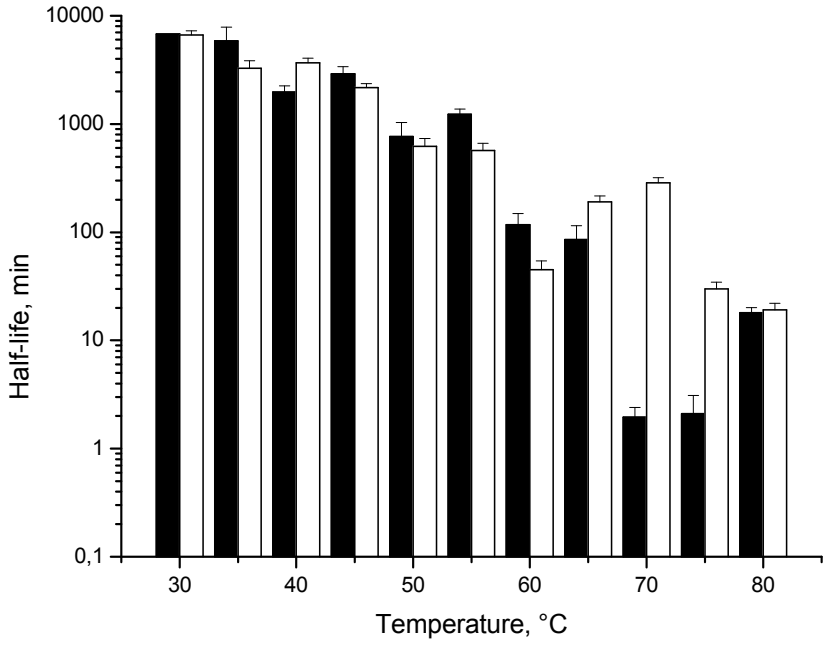

Figure 4-11. Thermal stability of the solid *Lb*ADHwt (black) and *Lb*ADH G37D (white). Heat inactivation experiments were performed with solid samples obtained after freeze-drying of 100 µl of the 0.1 mg/ml enzyme solution in 10 mM TEA, 1 mM $MgCl_2$, pH 7.5. Residual activity was measured after redisolving the thermally incubated samples by the standard activity assay (section 3.4.2.1). Data points at 30°C, 65°C and 70°C are hard to compare, because the slow inactivation at 30°C and considerably fast inactivation at 65°C and 70°C made half-life determination inaccurate.

As already reported for the solid dry pectin lyase from *Aspergillus niger* [230], structural decomposition is probably not the mechanism leading to the loss of enzymatic activity. Such reactions, as hydrophobic aggregation, deamidation,

racemization, cofactor release and/or destruction were suggested as alternative mechanisms of the inactivation of solid dry enzymes [227, 230, 231]. Local perturbations in the active site are also possible [227]. Interestingly, E_A values of 110-129 kJ mol^{-1} were found for the unfolding of α-helices and subsequent formation of ß-sheets in the process of amyloid fibrils formation [232, 233].

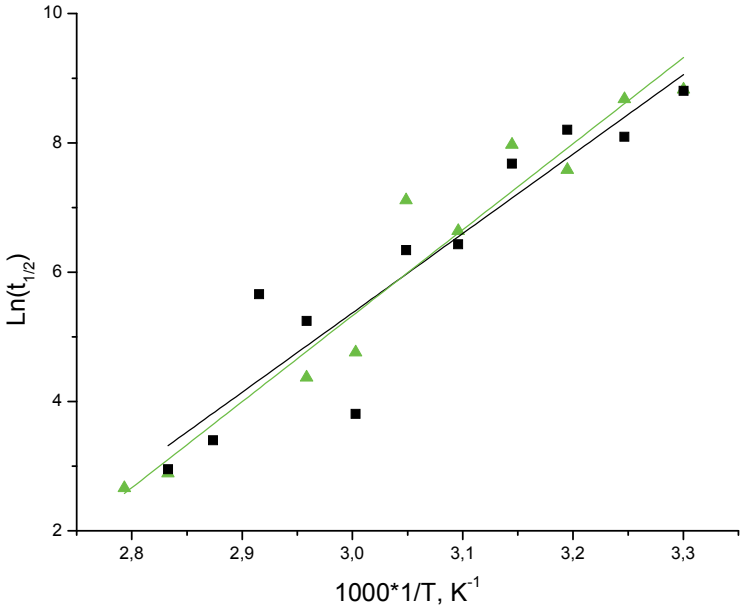

Figure 4-12. Arrhenius plot of inactivation constants of the solid *Lb*ADHwt ■ and *Lb*ADH G37D ▲. Heat inactivation experiments were performed with solid samples obtained after freeze-drying of 100 µl of 0.1 mg/ml enzyme solution in 10 mM TEA, 1 mM $MgCl_2$, pH 7.5. Residual activity was measured after redisolving the thermally incubated samples by the standard activity assay (section 3.4.2.1).

4.2.3 PH optimum

The catalytic activity of *Lb*ADHwt and *Lb*ADH G37D are strongly dependent on pH (Fig. 4-13). pH profiles, and, consequently, protonation status of the active site residues of the both enzymes were different. So, *Lb*ADHwt displayed detectable reduction activity in a range between pH 4.0 and 9.5, with a clear maximum at pH 7.5 (Fig. 4-13 A). Such a plot corresponded to the classical “bell-shaped” curve that demonstrated a presence of at least one acidic and one basic residue in the active site. Enzymatic activity at low pH is considered to be limited by protonation of basic amino acid side chains, whereas catalysis at high pH is slowed by deprotonation of the acidic one [234]. Non-linear regression analysis of the experimental data resulted in apparent pKa values of 6.8 and 8.5. The basic group that must be protonated for catalysis is probably the conserved Y155 of *Lb*ADHwt. Although pKa value of the hydroxyl group of free tyrosine equals to 9.7-10.1 [235],

it is considerably lowered in all SDR enzymes due to interaction with the neighbouring concerved lysine [63, 65]. The pKa value 6.8 lies in a normal pK range of histidine [235]. No histidine residue is present in close proximity to the active center of the *Lb*ADHwt [8, 67]. However, H39 is located in the surrounding of the cofactor and might be critical for its proper binding. Additionally, aspartic or glutamic acid can represent an alternative. Although free asparate and glutamate display pKa values of 3.7-4.0 and 4.2-4.5, respectively [235], these values may significantly raise in the protein microenvironment [236, 237]. The conserved D162, which is located in the cofactor-binding site and forms a hydrogen bond to the N6 atom of the adenine ring [63], is a probable candidate.

Oxidative activity of *Lb*ADHwt was determined in the range from 5.0 to 9.5. The plot had a typical sigmoidal shape with a transition point at approximately 6.2 (Fig. 4-13 A). The non-linear fit of the experimental data, however, suggested the presence of a second ionisable group with a pKa of about 11.2. Most likely, the exact amino acids displaying pH-dependent ionization in oxidative reactions are D162 and Y155. A pKa value of exactly 11.2 was obtained for Tyr155 by Karlsberg simulation [238, 239]. The large difference in the p*Ka* values of tyrosine in reduction and oxidation reactions was previously reported [240]. It was explained by the tendency of an enzyme to maintain a neutral net charge in its catalytic center by preferential ionization of tyrosine when the positively charged $NAD(P)^+$ was bound [240].

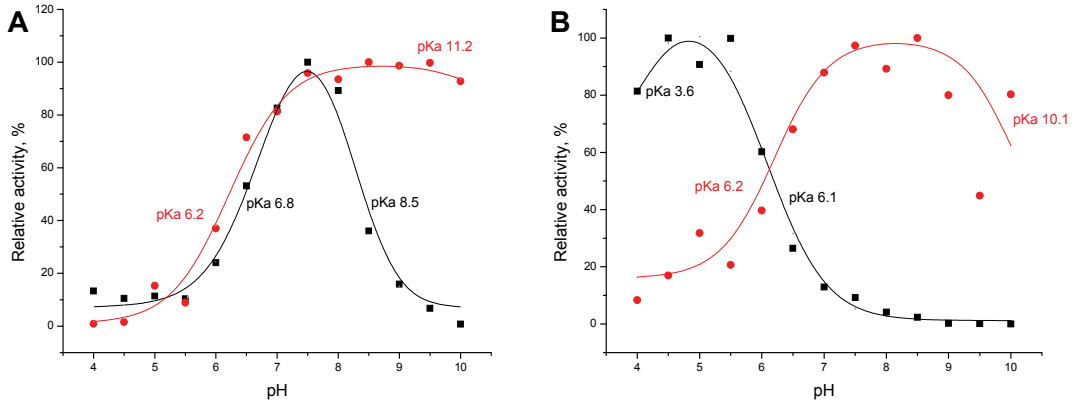

Figure 4-13. pH dependence of oxidative ● and reductive ■ activity of *Lb*ADHwt (A) and *Lb*ADH G37D (B). The experiments were performed with 11 mM acetophenone (reduction) and 200 mM isopropanol (oxidation), 10 mM of the corresponding cofactor, 1 mM $MgCl_2$ in 50 mM buffer.

The pH profile of oxidation catalyzed by *Lb*ADH G37D is shown in Fig. 4-13 B. It resembles that one catalyzed by *Lb*ADHwt. In contrast, reduction activity of *Lb*ADH G37D is greatly shifted to the lower pH-range compared to *Lb*ADHwt. pKa values of critical amino acids were found to be 3.6 for the acidic residue and 6.1 for the basic one. The data indicate that the substitution G37D drastically changed

electrostatic properties of the catalytic center, despite of its preserved topology [8, 67]. Obviously, introduction of the negatively charged residue into the close proximity to the cofactor binding region modified an internal electrostatic network connecting ionizable amino acid residues.

4.2.4 Substrate spectrum

The substrate spectra of *Lb*ADHwt and *Lb*ADH G37D are shown in Table 4-4 and 4-5. Despite of optimal reaction conditions applied to each of them, catalytic activity of the wild type enzyme is considerably higher in both the oxidation and the reduction direction. Both enzymes show a clear preference for the oxidation of secondary alcohols, whereas primary alcohols were not oxidized. Their catalytic activity steeply increases with the chain length of the substrates from 2-propanol to 2-hexanol for *Lb*ADHwt or 2-pentanol for *Lb*ADH G37D. Longer chain alcohols are less preferred and 2-octanol is not reduced at all (Table 4-4). *Lb*ADHwt can act on cyclic and aromatic substrates as well as on diols, which is not the case for *Lb*ADH G37D (Table 4-4).

Table 4-4. Substrate specificity of *Lb*ADHwt and *Lb*ADH G37D: oxidation. The experiments were performed with 10 mM substrate solution in 50 mM Tris-HCl, 1 mM $MgCl_2$, pH 8.0. The measurement was performed under standard assay conditions (section 3.4.2.1) in triplicates.

Substrate	**Structure**	**Activity, U/mg**	
		***Lb*ADHwt**	***Lb*ADH G37D**
methanol	—OH	0.003	0.005
ethanol		0.02	0.0005
1-propanol	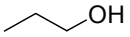	0.08	0.003
1-butanol	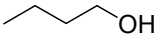	0.17	0.007
1-hexanol	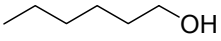	0.11	0.03
1-octanol	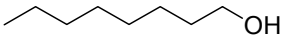	0.07	0.006
2-propanol		8.1	0.4
2-butanol	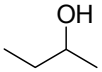	31.4	5.9
2-pentanol	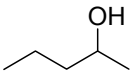	41.5	15.5
2-hexanol	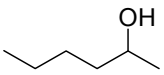	51	12

Table 4-4, continued. Substrate specificity of *Lb*ADHwt and *Lb*ADH G37D: oxidation. The experiments were performed with 10 mM substrate solution in 50 mM Tris-HCl, 1 mM $MgCl_2$, pH 8.0. The measurement was performed under standard assay conditions (section 3.4.2.1) in triplicates.

Substrate	Structure	Activity, U/mg	
		*Lb*ADHwt	*Lb*ADH G37D
2-heptanol	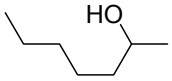	34.7	11
2-octanol	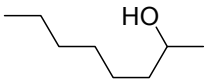	0.02	0.02
2-methyl-propanol	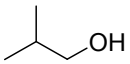	0.05	0.004
isoamylalcohol	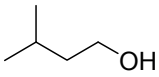	0.01	0.005
1-amino-2-propanol	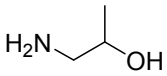	0.03	0.009
1-phenyl-2-propanol	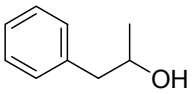	0.07	0.006
2-phenyl-1-propanol	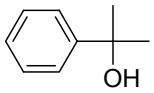	1.3	0.02
cyclohexanol	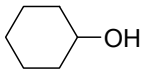	1.0	0.12
2-cyclohexen-1-ol	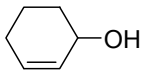	3.8	0.05
trans-2-hexen-1-ol	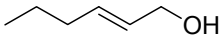	0.2	0.008
1,2-propandiol	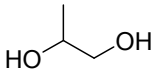	0.23	0.01
2,4-pentandiol	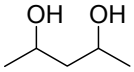	1.2	0.05

Table 4-5. Substrate specificity of *Lb*ADHwt and *Lb*ADH G37D: reduction. The experiments were performed with 10 mM substrate solution in 50 mM Tris-HCl, 1 mM $MgCl_2$, pH 7.5 or in 50 mM sodium acetate, 1 mM $MgCl_2$, pH 4.5 for *Lb*ADHwt and *Lb*ADH G37D, respectively. The measurement was performed under standard assay conditions, in triplicates. ND: not determined

Substrate	Structure	Activity, U/mg	
		***Lb*ADHwt**	***Lb*ADH G37D**
propionaldehyde	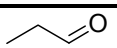	183.0	13.1
isovaleraldehyde	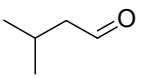	124.3	35.9
acetone		61.3	12.2
2-butanone	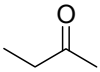	53.5	7.7
2-octanone	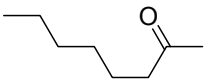	62.3	28.1
2-nonanone	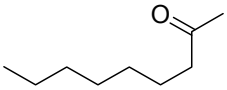	59.1	27.0
2-undecanone	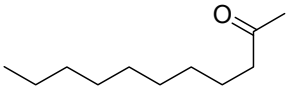	0.04	1.3
3-octanone	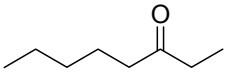	45.3	9.0
4-metyl-2-pentanone	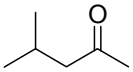	12.9	9.2
acetylacetone	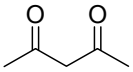	177.3	14.3
acetonylacetone	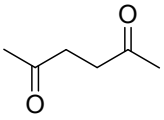	92.3	35.3
4-phenyl-2-butanone	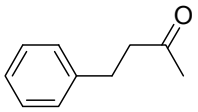	124.9	26.9
acetophenone	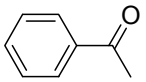	112.9	11.4
2-chloracetophenone	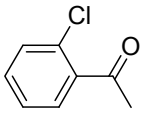	2.9	3.8
2,4-dichloracetophenone	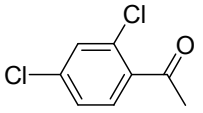	0.73	0.1

Table 4-5, continued. Substrate specificity of *Lb*ADHwt and *Lb*ADH G37D: reduction. The experiments were performed with 10 mM substrate solution in 50 mM Tris-HCl, 1 mM $MgCl_2$, pH 7.5 or in 50 mM sodium acetate, 1 mM $MgCl_2$, pH 4.5 for *Lb*ADHwt and *Lb*ADH G37D, respectively. The measurement was performed under standard assay conditions, in triplicates. ND: not determined

Substrate	Structure	Activity, U/mg	
		***Lb*ADHwt**	***Lb*ADH G37D**
4-isobutylacetophenone	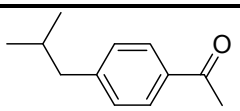	325.7	ND
3-methoxyacetophenone	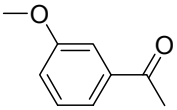	ND	ND
2,3-hexandione	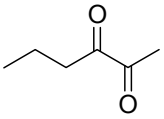	298.6	30.7
3,4-hexandione	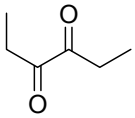	113.3	17.2
2,6,6-trimethyl-2-cyclohexene-1,4-dione	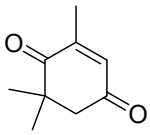	ND	ND

Compared to the oxidation reaction, both enzymes are significantly more active catalyzing the reduction of aldehydes and ketones (Table 4-5). *Lb*ADHwt and *Lb*ADH G37D accept linear and branched-chain, short and long chain aliphatic as well as sterically demanding aromatic ketones. Aromatic ring substitution significantly affected the reaction rate. Also diones were effectively reduced by both enzyme variants (Table 4-5).

The same phenomenon of higher reductive activity has already been reported for several SDR enzymes [79, 241, 242] and is usually explained by the physiological role performed by these enzymes in their host organisms. Most probably, it lies in the reduction of xenobiotic quinones or reactive carbonyl compounds, formed during lipid peroxidation [242]. However, the real physiological function remains unknown.

4.3 Inactivation mechanisms of *Lb*ADHwt and *Lb*ADH G37D in the dissolved and solid state

Heat-induced structural changes of the dissolved and solid *Lb*ADHwt and *Lb*ADH G37D were investigated by spectroscopic techniques. Tryptophan fluorescence spectroscopy was used to monitor changes in the 3D structure, CD spectroscopy for monitoring the changes in the 2D protein structure, and static light scattering spectroscopy was used for detection of aggregation.

First, the denaturation of *Lb*ADHwt and *Lb*ADH G37D to the random coil state by urea and GdnCl was performed in order to obtain reference data for the fully unfolded state. Tryptophan fluorescence emission measurements and CD spectra of respective samples incubated at defined concentrations of the chaotropic agents at room temperature were performed. Additionally the residual activity was recorded. The intrinsic tryptophan fluorescence emission spectra of the intact and denatured protein samples are shown in Fig. A-1 (Appendix).

The intensity of the emitted fluorescence is dependent on the concentration of denaturants. It monotonically decreases between 0 - 3 M urea for the wild type enzyme and between 0 - 4 M urea for the variant, indicating the structural transition region. At higher urea concentrations the signal did not considerably change (Fig. A-1) and stays at about 30% of the initial one. The quenching effect of GdnCl was more pronounced compared to urea in the same concentration range (Fig. A-1). The changes of the fluorescence emission maxima and the corresponding enzymatic activity in the presence of increasing concentrations of urea or GdnCl (24 h, RT) are shown in Fig. 4-14. The maximal fluorescence emission of the native *Lb*ADHwt and *Lb*ADH G37D was observed at 330.5 nm. Unfolding of the proteins by urea or GdnCl induces a red shift of the emission maximum to about 353 nm, which is characteristic for free tryptophan in aqueous solution [201]. Both enzyme variants show a typical two-state urea denaturation profile with overlapping inflecting points of the sigmoidal deactivation curves and the emission maxima. From the urea denaturation curves a higher stability can be deduced for the *Lb*ADH G37D, which reaches the inflection point with 2.5 M urea, whereas the wild type enzyme's inflection point is reached with 1 M urea (Fig. 4-14 A and B). As expected, GdnCl is the stronger denaturant as urea. So, *Lb*ADHwt was completely inactivated at GdnCl concentrations higher than 0.5 M, whereas 2.0 M urea was necessary to cause the same effect (Fig. 4-14).

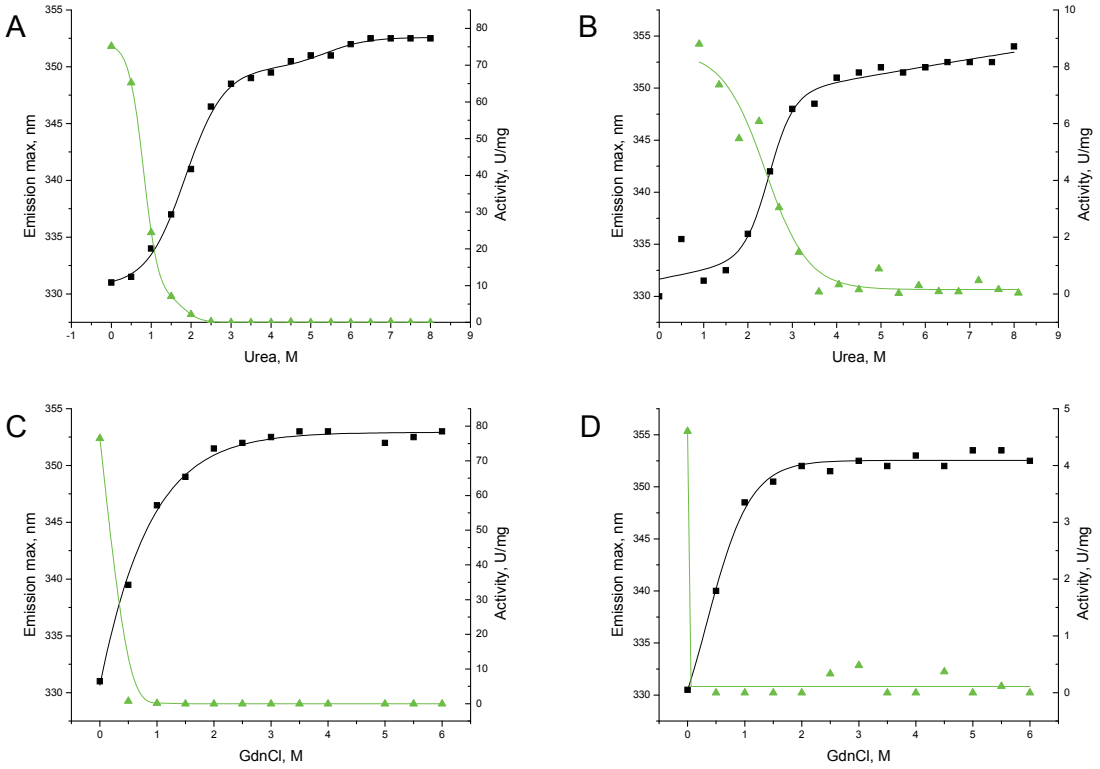

Figure 4-14. Unfolding of the *Lb*ADHwt and the *Lb*ADH G37D in urea and GdnCl by fluorescence emission spectroscopy. The fluorescence emission maxima are depicted in black squares ■, activity data are represented by green triangles ▲. A: *Lb*ADHwt denaturation in the presence of urea; B: *Lb*ADH G37D denaturation in the presence of urea; C: *Lb*ADHwt denaturation by GdnCl; D: *Lb*ADH G37D denaturation by GdnCl. Measurements were performed with a 0.1 mg/ml solution of the *Lb*ADHwt or the *Lb*ADH G37D in 10 mM TEA, 1 mM $MgCl_2$ buffer at pH 7.5 and the respective concentration of urea or GdnCl after incubation at RT for 24 h. Excitation wavelength 295 nm. Further experimental details are represented in section 3.6.1.2.

Investigation of the same samples with CD spectroscopy revealed a decrease of the CD signal amplitude with increasing denaturant concentrations (Fig. A-2, Appendix). The band's shape changes as well becoming more similar to the spectrum of a β-sheet [206]. Similar to the fluorescence studies, the largest change of the signal intensity occured between 0.0 M and 3.0 M urea for the *Lb*ADHwt and between 0.0 M and 4.0 M urea for the variant. The increase of the elipticity$_{222}$ signal was accompanied by a decay of the residual enzymatic activity (Fig. 4-15 C-D). The observed changes resulted in almost the same sigmoidal curves as was observed by fluorescence spectroscopy. The *Lb*ADH G37D variant was more stable than the wild type enzyme. The inflection point was observed at 2.0 M urea, whereas the wild type enzyme's inflection point was reached with 1.2 M urea.

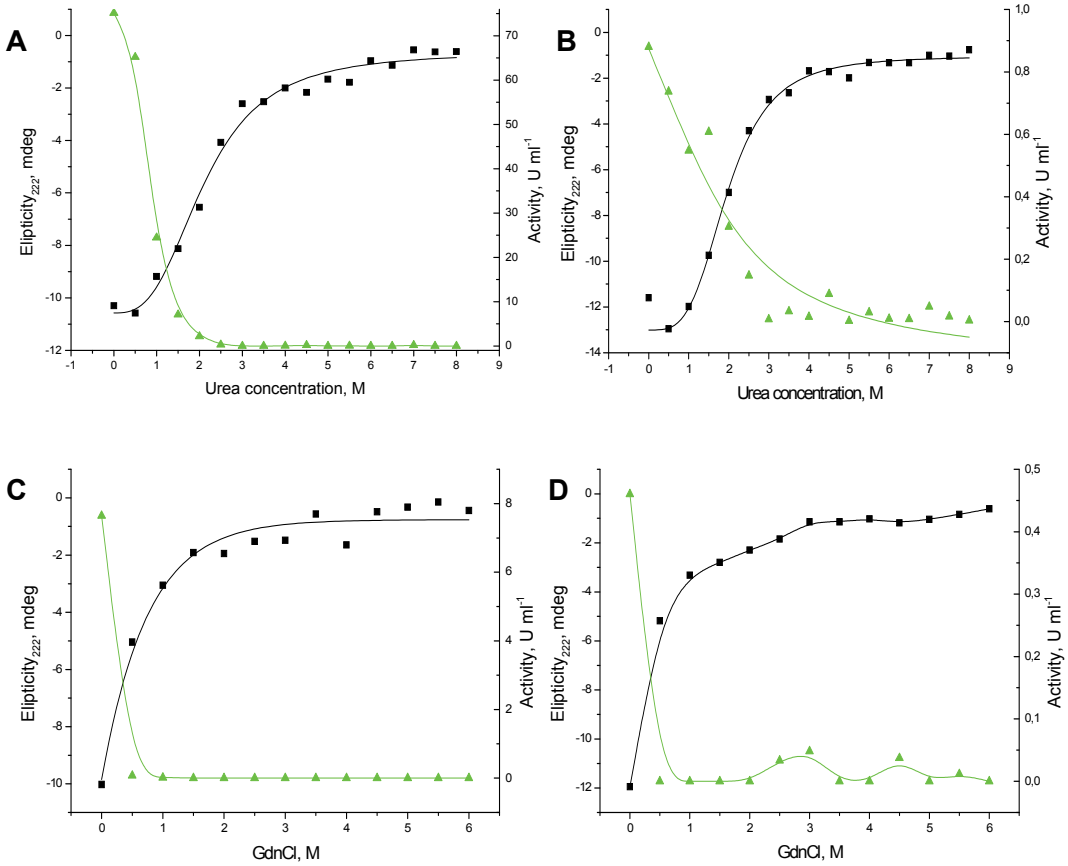

Figure 4-15. Unfolding of *Lb*ADHwt and the *Lb*ADH G37D in urea and GdnCl by CD spectroscopy. The elipticity$_{222}$ values are depicted in black squares ■, activity data are represented by green triangles ▲. A: *Lb*ADHwt denaturation in the presence of urea; B: *Lb*ADH G37D denaturation in the presence of urea; C: *Lb*ADHwt denaturation by GdnCl; D: *Lb*ADH G37D denaturation by GdnCl. Further experimental details are represented in section 3.6.2.2.

The detection of the residual activity showed that *Lb*ADHwt was completely inactivated at GdnCl concentrations higher than 0.5 M, whereas 2.0 M urea was necessary to cause the same effect (Fig. 4-14 and 4-15). Evidently, there was a correlation between enzymatic activity, CD, and fluorescence signals, which indicated, that perturbations of secondary and tertiary structure occurred simultaneously.

Thermal denaturation of both enzyme variants in the solid and dissolved states was comparatively studied using fluorescence and static light scattering spectroscopy methods paralleled by residual activity measurements. Experiments were designed such that heat-induced inactivation was completed in 30 min. As shown in Fig. A-3 (Appendix), the fluorescence intensity steeply declined with increase of the heating time in all cases. Thus, no clear division into transition and post-transition regions was detected.

As was already deduced from the residual activity measurements (Fig. 4-10), *Lb*ADHwt is less thermostable than *Lb*ADH G37D in aqueous solution. Using fluorescence spectroscopy, we could deduce these stability differences to the structural stability. The unfolding in solution at 50°C, which was detected by

analysis of the fluorescence emission maxima shift, occurred 2-fold faster for the wild type enzyme than for the G37D variant, which coincided with the residual activity (Fig. 4-16 A and B). Using the same experimental approach, it could be shown that the time-course of structural stability loss coincides with residual activity measurements also in the solid samples and does not show significant differences for the wild type enzyme and and the G37D variant (Fig. 4-16 C, D).
Detection of the intrinsic fluorescence emission was followed by static light scattering measurements. The intensity of scattered light is proportional to the concentration and absolute molecular weight (Mw) of the molecules (section 3.6.3.1). As in our experiments the protein concentration was kept constant, the increase of light scattering intensity reflects the protein aggregation. As represented in Fig. 4-17 A-B, heat-treatment of the dissolved *Lb*ADHwt and *Lb*ADH G37D at 50°C was followed by an increase of the light scattering intensity, which indicated the formation of aggregates. The curves were fitted with a sigmoidal function. The light scattering intensity of the heated dissolved *Lb*ADHwt normalized to the signal intensity of the intact enzyme increased by a factor of 15, whereas the intensity of *Lb*ADH G37D was 6 fold enhanced. The formation of the largest aggregates in both cases was achieved after about 15 min and stayed relatively constant afterwards, suggesting that a protein-aggregate equilibrium had been reached. Inflection points determined for the dissolved *Lb*ADHwt and *Lb*ADH G37D at 50°C by both spectroscopic techniques coinsided at 5 and 8 min, respectively.

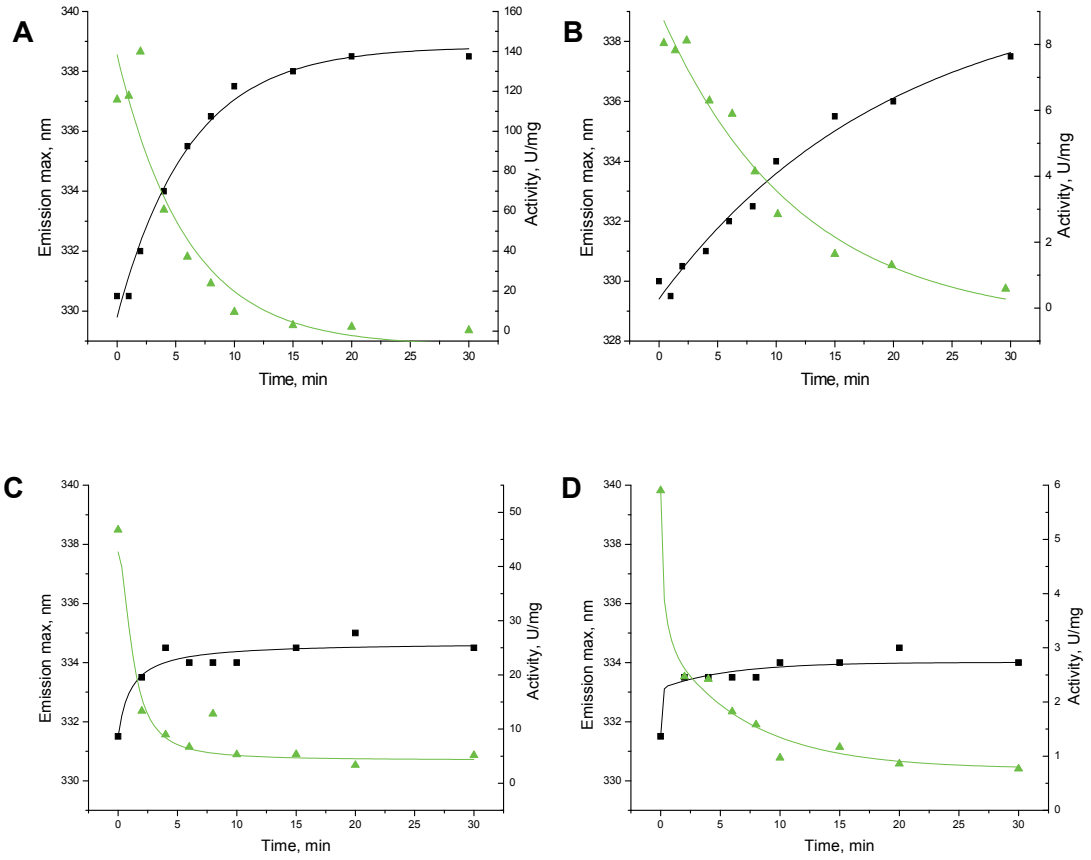

Figure 4-16. Thermal inactivation and unfolding of the *Lb*ADHwt and the *Lb*ADH G37D fluorescence emission spectroscopy. The fluorescence emission maxima are depicted in black squares ■, activity data are represented by green triangles ▲. A: dissolved *Lb*ADHwt at 50°C; B: dissolved *Lb*ADH G37D at 50°C; C: solid *Lb*ADHwt at a_w = 0.1 and T = 80°C; D: solid *Lb*ADH G37D at a_w = 0.1 and T = 80°C. To study the dissolved samples, 0.1 mg/ml solution of the *Lb*ADHwt or the *Lb*ADH G37D in 10 mM TEA, 1 mM $MgCl_2$ buffer at pH 7.5 was divided into 800 µl aliquots, heated at 50°C for 0-30 min and analyzed by fluorescence spectroscopy in correlation with enzymatic activity. The solid protein samples were equilibrated with saturated solution of LiCl for 24 h to reach a_w of 0.1, then heated at 80°C for 0-30 min, cooled down to room temperature, re-dissolved in 1 ml of distilled water, and immediately checked for fluorescence properties and enzymatic activity. Further experimental details are represented in section 3.6.3.2.

Thermal treatment of the solid *Lb*ADHwt and *Lb*ADH G37D preincubated at a_w 0.1 at 80°C resulted in structural changes of significantly lower degree (Fig. 4-17 C, D). Despite of exponential loss of catalytic activity, light scattering intensity of the re-dissolved enzyme samples did not follow an evident trend. A slight increase of intensity values, however, was observed in all the cases. This fact could indicate the presence of associated enzyme species in the samples. To verify this hypothesis and assess the amount of aggregated protein, which might be formed in the liquid and dry enzyme samples upon heating, the soluble protein concentration was checked for both dissolved enzyme variants incubated at 50°C

and for the solid protein probes, which were heat-inactivated at 80°C and then re-dissolved in water (Fig. 4-18).

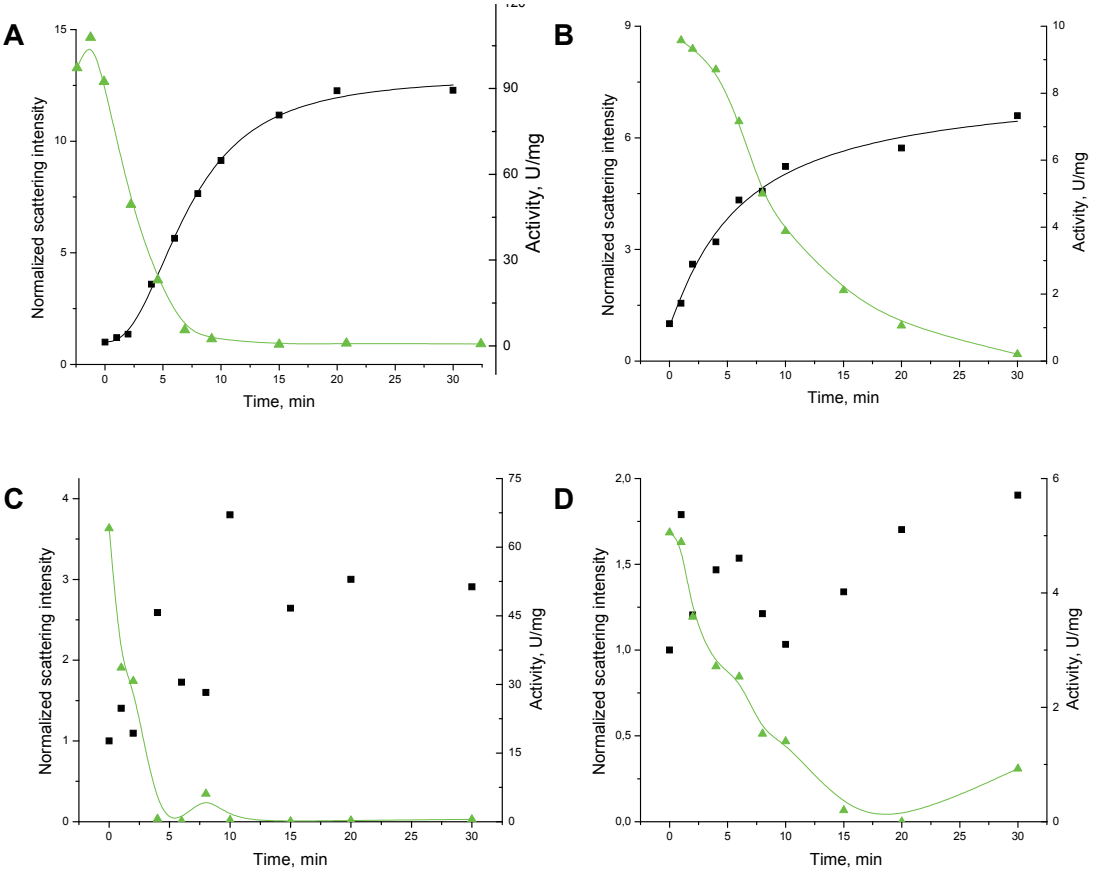

Figure 4-17. Thermal inactivation and unfolding of the *Lb*ADHwt and the *Lb*ADH G37D by static light scattering spectroscopy. The normalized light scattering intensity is depicted in black squares ■, activity data are represented by green triangles ▲. A: dissolved *Lb*ADHwt at 50°C; B: dissolved *Lb*ADH G37D at 50°; C: solid *Lb*ADHwt at aw=0.1 and T=80°C; D: solid *Lb*ADH G37D at aw=0.1 and T=80°C. To study the dissolved samples, 0.1 mg/ml solution of the *Lb*ADHwt or the *Lb*ADH G37D in 10 mM TEA, 1 mM $MgCl_2$ buffer at pH 7.5 was divided into 800 µl aliquots, heated at 50°C for 0-30 min and analyzed for light scattering at 450 nm, angle 90° in correlation with the residual enzymatic activity. The solid protein probes were equilibrated over a saturated solution of LiCl for 24 h to reach a_w of 0.1, then heated at 80°C for 0-30 min, cooled down to room temperature, re-dissolved in 1 ml of distilled water, and immediately checked for light scattering and enzymatic activity. Further experimental details are represented in section 3.6.3.2.

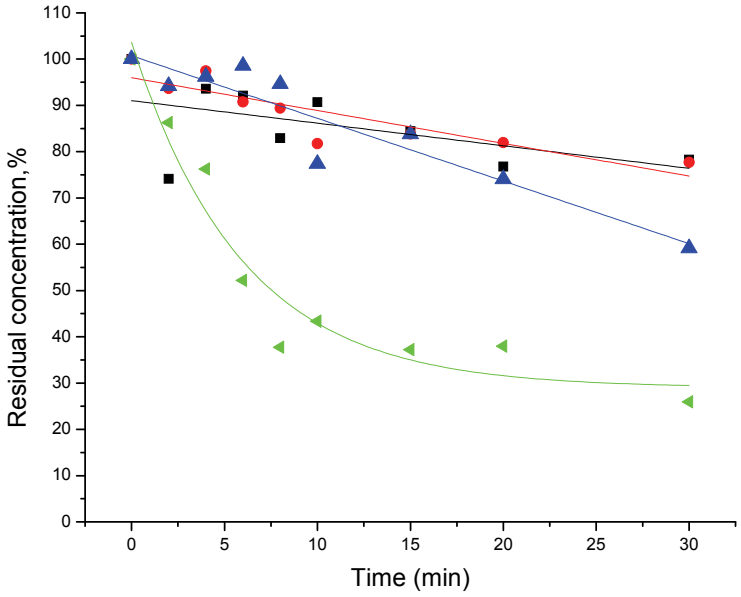

Figure 4-18. Thermal inactivation of the solid *Lb*ADHwt and *Lb*ADH G37D, solubility properties. The properties of the following samples were investigated: dissolved *Lb*ADHwt at 50°C, ■; dissolved *Lb*ADH G37D at 50°C, ●; solid *Lb*ADHwt at a_w=0.1 and T=80°C, ◀; solid *Lb*ADH G37D at a_w=0.1 and T=80°C, ▲. To study the dissolved samples, 0.1 mg/ml solution of *Lb*ADHwt or *Lb*ADH G37D in 10 mM TEA, 1 mM $MgCl_2$ buffer at pH 7.5 were divided into 800 µl aliquots, heated at 50°C for 0-30 min and analyzed for the content of soluble protein by the Bradford method. The solid protein samples were equilibrated over a saturated solution of LiCl for 24 h to reach a_w value of 0.1, then heated at 80°C for 0-30 min, cooled down to room temperature, re-dissolved in 1 ml of distilled water, incubated in water for 6 h and then assayed for protein concentration using the Bradford method (section 3.4.1).

The results revealed that protein solubility decreased linearly for the dissolved samples of both enzymes upon heating at 50°C and for the solid samples of *Lb*ADH G37D during its heating at 80°C, whereas the solubility of the solid *Lb*ADHwt decreased exponentially and to a much stronger extent after heating to 80°C. Thus, even for the dry solid samples, a significant aggregation is very probable.

In the dissolved state, no significant differences in the protein solubility between both variants were found. In contrast, *Lb*ADHwt samples lost solubility at 80°C significantly faster than the variant G37D. This effect could not be observed in Fig. 4-16 and 4-17, since the residual activity measurements were referred to the soluble protein amount. The different aggregation level of the solid samples of both enzyme variants may be restricted only to temperatures above 70°C where stronger deviation between half-life of the solid protein was observed (Fig. 4-11).

The dependence of thermal degradation of the *Lb*ADHwt and *Lb*ADH G37D on a_w was investigated by heating a single protein probe inside a CD-photometer with a constant speed. The dissolved protein samples were heated in a hermetically closed quartz cuvette, whereas the solid state studies were performed with the enzymes lyophilized on quartz glasses and pre-incubated at defined a_w. CD

spectra were recorded at a sample temperature, which excluded the possibility of renaturation. This method allowed monitoring of the stepwise conformational changes and determination of the midpoint temperature in the transition region. However, it was not possible to test the residual enzymatic activity.

CD spectra of the dissolved *Lb*ADHwt and *Lb*ADH G37D looked similar. They displayed two negative peaks at 222 nm and at 208 nm, and one positive peak near 192 nm (Fig. 4-19 A-B), which is characteristic for proteins rich in α-helices [201, 206]. No band between 250 and 300 nm was present. Therefore, the signal measured in the wavelength range of 200-260 nm was used for investigation of changes in the secondary structure elements content. In all experiments a high degree of data scattering was detected.

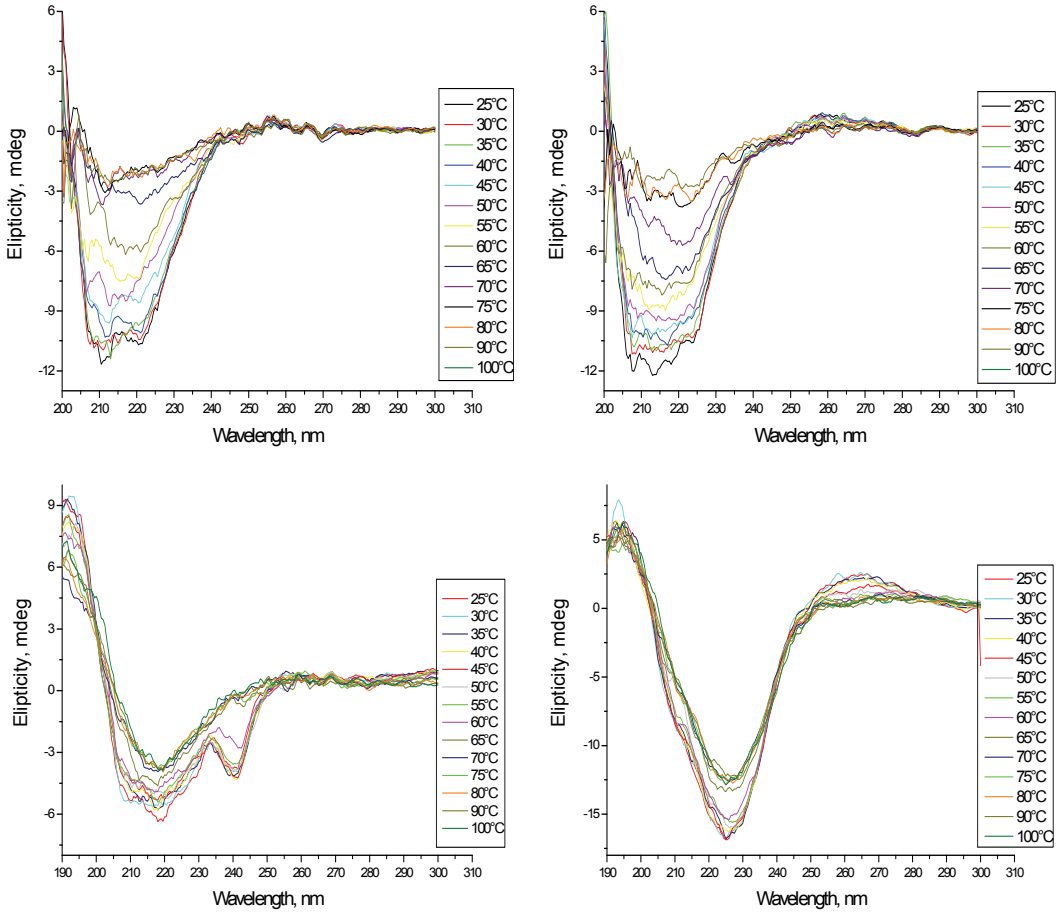

Figure 4-19. Temperature dependence of CD spectra of the dissolved and solid *Lb*ADHwt and *Lb*ADH G37D. A: dissolved *Lb*ADHwt at 50°C; B: dissolved *Lb*ADH G37D at 50°C; C: solid wt *Lb*ADH at a_w=0.9 and T=80°C; D: solid *Lb*ADH G37D at a_w=0.9 and T=80°C. . The experimental parameters are represented in section 3.6.2.2.

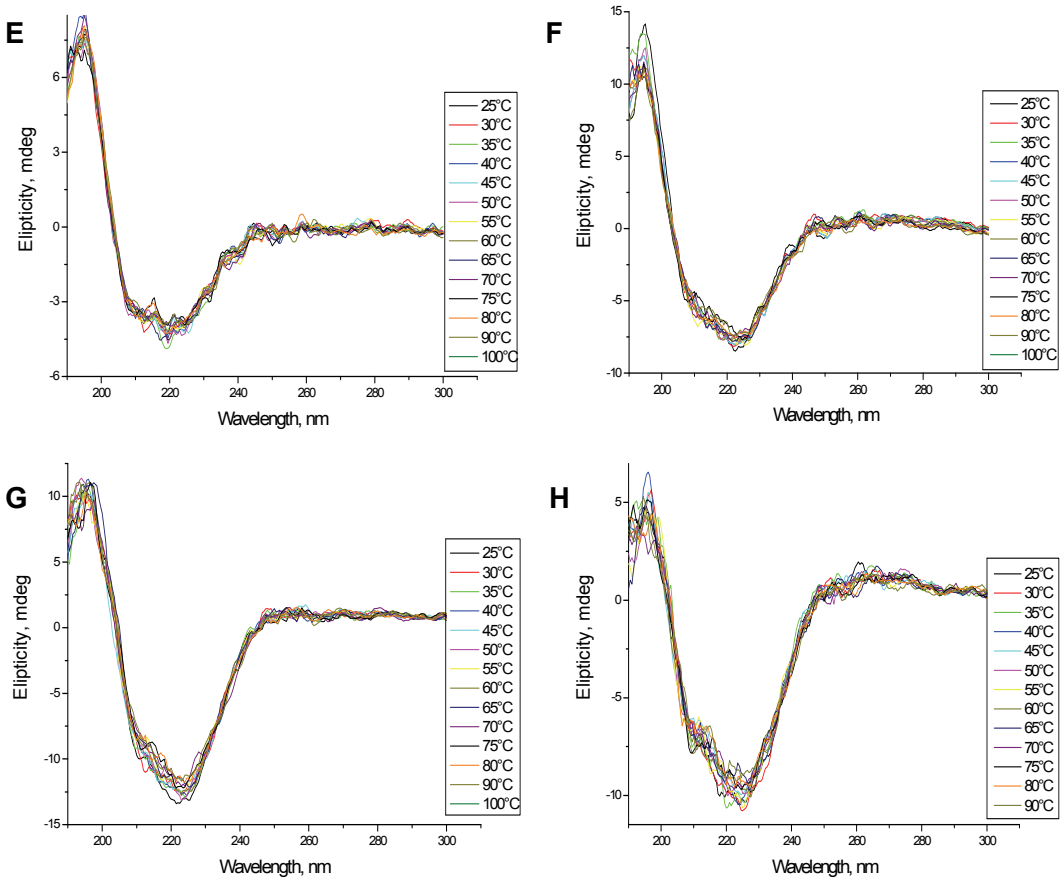

Figure 4-19, continued. Temperature dependence of CD spectra of the dissolved and solid *Lb*ADHwt and the *Lb*ADH G37D. E: solid *Lb*ADHwt at a_w=0.7 and T=80°C; F: solid *Lb*ADH G37D at a_w=0.7 and T=80°C; G: solid *Lb*ADHwt at a_w=0.1 and T=80°C; H: solid *Lb*ADH G37D at a_w=0.1 and T=80°C. The experimental parameters are represented in section 3.6.2.2.

The CD spectra of the dissolved *Lb*ADHwt and *Lb*ADH G37D heated up to 80°C with 5°C intervals are shown in Fig. 4-19 A-B. Both the shape and the amplitude of the negative peak at 205-240 nm were affected, indicating massive unfolding of α-helices. Plotting of the percentage of the initial helical content of *Lb*ADHwt and *Lb*ADH G37D against incubation temperature displayed sigmoidal melting curves with the midpoints at approximately 58°C for the wild type enzyme and at 65°C for the variant (Fig. 4-20 A-B). It is important to mention, that these values do not correspond to the melting temperatures of the enzymes due to cumulative effect induced by the stepwise heating in the protein structure.

The spectra of the solid enzymes at all tested a_w values were recorded with a high signal scattering. The spectra were found to differ from the ones of the dissolved proteins (Fig. 4-19). In particular, the peaks' magnitude was significantly lower, and the shape of CD spectra demonstrated a flattening of the trough at 208 nm. Rotation of the sample to 180°C did not change its spectra. The reduction of the signal amplitude could be explained by the significantly shortened optical pathway

used to detect CD spectra of the solid protein samples relative to a cuvette with a dissolved sample. Changes of the spectral shape could arise either from a contribution of differential scattering and absorption scattering effects below 230 nm or from a conformational change, which accompanied the freeze-drying of the protein [243]. Indirect support for the latter case would be the fact that lyophilization of the both *Lb*ADHwt and *Lb*ADH G37D led to a loss of about 20% of the initial catalytic activity. Similar changes of shape and magnitude of the CD spectra were also observed for RNase A placed on a thin-film and dried by a stream of N_2 [244], lyophilized fibronectin [245], crystals of proteorhodopsin [246] and subtilisin Carlsberg immobilized on silica particles [243]. Additionally, the lyophilization-promoted increase of the β-sheet content accompanied by lowering of the α-helical content was also found by other spectroscopic techniques, such as FTIR spectroscopy [246-249], VCD (Vibrational Circular Dichroism) spectroscopy [250], and hydrogen/deuterium exchange with mass spectrometry [248]. On the contrary, an extensive investigation of the drying process of thirteen different globular proteins, which was performed by synchrotron radiation vacuum CD spectroscopy, did not reveal considerable structure perturbations associated with dehydration [251].

As indicated in Fig. 4-19-1 C, the lyophilization-induced transition of α-helices to β-sheets in *Lb*ADHwt is reversible. After incubation at a_w 0.9 for 24 h the CD spectrum shows a pronounced minimum at 208 nm. Heating of the solid *Lb*ADHwt and *Lb*ADH G37D at lower a_w did not lead to changes of the negative peak shape (Fig. 4-19-2), but the signal magnitude reduces. Heating of the samples preincubated at a_w 0.9 led to the increase of elipticity$_{222}$ values, which indicated the decomposition of native protein structure (Fig. 4-20, red). Similar to the dissolved samples, the denaturation of the solid probes followed sigmoidal model. The degree of structural decomposition, however, was significantly lower. Heating of the solid samples with adjusted a_w to 0.7 resulted in monotonical decomposition of about 20% the native structure (Fig. 4-20, blue). Thermal incubation of the solid samples with a_w 0.5 and 0.1 showed neither significant change of elipticity$_{222}$ values and the corresponding structural content, nor considerable differences between these samples (Fig. 4-20, green and yellow). No more than 10% of the initial α-helical content was perturbed. With regard of inactivation of the solid *Lb*ADHwt and *Lb*ADH G37D at elevated temperatures (Fig. 4-11 and Table 4-3), one can conclude, that inactivation of the solid enzymes is caused by local effects, which can, however, entail a process analogous to aggregation (Fig. 4-18). Global unfolding of the native protein structure, which can be detected by spectroscopic methods, does not occur in solid state.

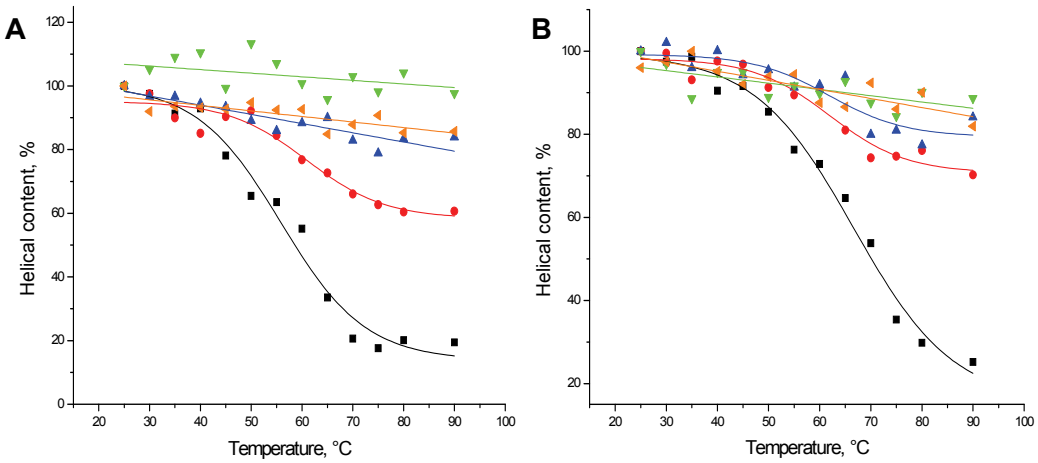

Figure 4-20. Thermal unfolding of *Lb*ADHwt and the *Lb*ADH G37D: percentage of the initial helical content. A: *Lb*ADHwt; B: *Lb*ADH G37D. Water activity was adjusted to 1.0 (■), 0.9 (●), 0.7 (▲), 0.5 (▼) and 0.1 (◀). The percentage of the initial structural content was calculated based on elipticity$_{222}$ values, which were obtained from CD cpectra measured according to the section 3.6.2.2.

Besides, thermal inactivation of the dissolved enzymes was irreversible (Fig. 4-21 A-B). Neither the shape nor the signal magnitude of the initial CD spectra of the native *Lb*ADHwt and *Lb*ADH G37D were restored when the samples were slowly cooled down after the thermal treatment.

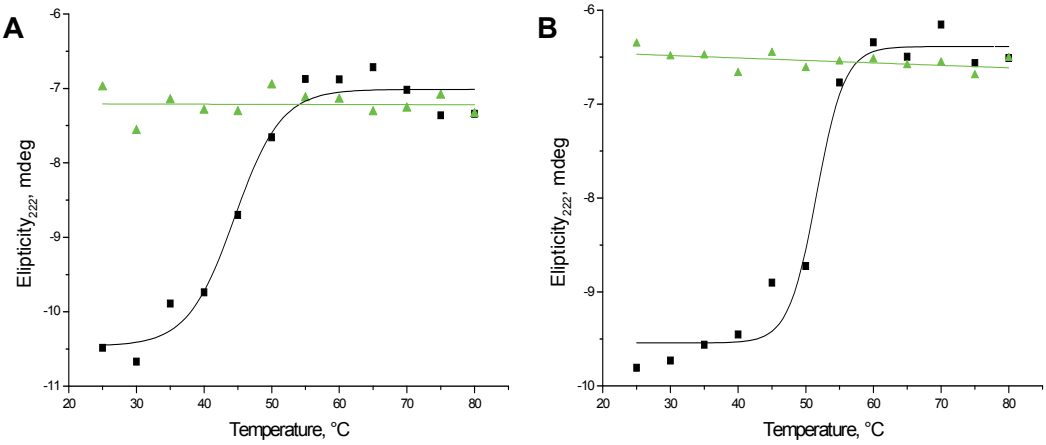

Figure 4-21. Elipticity$_{222}$ in the CD spectra of *Lb*ADHwt and *Lb*ADH G37D as a function of temperature during heating from 25 to 80 °C (■) and cooling from 80 to 25 °C (▲). A: dissolved *Lb*ADHwt; B: dissolved *Lb*ADH G37D. The experimental parameters are represented in section 3.6.2.2.

In summary, heat-induced minor unfolding of the protein structure in the solid state followed by irreversible intermolecular aggregation is the suggested process which could cause enzyme inactivation also for gas/solid catalysis, at least at higher temperatures (> 70°C) or upon prolonged heating at 40-50°C. In the reactive

system, however, the additional effects due to the presence of the substrates and co-substrates have to be considered, which might increase enzyme inactivation already at lower temperatures.

4.4 Generation of thermostable *Lb*ADH variants

As already shown in the section 4.2, the solid enzymes are significantly more stable than the dissolved ones. However, progressive inactivation of ADHs was observed under the gas/solid reactor conditions [6, 252-254]. So, Yang and Russell described the conversion of 3-methyl-2-buten-1-ol, catalyzed by immobilized yeast ADH in a continuous gas/solid reactor at 22-50°C at different water activities and observed steady-state periods of 4-16 days prior to progressive inactivation [6]. Reduction of acetophenone with the solid immobilized wild type *Lb*ADH performed in a continuous gas/solid reactor at 40°C and a water activity (a_w) of 0.5 revealed a half-life between 1 to more than 40 days for the enzymatic activity depending on the immobilization conditions [254]. In our gas/solid reactor studies, performed with *Lb*ADHwt and *Lb*ADH G37D and represented in the section 4.7, the specific initial reaction rates were strongly dependent on the water content. Reaction rates significantly increased with a_w, which, however, provoked a considerable decrease of the enzymatic stability at 40°C. Taking into consideration that potential application of the less volatile substrates into the gas/solid catalytic system would require a further increase of the operational temperature, the enzymatic stability under operational conditions represents a challenging task. Thus, generation of highly thermostable enzyme variants able to function at elevated temperatures and at higher water activities in the gas/solid reactor is desired.

As will be represented in the section 4.7, both the *Lb*ADH and the *Lb*ADH G37D can be successfully applied in the gas/solid reactor for the synthesis of chiral alcohol (*R)*-phenylethanol at 40°C. In these experiments, the thermostability of the solid enzymes determined “offline” in the absence of substrates (section 4.2.2) has been proven to be predictive for the operational stability in the gas/solid reactor with accuracy for the order of magnitude. This finding served for the establishment of a high throughput screening systems used in the current project. The novel screening system was applied for the selection of enzyme variants suitable for the gas/solid biocatalysis.

4.4.1 Construction and screening of an *Lb*ADH G37D mutant library

To make use of the advantages of NADH preference and higher thermostability (see the chapters 4.1 and 4.2), the variant *Lb*ADH G37D was chosen as a starting point to increase thermostability further by directed evolution. Since the X-ray structure of the *Lb*ADH G37D is already known (PBD ID 1ZJY), the B-fitter strategy

(see section 1.4.3.4), which is based on recognition and randomization of the mostly disordered amino acids in the protein, was exploited here [172]. The 42nd, 44th and 48th amino acids were selected with the help of the B-FITTER program and subjected to targeted randomization. Reasoning from the complex nature of protein thermostability and cooperative effects of small stabilizing interactions [114], randomization of the three codons was performed simultaneously. Degenerate PCR primers coding 12 different amino acids in the 42nd, 6 in the 44th and 20 in the 48th position were used to generate and a library with 6000 mutant variants.

Since the structural mechanisms leading to the thermoinactivation of the enzyme in the dissolved and solid state were different (see the chapter 4.3), selection of thermostable variants suitable for the gas/solid biocatalysis was performed in the solid state (the screening procedure is described in details in the section 4.4.2). This was done by assaying for residual activity after incubation of the lyophilized cell lysates at high temperature. However, the mutant library was additionally screened for thermostability in the dissolved state in order to entirely utilize the potential of the mutant library and preclude the possibility of missing some promising variants.

The screening of the library for improved thermostability was implemented in two stages. First, 4000 variants were assayed for higher thermostability in the solid state. Screening was done at 80°C for 10 min, since the half-life of the starting protein *Lb*ADH G37D at 80°C equaled to 10±2 min. This half-life value does not correspond to the previously mentioned half-life value of 19±3 min in (Table 4-3 in section 4.2.1) due to the fact, that the screening was performed with the lyophilized cell lysates, whereas the previously reported thermostability studies were carried out using the purified enzyme. Second, thermostability in the aqueous solution was estimated for all the 6000 variants for 10 min at 50°C. Although the half-life of the cell lysate containing *Lb*ADH G37D at 50°C was found to be 6.7 ± 0.2 min, it was prolonged to 10 min for technical reasons. The screening revealed 22 and 97 mutant variants, which showed higher thermostability than the *Lb*ADH G37D control in the solid and dissolved state, respectively. After isolation and additional screening on a larger scale, 12 variants were found to meet the statistical requirements. These variants were chosen for detailed characterization in the purified state.

4.4.2 Setup and validation of a high-throughput screening (HTS) system

The spectroscopic studies performed with *Lb*ADHwt and *Lb*ADH G37D revealed that the thermal inactivation of the dissolved and the solid enzymes occurs via different routes, which suggest different inactivation mechanisms in the solid and dissolved state (section 4.3). Therefore, a variant with higher thermostability in the solid state can most probably not be identified from you a usual screening in

solution. Thus, screening was performed with solid dry enzyme samples. The design of an appropriate HTS system is represented in Fig. 4-22.

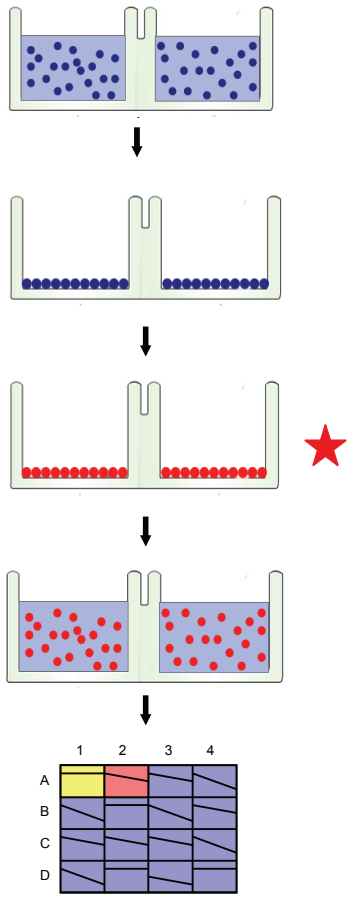

- Cooling down, addition of water, screening for *LB*ADH G37D activity
- Screening for *Lb*ADH G37D activity in liquid phase, selection of active variants
- Water evaporation in the dissicator/ lyophillisation
- Heat treatment of the solid sample at 80°C for 10 min
- Evaluation of selected variants

Figure 4-22. Schematic representation of the HTS system design.

The screening for improved variants suitable for the gas/solid biocatalysis included determination of the initial catalytic activity of the cell lysates containing the overexpressed enzyme variants at room temperature with subsequent lyophilization and screening for the residual enzymatic activity after incubation of a dried cell lysate at 80°C for its half-life time. During the course of this PhD project, the system was continuously validated, optimized, and used for the screening of 4000 enzyme variants. The most important factors for successful screening are the following:

- overexpression in autoinduction medium (according to Reetz and Carballeira, [172]);
- appropriate dilution of the cell lysates in ddH_2O prior to the freeze-drying;
- moderate vacuum strength of lyophilization process.

The final version of the HTS is represented in the section 3.5.2.2/3 of the “Materials and Methods” chapter. Validation of this system was based on commonly accepted parameters, which are described in details in the section 3.5.2.3. The results are

summarized in the Table 4-6. Despite the higher value of the Z factor, which estimates the separation of a signal from a background, the quality of the HTS system was considered as sufficient for the quantitative screening of the mutant library.

Table 4-6. Statistical evaluation of the HTS reliability.

Statistical parameter	Calculated value	Acceptable value
S/B	9.2	> 3
S/N	20.4	> 10
CV	8%	<10 %
Z factor	0.94	< 0,4

Since the thermostability of the solid enzymes was found to reflect the operational stability in the gas/solid reactor with accuracy for the order of magnitude (section 4.7), no other influencing factors (*e.g.* influence of thermodynamic activity of water or/and substrates) have been considered.

4.4.3 Characterization of selected stabilized *Lb*ADH variants

The attempt to increase thermal stability of the *Lb*ADH G37D by constructing and screening of a mutant library resulted in selection of 11 potential candidates with increased thermostability in the dissolved or solid state (the amino acid substitutions present in these variants are summarized in Table 4-7, section 4.4.4). To exclude possible stabilizing effects of the crude extract components, these variants were expressed on a larger scale, and purified using ion-exchange chromatography (section 3.3.1). Thermal stability of the selected hints was investigated in the dissolved and solid state by measuring the residual enzymatic activity after 60 min incubation at different temperatures, according to Bogin et al. [255]. As shown in Fig. 4-23, the residual enzymatic activity of the dissolved enzyme variants plotted against the temperature displayed a sigmoid shape, with midpoints of the thermal inactivation curves of about 41.0°C and 45.0°C for the *Lb*ADHwt and *Lb*ADH G37D, respectively. The selected randomized variants display a similar shape of the inactivation curves. The transition region of some selected variants LK18 G4 (T_{md} = 47.3°C), LK19 A11 (T_{md} = 47.0°C), LK19 F11 (T_{md} = 47.5°C), LK34 G3 (T_{md} = 46.5°C), LK41 C12 T_{md} = 50°C), and LK41 H7 (T_{md} = 47.9°C) were shifted to higher temperatures compared to *Lb*ADH G37D. Since the increase of enzymatic thermostability is considered to be associated with an increase of the long-term stability at lower temperatures [256], half-lifes of the mentioned variants at 40°C (operation temperature of the gas-solid reactor) might be prolonged in comparison to *Lb*ADH G37D.

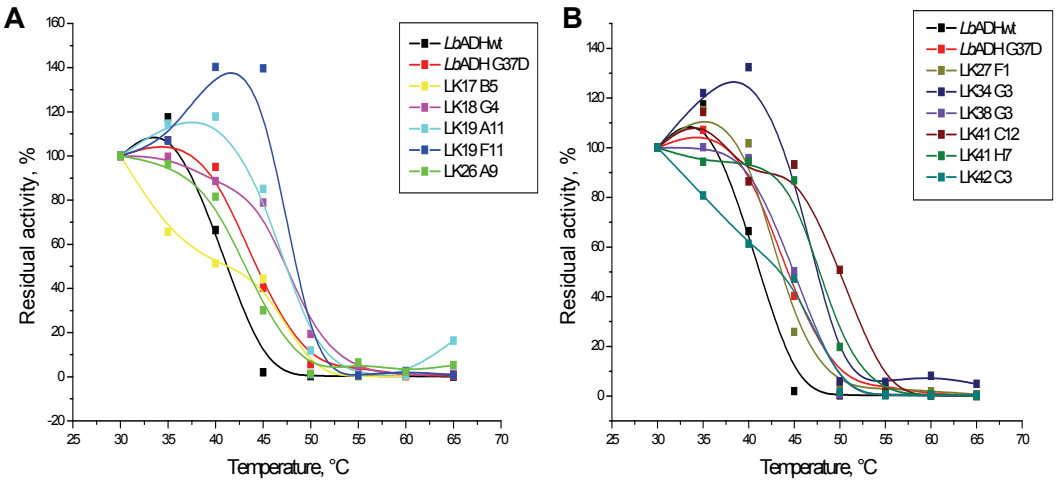

Figure 4-23. Thermal inactivation of 42/44/48-randomized *Lb*ADH G37D variants after 60 min incubation at different temperatures in aqueous solution. Heat inactivation experiments were performed with 100 µl of the 0.1 mg/ml enzyme solution in 10 mM TEA, 1 mM $MgCl_2$, pH 7.5. Residual activity was measured in duplicates using the standard photometric assay (section 3.4.2.1). Thermoinactivation profiles of the variants are highlighted as following: *Lb*ADHwt – red, *Lb*ADH G37D - black, LK17 B5 - green, LK18 G4 – blue, LK19 A11 – cyan, LK19 F11 – magenta, LK26 A9 – yellow, LK27 F1 – dark yellow, LK34 G3 – navy, LK38 G3 – purple, LK41 C12 – wine, LK41 H7 – olive, and LK42 C3 – dark cyan, respectively.

A temperature of 45°C, which corresponded to the midpoint of thermal inactivation curve of the "starting enzyme" *Lb*ADH G37D in the dissolved state, was chosen for further comparison of the randomized variants. Fig. 4-24, which represents the residual activity of the selected variants after incubation at 45°C for 60 min, clearly demonstrates their higher thermostability.

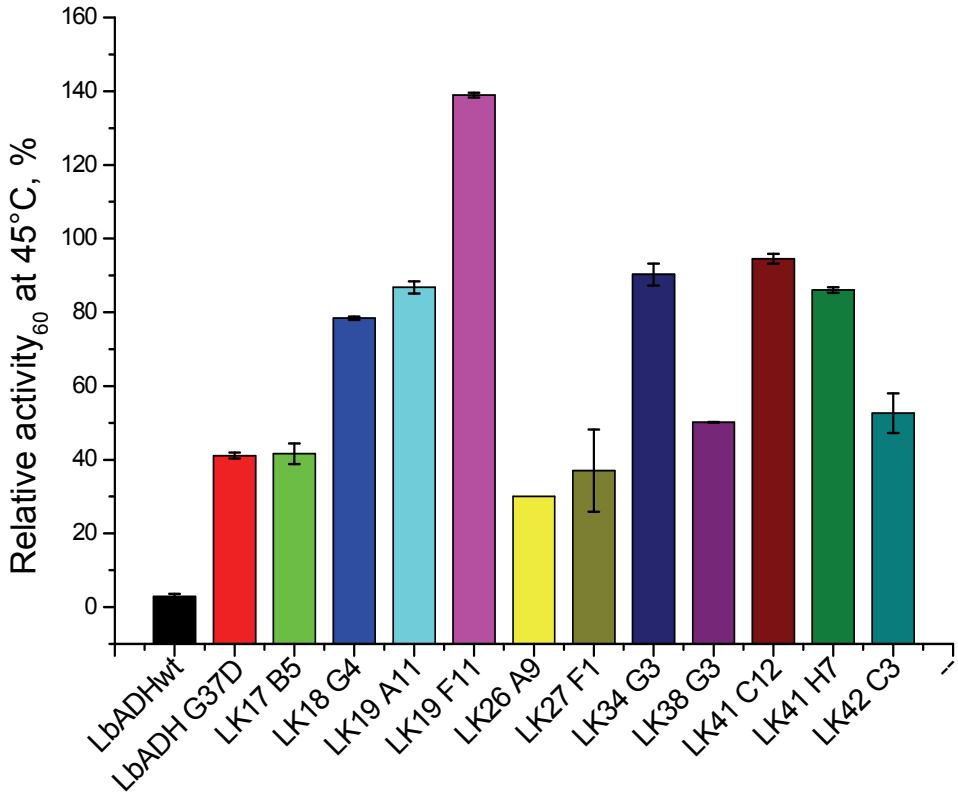

Figure 4-24. The residual activity the 42/44/48-randomized *Lb*ADH G37D variants after incubation at 45°C for 60 min in aqueous solution. The experiments were performed in 10 mM TEA, 1 mM $MgCl_2$, pH 7.5. The residual catalytic activity was determined using standard photometric assay in duplicates; two independent experiments were performed for each of the variants. Color code of the variants is the following: *Lb*ADHwt – red, *Lb*ADH G37D - black, LK17 B5 - green, LK18 G4 – blue, LK19 A11 – cyan, LK19 F11 – magenta, LK26 A9 – yellow, LK27 F1 – dark yellow, LK34 G3 – navy, LK38 G3 – purple, LK41 C12 – wine, LK41 H7 – olive, and LK42 C3 – dark cyan, respectively.

The inactivation of all the 42/44/48-randomized *Lb*ADH G37D variants in the solid state correlated linearly with increasing temperature (Fig. 4-25), which was in good accordance to the previously reported results of inactivation of the solid *Lb*ADHwt and *Lb*ADH G37D. It is obvious that most candidates in the solid state are inactivated even faster than the solid *Lb*ADH G37D control. The variant LK41 H7, however, displayed an extraordinary stability being inactivated in the range from 30 to 75°C (Fig. 4-25 B, olive).

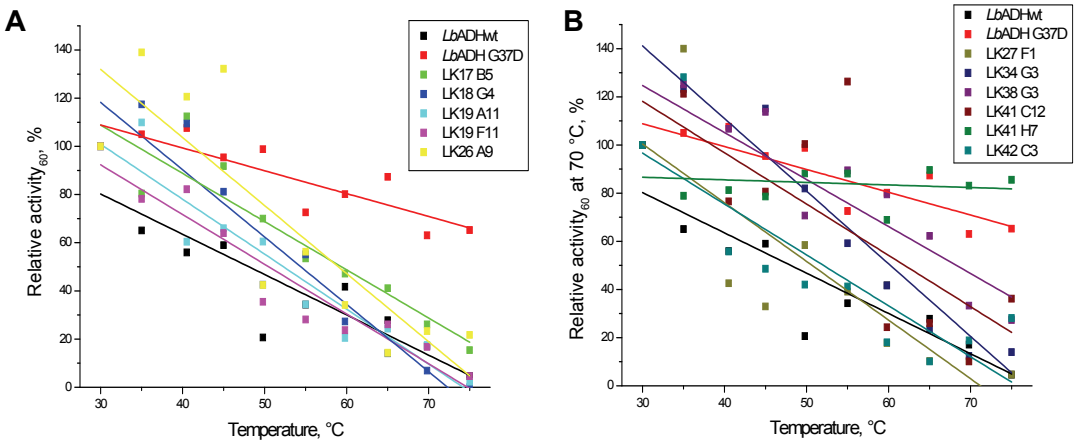

Figure 4-25. Thermal inactivation of the 42/44/48-randomized *Lb*ADH G37D variants after 60 min incubation at different temperatures in the solid state after 60 min incubation at different temperature. Heat inactivation experiments were performed with the solid probe obtained after freeze-drying of 100 µl of the 0.1 mg/ml enzyme solution in 10 mM TEA, 1 mM $MgCl_2$, pH 7.5. Residual activity was measured in duplicates after redisolving the thermally incubated samples by the standard activity assay (section 3.4.2.1). Thermoinactivation profiles of the *Lb*ADHwt and *Lb*ADH G37D are highlighted with bold lines. Thermoinactivation profiles of the variants are highlighted as following: *Lb*ADHwt – red, *Lb*ADH G37D - black, LK17 B5 - green, LK18 G4 – blue, LK19 A11 – cyan, LK19 F11 – magenta, LK26 A9 – yellow, LK27 F1 – dark yellow, LK34 G3 – navy, LK38G3 – purple, LK41 C12 – wine, LK41 H7 – olive, and LK42 C3 – dark cyan, respectively.

A temperature of 70°C, which corresponds to approximately 30% inactivation of the solid *Lb*ADH G37D, was chosen for the further comparison of the enzymes, because it was the lowest value of the residual activity determined experimentally for all the variants with high accuracy. The residual activity of all the selected variants after incubation at 70°C for 60 min is represented in Fig. 4-26. The residual activity demonstrated by the variant LK41 H7 in the solid state is significantly higher than the activity of the *Lb*ADH G37D and the other randomized variants. Since the variant LK41 H7 demonstrates higher thermostability in the dissolved state, too, it was selected as a most promising candidate for the later gas/solid reactor experiments.

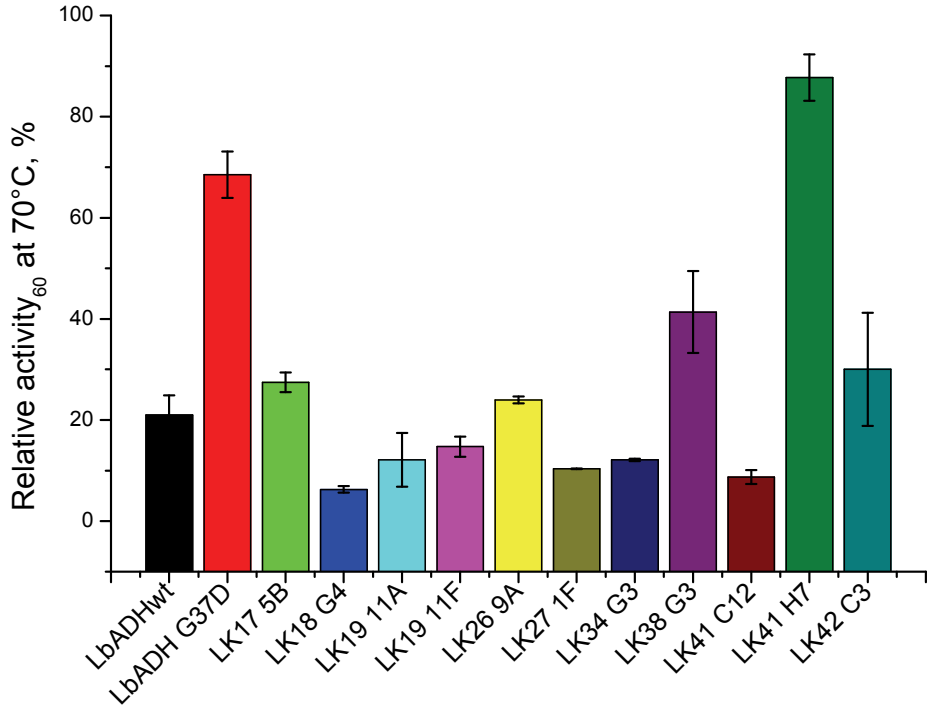

Figure 4-26. The residual activity of selected 42/44/48-randomized *Lb*ADH G37D variants after incubation at 70°C for 60 min in the solid state. The experiments were performed with the solid samples obtained after lyophilization of of 100 µl of the 0.1 mg/ml enzyme solution in 10 mM TEA, 1 mM $MgCl_2$, pH 7.5. Residual activity was measured in duplicates after redisolving the thermally incubated samples by the standard activity assay (section 3.4.2.1); two independent experiments were performed for each of the variants. Color code of the variants is the following: *Lb*ADHwt – red, *Lb*ADH G37D - black, LK17 B5 - green, LK18 G4 – blue, LK19 A11 – cyan, LK19 F11 – magenta, LK26 A9 – yellow, LK27 F1 – dark yellow, LK34 G3 – navy, LK38 G3 – purple, LK41 C12 – wine, LK41 H7 – olive, and LK42 C3 – dark cyan, respectively.

4.4.4 Explanation of stabilizing effects on the molecular level

The amino acid substitutions involved in the thermostabilization of *Lb*ADH G37D are summarized in Table 4-7. The variant LK19 A11 containes a single exchange V42D, while the further variants are mutated in all three positions. The triple mutant V42D/E44Y/K48E was selected twice, as LK41 C12 and LK34 G3. The most promising candidate LK41 H7 contains a combination of exchanges V42F/E44C/K48Q.

As already mentioned in section 4.2.1, the exchange G37D, which is located in a β-turn connecting the αB- and αC-helices in close proximity to the NADH binding region (Fig. 4-27 and 4-28), considerably increases the thermal stability of the variant *Lb*ADH G37D compared to *Lb*ADHwt. The βB-turn connecting two α-helices is known to be the thermo-sensitive part of the enzyme [146, 150, 151]. Manipulations in this region, such as partial deletions or point mutations, may significantly affect the local and even global flexibility of protein molecule, and, therefore, its thermal stability.

Table 4-7. 42/44/48-randomized variants of *Lb*ADH G37D variants with increased thermostability. X: Increased thermostability observed in comparison to *Lb*ADH G37D; -: no improvement of thermostability found.

Variant	The state of increased thermostability		Position 42	Position 44	Position 48
	Dissolved	Solid			
*Lb*ADH G37D			V	E	K
LK17 B5	-	-	F	N	R
LK18 G4	x	-	D	N	Q
LK19 A11	x	-	D	E	K
LK19 F11	x	-	L	Y	E
LK26 A9	-	-	I	Y	R
LK27 F1	-	-	I	F	L
LK34 G3	x	-	D	Y	E
LK38 G3	-	-	I	S	K
LK41 C12	x	-	D	Y	E
LK41 H7	x	x	F	C	Q
LK42 C3	x	-	V	F	E

Position 42 is located in the α-helix next to the βB-turn. Thus, this position can be considered in connection to the β-turn and the cofactor binding site. As a charged aspartate residue replaces the valine in postion 42, this additional charge might rigidify the whole α-β-α joint through additional electrostatic interactions with R38,

which is located in position i-1, whereas the contact with K45 (located in position i+3) could stabilize the α-helix. Additionally, exclusion of the ß-branched V42 from the α-helix eliminated conformational constraints caused by this residue.
Positions 44 and 48 are situated in the α-helix more distant from the β-turn. Mutations in these positions may perturb the formation of the helix, stabilizing or destabilizing it. As the αC-helix is located in proximity to the cofactor binding pocket, these changes can also have effect on the cofactor association and dissociation. Additionally, three simultaneous mutations in the α-helix are able to drastically affect the structure of the whole subunit via changes in interaction with solvent molecules and internal water network. This might further affect the assembly of subunits in the active form of the enzyme. However, the detailed evaluation of all the mentioned mechanisms requires further investigation, such as MD simulation coupled with rational creation of point mutants, which should be done in the future.

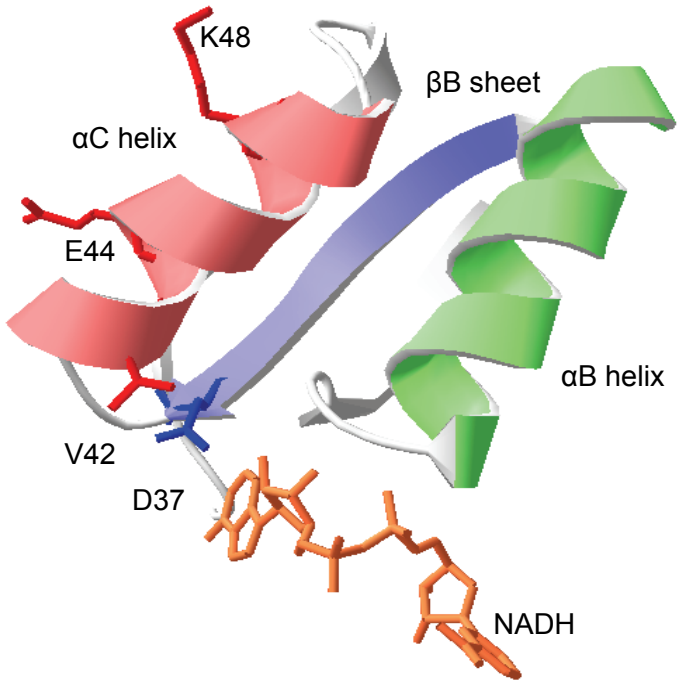

Figure 4-27. Location of amino acids 37, 42, 44 and 48 in the tertiary structure of *Lb*ADH G37D. The N-terminal region of the *Lb*ADH G37D until its 64th residue is represented. NADH (orange), G37 (blue), and the randomized amino acids V42, E44 and K48 (red) are marked. The structure was derived from the database PDB, entry 1zk1.

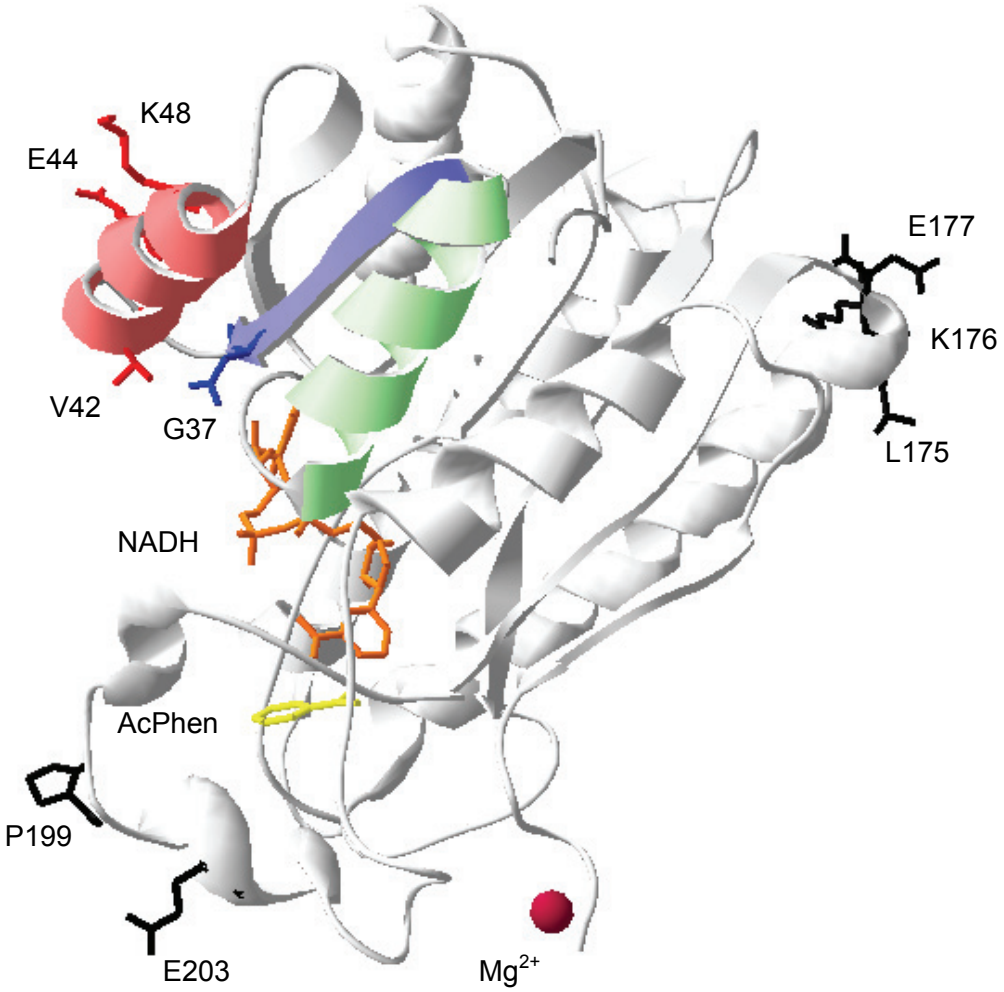

Figure 4-28. Tertiary structure of *Lb*ADH G37D. The αB- and αC-helices are represented in green and red, respectively; the ßB-sheet is marked by blue. NADH is highlighted in orange, acetophenone is shown in yellow, the residue G37 is marked in blue, the randomized amino acids V42, E44 and K48 are colored red, and the interfacing residues L175, K176, E177, P199 and E203 are black. The structure was derived from the database PDB, entry 1zk1; interfacing residues are derived with PISA analysis [257].

4.5 Characterization of further thermostable wildtype alcohol dehydrogenases

As shown in the section 4.1, the stability of redox cofactors in the solid state is significantly higher than in aqueous solution, with the higher stability of NADH compared to NADPH in the solid state as well. Therefore, the use of NADH-dependent oxidoreductases in gas/solid system could represent a possibility to increase the stability of such a system. In spite of this expectation, as will be described in the section 4.6, the cofactor stability was found not to be the decisive parameter determining operational stability of *Lb*ADHwt and *Lb*ADH G37D in the gas/solid reactor. The protein thermostability, in contrast, had the major influence. Nevertheless, the data were obtained for *Lb*ADHwt and *Lb*ADH G37D with no clear evidence if they represent a particular case or a general trend. Taking into account both possibilities, highly thermostable NADH-dependent ADHs are the best candidates to perform well in the gas/solid reactor.

Recently discovered NADH-dependent highly thermostable alcohol dehydrogenases from *Thermus thermophillus* (*T*ADH) [75] and from *Flavobacterium frigidimaris* (*Ff*ADH) [79] have already shown a big potential for biotechnological applications [49, 76]. These enzymes were suggested as promising candidates for the gas/solid biocatalysis with intention to check their behaviour under operational conditions.

Both enzymes were recombinantely expressed in *E. coli* BL21 (DE3) and characterized in solution in respect of their substrate scope, pH and temperature reaction optima. As shown in Tab. 4-8 and in Tab. 4-9, *T*ADH shows the comparatively highest reaction rates with primary alcohols and the corresponding aldehydes. Its activity increases with increase of the length of the aliphatic chain to C7- and decreases when longer chained substrates were applied. The results are in good accordance with the observations of Höllrigl et al. [75]. *Ff*ADH also prefers aldehydes, but is inactive with primary alcohols. The last result contradicts the data of Kazuoka et al., who observed significant activity of *Ff*ADH with primary alcohols [79]. Interestingly, both enzymes are able to reduce aliphatic, cyclic and some aromatic ketones with reliable reaction rates. Moreover, derivatives of cyclohexanone were found to be good substrates for *T*ADH. Therefore, both enzymes possess relatively broad substrate spectra. Thus, they are potentially interesting for the development of synthetic applications.

Similar to *Lb*ADH, both enzymes showed higher specific activities for the reduction reactions than for the oxidation.

Table 4-8. Substrate specificity of *T*ADH and *Ff*ADH: oxidation. The experiments were performed with 10 mM substrate solution in 50mM Tris-HCl, pH 7.5 for *T*ADH or in 100 mM Kpi buffer, pH 7.0 for *Ff*ADH at RT. Measurements were performed using the crude extracts of *E. coli* cells with recombinantly expressed *T*ADH or *Ff*ADH by the photometric assay given in chapters 3.4.3 and 3.4.4 in triplicates. ND: not determined

Substrate	Structure	Activity, U mg^{-1}	
		*T*ADH	*Ff*ADH
methanol		0.029 ± 0.007	0.05 ± 0.02
ethanol		0.25 ± 0.05	0.18 ± 0.09
1-propanol	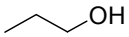	0.53 ± 0.06	0 ± 0.03
1-butanol	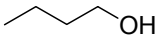	0.38 ± 0.03	0 ± 0.03
1-hexanol	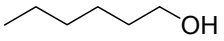	0.19 ± 0.05	0 ± 0.01
1-heptanol		0.24 ± 0.04	0 ± 0.04
1-octanol	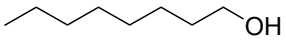	0.07 ± 0.04	0 ± 0.03
2-propanol		0.03 ± 0.02	0.88 ± 0.06
2-butanol	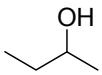	0.06 ± 0.04	0.52 ± 0.04
2-pentanol	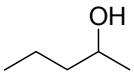	0.18 ± 0.03	0.96 ± 0.03
2-hexanol	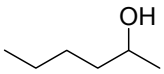	0.08 ± 0.04	0.5 ± 0.05
2-heptanol	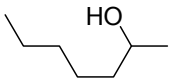	0.19 ± 0.05	0.67 ± 0.03
isoamylalcohol	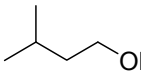	0.44 ± 0.03	0.01 ± 0.02
1-amino-2-propanol	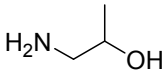	ND	0 ± 0.002
2-amino-1-propanol		0.04 ± 0.02	0 ± 0.006
2-dimethylamino-2-methyl-1-propanol	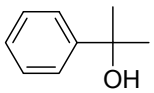	0.05 ± 0.03	ND
cyclohexanol	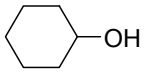	0.24 ± 0.05	0.05 ± 0.01
2-cyclohexen-1-ol	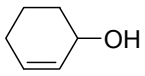	ND	0.08 ± 0.02
2,2,2 - trichlorethanol	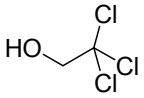	ND	ND

Table 4-9. Substrate specificity of *T*ADH and *Ff*ADH: reduction. The experiments were performed with 10 mM substrate solution in 50mM Tris-HCl, pH 7.5 for *T*ADH or in 100 mM Kpi buffer, pH 7.0 for *Ff*ADH at RT. Measurements were performed using the crude extracts of *E. coli* cells with recombinantly expressed *T*ADH or *Ff*ADH by the photometric assay given in chapters 3.4.3 and 3.4.4 in triplicates. ND: not determined.

Substrate	Structure	Activity, U/mg	
		***T*ADH**	***Ff*ADH**
acetaldehyde		0.41 ± 0.06	8.8 ± 0.5
propionaldehyde	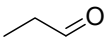	0.81 ± 0.08	19 ± 1
butyraldehyde	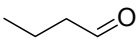	0.43 ± 0.03	10.9 ± 0.6
valeraldehyde	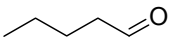	0.16 ± 0.04	22 ± 3
isovaleraldehyde	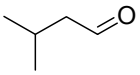	0.19 ± 0.07	1.1 ± 0.1
hexanal	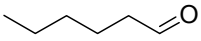	0.5 ± 0.2	7.0 ± 0.5
octanal	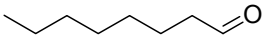	0.15 ± 0.08	1.1 ± 0.4
2-methyl-butyraldehyde	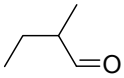	1,10 ± 0.2	8.6 ± 0.9
3,3 – dimethyl-butyraldehyde	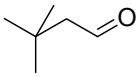	0.26 ± 0.08	1.6 ± 0.3
benzaldehyde	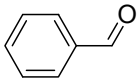	0.26 ± 0.03	0.4 ± 0.1
2-chloro-benzaldehyde	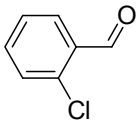	0.13 ± 0.02	0.20 ± 0.06
3-bromo-benzaldehyde	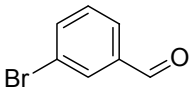	0.9 ± 0.3	1.4 ± 0.2
o-tolualdehyde	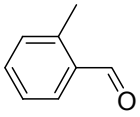	0.3 ± 0.1	0 ± 0.04
acetone		0.32 ± 0.05	0.99 ± 0.03
2-butanone	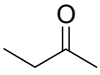	0.4 ± 0.1	1.099 ± 0.005
2-pentanone	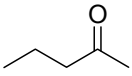	0.5 ± 0.1	-
2-heptanone	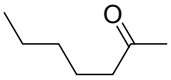	0.8 ± 0.3	1.1 ± 0.3
2-decanone	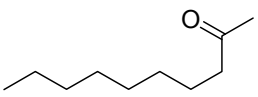	0.8 ± 0.3	0.5 ± 0.1

Table 4-9, continued. Substrate specificity of *T*ADH and *Ff*ADH: reduction. The experiments were performed with 10 mM substrate solution in 50mM Tris-HCl, pH 7.5 for *T*ADH or in 100 mM Kpi buffer, pH 7.0 for *Ff*ADH at RT. Measurements were performed using the crude extracts of *E. coli* cells with recombinantly expressed *T*ADH or *Ff*ADH by the photometric assay given in chapters 3.4.3 and 3.4.4 in triplicates. ND: not determined.

Substrate	Structure	Activity, U/mg	
		***T*ADH**	***Ff*ADH**
2-undecanone	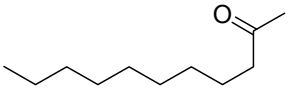	0.7 ± 0.2	0.7 ± 0.1
2-pentadecanone	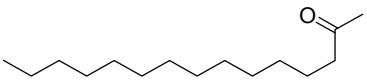	ND	0.4 ± 0.1
3-octanone	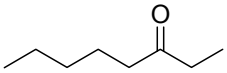	0.4 ± 0.1	0.55 ± 0.02
3-nonanone	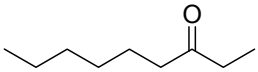	0.7 ± 0.2	0.49 ± 0.08
4-phenyl-2-butanone	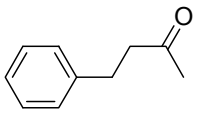	ND	1.4 ± 0.1
3-phenyl-propionaldehyde	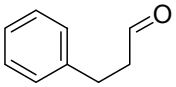	ND	7.3 ± 0.6
phenylacetaldehyde	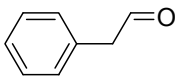	ND	1.0 ± 0.1
acetophenone	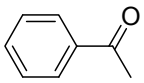	0.24 ± 0.04	0.30 ± 0.08
2-fluoro-acetophenone	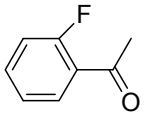	ND	0.6 ± 0.1
4-fluoro-acetophenone	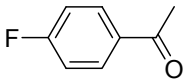	ND	0.6 ± 0.2
cyclopropan-carboxaldehyde	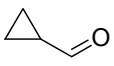	ND	1.7 ± 0.2
2-methyl-cyclohexanone	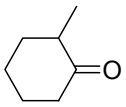	0.22 ± 0.9	ND
3-methyl-cyclohexanone	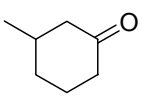	ND	0.6 ± 0.1
3,3,5-trimethyl-cyclohexanone	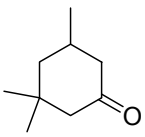	ND	0.6 + 0.2

Optimal experimental conditions of enzymatic reactions were checked using 1-propanol as a model substrate for *T*ADH and 2-propanol as a model substrate for *Ff*ADH. Whereas *T*ADH proved to be very thermostable showing the highest activity at 70°C, *Ff*ADH reaches its maximal activity in the range of 45-55°C (Fig. 4-29 A). The most favourable pH for initial rate measurements was 10.0 for *T*ADH and 7.5 for *Ff*ADH (Fig. 4-29 B). No stability data were obtained.

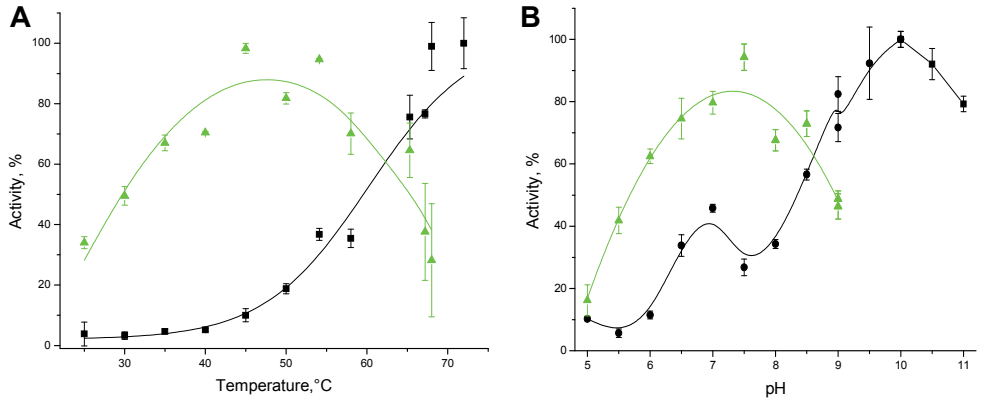

Figure 4-29. pH and temperature optima of *T*ADH (■) and *Ff*ADH (▲). A: effect of temperature on the initial rate activity of *T*ADH and *Ff*ADH; B: effect of pH on the initial rate activity (oxidation) of *T*ADH and *Ff*ADH. Temperature influence was assayed with 25 mM 1-propanol, 10 mM NAD^+ in 50 mM glycine buffer, pH 11.0 for *T*ADH and with 25 mM isopropanol, 10 mM NAD^+ in 50 mM Tris, pH 7.5 for *Ff*ADH. The influence of pH on enzymatic activity was determined in the pH range of 4-12 and otherwise under standard assay conditions. Concentration of buffering component was always 50 mM (sections 3.5.5 and 3.5.6).

Initial activity measurements indicated that the temperature and pH profiles of *T*ADH are shifted to extremely high values, whereas *Ff*ADH demonstrates significant enzymatic activity at a broad range of moderate temperatures and pH values (Fig. 4-29). Considering the facts that a pH of 7.0 was found to be optimal for the immobilization of nicotinamide cofactors [31], a well-known pH memory effect is usually observed after immobilization of enzymes [258], and operational temperature of a gas/solid reactor equals to 40-50°C [3, 7, 31, 259], *Ff*ADH would probably represent the more attractive candidate for the gas/solid experiments. However, detailed experiments are necessary to estimate the long-term behaviour of the enzymes under gas/solid reactor conditions.

4.6 Gas/solid reactor experiments

In contrast to enzymatic reactions performed in solution, gas/solid reactor system ensures a precise control of the thermodynamic parameters (such as water activity, pressure, temperature etc.) [3]. In this type of experiments, the 'key parameter' in gaseous mixture can be varied, keeping all the other reaction conditions constant. This setup represents a powerful tool for the studies of enzyme hydration and solvent influences.

A direct comparison of the *Lb*ADHwt and *Lb*ADH G37D in the gas/solid reactor was performed in close collaboration with K. Dimoula and M. Jordan, AVT, RWTH Aachen University. To avoid potential experimental inaccuracies, the following set up was chosen:

(i) The molar amount of the wild type enzyme and the variant deposited on 1 g of the glass beads was always identical.

(ii) The immobilization of the both *Lb*ADHwt and *Lb*ADH G37D was performed at pH 7.0, although this pH value was not optimal for the activity of both enzymes, at least in solution (Fig. 4-13). However, this pH value was found to be optimal for immobilization efficiency of the nicotinamide cofactor [31].

(iii) The molar amount of the co-immobilized cofactor $NAD(P)^+$ was 12 times higher than the molar amount of the enzymes in the both cases.

(iv) 50 mg of the glass beads with immobilized *Lb*ADHwt or 100 mg of the glass beads with immobilized *Lb*ADH G37D were used in a single experiment with the gas/solid reactor.

As shown before (section 4.2.1), the wild type enzyme has a 12-fold higher specific activity than the variant in aqueous solution at pH 7.0. Since the deposition of the enzyme on the carrier was also performed at pH 7.0, the whole mass of the *Lb*ADH G37D used for deposition on 1 g of the carrier contained just 2 Units of enzymatic activity in solution. Thus, the expected reaction rate of the *Lb*ADH G37D in the gas/solid reactor was negligible. In order to compensate the expected low enzymatic activity and obtain measurable reaction rates, a higher amount of *Lb*ADH G37D had to be used. However, the higher amount of the glass beads with immobilized *Lb*ADH G37D could cause potential differences in the micro-environment of the two enzyme preparations, such as different levels of adsorption of water and substrates. This might influence activity and stability in the gas/solid reactor and complicate the direct comparison of the two enzyme variants [260]. Therefore, an influence of the amount of the deposited carrier on the stability of the enzyme in the gas/solid reactor was studied. For this purpose, different amounts of the carrier covered by the immobilized enzyme were placed into the reactor. In these experiments all the thermodynamic parameters and the amount of lyophilized protein per gram of carrier were kept constant. As indicated in Fig. 4-30, the increasing amount of loaded carrier from 50 to 400 mg in the reactor did not influence the stability of *Lb*ADH G37D, which remained almost constant.

The loading of the reactor does not influence the stability of the deposited enzyme, as depicted in Fig. 4-30. The remaining parameters, namely thermodynamic activity of water (a_w) and acetophenone, were studied with 50 mg and 100 mg carriers, for the wild type enzyme and the variant, respectively.

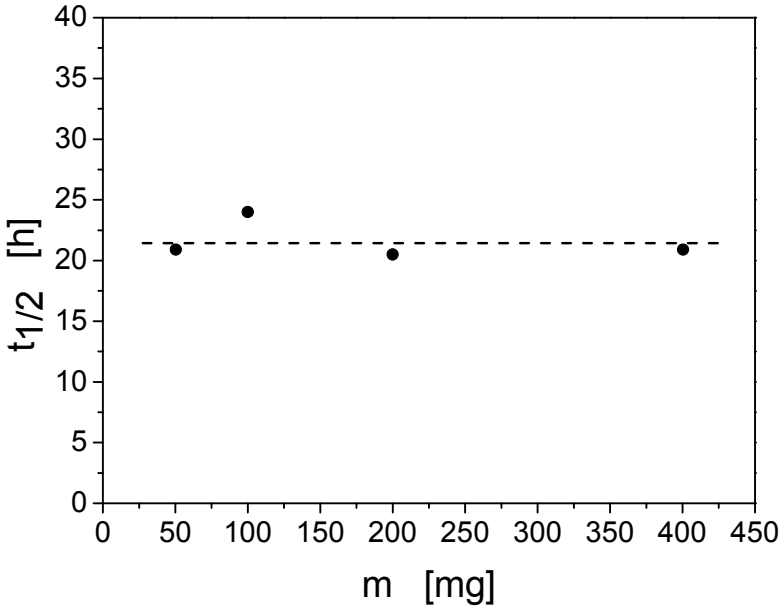

Figure 4-30. The effect of the deposited enzyme amount (*Lb*ADH G37D) on the stability in the gas/solid reactor. Experimental conditions: α_{AcPh}=0.3, α_w=0.56, $n_{2\text{-}prop}/n_{AcPh}$=60, V_{tot}=20 mL/min, T=40°C. Performed by Dr. K. Dimoula, [259].

The effect of a_w on the operational activity and stability of *Lb*ADHwt and *Lb*ADH G37D was investigated. In these experiments, a_w in the gaseous reaction mixture was individually adjusted, whereas the further parameters (namely, temperature, thermodynamic activities of the both substrates, and flow rate of the gaseous mixture) were kept constant. The experiments were performed at 40°C and an a_w of 0.4, 0.5, 0.6 and 0.7. A typical result of the gas/solid experiment is represented in Fig. 4-31. After equilibration of the gaseous mixture, the reaction was started by allowing the equilibrated gaseous mixture to pass through the carrier bed. After a certain equilibration time, the maximal reaction rate was observed. The progress of the gas/solid reaction was monitored for additional 16-22 h. During this period, the reaction rate constantly decreased, which could be described by a single-order exponential decay model. The stability of *Lb*ADHwt and *Lb*ADH G37D was estimated as a half-life value, which was calculated from the reaction profiles according to the model.

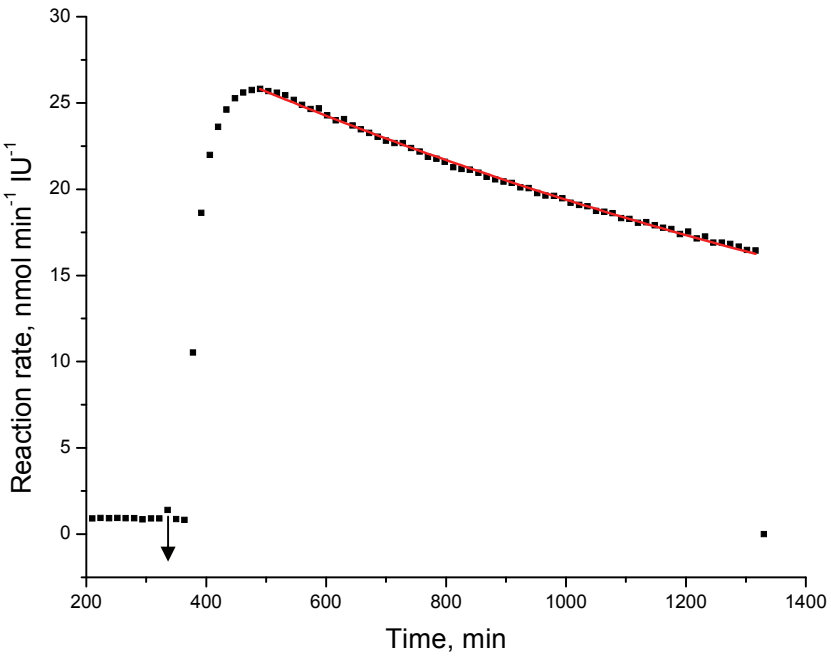

Figure 4-31. Acetophenone conversion catalyzed by *Lb*ADH G37D. Reaction conditions: 40°C, a_w = 0.6; a_{acphen} = 0.3, a_{iso} = 0.21. The reaction progress was fitted by the one-order exponential decay model (red line). The time point when the substrate-containing gas mixture was allowed to pass through the reactor is highlighted by an arrow.

In contrast to earlier expectations, the specific reaction rates of *Lb*ADHwt and *Lb*ADH G37D normalized on the amount of the deposited protein (µmol min^{-1} $mg_{protein}^{-1}$) were found to be of the same order of magnitude (Fig. 4-32 and Table 4-10). Therefore, the performance of the G37D variant in the gas/solid system was found to be improved, compared to its performance in solution. Thus, this variant can be considered as a promising candidate, especially due to its NADH dependency. The initial reaction rate of *Lb*ADHwt and *Lb*ADH G37D increased continuously with increasing a_w (Fig. 4-32).

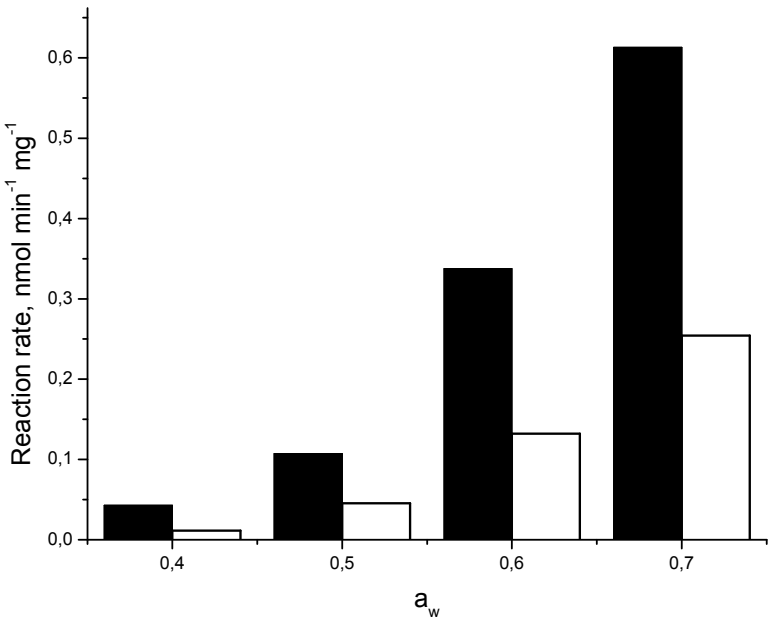

Figure 4-32. Effect of water activity on initial reaction rate of *Lb*ADHwt (black) and *Lb*ADH G37D (white). The reaction rate was normalized to the deposited protein amount. Experimantal setup: α_{AcPh} = 0.3, $n_{2\text{-}prop}/n_{AcPh}$ = 60, m = 50 mg (*Lb*ADHwt), m = 100 mg (*Lb*ADH G37D), V_{tot} = 20 mL/min, T = 40°C. Data for the *Lb*ADHwt were obtained by Dr. K. Dimoula, [259].

In contrast to the activity of the variant, its operational stability was significantly lower than the stability of the wild type enzyme at all tested a_w values (Fig. 4-32 and Table 4-10). The half-life of NADPH-dependent *Lb*ADHwt varied between 30 and 80 h, which amounted to 2 – 4 fold the half-life of the NADH-dependent LbADH G37D (Fig. 4-32 and Table 4-10). With regard to the high stability of both cofactors in the dry state (Fig. 4-3), this fact indicates that stability of the cofactor is probably not the decisive parameter for the enzyme stability in the gas/solid reaction system.

The stability of the wild type enzyme showed a maximum at a_w 0.5 (Fig. 4-32). This result contradicts previous findings of Trivedi et al. [25], who evidenced a continuous decrease of the stability of the deposited crude cell extract of *Lb*ADHwt with increasing a_w. The results, however, are in line with studies of Mikolajek *et al.*, performed on purified thiamine diphosphate-dependent enzymes revealing also an optimal stability at a water activity of 0.5 [26]. The stability of deposited lyophilized *Lb*ADH G37D, however, was almost constant below a_w value of 0.7 (Fig. 4-33).

Table 4-10. Kinetic parameters of the gas/solid reactions. Experimental conditions: α_{AcPh}=0.3, α_w=0.56, $n_{2\text{-prop}}/n_{AcPh}$=60, V_{tot}=20 mL/min, T=40°C. Data for the *Lb*ADHwt were obtained by Dr. K. Dimoula, [259].

Enzyme	Amount per reaction, mg	Specific activity in aq. solution, U/g	A_w	Maximal conversion, %	Vmax, nmol/min/U	$T_{1/2}$, h
*Lb*ADHwt	50 mg	4.14	0.4	0.81	0.72	29
		2.67	0.4	0.58	0.80	27
		2.55	0.5	1.46	2.1	52
		1.48	0.6	4.54	11.4	145
		1.31	0.7	8.27	23.4	20
*Lb*ADH G37D	100 mg	0.18	0.4	0.31	6.3	17
		0.12	0.5	1.26	38	21
		0.07	0.6	3.35	188.6	19
		0.05	0.7	3.27	125	9.9

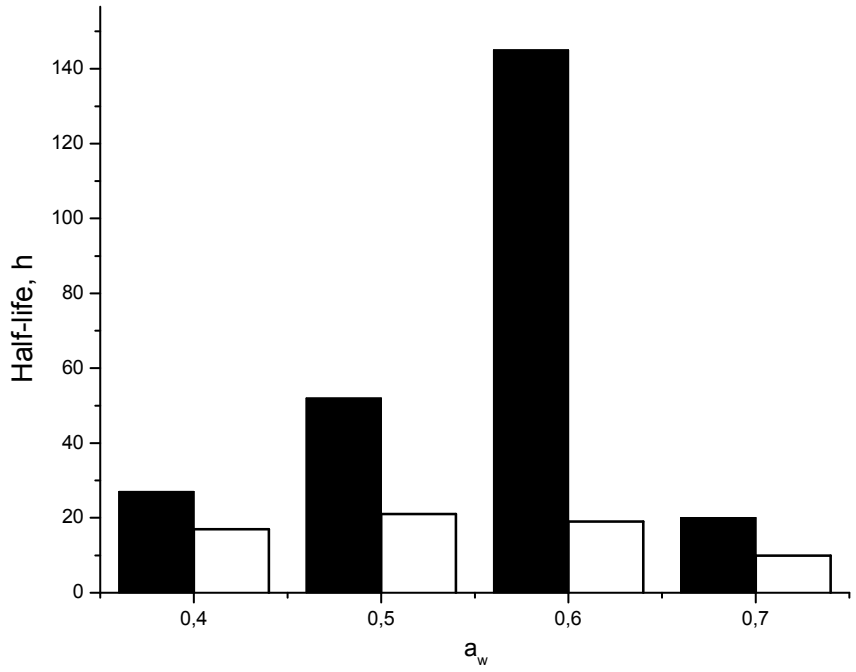

Figure 4-33. Effect of the water activity on the stability of *Lb*ADHwt (black) and *Lb*ADH G37D (white). Experimental conditions: α_{AcPh} = 0.3, $n_{2\text{-prop}}/n_{AcPh}$ = 60, m = 50 mg (*Lb*ADHwt), m = 100 mg (*Lb*ADH G37D), V_{tot} = 20 mL/min, T = 40°C. Data for the *Lb*ADHwt were obtained by Dr. K. Dimoula, [259].

As reported in section 4.2.2, the activation energies of heat inactivation in the solid state were found to be 135 and 102 kJ mol^{-1} for *Lb*ADHwt and *Lb*ADH G37D,

respectively. Thus, lower stability of *Lb*ADH G37D can be partially explained by lower E_A of heat inactivation. The most probable reason for inactivation of the immobilized dry *Lb*ADH G37D in gas/solid reactor, however, could be a substrate inhibition effect. The influence of thermodynamic activity of the substrate (a_{AcPh}) on the activity and stability of *Lb*ADHwt and *Lb*ADH G37D was investigated by K. Dimoula and M. Jordan at fixed a_w of 0.5, for which maximal stability of the wild type enzyme was observed. The a_{AcPh} values were varied between 0.14 and 0.3, with simultaneous variation of the activity of isopropanol and thus keeping the molar ratio of the two substrates constant (Fig. 4-34).

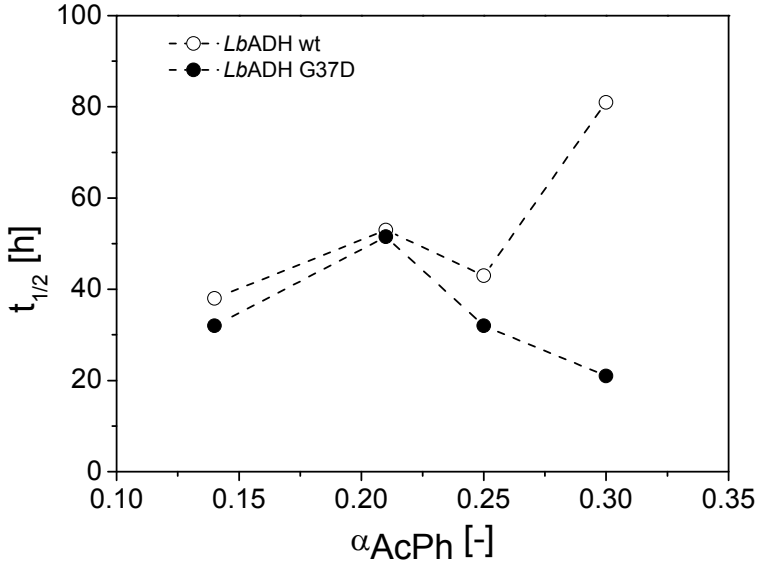

Figure 4-34. Influence of the thermodynamic activity of acetophenone on the operational stability of the deposited lyophilized *Lb*ADHwt (black) and variant *Lb*ADH G37D (white). Experimental conditions: αw=0.50, n2-prop/nAcPh=60, m= 50 mg (for *Lb*ADHwt), m=100 mg (for *Lb*ADH G37D), Vtot=20 mL/min, T=40°C. Performed by Dr. K. Dimoula [259].

*Lb*ADH G37D had approximately the same operational stability as the wild type enzyme, with the highest difference in half-life of 60 h at the highest acetophenone activity investigated. At substrate activities of 0.14 – 0.25 the differences in half-life between the variants ranged within the experimental error of 1–5 h. The variant *Lb*ADH G37D showed a maximal stability at an intermediate a_{AcPh} of 0.21, nearly matching the half-life of *Lb*ADHwt under these conditions (52 h). In contrast, *Lb*ADHwt exhibited an increasing stability with increasing substrate activity (Fig. 4-33).

The influence of the a_{AcPh} on the specific reaction rate is shown in Fig. 4-34. Similar to the water activity studies, the specific reaction rates of both enzymes were of the same order of magnitude. The increase of a_{AcPh} led to an almost linear increase of the initial reaction rate of *Lb*ADH G37D, which indicated that no substrate

saturation was observed within the tested substrate activity range. In contrast to this, the wild type enzyme had a clear optimum at a_{AcPh} of 0.25 (Fig. 4-35).

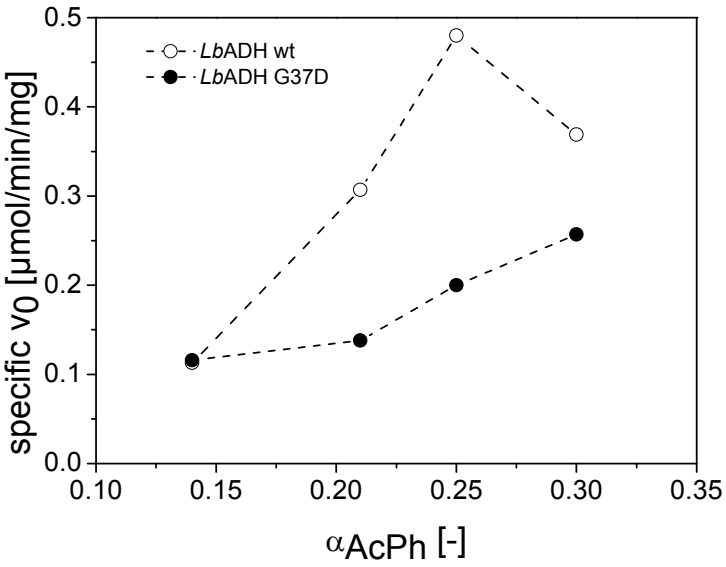

Figure 4-35. Influence of thermodynamic activity of acetophenone on the initial specific reaction rate of the deposited lyophilized *Lb*ADHwt (black) and variant *Lb*ADH G37D (white). Experimental conditions: αw=0.50, n2-prop/nAcPh=60, m= 50 mg (for *Lb*ADHwt), m=100 mg (for *Lb*ADH G37D), Vtot=20 mL/min, T=40°C. Performed by Dr. K. Dimoula, [259].

The observed phenomenon can probably be explained by an impact of the single exchange G37D into the catalytic properties of the enzymes, such as interaction with substrate, cofactor and water molecules. These effects could overlap with the high protein stability in the presence of the substrates.The hypothesis corresponds to the data obtained by Schlieben *et al.* for the dissolved *Lb*ADHwt and *Lb*ADH G37D. In aqueous solution, the variant exhibited lower Km values both for its cofactor and both substrates, thus increasing the saturation level in solution significantly [11] (Table 4-11). For example, Km values for acetophenone equaled to 2.8 mM and 10.9 mM (1.4 mM and 7.9 mM in our studies) for the *Lb*ADHwt and *Lb*ADH G37D, respectively [11], whereas the cofactors' Km values amounted to 0.04 mM of NADPH for *Lb*ADHwt, and 1.6 mM of NADH for *Lb*ADH G37D.

Table 4-11. Kinetic parameters of *Lb*ADHwt and *Lb*ADH G37D, reprinted from Schlieben *et al.* [8]. Enzymatic activity was determined in triplicates using the photometric assay identical to the one described in section 3.4.2.1. (ND: not determined).

A: Kinetic parameters for NAD, NADP, NADH and NADPH (substrate saturation).

NAD/NADP reduction						
	NADP			NAD		
	K_m (mM)	k_{cat} (s^{-1})	k_{cat}/K_m (M^{-1} s^{-1})	K_m (mM)	k_{cat} (s^{-1})	k_{cat}/K_m (M^{-1} s^{-1})
*Lb*ADHwt	0.015 ± 0.0004	4.4 ± 0.1	2.9×10^5	No reaction		
*Lb*ADH G37D	9.1 ± 1.5	5.9 ± 1.0	6.5×10^5	0.75 ± 0.07	9.9 ± 0.9	1.3×10^4
NADH/NADPH oxidation						
	NADPH			NADH		
*Lb*ADHwt	0.04 ± 0.005	38.1 ± 4.7	9.5×10^5	No reaction		
*Lb*ADH G37D	ND			1.6 ± 0.5	36.6 ± 10.5	2.3×10^4

B: Kinetic parameters for acetophenone and phenylethanol (cosubstrate saturation).

Acetophenone reduction						
	With NADPH			With NADH		
	K_m (mM)	k_{cat} (s^{-1})	k_{cat}/K_m (M^{-1} s^{-1})	K_m (mM)	k_{cat} (s^{-1})	k_{cat}/K_m (M^{-1} s^{-1})
*Lb*ADHwt	2.8 ± 0.2	44.5 ± 3.7	1.6×10^4	No reaction		
*Lb*ADH G37D	ND			10.9 ± 1.1	35.7 ± 3.6	3.3×10^3
Phenylethanol oxidation						
	With NADP			With NAD		
*Lb*ADHwt	2.9 ± 0.2	5.4 ± 0.3	1.9×10^3	No reaction		
*Lb*ADH G37D	55.5 ± 6.8	8.2 ± 1.0	1.5×10^2	10.8 ± 1.6	9.5 ± 1.4	8.8×10^2

Obviously, the single amino acid exchange G37D has a significant impact on the kinetic parameters. Thus, in order to fully understand the operational stability of the two variants, the influence of the substrate activity, both under reactive and non-reactive conditions should be further investigated in the future, at different water activity levels and probably also at varying relative and/or absolute isopropanol and acetophenone activity levels.

Chapter 5
Conclusions and outlook

Gas/solid biocatalysis represents a perspective biotechnological approach, in which a dry enzyme catalyzes the reaction of a gaseous substrate to a gaseous product. Studies of the temperature-dependent performance of the solid enzymes are important for both fundamental scientific understanding and the engineering of novel thermostable biocatalysts for the gas/solid biocatalysis. In this thesis, the stability of enzymes was characterized both in non-reactive and in the reaction systems. The aim was to elucidate factors that affect in the operational stability in the gas/solid reactor and find parameters that may predict the biocatalyst performance in the gas/solid system. Two single-amino acid exchange enzyme variants, the NADPH-dependent *Lb*ADHwt and the NADH-dependent *Lb*ADH G37D were used as model enzymes. Special emphasis was placed on (i) thermal stability of the solid cofactors, (ii) thermal stability of the solid proteins, (iii) design of a high-throughput screening system and optimization of target enzymes for gas/solid application.

It was proven that in spite of a lower thermostability and increased number of degradation products of the cofactor NADPH in comparison to NADH both in the dissolved and solid state, the cofactor stability was not the decisive parameter for the operational stability in the gas/solid reactor system. Measurement of the thermal stabilities of enzymes in solution in the absence of substrates and products was also not indicative for operational stability. In contrast, the thermostability of the dry enzymes without substrates has been demonstrated to be predictive for the order of magnitude of the operational stability in the gas/solid reactor. Subsequently, this factor served for the establishment of a high throughput screening system. Application of this system for the screening of a mutant library allowed identification of the variant G37D/V42F/E44C/K48Q as potentially suitable for the gas/solid biocatalysis. Together with the highly thermostable alcohol dehydrogenases *T*ADH and *Ff*ADH, this variant is suggested as promising candidate for the investigation in the gas/solid reactor system in the future. Additionally, identification of further influencing factors would yield the necessary information for an optimization of the gas/solid reactor system for long-term productivity by engineering either the enzyme or the gas/solid reactor's operating conditions.

Increasing thermodynamic activities of water and substrate in the gas/solid reactor caused differences in the operational stability of the two enzyme variants. The observed phenomenon can probably be explained by an impact of the single exchange G37D into the catalytic properties of the enzymes, such as substrate and co-substrate affinity or substrate inhibition. These effects could overlap with

the high protein stability in the presence of the substrates. Importantly, some of these differences, i.e. the lower affinity of *Lb*ADH G37D to the substrate, were observed in the aqueous medium. Thus, future studies need to further analyze the interaction of substrate and co-substrate with the enzyme and its effect on the thermostability under non-reactive conditions as well as the effects of variation of the substrate and water activity in the reactive gas/solid reactor system.

Chapter 6
References

[1] B. Erable, I. Goubet, S. Lamare, M.D. Legoy, T. Maugard, Chemosphere. 65 (2006) 1146-1152.
[2] J.W. Barton, E.K. Reed, B.H. Davison, Biotechnology Techniques. 11 (1997) 747-750.
[3] S. Lamare, M.D. Legoy, M. Graber, Green Chemistry. 6 (2004) 445-458.
[4] E. Barzana, M. Karel, Biotechnology and Bioengineering. 34 (1989) 1178-1185.
[5] E. Barzana, A. Klibanov, M. Karel, Applied Biochemistry and Biotechnology. 15 (1987) 25-34.
[6] F. Yang, A.J. Russel, Biotechnology and Bioengineering. 49 (1996) 709-716.
[7] C. Ferloni, M. Heinemann, W. Hummel, T. Daussmann, J. Büchs, Biothechnology progress. 20 (2004) 975-978.
[8] N.H. Schlieben, K. Niefind, J. Müller, B. Riebel, W. Hummel, D. Schomburg, Journal of Molecular Biology. 349 (2005) 801-813.
[9] S. Cantone, U. Hanefeld, A. Basso, Green Chemistry. 9 (2007) 954-971.
[10] A. Zaks, Current Opinion in Chemical Biology. 5 (2001) 130-136.
[11] S. Danke, M. Held, M. Wubbolts, Current Opinion in Biotechnology. 15 (2004) 272-279.
[12] M. Leisola, J. Jokela, O. Pastinen, O. Turunen, Industrial use of enzymes, Eolas Publishers, Oxford, 2001.
[13] C. Wandrey, A. Liese, D. Kihumbu, Organic process research and development. 4 (2000) 286-290.
[14] A.J.J. Straathof, S. Panke, A. Schmid, Current Opinion in Biotechnology. 13 (2002) 548-556.
[15] A. Schmid, J.S. Dordick, B. Hauer, A. Kiener, M. Wubbolts, B. Witholt, Nature. 409 (2001) 258-268.
[16] M.H. Vermue, J. Tramper, Pure and Applied Chemistry. 67 (1995) 345-373.
[17] S. Lütz, L. Giver, J. Lalonde, Biotechnology and Bioengineering. 101 (2008) 647-653.
[18] S. Lamare, M.D. Legoy, Biotechnology Techniques. 9 (1995) 127-132.
[19] F. Parvaresh, H. Robert, D. Thomas, M.D. Legoy, Biotechnology and Bioengineering. 39 (1992) 467-473.
[20] V. Leonard, L. Fransson, S. Lamare, K. Hult, M. Graber, ChemBioChem. 8 (2007) 662-667.
[21] S. Lamare, M.D. Legoy, Trends in Biotechnology. 11 (1993) 413-418.

[22] R.V. Dunn, R.M. Daniel, Philosophical Transactions of the Royal Society B. 359 (2004) 1309-1320.
[23] S. Lamare, M.D. Legoy, Biotechnology and Bioengineering. 45 (1995) 387-397.
[24] S. Pulvin, M.D. Legoy, R. Lortie, M. Pensa, T. D., Biotechnology Letters. 8 (1986) 783-784.
[25] A.H. Trivedi, A.C. Spiess, T. Daussmann, J. Büchs, Biotechnology Progress. 22 (2006) 454-458.
[26] R. Mikolajek, A.C. Spiess, M. Pohl, S. Lamare, J. Büchs, Chembiochem. 8 (2007) 1063-1070.
[27] B.C. Dravis, K.E. LeJeune, A.D. Hetro, A.J. Russel, Biotechnology and Bioengineering. 69 (2000) 235-241.
[28] B. Erable, I. Goubet, S. Lamare, M.D. Legoy, T. Maugard, Biotechnology and Bioengineering. 86 (2004) 47-54.
[29] J.-K. Park, H.-J. Yee, S.-T. Kim, Biosensors and Bioelectronics. 10 (1995) 587-594.
[30] S. Lamare, R. Lortie, M.D. Legoy, Biotechnology and Bioengineering. 56 (1997) 1-7.
[31] A.H. Trivedi, PhD thesis, RWTH Aachen University (2005).
[32] T. Maugard, S. Lamare, M.D. Legoy, Biotechnology and Bioengineering. 73 (2001) 164-168.
[33] V. Leonard-Nevers, Z. Marton, S. Lamare, K. Hult, M. Graber, Journal of Molecular Catalysis B: Enzymatic. 59 (2009) 90-95.
[34] V. Leonard, S. Lamare, M.D. Legoy, M. Graber, Journal of Molecular Catalysis B: Enzymatic. 32 (2004) 53-59.
[35] F. Letisse, S. Lamare, M.D. Legoy, M. Graber, Biochimica et Biophysica Acta-Proteins and Proteomics. 1652 (2003) 27-34.
[36] M. Graber, R. Iragüe, E. Rosenfeld, S. Lamare, L. Franson, K. Hult, Biochimica et Biophysica Acta. 1774 (2007) 1052-1057.
[37] S. Lamare, M.D. Legoy, Annals of the New York Academy of Sciences. 799 (1997) 563-568.
[38] B.C. Dravis, P.E. Swanson, A.J. Russel, Biotechnology and Bioengineering. 75 (2001) 416-423.
[39] A. Trivedi, M. Heinemann, A.C. Spiess, T. Daussmann, J. Büchs, Journal of Bioscience and Bioengineering. 99 (2005) 340-347.
[40] B. Erable, T. Maugard, I. Goubet, S. Lamare, M.D. Legoy, Process Biochemistry. 40 (2005) 45-51.
[41] A.H. Trivedi, A.C. Spiess, T. Daussmann, J. Büchs, Applied Microbiology and Biotechnology. 71 (2006) 407-414.
[42] T. Yagi, M. Tsuda, Y. Mori, H. Inokuchi, Journal of American Chemical Society. 91 (1969) 2801.

[43] K. Kimura, A. Suzuki, H. Inokuchi, T. Yagi, Biochimica et Biophysica Acta. 567 (1979) 96-105.
[44] R. Mikolajek, A.C. Spiess, J. Büchs, Journal of Biotechnology. 129 (2007) 723-725.
[45] H.H.J. Cox, M.A. Deshusses, Current Opinion in Biotechnology. 9 (1998).
[46] W. Hummel, Trends in Biotechnology. 17 (1999) 487-492.
[47] W. Hummel, New alcohol dehydrogenases for the synthesis of chiral compounds, Springer, Berlin / Heidelberg, 1997.
[48] S. Pulvin, F. Parvaresh, D. Thomas, M.D. Legoy, Annals of the New York Academy of Sciences. 542 (1988) 434-439.
[49] D.A. Ullish, Master thesis, RWTH Aachen University (2007).
[50] H. Uchiyama, K. Oguri, O. Yagi, E. Kokufuta, Biotechnology Letters. 14 (1992) 619-622.
[51] M. Zilli, A. Converti, A. Lodi, M. Delborghi, G. Ferraiolo, Biotechnology and Bioengineering. 41 (1993) 693-699.
[52] M. Zilli, G. Camogli, C. Nicolella, Biotechnology and Bioengineering. 91 (2005) 707-714.
[53] I. Goubet, T. Maugard, S. Lamare, M.D. Legoy, Enzyme and Microbial Technology. 31 (2002) 425-430.
[54] H. Jörnvall, J.-O. Höög, B. Persson, European Journal of Biochemistry. 445 (1999) 261-264.
[55] E. Nordling, H. Jörnvall, B. Persson, European Journal of Biochemistry. 269 (2002) 4267-4276.
[56] P. Tse, R.K. Scopes, A.G. Wedd, Journal of the American Chemical Society. 111 (1989) 8703-8706.
[57] V.M. Williamson, C.E. Paquin, Molecular & General Genetics. 209 (1987) 374-381.
[58] K.L. Kavanagh, H. Jörnvall, B. Persson, U. Oppermann, Cellular and Molecular Life Sciences. 65 (2008) 3895-3906.
[59] J. Benach, S. Atrian, R. Gonzalez-Duarte, R. Ladenstein, Journal of Molecular Biology. 282 (1998) 383-399.
[60] S.T. Rao, M.G. Rossmann, Journal of Molecular Biology. 76 (1973) 241-256.
[61] Y. Kallberg, U. Oppermann, H. Jörnvall, B. Persson, European Journal of Biochemistry. 269 (2002) 4409-4417.
[62] R. Machielsen, L.L. Looger, J. Raedts, S. Dijkhuizen, W. Hummel, H.-J. Hennemann, T. Daussmann, J. Van der Oost, Engineering in Life Sciences. 9 (2009) 38-44.
[63] C. Filling, K.D. Berndt, J. Benach, S. Knapp, T. Prozorovski, E. Nordling, R. Ladenstein, H. Jornvall, U. Oppermann, Journal of Biological Chemistry. 277 (2002) 25677-25684.

[64] C. Notredame, D.G. Higgins, J. Heringa, Journal of Molecular Biology. 302 (2000) 205-217.
[65] N. Tanaka, T. Nonaka, K.T. Nakamura, A. Hara, Current Organic Chemistry. 5 (2001) 89-111.
[66] J. Benach, S. Atrian, R. Gonzalez-Duarte, R. Ladenstein, Journal of Molecular Biology. 289 (1999) 335-355.
[67] K. Niefind, J. Müller, B. Riebel, W. Hummel, D. Schomburg, Journal of Molecular Biology. 327 (2003) 317-328.
[68] F. Hildebrand, S. Lütz, Tetrahedron-Asymmetry. 17 (2006) 3219-3225.
[69] M. Wolberg, M. Villela, S. Bode, P. Geilenkirchen, R. Feldmann, A. Liese, W. Hummel, M. Müller, Bioprocess and Biosystems Engineering. 31 (2008) 183-191.
[70] S. Lüdeke, M. Richter, M. Müller, Advanced Synthesis & Catalysis. 351 (2009) 253-259.
[71] T. Schubert, W. Hummel, M.R. Kula, M. Müller, European Journal of Organic Chemistry (2001) 4181-4187.
[72] K. Goldberg, K. Schroer, S. Lütz, A. Liese, Applied Microbiology and Biotechnology. 76 (2007) 249-255.
[73] A.S. Bommarius, B.R. Riebel, Biocatalysis - Fundamentals and Applications, Wiley-CH, 2003.
[74] B.M. Anderson, C.D. Anderson, The Journal of Biological Chemistry. 238 (1963) 1475-1478.
[75] V. Höllrigl, F. Hollmann, A.C. Kleeb, K. Buehler, A. Schmid, Applied Microbiology and Biotechnology. 81 (2008) 263-273.
[76] V. Höllrigl, K. Otto, A. Schmid, Advanced Synthesis & Catalysis. 349 (2007) 1337-1340.
[77] F. Hollmann, A.C. Kleeb, K. Otto, A. Schmid, Tetrahedron: *Asymmetry*. 16 (2005) 3512-3519.
[78] Y. Nogi, K. Soda, T. Oikawa, Systematic and Applied Microbiology. 28 (2005) 310-315.
[79] Y. Kazuoka, T. Oikawa, I. Muraoka, S. Kuroda, K. Soda, Extremophiles. 11 (2007) 257-267.
[80] B. Alberts, A. Johnson, J. Lewis, M. Raff, K. Roberts, P. Walter, Molecular biology of the cell, Garland Science, New York, 2002.
[81] R.M.C. Dawson, D.C. Elliott, W.H. Elliott, K.M. Jones, Data for biochemical research, Oxford University Press, New York, 1989.
[82] J.R. Lakowicz, H. Szmacinski, K. Nowaczyk, M.L. Johnson, Protocols of National Academy of Science USA. 89 (1992) 1271-1275.
[83] C.-H. Wong, G.M. Whitesides, Protocols of American Chemical Society. 103 (1981) 4890-4899.
[84] H.K. Chenault, G.M. Whitesides, Applied Biochemistry and Biotechnology. 14 (1987) 147-197.

[85] O.H. Lowry, M.K. Rock, J.V. Passonneau, Journal of Biological Chemistry. 236 (1961) 2756-2759.
[86] S.L. Johnson, P.T. Tuazon, Biochemistry. 16 (1977) 1175-1183.
[87] N. Oppenheim, N.O. Kaplan, Biochemistry. 13 (1974) 4675-4685.
[88] J.T. Wu, L.H. Wu, J.A. Knight, Clinical Chemistry. 32 (1986) 314-319.
[89] K.A. Markham, R.S. Sikorski, A. Kohem, Analytical Biochemistry. 322 (2003) 26-32.
[90] E. Bernt, H. Bergmeyer, M. Grassl, W. Gruber, K. Beaucamp, Patent (1974).
[91] W.A. Van der Donk, H. Zhao, Current Opinion in Biotechnology. 14 (2003) 421-426.
[92] M. Eckstein, T. Daussmann, U. Kragl, Biocatalysis and Biotransformation. 22 (2004) 89-96.
[93] W.F. Liu, P. Wang, Biotechnology Advances. 25 (2007) 369-384.
[94] D. Westerhausen, S. Herrmann, W. Hummel, E. Steckhan, Angewandte Chemie-International Edition in English. 31 (1992) 1529-1531.
[95] H. Gröger, W. Hummel, C. Rollmann, F. Chamouleau, H. Hüsken, H. Werner, C. Wunderlich, K. Abokitse, K. Drauz, S. Buchholz, Tetrahedron. 60 (2004) 633-640.
[96] F.M. Bastos, A.G. Santos, J.J. Jr, E.G. Oestreicher, G.F. Pinto, L.M.C. Paiva, Biotechnology Techniques. 13 (1999) 661-664.
[97] A. Andreadeli, D. Platis, V. Tishkov, V. Popov, N.E. Labrou, European Journal of Biochemistry. 275 (2008) 3859-3869.
[98] R. Woodyer, H. Zhao, W.A. Van der Donk, European Journal of Biochemistry. 272 (2005) 3816-3827.
[99] C. Kohlmann, W. Märkle, S. Lütz, Journal of Molecular Catalysis B: Enzymatic. 51 (2008) 57-72.
[100] Y.H. Kim, Y.J. Yoo, Enzyme and Microbial Technology. 44 (2009) 129-134.
[101] F. Hildebrand, C. Kohlmann, A. Franz, S. Lütz, Advanced Synthesis & Catalysis. 350 (2008) 909-918.
[102] E. Steckhan, Topics in current Chemistry. 170 (1994) 83-111.
[103] K. Délécouls-Servat, R. Basséguy, A. Bergel, Chemical Engineering Science. 57 (2002) 4633-4642.
[104] R. Yuan, S. Watanabe, S. Kuwabata, H. Yoneyama, Journal of Organic Chemistry. 62 (1997) 2494-2499.
[105] F. Hildebrand, S. Lütz, Tetrahedron-Asymmetry. 18 (2007) 1187-1193.
[106] F. Hildebrand, S. Lütz, Chemistry - A European Journal. 15 (2009) 4998-5001.
[107] D. Mandler, I. Willner, Journal of the Chemical Society, Perkin Transactions 2 (1986) 805-811.
[108] K. Nakamura, R. Yamanaka, Chemical communications (2002) 1782-1783.
[109] T. Endo, S. Koizumi, Advanced Synthesis & Catalysis. 343 (2001) 521-526.

[110] C. Vieille, J.G. Zeikus, Trends in Biotechnology. 14 (1996) 183-190.
[111] W.F. Li, X.X. Zhou, P. Lu, Biotechnology Advances. 23 (2005) 271-281.
[112] A. Razvi, J.M. Scholtz, Protein Science. 15 (2006) 1569-1578.
[113] H. Radianingtyas, P.C. Wright, Fems Microbiology Reviews. 27 (2003) 593-616.
[114] S. Kumar, C.-J. Tsai, R. Nussinov, Protein Engineering. 13 (2000) 179-191.
[115] K. Yokota, K. Satou, S. Ohki, Science and Technology of Advanced Materials. 7 (2006) 255-262
[116] X.X. Zhou, Y.B. Wang, Y.J. Pan, W.F. Li, Amino Acids. 34 (2008) 25-33.
[117] S.P. Pack, Y.J. Yoo, Journal of Biotechnology. 111 (2004) 269-277.
[118] A.M. Facchiano, G. Colonna, R. Ragone, Protein Engineering. 11 (1998) 753-760.
[119] G. Vogt, S. Woell, P. Argos, Journal of Molecular Biology. 269 (1997) 631-643.
[120] R.L. Baldwin, Journal of Molecular Biology. 371 (2007) 283-301.
[121] C.N. Pace, B.A. Shirley, M. McNutt, K. Gajiwala, The Journal of the Federation of American Societies of Experimental Biology. 10 (1996) 75-83.
[122] C.N. Pace, Journal of Molecular Biology. 226 (1992) 29-35.
[123] K. Ishikawa, H. Nakamura, K. Morikawa, S. Kanaya, Biochemistry. 32 (1993) 6171-6178.
[124] M.-S. Kim, X. Lei, Applied Microbiology and Biotechnology. 79 (2008) 69-75.
[125] M.-S. Kim, J.D. Weaver, X.G. Lei, Applied Microbiology and Biotechnology. 79 (2008) 751-758.
[126] V.G. Eijsink, G. Vriend, G.R. Van der Zee, B. Van den Burg, G. Venema, Biochemical Journal. 285 (1992) 625-628.
[127] S. Sakasegawa, H. Takehara, I. Yoshioka, H. Misaki, H. Sakuraba, T. Ohshima, Bioscience, Biotechnology, and Biochemistry. 66 (2002) 1374-1377.
[128] S.-Y. Tang, Q.-T. Le, J.-H. Shim, S.-J. Yang, J.-H. Auh, C. Park, K.-H. Park, European Journal of Biochemistry. 273 (2006) 3335 - 3345.
[129] C. Vieille, J.G. Zeikus, Microbiology and Molecular Biology Reviews. 65 (2001) 1-43.
[130] S. Kawamura, I. Tanaka, N. Yamasaki, M. Kimura, Journal of Biochemistry. 121 (1997) 448-455.
[131] G. Pappenberger, H. Schurig, R. Jaenicke, Journal of Molecular Biology. 274 (1997) 676-683.
[132] A.V. Grinberg, R. Bernhardt, Archives of Biochemistry and Biophysics. 396 (2001) 25-34.
[133] A. Merz, T. Knöchel, J.N. Jansonius, K. Kirschner, Journal of Molecular Biology. 288 (1999) 753-763.
[134] L.J. Perry, R. Wetzel, Science 226 (1984) 555-557.

[135] O.R. Siadat, A. Lougarre, L. Lamouroux, C. Ladurantie, D. Fournier, BMC Biochemistry. 7 (2006) 1-7.
[136] H.M. Yang, B. Yao, K. Meng, Y.R. Wang, Y.G. Bai, N.G. Wu, Journal of Industrial Microbiology & Biotechnology. 34 (2007) 213-218.
[137] S. Kanaya, C. Katsuda, S. Kimura, T. Nakai, E. Kitakuni, H. Nakamura, K. Katayanagi, K. Morikawa, M. Ikehara, Journal of Biological Chemistry. 266 (1991) 6038-6044.
[138] S.-J. Lin, E. Yoshimura, H. Sakai, T. Wakagi, H. Matsuzawa, Biochimica et Biophysica Acta (BBA)/Protein Structure and Molecular Enzymology. 1433 (1999) 132-138.
[139] T.C. Khoo, D.A. Cowan, R.M. Daniel, H.W. Morgan, Biochemical Journal. 221 (1984) 407-413.
[140] S.V. Story, A.M. Grunden, M.W. Adams, Journal of Bacteriology. 183 (2001) 4259-4268.
[141] M. Nishioka, K. Tanimoto, N. Higashi, H. Fukada, K. Ishikawa, M. Taya, Biotechnology Letters. 30 (2008) 1573-6776.
[142] R. Scandurra, V. Consalvi, R. Chiaraluce, L. Politi, P.C. Engel, Biochimie. 80 (1998) 933-941.
[143] S. Bershtein, D.S. Tawfik, Current Opinion in Chemical Biology. 12 (2008) 151-158.
[144] R.J. Russell, J.M. Ferguson, D.W. Hough, M.J. Danson, G.L. Taylor, Biochemistry. 36 (1997) 9983-9994.
[145] S. Kawamura, Y. Abe, T. Ueda, K. Masumoto, T. Imoto, N. Yamasaki, M. Kimura, Journal of Biological Chemistry. 273 (1998) 19982-19987.
[146] S. Kawamura, Y. Kakuta, I. Tanaka, K. Hikichi, S. Kuhara, N. Yamasaki, M. Kimura, Biochemistry. 35 (1996) 1195-1200.
[147] S. Kimura, S. Kanaya, H. Nakamura, Journal of Biological Chemistry. 267 (1992) 22014-22017.
[148] K. Takano, Y. Yamagata, K. Yutani, Proteins-Structure Function and Genetics. 44 (2001) 233-243.
[149] K. Takano, Y. Yamagata, K. Yutani, Proteins-Structure Function and Genetics. 45 (2001) 274-280.
[150] S.R. Trevino, S. Schaefer, J.M. Scholtz, C.N. Pace, Journal of Molecular Biology. 373 (2007) 211-218.
[151] H. Fu, G.R. Grimsley, A. Razvi, J.M. Scholtz, C.N. Pace, Proteins-Structure Function and Bioinformatics. 77 (2009) 491-498.
[152] J.M. Richardson, M.M. Lopez, G.I. Makhatadze, Protocols of National Academy of Science USA. 102 (2005) 1413-1418.
[153] C. Vetriani, D.L. Maeder, N. Tolliday, K.S.-P. Yip, T.J. Stillman, K.L. Britton, D.W. Rice, H.H. Klump, F.T. Robb, Protocols of National Academy of Science USA. 95 (1998) 12300-12305.

[154] F. Van den Akker, I.K. Feil, C. Roach, A.A. Platas, E.A. Merritt, W.G. Hol, Protein Science. 6 (1997) 2644–2649.
[155] E. Goihberg, O. Dym, S. Tel-Or, I. Levin, M. Peretz, Y. Burstein, Proteins-Structure Function and Bioinformatics. 66 (2007) 196-204.
[156] H. Kaneka, H. Minagawa, J. Shimada, Biotechnology Letters. 27 (2005) 1777-1784.
[157] J.D. Bloom, F.H. Arnold, Proceedings of the National Academy of Sciences of the United States of America. 106 (2009) 9995-10000.
[158] A.V. Shivange, J. Marienhagen, H. Mundhada, A. Schenk, U. Schwaneberg, Current Opinion in Chemical Biology. 13 (2009) 19-25.
[159] D.A. Drummond, B.L. Iverson, G. Georgiou, F.H. Arnold, Journal of Molecular Biology. 350 (2005) 806-816.
[160] B.M. Hoeller, B. Reiter, S. Abad, I. Graze, A. Glieder, Journal of Microbiological Methods. 75 (2008) 251-257.
[161] A.J. Baldwin, K. Busse, A.M. Simm, D.D. Jones, Nucleic Acids Research. 36 (2008) 1-9.
[162] W.P. Stemmer, Nature. 370 (1994) 389-391.
[163] J.M. Joern, DNA Shuffling, Humana Press, 2003.
[164] S.Y. Tang, Q.T. Le, J.H. Shim, S.J. Yang, J.H. Auh, C. Park, K.H. Park, European Journal of Biochemistry. 273 (2006) 3335-3345.
[165] H. Minagawa, H. Kaneko, Biotechnology Letters. 22 (2000) 1131-1133.
[166] C. Shi, X. Lu, C. Ma, X. Fu, W. Yu, Applied Biochemistry and Biotechnology. 15 (2008) 51-59.
[167] W.-N. Niu, Z.-P. Li, D.-W. Zhang, M.-R. Yu, T.-W. Tan, Journal of Molecular Catalysis B: Enzymatic. 43 (2006) 33-39.
[168] H. Shibuya, S. Kaneko, K. Hayashi, Biochemical Journal. 349 (2000).
[169] T. Kaper, S.J.J. Brouns, A.C.M. Geerling, W.M. De Vos, J. Van der Oost, Biochemical Journal. 368 (2002) 461-470.
[170] A.-S. Xiong, R.-H. Peng, Z.-M. Cheng, Y. Li, J.-G. Liu, J. Zhuang, F. Gao, F. Xu, Y.-S. Qiao, Z. Zhang, J.-M. Chen, Q.-H. Yao, Protein Engineering Design & Selection (2007) 1-7.
[171] J.F. Chaparro-Riggers, B.L.W. Loo, K.M. Polizzi, P.R. Gibbs, X.-S. Tang, M.J. Nelson, A.S. Bommarius, BMC Biotechnology. 7 (2007) 1-7.
[172] M.T. Reetz, J.D. Carballeira, Nature Protocols. 2 (2007) 891-903.
[173] M. Lehmann, L. Pasamontes, S.F. Lassen, M. Wyss, Biochimica et Biophysica Acta. 1543 (2000) 408-415.
[174] A.S. Bommarius, J.M. Broering, J.F. Chaparro-Riggers, K.M. Polizzi, Current Opinion in Biotechnology. 17 (2006) 606-610.
[175] A. Hidalgo, A. Schließmann, R. Molina, J. Hermoso, U.T. Bornscheuer, Protein Engineering Design & Selection. 21 (2008) 567-576.
[176] A. Herman, D.S. Tawfik, Protein Engineering Design & Selection. 20 (2007) 219-226.

[177] P. Heinzelman, C.D. Snow, M.A. Smith, X.L. Yu, A. Kannan, K. Boulware, A. Villalobos, S. Govindarajan, J. Minshull, F.H. Arnold, The Journal of Biological Chemistry. 284 (2009) 26229-26233.
[178] M.M. Meyer, L. Hochrein, F.H. Arnold, Protein Engineering Design & Selection. 19 (2006) 563-570.
[179] C.A. Voigt, S.L. Mavo, F.H. Arnold, Z.-G. Wang, Proceedings of the National Academy of Sciences of the United States of America. 98 (2001) 3778–3783.
[180] O. Alvizo, B.D. Allen, S. Mayo, BioTechniques. 42 (2007) 31-39.
[181] S.M. Lippow, B. Tidor, Current Opinion in Biotechnology. 18 (2007) 305-311.
[182] L. Montanucci, P. Fariselli, P.L. Martelli, R. Casadio, Bioinformatics. 24 (2008) 190-195.
[183] I.A. Noorbatcha, M.A. Hadi, A.F. Ismail, H.M. Salleh, Journal of Applied Science. 9 (2009) 3184-3187.
[184] M. Kankainen, A. Löytynoja, BMC Bioinformatics. 8 (2007) 189.
[185] E. Alsop, M. Silver, D.R. Livesay, Protein Engineering Design & Selection. 16 (2003) 871-874.
[186] M. Torrez, M. Schultehenrich, D.R. Livesay, Biophysical Journal. 85 (2003) 2845-2853.
[187] P.S. Shah, G.K. Hom, S.A. Ross, J.K. Lassila, K.A. Crowhurst, S.L. Mayo, Journal of Molecular Biology. 372 (2007) 1-6.
[188] M.T. Reetz, D. Kahakeaw, R. Lohmer, ChemBioChem. 9 (2008) 1797-1804.
[189] C. Bösing, Bachelor theis, Heinrich-Heine-Universität Düsseldorf 2009).
[190] W.J. Dower, J.F. Miller, C.F. Ragsdale, Nucleic Acids Research. 16 (1988) 6127-6145.
[191] D. Hanahan, Journal of Molecular Biology. 166 (1983) 557-580.
[192] J.C. Fieschko, Fermentation technology using recomvinant microorganisms, VCH Verlagsgesellschaft, 1989.
[193] W.F. Studier, Protein Expression and Purification. 41 (2005) 207-234.
[194] U.K. Laemmli, Nature. 227 (1970) 680-685.
[195] B. Riebel, PhD thasis, Heinrich-Heine University Düsseldorf (1996).
[196] M.M. Bradford, Analytical Biochemistry. 72 (1976) 248-254
[197] J.-H. Zhang, Journal of Biomolecular Screening. 4 (1999) 67-73.
[198] J.R. Lakowicz, Principles of Fluorescence Spectroscopy, Springer Science and Business Media, Singapore, 2006.
[199] http://web.uvic.ca/ail/techniques/epi-fluorescence.html.
[200] B.A. Shirley (Ed.), Protein stability and folding: theory and practice, Humana Press, New Jersey, 1995.
[201] T.E. Creighton, Protein structure: a practical approach, Oxford University Press, Oxford, New York, Tokyo, 1989.

[202] N. Berova, K. Nakanishi, R. Woody, Circular dichroism: principles and applications, Wiley-VCH, New York, 2000.
[203] N. Greenfield, G.D. Fasman, Biochemistry. 8 (1969) 4108-4116.
[204] J.T. Pelton, L.R. McLean, Analytical Biochemistry. 277 (2000) 167-176.
[205] A. Rodger, B. Norden, Circular dichroism and Linear dichroism, Oxford Chemistry Press, New York (1997).
[206] G.D. Fasman, Circular dichroism and the conformational analysis of biomolecules, Springer, Berlin (1996).
[207] C. Jones, B. Mulloy, A.H. Thomas, Microscopy, optical spectroscopy, and macroscopic technology, Humana Press, New Jersey (1994).
[208] J.S. Philo, Current Pharmaceutical Biotechnology. 10 (2009) 359-372.
[209] C. Fernandez, A.P. Minton, Analytical Biochemistry. 381 (2008) 254-257.
[210] A.P. Minton, Biophysical Journal. 93 (2007) 1321-1328.
[211] A.K. Attri, A.P. Minton, Analytical Biochemistry. 337 (2005) 103-110.
[212] J.Z. Xia, T. Aerts, K. Donceel, J. Clauwaert, Biophysical Journal. 66 (1994) 861-872.
[213] A. Saluja, D.S. Kalonia, International Journal of Pharmaceutics. 358 (2008) 1-15.
[214] A.K. Attri, A.P. Minton, Analytical Biochemistry. 346 (2005) 132-138.
[215] N. Zhelev, S. Barudov, Biotechnology and Bioengineering. 3 (2005) 1-8.
[216] H. Matsunami, C. Fujita, K. Ogawa, E. Kokofuta, Colloids and Surfaces B: Biointerfaces. 56 (2006) 149-154
[217] K. Kameyama, A.P. Minton, Biophysical Journal. 90 (2006) 2164-2169.
[218] V.A. Bloomfield, Biopolymers. 54 (2000) 168-172.
[219] A.J. Alpert, Journal of Chromatography. 499 (1990) 177-196.
[220] O.H. Lowry, J.V. Passonneau, D.W. Schulz, M.K. Rock, The Journal of Biological Chemistry. 236 (1961) 2746-2755.
[221] A. Illanes, Enzyme Biocatalysis: Principles and Applications, Springer Science and Business Media (2008).
[222] J.F. Nicholas, The Journal of Chemical Physics. 31 (1959) 922-925.
[223] R. Lumry, H. Eyling, Journal of Physical Chemistry. 58 (1954) 110-120.
[224] S.E. Zale, A.M. Klibanov, Biotechnology and Bioengineering. 25 (1983) 2221-2230.
[225] E.Y. Chi, S. Krishnan, T.W. Randolph, J.F. Carpenter, Pharmaceutical Research. 20 (2003) 1325-1336.
[226] J.M. Sanchez-Ruiz, J.L. Lopez-Lacomba, M. Cortijo M, P.L. , Biochemistry. 27 (1988) 1648-1652.
[227] G.F. Gutierrez-Lopez, G.B. Barbosa-Canovas, Food science and food biotechnology, CRC Press (2003).
[228] F. Dannenberg, H.-G. Kessler, Journal of Food Science. 53 (1988) 258-263.
[229] J. Hinrichs, B. Rademacher, Journal of Dairy Research. 71 (2004) 480-488.
[230] V.M. Taragano, A.M. Pilosof, Biotechnology Progress. 17 (2001) 775-777.

[231] M. Karel, O.R. Fennema, D.B. Lund, Physical principles of food preservation, Marcel Dekker (1975).
[232] J. Johansson, Swiss Medical Weekly. 133 (2003) 275-282.
[233] S. Jain, J.B. Udgaonkar, Journal of Molecular Biology. 382 (2008) 1228-1241.
[234] A. Pingoud, C. Urbanke, J. Hoggett, A. Jeltsch, Biochemical methods, Wiley-VCH, Weinheim (2002.)
[235] http://homepage.smc.edu/kline_peggy/Organic/Amino_Acid_pKa.htm.
[236] M.D. Joshi, G. Sidhu, J.E. Nielsen, G.D. Brayer, S.G. Withers, L.P. McIntosh, Biochemistry. 40 (2001) 10115-10139.
[237] J.E. Nielsen, J.A. McCammon, Protein Science. 12 (2003) 313-326.
[238] B. Rabenstein, G.M. Ullmann, E.W. Knapp, European Biophysics Journal 27 (1998) 626-637.
[239] http://agknapp.chemie.fu-berlin.de/karlsberg_old/doc/.
[240] R. Kratzer, B. Nidetzky, Biochemical Journal. 389 (2005) 507-515.
[241] R. Machielsen, A.R. Uria, S.W.M. Kengen, J. Van der Oost, Applied and Environmental Microbiology. 72 (2006) 233-238.
[242] U.C. Oppermann, E. Maser, Toxicology. 144 (2000) 71-81.
[243] A. Ganesan, N.C. Price, S.M. Kelly, I. Petry, B.D. Moore, P.J. Halling, Biochimica et Biophysica Acta. 1764 (2006) 1119-1125.
[244] J. Safar, P.P. Roller, G.C. Ruben, D.C. Gajdusek, C.J. Gibbs, Biopolymers. 33 (1993) 1461-1476.
[245] P. Pereira, S.M. Kelly, A. Cooper, H.J. Mardon, P.R. Gellert, C.F. Van der Walle, European Journal of Pharmaceutics and Biopharmaceutics 67 (2007) 309-319.
[246] G. Schäfer, S. Shastri, M.-K. Verhoefen, V. Vogel, K. Glaubitz, J. Wachtveitl, W. Mäntele, Photochemistry and Photobiology. 85 (2009) 529-534.
[247] K. Griebenow, A.M. Klibanov, Proceedings of the National Academy of Sciences of the United States of America. 92 (1995) 10969-10976.
[248] S. Sinha, Y.S. Li, T.D. Williams, E.M. Topp, Biophysical Journal. 95 (2008) 5951-5961.
[249] A. Sachdeva, S.W. Cai, Applied Spectroscopy. 63 (2009) 458-464.
[250] G. Shanmugam, P.L. Polavarapu, Journal of the American Chemical Society. 126 (2004) 10292-10295.
[251] L.W. Nesgaard, S.V. Hoffmann, C.B. Andersen, A. Malmendal, D.E. Otzen, Biopolymers. 89 (2008) 779-795.
[252] E. Barzana, M. Karel, A.M. Klibanov, Biotechnology and Bioengineering. 34 (1989) 1178-1185.
[253] E. Barzana, A.M. Klibanov, M. Karel, Applied Biochemistry and Biotechnology. 15 (1987) 25-34.
[254] C. Ferloni, M. Heinemann, W. Hummel, T. Daussmann, J. Buchs, Biotechnol Progr. 20 (2004) 975-978.

[255] O. Bogin, M. Peretz, Y. Burstein, Letters in Peptide Sciences. 5 (1998) 399-408.
[256] V. Renugopalakrishnan, X. Wei, G. Narasimhan, C.S. Verma, L. Pingzuo, A. Anumanthan, Bionanotechnology: proteins to nanodevices, Springer Netherlands, 2006.
[257] http://www.ebi.ac.uk/msd-srv/prot_int/pistart.html.
[258] A. Zaks, A.M. Klibanov, Protocols of National Academy of Science USA. 82 (1985) 3192-3196.
[259] K. Dimoula, PhD thesis, RWTH Aachen University (2009).
[260] K. Dimoula, M. Pohl, J. Büchs, A.C. Spiess, Biotechnology Journal. 4 (2009) 712-721.

Appendix

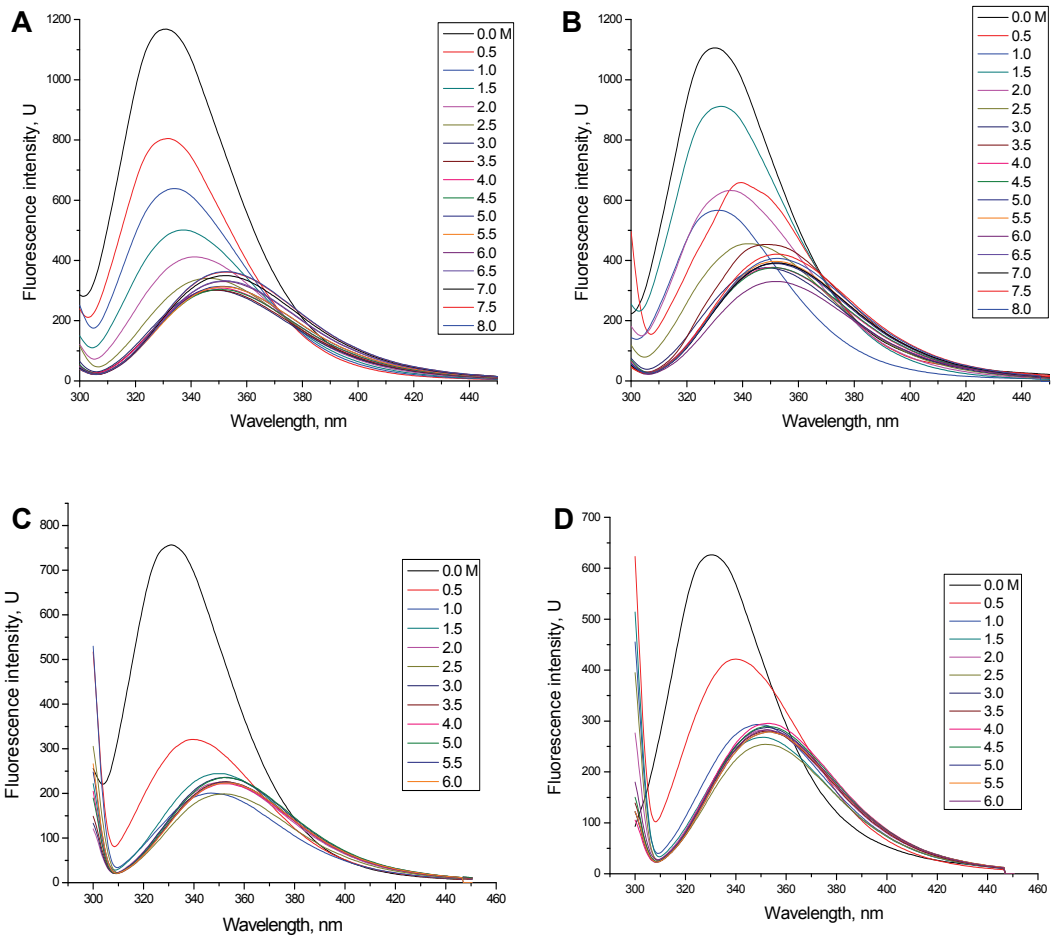

Figure A-1. Unfolding of *Lb*ADHwt and the *Lb*ADH G37D in the presence of urea and GndCl: tryptophan fluorescence emission spectra. A: *Lb*ADHwt denaturation by urea; B: *Lb*ADH G37D denaturation by urea; C: *Lb*ADHwt denaturation by GdnCl; D: *Lb*ADH G37D denaturation by GdnCl. Measurements were performed with a 0.1 mg/ml solution of the *Lb*ADHwt or the *Lb*ADH G37D in 10 mM TEA, 1 mM $MgCl_2$ buffer at pH 7.2 and the respective concentration of urea or GdnCl after incubation at RT for 24 h. Excitation wavelength 295 nm. . Further experimental details are represented in section 3.6.1.2.

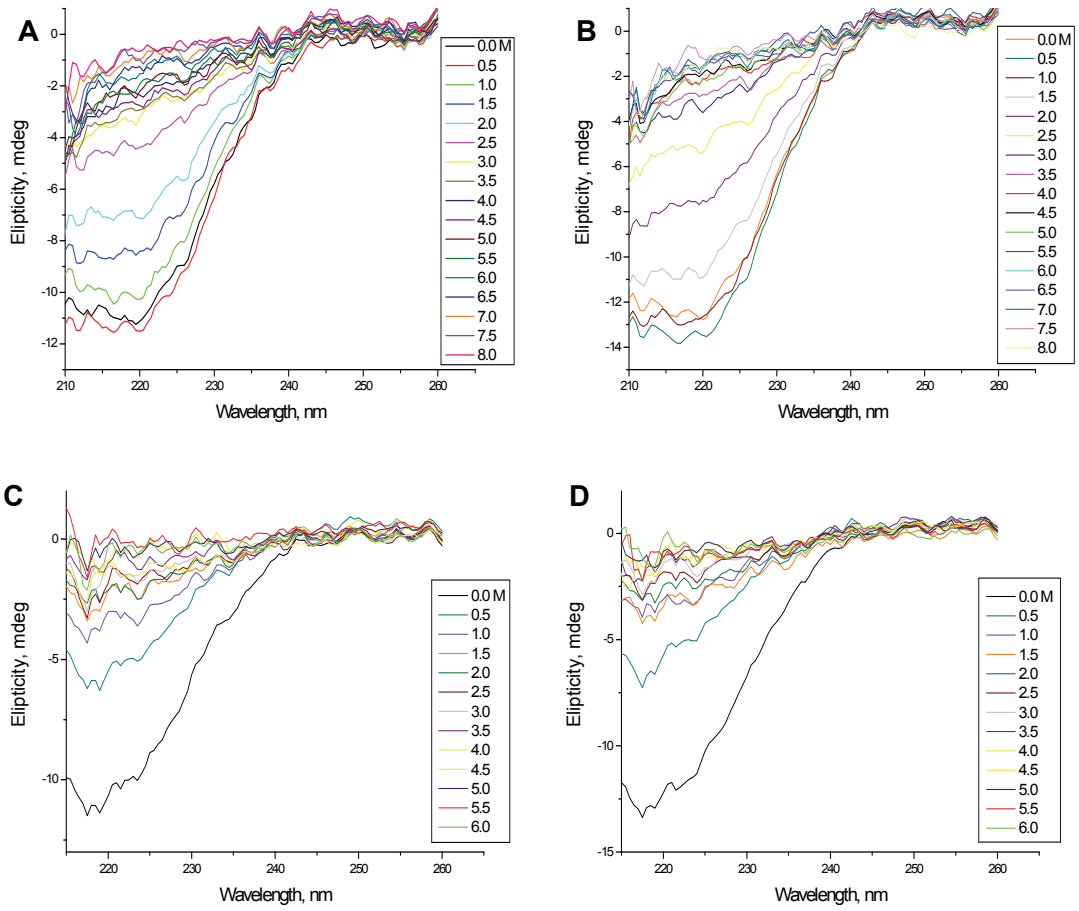

Figure A-2. Unfolding of *Lb*ADHwt and the *Lb*ADH G37D in urea and GdnCl: CD spectra. A: *Lb*ADH denaturationwt by urea; B: *Lb*ADH G37D denaturation by urea; C: *Lb*ADHwt denaturation by GdnCl; D: *Lb*ADH G37D denaturation by GdnCl. Experiments were performed with the 0.1 mg/ml solution of the *Lb*ADHwt or the *Lb*ADH G37D in 10 mM TEA, 1 mM $MgCl_2$ buffer at pH 7.2 and the respective concentration of urea or GdnCl after incubation at RT for 24h. . Further experimental details are represented in section 3.6.2.2.

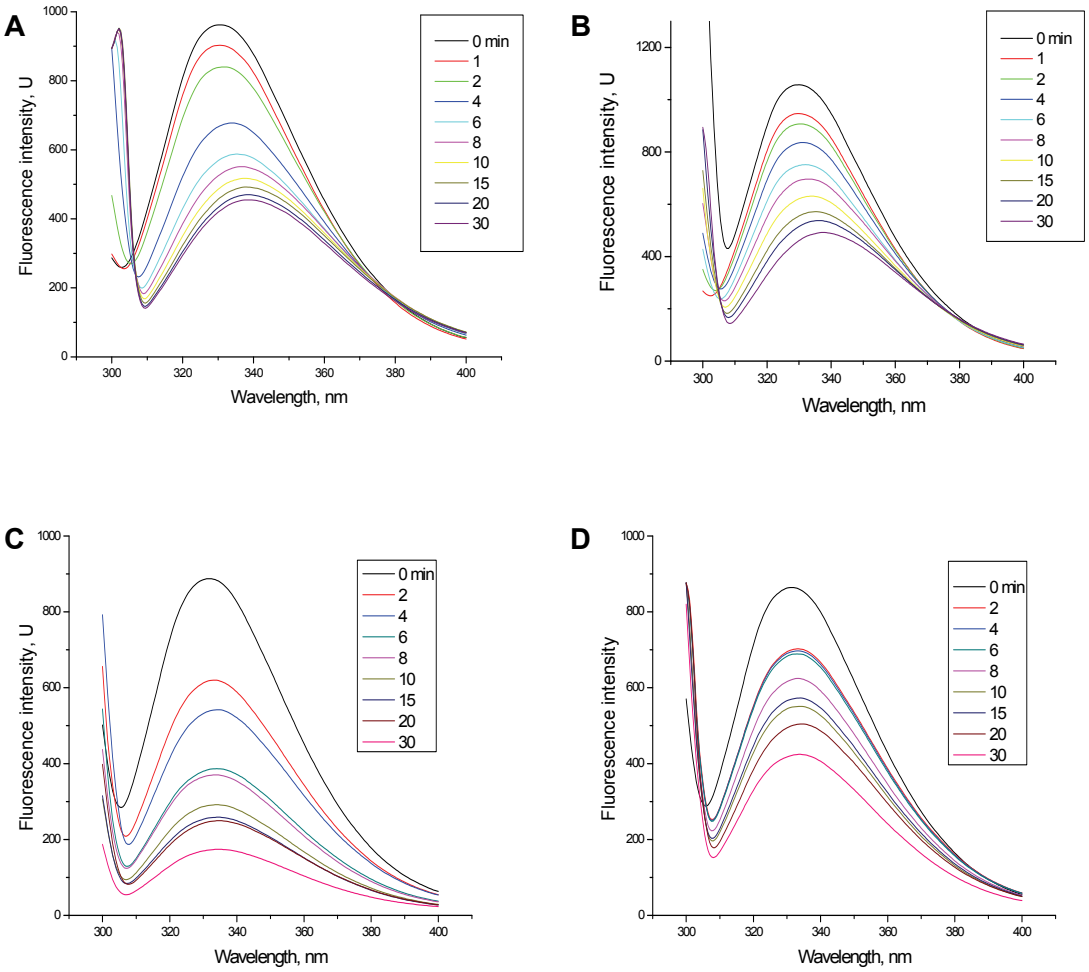

Figure A-3. Temperature dependence of fluorescence emission spectra of the dissolved and solid *Lb*ADHwt and the *Lb*ADH G37D. A: dissolved *Lb*ADHwt at 50°C; B: dissolved *Lb*ADH G37D at 50°C; C: solid *Lb*ADHwt at a_w = 0.1 and T = 80°C; D: solid *Lb*ADH G37D at a_w = 0.1 and T = 80°C. The studies of the dissolved samples, *Lb*ADHwt or the *Lb*ADH G37D (each 0.1 mg/ml) were performed in 10 mM TEA, 1 mM $MgCl_2$ buffer at pH 7.2. Each sample was divided into 800 µl aliquots, heated at 50°C for 0-30 min and analyzed by fluorescence spectroscopy in correlation with enzymatic activity. The solid enzyme samples were equilibrated over saturated salt solutions for 24 h to reach defined values of water activity, then heated at 80°C for 0-30 min, cooled down to room temperature, re-dissolved in 1 ml of distilled water, and immediately checked for fluorescence properties and enzymatic activity. Excitation was performed at 295 nm. . Further experimental details are represented in section 3.6.1.2.